WAVELET-BASED ADAPTIVE CONTROL OF STRUCTURES UNDER SEISMIC AND WIND LOADS

DISSERTATION

Presented in Partial Fulfillment of the Requirements for

the Degree Doctor of Philosophy in the Graduate

School of The Ohio State University

By

Hongjin Kim, M.S.

* * * * *

The Ohio State University
2002

Dissertation Committee:

Professor Hojjat Adeli, Advisor

Professor Shive Chaturvedi

Dr. Kaveripa V. Balasubramanyam

Approved by

____

Advisor
Graduate Program in Civil Engineering

ABSTRACT

A new control algorithm, wavelet-hybrid feedback LMS algorithm, is developed to overcome the shortcomings of the classical feedback control algorithms and the filtered-x LMS control algorithm. It integrates a feedback control algorithm such as the LQR or LQG algorithm with the filtered-x LMS algorithm and utilizes a wavelet multi-resolution analysis for the low-pass filtering of external dynamic excitations. Since the control forces determined by the filtered-x LMS algorithm are adapted by updating the FIR filter coefficients at each sampling time until the output error is minimized, the new control algorithm is effective in control of both steady-state and transient vibrations. It is shown that the algorithm is capable of suppressing vibrations over a range of input excitation frequencies unlike the classic feedback control algorithms whose control effectiveness decreases considerably when the frequency of the external disturbance differs from the fundamental frequency of the system. Further, results demonstrate that the wavelet transform can be effectively used as a low-pass filter for control of civil structures without any significant additional computational burden.

A new hybrid control system, hybrid damper-TLCD system, is developed through judicious integration of a passive supplementary viscous fluid damping system with a semi-active TLCD system, and its performance is evaluated for control of responses of 3D irregular buildings under various seismic excitations and for control of wind-induced motion of high-rise buildings. The new hybrid control system utilizes the advantages of both passive and semi-active control systems along with improving the overall performance and eliminating the need for a large power requirement, unlike other proposed hybrid control systems where active and passive systems are combined. Simulation results show that the new hybrid control system is effective in reducing the response of structures significantly under seismic excitations as well as wind loads. It is also demonstrated that the hybrid control system provides increased reliability and maximum operability during normal operations as well as a power or computer failure.

Dedicated to my wife Jayoung and daughter Soohyun

ACKNOWLEDGEMENTS

It is my sincere pleasure to acknowledge the contribution of my advisor Dr. Hojjat Adeli. His encouragement, enthusiasm, and invaluable wisdom made it possible for me to complete this dissertation. I cannot thank him enough for hundreds of hours on Saturdays and Sundays that he has worked with me for my dissertation. Moreover, I appreciate the opportunities he has given me as well as the insight he has instilled.

I would like to express my gratitude to Professor Shive K. Chaturvedi and Dr. Kaveripa V. Balasubramanyam for serving as my dissertation committee. I also extend my gratitude to thank the faculty members, staffs, colleagues, and friends from the Department of Civil and Environmental Engineering and Geodetic Science for their help, assistance, and support throughout the my graduate studies.

The financial support provided as a Graduate Research Associate and PEGS Fellow at The Ohio State University during part of my Ph. D. studies is acknowledged and appreciated.

Last, but not least, I want to thank my parents, my wife, and her parents, who provided continuous support, encouragement and love.

VITA

November 22, 1969............................Born

1993..B.S. Architectural Engineering, Seoul National University, Seoul Korea

1999..M.S. Civil Engineering, The Ohio State University

1999 – present...............................Graduate Research Associate, The Ohio State University

PUBLICATIONS

Research Publication

Adeli, Hojjat and Kim, Hongjin (2000), "Web-based interactive courseware for structural steel design using Java," *Computer-Aided Civil and Infrastructure Engineering*, Vol. 15, No. 2, pp. 158-166.

Kim, Hongjin and Adeli, Hojjat (2001), "Discrete cost optimization of composite floors using floating-point genetic algorithm," *Engineering Optimization*, Vol. 33, No. 4, pp. 485-501.

Adeli, Hojjat and Kim, Hongjin (2001), "Cost optimization of composite floors using neural dynamics model," *Communications in Numerical Methods in Engineering*. Vol. 17, No. 11, pp. 771-787.

FIELDS OF STUDY

Major Field: Graduate Program in Civil Engineering (Structures)

Minor Field: Computer Information Science

TABLE OF CONTENTS

LIST OF TABLES

LIST OF FIGURES

CHAPTER 1

INTRODUCTION

1.1 Control Algorithms

Since Yao (1972) introduced the control concept to structural engineers, a number of control algorithms have been used for structural problems. The Linear Quadratic Regulator (LQR) feedback control algorithm (Soong, 1990) and the Linear Quadratic Gaussian (LQG) control algorithm (Stein and Athans, 1987; Dyke et al., 1996b) are among the most popular optimal feedback control algorithms mainly due to their simplicity and ease of implementation. These algorithms achieve a significant level of attenuation in the vicinity of the natural frequencies of the structure. However, they fail to suppress the vibrations when frequency of the external disturbance differs from the natural frequencies of the structure. Further, these algorithms are susceptible to parameter uncertainty and modeling error (Prakah-Asante and Craig, 1994) and they present optimum solutions in a narrow sense only because the external excitation term is ignored in their formulation and solution. In these algorithms, a pre-defined performance index is minimized where only the responses of the system and control effort are included.

Yang et al. (1987) attempted to include the external excitation in the formulation by proposing an instantaneous optimal control algorithm that minimizes the performance index at every instant of time within control interval. This algorithm, however, is much more dependent on the choice of weighting matrices than the LQR and LQG algorithms, thus requiring careful considerations in order to achieve desirable control results (Soong, 1990). Further, the stability of the control system is not guaranteed (Yang and Li, 1991). Suhardjo et al. (1992) include the external excitation in the frequency domain in an optimal feedback-feedforward control algorithm in their study of control of wind-excited building structures. Wind loads are modeled in the frequency domain as stochastic processes by their spectral density matrices. The authors combine the external wind loads with a feedback controller in the form of feedforward filters in the formulation of control problem.

To overcome the aforementioned limitations of the classic optimal control algorithms, researchers have recently explored the use of soft computing approaches such as neural networks and fuzzy logic (Adeli and Hung, 1995). Neural networks are capable of learning and generalizing. A review of the civil engineering applications of neural networks is presented by Adeli (2001). Backpropagation (BP) neural network learning algorithm is the most widely-used neural network algorithm because of its simplicity. Ghaboussi and Joghataie (1995) and Chen et al. (1995) present active control algorithms using the BP neural networks. The BP algorithm is used first to predict the desired responses subjected to control forces and again to predict the control forces given the desired responses and the external excitation. Chen et al. (1995) define the instantaneous error function as the summation of error between actual and desired responses. Then, the BP training rule is applied to minimize the error function. The desired response is set to zero in each time step. Ghaboussi and Joghataie (1995), however, set the average of expected responses for a few future time steps to zero. As such, in the BP-based control algorithm, the desired output is selected somewhat arbitrarily and may not be optimal. The BP algorithm is used for function approximation. To achieve satisfactory results, a hidden layer with a large number of nodes is needed resulting in a very slow learning process and a very large number of iterations for solution convergence. Moreover, the BP algorithm suffers from the hill climbing problem, that is, the solution can be trapped in a local minimum during the training (Bakshi and Stephanopoulos, 1993; Adeli and Hung, 1994).

The adaptive filtered-x Least Mean Square (LMS) control algorithm has been used successfully in acoustic, electrical, and aerospace engineering problems (Widrow and Stearns, 1985). This algorithm is based on the integration of the adaptive filter theory used for system identification in real time and the feedforward control approach. The advantage of this method is that the external excitation is included in the formulation. This algorithm was used by Burdisso et al. (1994) for active control of a three-story two-dimensional frame subjected to earthquake loading. They point out that this algorithm can handle the modeling error including the effect of soil-structure interaction. Since the control forces determined are adapted by updating the finite-impulse-response (FIR) filter coefficients at each sampling time until the output error is minimized, the filtered-x LMS control scheme minimizes vibrations over the entire frequency range and thus is less susceptible to modeling errors and inherently more stable. However, it is not as effective for short transient vibrations such as peaks because it requires adaptation time.

1.2 Passive, Semi-Active, and Hybrid Control of Structures

Passive control refers to systems that do not require an external power source. It includes base isolation, supplementary damper, and tuned mass damper (TMD) systems. A base isolation system (Figure 1.1(a)) attempts to reduce the response of structures subjected to seismic ground excitations by isolating the structure from the external seismic excitations. The seismic isolation system is usually applied to relatively massive buildings that are housing sensitive equipments such as computer centers, emergency operation centers, hospitals, and nuclear power plants, and to the rehabilitation of historic-landmark buildings such as the Los Angeles City Hall (Youssef et al., 2000) and the Ninth Circuit U.S. Court of Appeals building located in San Francisco (Mokha et al., 1996). The base isolation systems used in these applications are often large, heavy, and costly.

The supplementary damper system (Figure 1.1(b)) has been widely used for the vibrations suppression in general. In this system mechanical devices increase the existing inherent damping of the structure and help dissipate the energy of the external excitation.

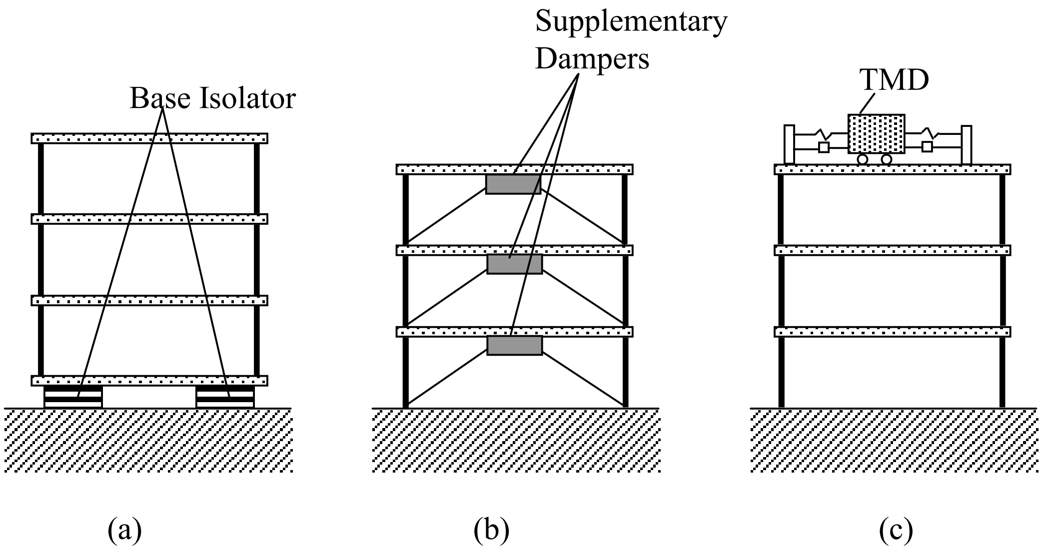

Figure 1.1: Three typical passive control devices: (a) base isolation system, (b) supplementary damper system, (c) TMD system

The mechanical dampers in buildings are usually installed as part of its bracing system, such as diagonal or Chevron bracings (Figure 1.1(b)). Examples include an eleven story steel building located in Sacramento, California (Miyamoto and Scholl, 1998) and the seismic upgrade of a 13-story concrete frame structure located in Los Angeles, California (Hanson and Soong, 2001). Supplementary dampers are sometimes used with other types of passive and/or active devices in order to maximize the suppression capacity (Youssef et al., 2000).

A TMD system (Figure 1.1(c)) relies on the damping forces introduced through the inertia force of a secondary system attached to the main structure in order to reduce the response of the main structure. The secondary mass is designed to have dynamic characteristics that are closely related to those of the primary structure. The most important characteristics are the mass ratio of the secondary mass to the primary system, the frequency ratio of the two systems, and the damping ratio of the secondary system. By varying these three ratios, the frequency response function of the primary system can be modified so that the response of the primary system is reduced. Examples can be found in the John Hancock tower in Boston and the Citicorp Building in New York City (Housner et al., 1997).

In a TMD system, the secondary mass, which is usually made of concrete, is attached to the main structure through a spring and a dashpot. The parameters of mass, spring, and dashpot are often tuned for the fundamental natural frequency of the structures so that the maximum response reduction occurs near that frequency. The drawback of this approach is that a TMD system provides protection against external dynamic disturbances with a frequency only in the vicinity of the natural frequency of the structure and not for a range of frequencies or bandwidth normally found in environmental forces. Moreover, to find the optimal values of parameters for a TMD system, the magnitude of the external excitation must be established *a priori*, which is not practical considering the variable nature of environmental forces. To overcome these shortcomings, active and semi-active TMD systems have been proposed where values of the parameters are changed based on the frequency and the amplitude of excitation in real time (Hrovat et al., 1983; Abe, 1996). Others have proposed the Multiple-TMD system where more than one TMD system are designed and distributed within the structure to cover a range of dominant frequencies (Kareem and Kline, 1995).

More recently, the tuned liquid column damper (TLCD) has received the attention of researchers (Sakai et al., 1989; Kareem 1994; Won et al, 1996; Yalla et al., 2001) as another type of secondary mass system. Similar to a TMD system, a TLCD system can reduce the response of the primary system by modifying its frequency response function. In a TLCD system, the secondary mass is liquid and damping forces are introduced through the motion of liquid in a U-shape tube container. When the same mass is used and other parameters are properly tuned, a TLCD system provides performance similar to a TMD system (Samali et al., 1998). In addition to reducing building responses, a TLCD system provides several advantages over a TMD system, which will be discuused in Chapter 4.

Because of advantages, a growing number of bridge and building structures have been built with the TLCD system over the past decade or so. Examples include the Higash-Kobe cable-stayed bridge in Japan (Sakai et al., 1991), the 106.2-m high Hotel Cosima in Tokyo (Teramura and Yoshida, 1996), and the 194.4-m high Shin Yokohama Prince Hotel in Japan (Kareem, 1994). Recently, a TLCD system was used in the 48-story One Wall Centre, the tallest building in Vancouver, British Columbia. Two specially-designed U-shaped tanks, each containing about 50,000 gallon (189 tons) of water, are installed in the tower's mechanical penthouse in order to lessen the lateral movement of building against both earthquakes and strong winds. According to Fortner

(2001), the TLCD system has saved at least 2 million dollars in construction cost compared to the conventional TMD system. This is because the TLCD system eliminates the installation of a pump station and a backup generator required for fire suppression. If the water is used for extinguishing a fire, the effectiveness of the TLCD system is reduced. When a fire occurs during an earthquake the TLCD system will protect the structure during ground motions. The water in the TLCD system can then be used to extinguish any ensuing fire. In addition, the water tanks are used as heat sinks for building's heat pump, and thick concrete water tank walls on the roof level act as outrigger walls.

As in TMD systems, however, the effectiveness of a TLCD system depends on proper tuning of design parameters. The optimum values of design parameters of a TLCD system are obtained only for any given external excitations with fixed frequency bandwidth and amplitude. In other words, these values are optimal only for the design excitation and not any other external excitation. This shortcoming can be overcome by utilizing semi-active or active control strategies.

In order to improve the performance of passive control systems, active control systems have been proposed where sensors measure the motions of the structure and actuators and a feedback control strategy exert counteracting forces to compensate for the effect of external excitations (Adeli and Saleh, 1997 and 1999; Christenson et al., 2003). A shortcoming of active control of structures is its dependency on a large power requirement for the control system. An active control system will not operate when a strong earthquake causes the failure of the electric power system unless there is a large properly operating backup battery system.

Semi-active control strategies have been proposed by researchers to increase the overall reliability as well as the efficacy of the control system (Housner et al., 1997). Semi-active control systems are physically similar to passive control systems but computationally similar to active control systems. Developed from passive control devices, semi-active control devices are designed to operate with a very small power (e.g. a battery) thus eliminating to need for a large external electric power source. They control the response of the structure by actively changing the properties of controllers when power is supplied, but behave like passive control systems when the power source is cut off or when there is a computer system failure. As such, semi-active control systems provide a more reliable and stable way of controlling structures compared with active control systems.

There is another strategy to overcome the vulnerability of active control systems, called hybrid control, where two distinct systems are employed together. Traditionally, an active control system is used in conjunction with a passive control system (Soong and Reinhorn, 1993; Lee-Glauser et al., 1997). When there is power (normally electric power) the two systems work simultaneously. When the external power fails the passive control system still works, thus reducing the response of the structure at least to some extent even after the active control system stops functioning. The shortcoming of this approach is that in the event of power failure during a catastrophic or maximum probable earthquake only one half of the earthquake resistant system is available and safety of the structural system is not guaranteed.

1.3 Objectives and Outline of Dissertation

The first objective of this study is to develop a new control algorithm for robust control of civil structures subjected to destructive environmental forces such as earthquakes and winds. The new control algorithm, wavelet-hybrid feedback LMS algorithm, integrates a feedback control algorithm such as the LQR or LQG algorithm with the filtered-x LMS algorithm and utilizes a wavelet multi-resolution analysis for the low-pass filtering of external dynamic excitations. The goals are to achieve optimum control under external dynamic disturbances in real time and to overcome shortcomings of the existing feedback control algorithms and the filtered-x LMS algorithm described earlier.

In Chapter 2, a hybrid feedback-LMS algorithm, which integrates a feedback control algorithm such as LQR and LQG algorithms and the filtered-x LMS algorithm, is introduced. The hybrid feedback-LMS control algorithm is intended to achieve faster vibration suppression than the filtered-x LMS algorithm, and to be capable of suppressing vibrations over a range of input excitation frequencies unlike the classic feedback control algorithms whose control effectiveness decreases considerably when the frequency of the external disturbance differs from the fundamental frequency of the system.

In Chapter 3, the wavelet-hybrid feedback LMS algorithm is developed through judicious integration of the hybrid feedback-LMS algorithm and a wavelet low-pass filter. The wavelet low-pass filter is introduced for better stabilization of the FIR filter during adaptation when applying the algorithm to the control of civil structures against real environmental forces.

The second objective of this study is to devise a new hybrid control system, hybrid damper-TLCD system. The new hybrid control system, which combines passive and semi-active control systems, is intended to achieve increased reliability and maximum operability of the control system during power failure, and to eliminate the need for a large power requirement unlike other proposed hybrid control systems where active and passive systems are combined.

In Chapter 4, the hybrid damper-TLCD system is developed through integration of a passive supplementary damping system with a semi-active TLCD system. The wavelet-hybrid feedback LMS control algorithm, presented in Chapters 2 and 3, is applied to find optimum control forces.

In Chapters 5 and 6, the hybrid damper-TLCD system is further investigated for control of responses of 3-dimensional (3D) irregular buildings and high-rise buildings. In Chapter 5, the effectiveness and robustness of the proposed hybrid system in reducing the vibrations of 3D irregular buildings under various seismic excitations are evaluated. Two multistory moment-resisting steel building structures with vertical and plan irregularities, respectively, are designed and used to investigate the effectiveness of the hybrid system. In Chapter 6, the effectiveness of hybrid system is investigated for the control of wind-induced motion of high-rise buildings. Simulations are performed on a benchmark 76-story reinforced concrete building.

In Chapter 7, the wavelet-hybrid feedback LMS control algorithm is applied for control of cable-stayed bridge subjected to strong seismic motions. Simulations are performed on a benchmark cable-stayed bridge under various seismic excitations. Chapter 8 summarizes the conclusions from this study.

CHAPTER 2

HYBRID FEEDBACK-LMS ALGORITHM

2. 1 Introduction

In this chapter, a hybrid feedback-LMS model is presented for control of structures through integration of a feedback control strategy such as the LQR or LQG algorithm and the filtered-x LMS algorithm. The goal is to achieve optimum control under external dynamic disturbances such as earthquake and wind in real time. In the following sections, first two classical feedback control methods are reviewed briefly. Next, the adaptive filtered-x LMS algorithm is introduced. Then, a hybrid LMS feedback control algorithm is presented and applied to the active tuned mass damper (ATMD) system subjected to harmonic loadings.

2. 2 Equation of Motion

A major reason for the use of active control is to minimize the displacements and stresses under severe dynamic loading conditions. As such, the structural response will be limited to the elastic range. The control algorithms presented in this section are based on the assumption that the structure is time-invariant and behaves linearly.

When an m-degree-of-freedom (DOF) discrete system is subjected to external excitation and control forces, its governing equation of motion can be written as (Soong, 1990)

$$\boldsymbol{M}\ddot{\boldsymbol{u}}(t) + \boldsymbol{C}\dot{\boldsymbol{u}}(t) + \boldsymbol{K}\boldsymbol{u}(t) = \boldsymbol{B}_c\boldsymbol{f}(t) + \boldsymbol{E}_c\boldsymbol{f}_e(t) \tag{2.1}$$

where $\boldsymbol{M}$, $\boldsymbol{C}$, and $\boldsymbol{K}$ are $m \times m$ mass, damping, and stiffness matrices, respectively; $\boldsymbol{u}(t)$ = $m \times 1$ displacement vector; $\boldsymbol{f}(t) = l \times 1$ control force vector; $\boldsymbol{f}_e(t) = r \times 1$ external dynamic force vector; $\boldsymbol{B}_c$ and $\boldsymbol{E}_c$ are $m \times l$ and $m \times r$ location matrices which define locations of the control forces and the external excitations, respectively, and t is the time. In state-space form, Eq. (2.1) can be written in the form

$$\dot{\boldsymbol{z}}(t) = \boldsymbol{A}\boldsymbol{z}(t) + \boldsymbol{B}\boldsymbol{f}(t) + \boldsymbol{E}\boldsymbol{f}_e(t) \tag{2.2}$$

where

$$\boldsymbol{z}(t) = \begin{bmatrix} \boldsymbol{u}(t) \\ \dot{\boldsymbol{u}}(t) \end{bmatrix} \tag{2.3}$$

is the $2m \times 1$ state vector, and

$$\boldsymbol{A} = \begin{bmatrix} \boldsymbol{0} & \boldsymbol{I} \\ -\boldsymbol{M}^{-1}\boldsymbol{K} & -\boldsymbol{M}^{-1}\boldsymbol{C} \end{bmatrix} \tag{2.4}$$

$$\boldsymbol{B} = \begin{bmatrix} \boldsymbol{0} \\ \boldsymbol{M}^{-1}\boldsymbol{B}_c \end{bmatrix} \tag{2.5}$$

$$\boldsymbol{E} = \begin{bmatrix} \boldsymbol{0} \\ \boldsymbol{M}^{-1}\boldsymbol{E}_c \end{bmatrix} \tag{2.6}$$

are $2m \times 2m$, $2m \times l$, and $2m \times r$ system, control location, and external excitation location matrices, respectively. The matrices $\boldsymbol{0}$ and $\boldsymbol{I}$ in Eqs (2.4) to (2.6) denote, respectively, the zero and identity matrices of size $m \times m$.

2.3 Feedback Control Algorithms

2.3.1 LQR Control Algorithm

The LQR optimal control algorithm is one of the most widely used feedback algorithms in structural control mainly due to its simplicity and relative ease of implementation (Adeli and Saleh, 1999; Kurata et al., 1999). The optimal control is defined by a given vector of controllers and predefined state variable performance weighting matrix, $\boldsymbol{Q}$, and control effort weighting matrix, $\boldsymbol{R}$. The problem is then expressed as finding the appropriate state-feedback control forces that minimize the following performance index:

$$J = \int_0^\infty \left[\boldsymbol{z}^{\mathrm{T}}(t)\boldsymbol{Q}\boldsymbol{z}(t) + \boldsymbol{f}^{\mathrm{T}}(t)\boldsymbol{R}\boldsymbol{f}(t)\right]dt \tag{2.7}$$

where the superscript $^{\mathrm{T}}$ denotes the transpose of a matrix. Then, optimal state-feedback control forces are obtained from

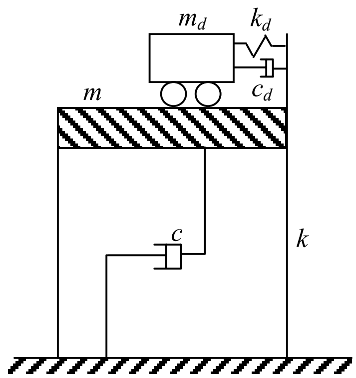

Figure 2.1: Active Tuned Mass Damper (ATMD) system

$$\boldsymbol{f}(t) = -\boldsymbol{G}\boldsymbol{z}(t) = -\boldsymbol{R}^{-1}\boldsymbol{B}^{\mathrm{T}}\boldsymbol{P}\boldsymbol{z}(t) \tag{2.8}$$

where $\boldsymbol{G}$ is the gain matrix and $\boldsymbol{P}$ is obtained from the solution of the algebraic Riccati equation:

$$-\boldsymbol{P}\boldsymbol{A} - \boldsymbol{A}^{T}\boldsymbol{P} - \boldsymbol{Q} + \boldsymbol{P}\boldsymbol{B}\boldsymbol{R}^{-1}\boldsymbol{B}^{T}\boldsymbol{P} = \boldsymbol{0} \tag{2.9}$$

where the superscript $^{-1}$ denotes the inverse of a matrix. The solution of the Riccati equation can be obtained by the generalized eigenproblem algorithm (Arnold, 1984) or other methods (Lewis and Syrmos, 1995; Saleh and Adeli, 1997). Substituting Eq. (2.8) into Eq. (2.2), the behavior of the optimally controlled structure can be obtained by

$$\dot{\boldsymbol{z}}(t) = (\boldsymbol{A} - \boldsymbol{B}\boldsymbol{G})\boldsymbol{z}(t) + \boldsymbol{E}\boldsymbol{f}_e(t) \tag{2.10}$$

The example structure considered in this chapter is the active tuned mass damper (ATMD) control model, shown in Figure 2.1, presented at the web site "*Java Powered*

Simulator for Structural Vibration and Control" (Yang and Satoh, 2001). Structural properties of the ATMD system are presented in Appendix I. The fundamental natural frequency of the system, ω_n, is 1 Hz. Figure 2.2 shows the comparison of the frequency responses of the ATMD system with and without LQR control in decibels (dB). Decibel is a logarithmic unit defined as $20\log_{10}X$, where X is the root mean square quantity. The gain matrix $\boldsymbol{G}$ calculation is done using the Matlab (2000) *LQR* routine. As seen in Figure 2.2, a significant level of attenuation is achieved in the vicinity of the resonance frequency of the ATMD system. However, the level of attenuation reduces drastically when the frequency of the external disturbance differs from the fundamental frequency of the ATMD system.

Consequently, the LQR control method results in very little suppression of vibration for the latter case, as demonstrated in Figure 2.3. Figure 2.3(a) shows the displacement of the system when the disturbance frequency, ω, is same as the natural frequency of the system and substantial suppression of vibrations is achieved. In contrast, Figure 2.3(b) shows the displacement when the disturbance frequency is 1.2 times the fundamental frequency of the ATMD system. In this case, the vibration suppression is minimal and diminishes as times go on. Table 2.1 summarizes the maximum responses and the root mean square (RMS) displacements with reduction ratios presented in parentheses. The results clearly show that the control effectiveness decreases considerably when the frequency of the external disturbance differs from the fundamental frequency of the ATMD system.

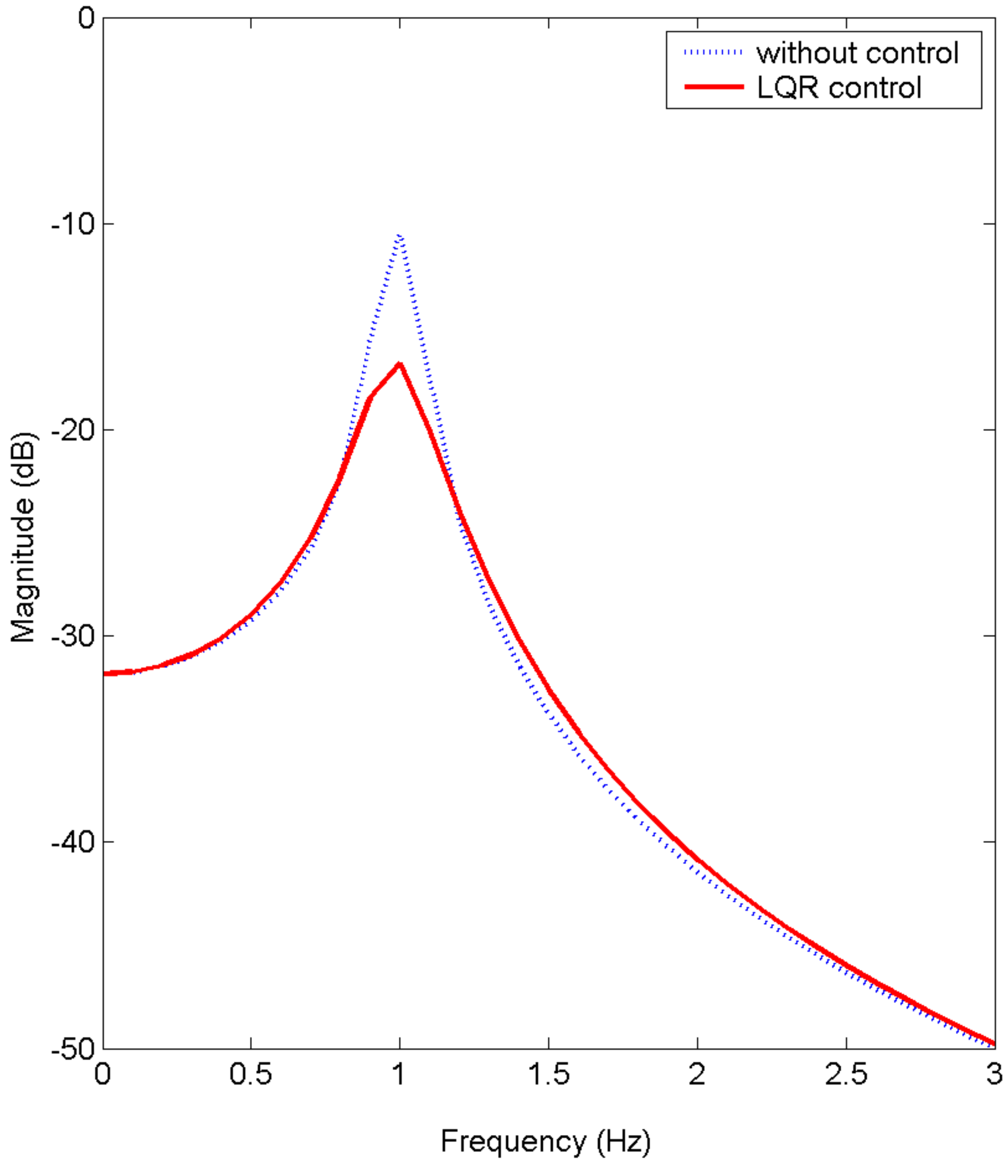

Figure 2.2: Frequency responses of the ATMD system with and without LQR control

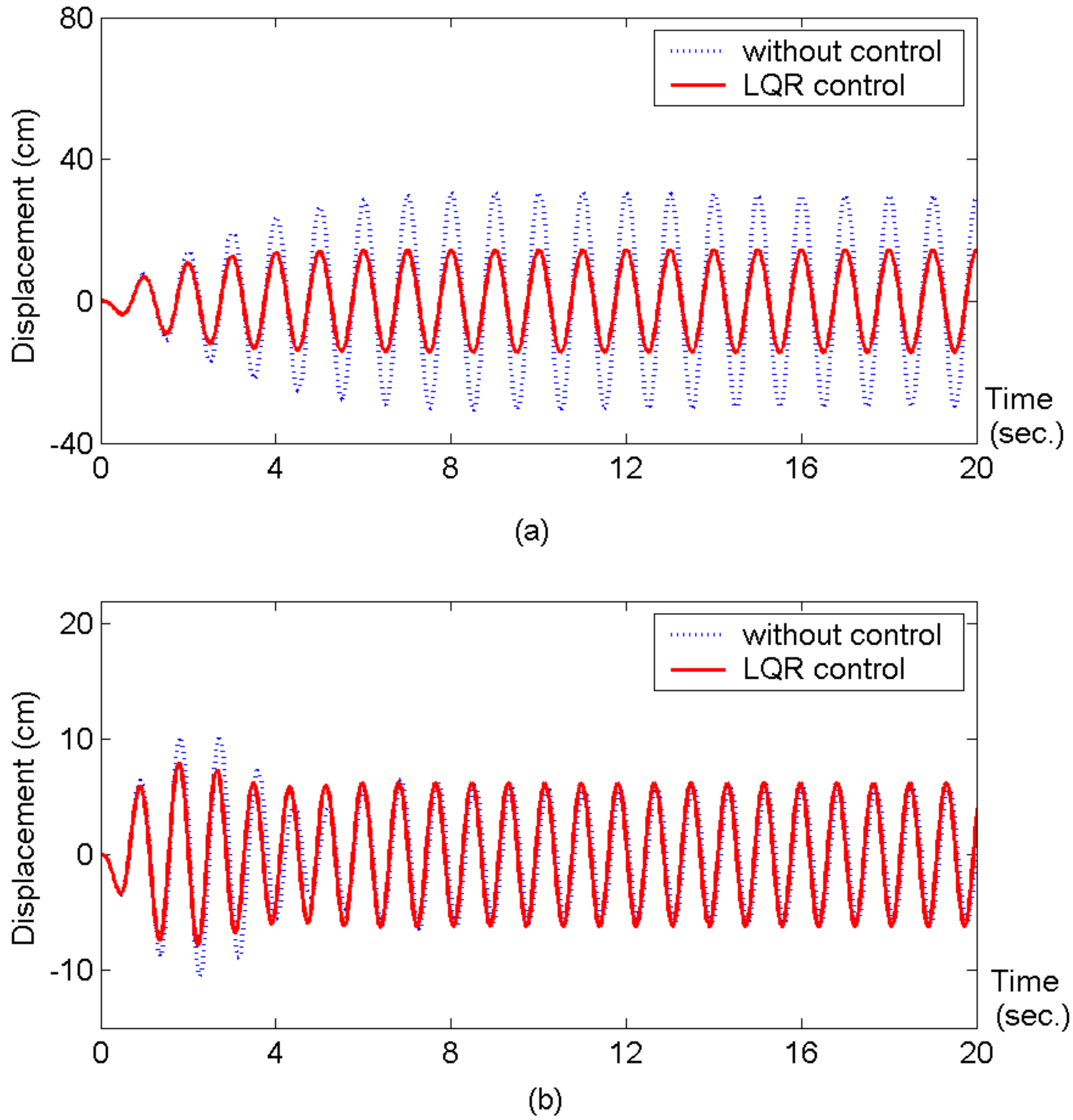

Figure 2.3: LQR control of the ATMD system, (a) $\omega = 1.0\ \omega_n$, (b) $\omega = 1.2\ \omega_n$

Disturbance frequency	Uncontrolled responses		LQR controlled responses	
	Maximum displacement (cm)	RMS displacement (cm)	Maximum displacement (cm)	RMS displacement (cm)
$\omega = 1.0\ \omega_n$	30.9	20.0	14.4 (53.2%)	9.84 (50.8%)
$\omega = 1.2\ \omega_n$	10.7	4.43	8.02 (24.9%)	4.46 (-0.68 %)

Table 2.1: Responses of the ATMD system subjected to the disturbances with frequencies the same as and 1.2 times the natural frequency of the system

2.3.2 LQG Control Algorithm

Another commonly used feedback control algorithm in structural control is the LQG control algorithm (Dyke et al., 1996a; Spencer et al., 1998). In this approach, the measured outputs are assumed to be the desired system response plus noise. This consideration is due to the fact that there are inherent errors in the structure modeling as well as in the output sensoring. Considering noise in the measured response, the controlled response, $\boldsymbol{y}_c$, and measured response, $\boldsymbol{y}_m$, are given by

$$\boldsymbol{y}_c = \boldsymbol{C}_c \boldsymbol{z} + \boldsymbol{D}_c \boldsymbol{f} + \boldsymbol{F}_c \boldsymbol{f}_e \tag{2.11}$$

and

$$\boldsymbol{y}_m = \boldsymbol{C}_m \boldsymbol{z} + \boldsymbol{D}_m \boldsymbol{f} + \boldsymbol{F}_m \boldsymbol{f}_e + \boldsymbol{v} \tag{2.12}$$

respectively, where $\boldsymbol{C}_c$, $\boldsymbol{D}_c$, $\boldsymbol{F}_c$, $\boldsymbol{C}_m$, $\boldsymbol{D}_m$, and $\boldsymbol{F}_m$ are mapping matrices with appropriate dimensions and $\boldsymbol{v}$ is the measurement noise vector.

For LQG feedback control algorithm, the optimal control problem is expressed as finding the appropriate state-feedback control forces that minimize the following performance index:

$$J = E\left\{ \lim_{t_f \to \infty} \frac{1}{t_f} \int_0^{t_f} \left[(\boldsymbol{C}_c \boldsymbol{z} + \boldsymbol{D}_c \boldsymbol{z})^{\mathrm{T}} \boldsymbol{Q} (\boldsymbol{C}_c \boldsymbol{z} + \boldsymbol{D}_c \boldsymbol{z}) + \boldsymbol{f}^{\mathrm{T}} \boldsymbol{R} \boldsymbol{f} \right] dt \right\} \tag{2.13}$$

where $E\{\}$ denotes the expected value operator. The control force is obtained as

$$\boldsymbol{f} = -\boldsymbol{G}\hat{\boldsymbol{z}} \tag{2.14}$$

where $\hat{\boldsymbol{z}}$ is the Kalman Filter estimator of the state vector, which is given by

$$\dot{\hat{\boldsymbol{z}}} = \boldsymbol{A}\hat{\boldsymbol{z}} + \boldsymbol{B}\boldsymbol{f} + \boldsymbol{L}(\boldsymbol{y}_m - \boldsymbol{C}_m \hat{\boldsymbol{z}} - \boldsymbol{D}_m \boldsymbol{f}) \tag{2.15}$$

where matrix $\boldsymbol{L}$ is determined by using the standard Kalman Filter estimator technique (Dorato et al., 1995; Spencer et al., 1998; Skelton, 1988). Substituting Eq. (2.14) into Eq. (2.15) yields the closed-loop form as

$$\dot{\hat{\boldsymbol{z}}} = (\boldsymbol{A} - \boldsymbol{B}\boldsymbol{G} - \boldsymbol{L}\boldsymbol{C}_m + \boldsymbol{L}\boldsymbol{D}_m \boldsymbol{G})\hat{\boldsymbol{z}} + \boldsymbol{L}\boldsymbol{y}_m \tag{2.16}$$

The frequency response of the ATMD system using the LQG control is not presented here because it is very similar to that shown in Figure 2.2 for the LQR method. The LQG control method also suppresses the vibrations effectively only when the external disturbance frequency is near the fundamental frequency of the system.

Both LQR and LQG control algorithms are sensitive to structural modeling and discretization errors and vibrations in the sensoring equipment (Prakah-Asante and Craig, 1994). They present optimum solutions in a narrow sense only because the external excitation term is ignored in their formulation and solution. In these algorithms, a pre-defined performance index is minimized where only the responses of the system and control effort are included. This limitation of classical optimal control algorithms is due to the fact that the input excitation must be known *a priori* which is not the case for earthquake or wind loads.

2.4 Filtered-x LMS Control Algorithm

2.4.1 Adaptive LMS Filter

The adaptive LMS filter algorithm was developed in the system identification field (Widrow and Stearns, 1985). Figure 2.4 shows an adaptive filter in the form of system identification. An external input signal, $x(n)$, is fed into both the unknown system and the filter, and the outputs of unknown system and filter, $d(n)$ and $y(n)$, are subtracted to find an error signal, $e(n)$.

$$e(n) = d(n) - y(n) \tag{2.17}$$

where n is an integer defining the nth discrete time step. The aim of the adaptive algorithm is to adapt the filter coefficients such that the error sequence is as close to zero as possible in a squared mean sense.

When the FIR filter is used, the output of a FIR filter is expressed in terms of input as

$$y(n) = \sum_{i=0}^{L-1} w_i(n)x(n-i) = \boldsymbol{w}(n)^{\mathrm{T}}\boldsymbol{x}(n) \tag{2.18}$$

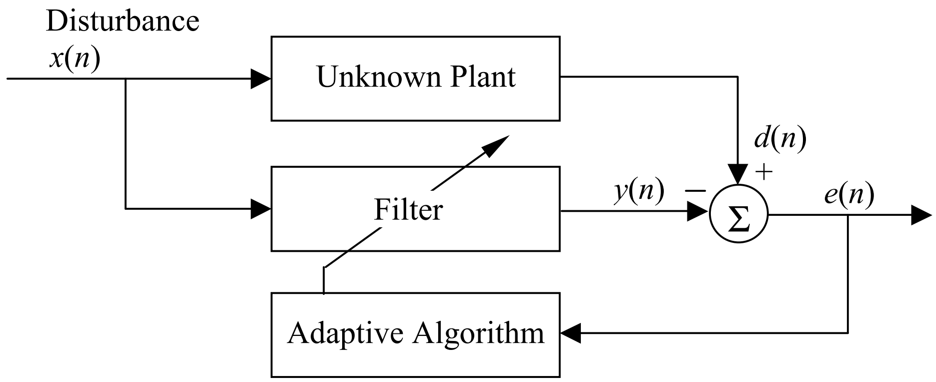

Figure 2.4: Adaptive filter adjusted to emulate the response of an unknown system

where L = order of filter; w_i = ith coefficient; $\boldsymbol{w}(n)$ = $[w_0(n)\ w_1(n)\ \ldots\ w_{L\text{-}1}(n)]^{\mathrm{T}}$ = coefficient vector; and $\boldsymbol{x}(n) = [x(n)\ x(n\text{-}1)\ \ldots\ x(n\text{-}L\text{+}1)]^{\mathrm{T}}$ = input signal vector.

In the adaptive LMS filter, the coefficients vector $\boldsymbol{w}(n)$ is adapted by using the LMS algorithm to minimize the error signal, $e(n)$. A cost function to be minimized is defined by

$$
\begin{aligned}
J(n) &= E\{e(n)\}^2 \\
&= E\{d(n) - \boldsymbol{w}^{\mathrm{T}}(n)\boldsymbol{x}(n)\}^2 \\
&= E\{d(n)^2\} - 2\boldsymbol{w}^{\mathrm{T}}(n)\boldsymbol{R}_{dx} + \boldsymbol{w}^{\mathrm{T}}(n)\boldsymbol{R}_{xx}\boldsymbol{w}(n) \qquad (2.19)
\end{aligned}
$$

where

$$\boldsymbol{R}_{dx} = E\{d(n)\boldsymbol{x}(n)\}$$

$$\boldsymbol{R}_{xx} = E\{\boldsymbol{x}(n)\boldsymbol{x}(n)^{\mathrm{T}}\} \tag{2.20}$$

The square matrix $\boldsymbol{R}_{xx}$ is the input correlation matrix, and the vector $\boldsymbol{R}_{dx}$ is the set of cross-correlation between the desired response and the input signals.

Widrow and Stearns (1985) proposed the simple and effective LMS algorithm to find the minimum mean-squared error as

$$w_i(n+1) = w_i(n) - \mu \frac{\partial J(n)}{\partial w_i(n)} \tag{2.21}$$

where μ = gain constant that regulates the speed and stability of the adaptive algorithm. Taking derivatives of $J(n)$ with respect to the elements of $\boldsymbol{w}(n)$ yields

$$\frac{\partial J(n)}{\partial w_i(n)} = 2E\left\{e(n)\frac{\partial e(n)}{\partial w_i(n)}\right\} \qquad i = 0,\ldots, L\text{-}1 \tag{2.22}$$

Using the instantaneous values to approximate expected values of the gradient, Eq. (2.22) can be simplified as

$$\frac{\partial J(n)}{\partial w_i(n)} = 2e(n)\frac{\partial e(n)}{\partial w_i(n)} \qquad i = 0,\ldots, L\text{-}1 \tag{2.23}$$

Combining Eqs. (2.17), (2.18) and (2.23) we obtain

$$\frac{\partial J(n)}{\partial w_i(n)} = -2e(n)x(n-i) \qquad i = 0,\ldots, L\text{-}1 \tag{2.24}$$

Substituting Eq. (2.24) into Eq. (2.21) we find

$$w_i(n+1) = w_i(n) + 2\mu e(n)x(n-i) \qquad i = 0,\ldots, L\text{-}1 \tag{2.25}$$

Or, in vector form

$$\boldsymbol{w}(n+1) = \boldsymbol{w}(n) + 2\mu e(n)\boldsymbol{x}(n) \tag{2.26}$$

The bound on μ for stability is derived as (Widrow and Stearns, 1985)

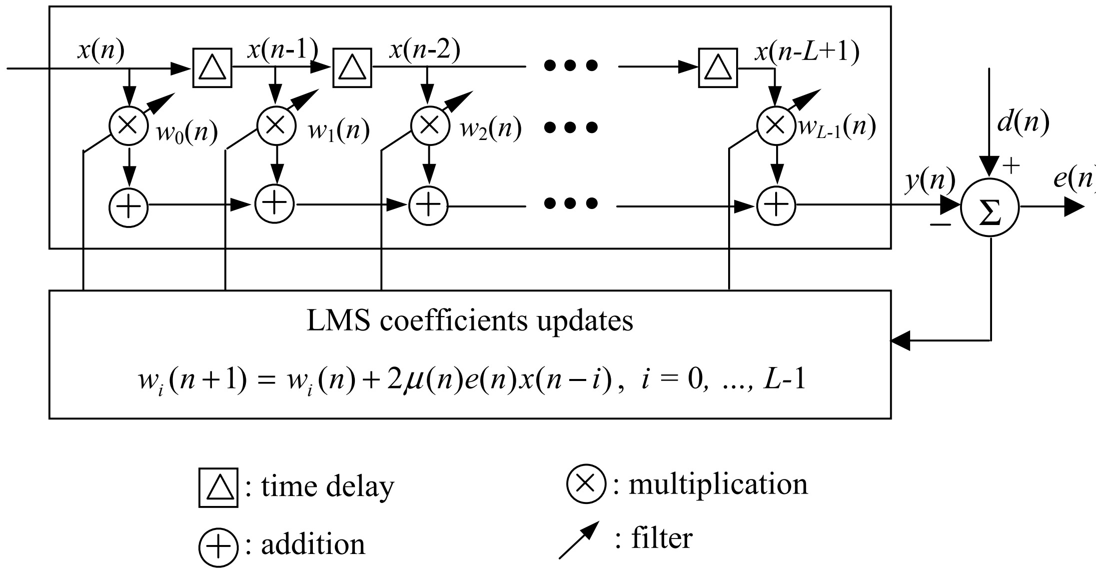

Figure 2.5: Adaptive FIR filter updated using the NLMS algorithm

$$0 < \mu < \frac{1}{\lambda_{\max}} \tag{2.27}$$

where $\lambda_{\max}$ is the largest eigenvalue of the input correlation matrix $\boldsymbol{R}_{xx}$. In this work, we use the Normalized-LMS (NLMS) algorithm where the constant μ is substituted by a time-varying function $\mu(n)$ defined as

$$\mu(n) = \frac{1}{a + \boldsymbol{x}(n)^{\mathrm{T}}\boldsymbol{x}(n)} \tag{2.28}$$

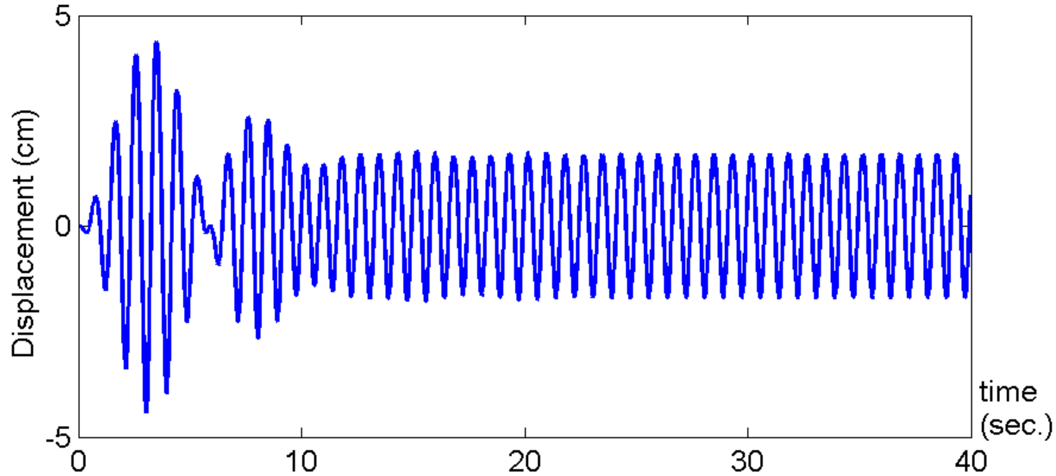

(a)

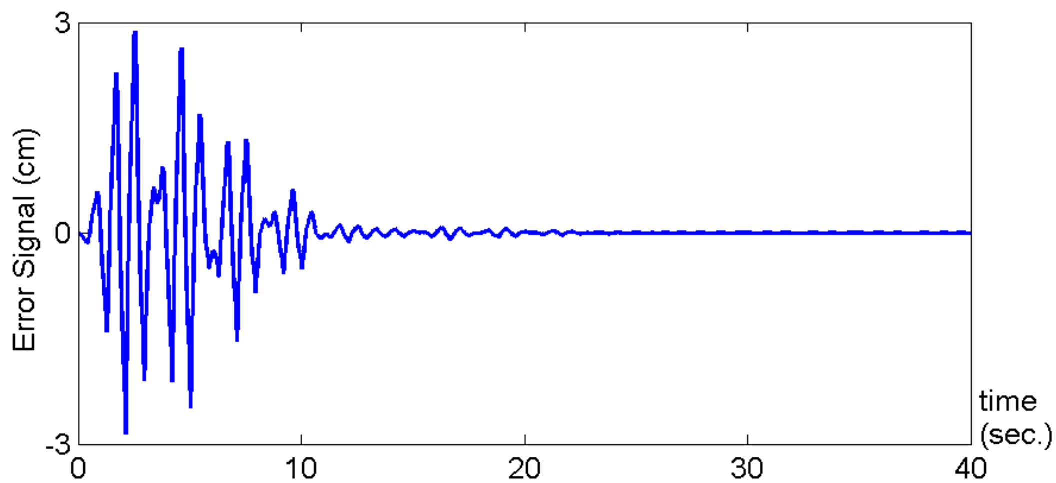

(b)

Figure 2.6: Simulation of system identification process for single harmonic disturbance on the ATMD system, (a) displacement, $d(n)$, (b) error signal, $e(n)$

where a = a small positive constant to overcome the potential numerical instability in the filter coefficients update. The advantage of using the NLMS algorithm over the constant LMS algorithm is that the adaptation is inherently stable (Tarrab and Feuer, 1988).

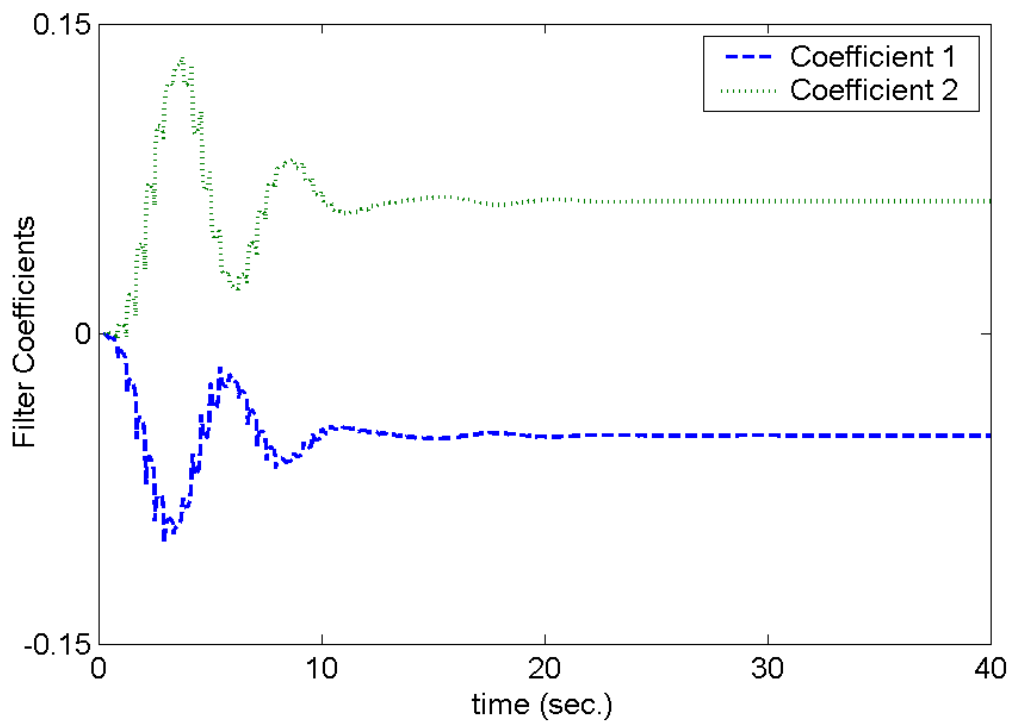

Figure 2.7: Adaptation of two filter coefficients during simulation

Figure 2.5 summarizes the above process by showing a FIR filter that is updated using the NLMS algorithm. Figure 2.6 shows the simulation of system identification process using a single-frequency infinite harmonic disturbance with sampling frequency of 50 Hz (time step of 0.02 seconds) for the ATMD system. Figure 2.6(a) shows the actual response of the ATMD system to the single-frequency harmonic motion. Figure 2.6(b) shows the error signal as defined by Eq. (2.17). It is observed that the error signal is reduced to zero after about 20 seconds (that means the system is fully identified after 20 seconds). Adaptation of two filter coefficients (w_i) over time is presented in Figure 2.7. Note that a second order filter with two filter coefficients is sufficient for identification of the ATMD system subjected to a single-frequency sinusoidal external disturbance.

2.4.2 Filtered-x LMS Control Algorithm

The direct form of the LMS algorithm cannot be used for active control of structures because the response of the system depends not only on the external disturbance but also on the control forces. In Figure 2.8 the entire plant is divided into two systems; the structural and control systems. The structural system represents the external disturbance-to-output relationship of the plant expressed with state-space matrices $\boldsymbol{A}$ and $\boldsymbol{E}$ and the control system represents the control force-to-output relationship of the plant expressed with state-space matrices $\boldsymbol{A}$ and $\boldsymbol{B}$ in Eq. (2.2). In practice, the control force-to-output relationship is estimated by a FIR or infiniteimpulse-response (IIR) filter coefficients, and these filter coefficients are obtained in the offline LMS implementation. In the following paragraphs, for the derivation of the filtered-x LMS control algorithm, this relationship denoted by discrete filter coefficients $h_c(n)$ in Figure 2.8 is estimated by a FIR filter of order K.

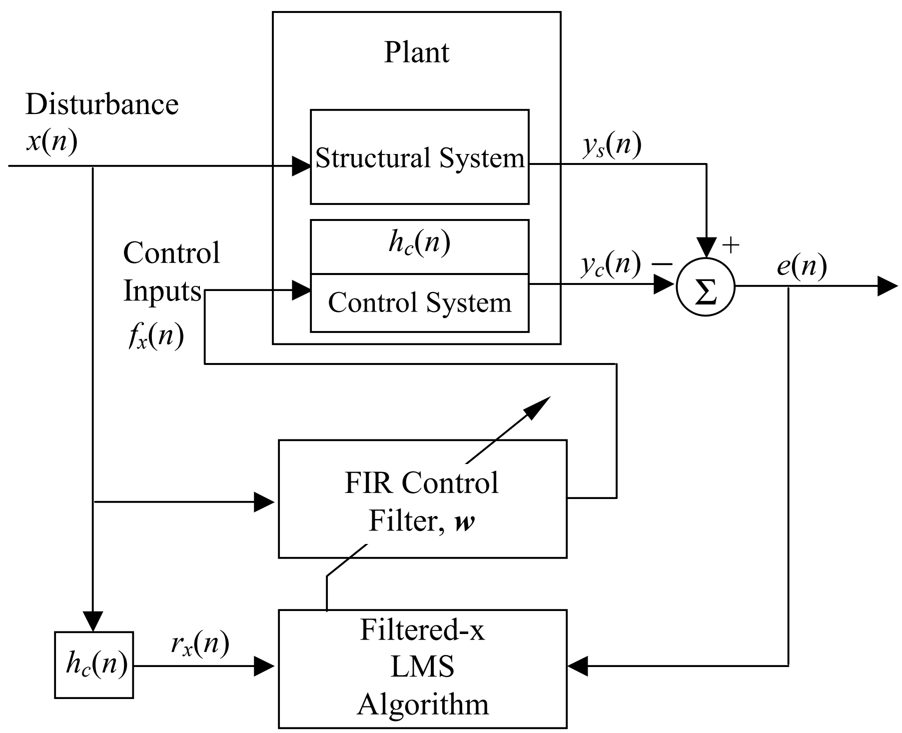

Figure 2.8: Adaptive filter being updated using the Filtered-x LMS algorithm

The output of the control filter $f_x(n)$ (the input to the control system) is expressed in terms of the FIR filter coefficients $w_i(n)$ and the external disturbance input signal $x(n\text{-}i)$ as

$$f_x(n) = \sum_{i=0}^{L-1} w_i(n)x(n-i) \tag{2.29}$$

The output of the control system due to control input only is obtained as follows (Widrow and Stearns, 1985):

$$\begin{aligned} y_c(n) &= \sum_{j=0}^{K-1} h_c(j) f_x(n-j) \\ &= \sum_{j=0}^{K-1} h_c(j) \sum_{i=0}^{L-1} w_i(n)x(n-i-j) \end{aligned} \tag{2.30}$$

Then, the output error, the net output of the system $e(n)$, is taken as the difference between the output of the structural system $y_s(n)$ and that of the control plant $y_c(n)$:

$$e(n) = y_s(n) - \sum_{j=0}^{K-1} h_c(j) \sum_{i=0}^{L-1} w_i(n)x(n-i-j) \tag{2.31}$$

Since the order of convolution can be interchanged without affecting the summation result, we can rewrite Eq. (2.31) as

$$e(n) = y_s(n) - \sum_{i=0}^{L-1} w_i(n) \sum_{j=0}^{K-1} h_c(j)x(n-i-j) \tag{2.32}$$

which can be further simplified as

$$e(n) = y_s(n) - \sum_{i=0}^{L-1} w_i(n) r_x(n-i) \tag{2.33}$$

where

$$r_x(n-i) = \sum_{j=0}^{K-1} h_c(j)x(n-i-j) \tag{2.34}$$

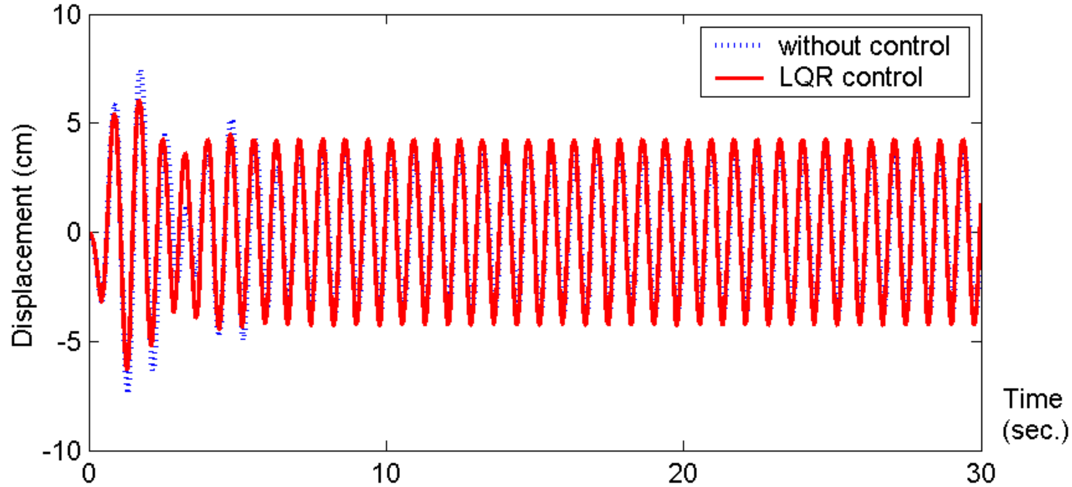

(a) LQR Control

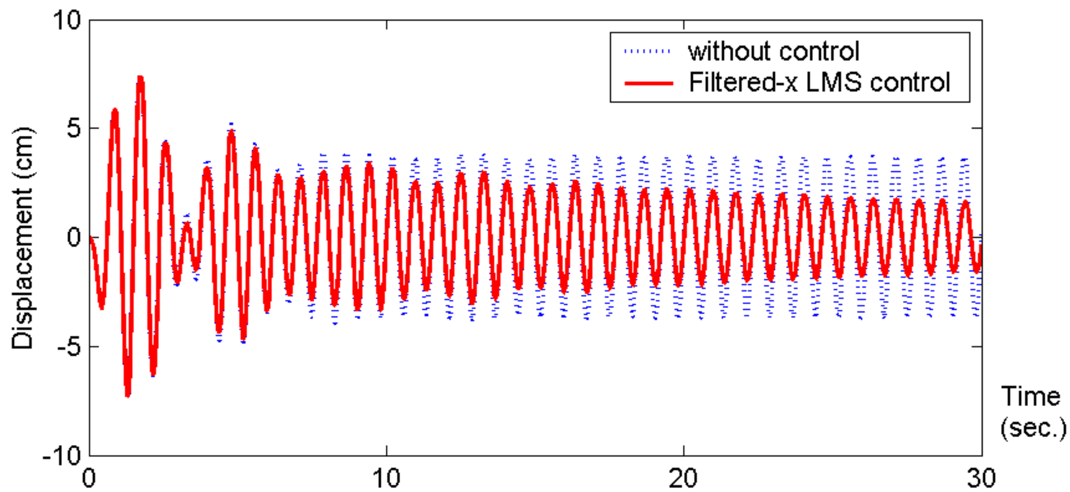

(b) Filtered-x LMS Control

Figure 2.9: Filtered-x LMS control of the ATMD system, $\omega = 1.2\ \omega_n$

This procedure to produce the resultant output r_x by rearranging convolution is dubbed the filtered-x operation (Widrow and Stearns, 1985). The term "filtered-x" refers to the input signal x.

The gradient of the cost function $J(n)$ defined by Eq. (2.19) then becomes

$$\frac{\partial J(n)}{\partial w_i(n)} = -2r_x(n-i)e(n) \qquad i = 0,\ldots, L\text{-}1 \tag{2.35}$$

The filter coefficients of the control system are updated and adapted according to Eq. (2.21) yielding

$$w_i(n+1) = w_i(n) + 2\mu(n)r_x(n-i)e(n) \qquad i = 0,\ldots, L\text{-}1 \tag{2.36}$$

The control forces are adapted at each sampling time using Eq. (2.34) with the updated filter coefficients obtained from Eq. (2.36) until the output error is minimized. In other words, the filtered-x LMS algorithm finds an optimal value of the cost function in real time by adapting its values of coefficients, while cost function (performance index) of the LQR/LQG control algorithm is optimized offline.

Figure 2.9 presents the results of filtered-x LMS control for the same ATMD system used earlier. The frequency of the external disturbance is set to 1.2 times the fundamental frequency of the system (ω = 1.2ω_n) where both LQR and LQG control algorithms are limited in suppressing the vibration, as discussed in a previous section. Figure 2.9(a) is the same as the Figure 2.3(b) and is presented here again for better comparison. At the beginning as seen in Figure 2.9(b), the filtered-x LMS control algorithm shows little vibration suppression compared to LQR control algorithm, but more and more vibration suppression is made as time goes on. This is due to the fact that the filtered-x LMS control algorithm requires time of filter adaptation for control. Consequently, it can be concluded that this filtered-x LMS algorithm is not as effective for short transient vibrations such as peaks since it requires adaptation time, but is effective in suppressing the system vibration outside the resonance frequency.

2.5 Hybrid Feedback-LMS Control Algorithm

A hybrid feedback-LMS control algorithm is introduced in this section combining the feedback and filtered-x LMS control algorithms. The feedback control methods are susceptible to modeling errors, which affect their stability as described earlier. Though the filtered-x LMS control scheme minimizes vibrations over the entire frequency range and thus is less susceptible to modeling errors and inherently more stable, it is not as effective for short transient vibrations such as peaks since it requires adaptation time.

The hybrid feedback-LMS control algorithm introduced in this chapter is intended to minimize vibrations for both steady state and transient vibrations by combining the feedback control together with a robust adaptive filtered-x LMS algorithm. The resulting new algorithm is robust because it takes into account different external disturbances and a large frequency range. The hybrid control algorithm, shown in Figure 2.10, can be a combination of LQR or LQG and the filtered-x LMS algorithms. In this algorithm, the external disturbance signal, $x(n)$, is simultaneously fed into the structural system and filtered-x LMS adaptive controller. The control force, $f_x(n)$, obtained through the filtered-x LMS adaptive controller is added to the feedback control force, $f_b(n)$, to yield the total control force, $f_c(n)$, and applied to the structural system to be controlled. The response of structure, $y(n)$, is then fed back into both feedback controller to obtain the feedback control force, $f_b(n)$, and filtered-x LMS adaptive controller to update FIR filters and obtain the control force, $f_x(n)$.

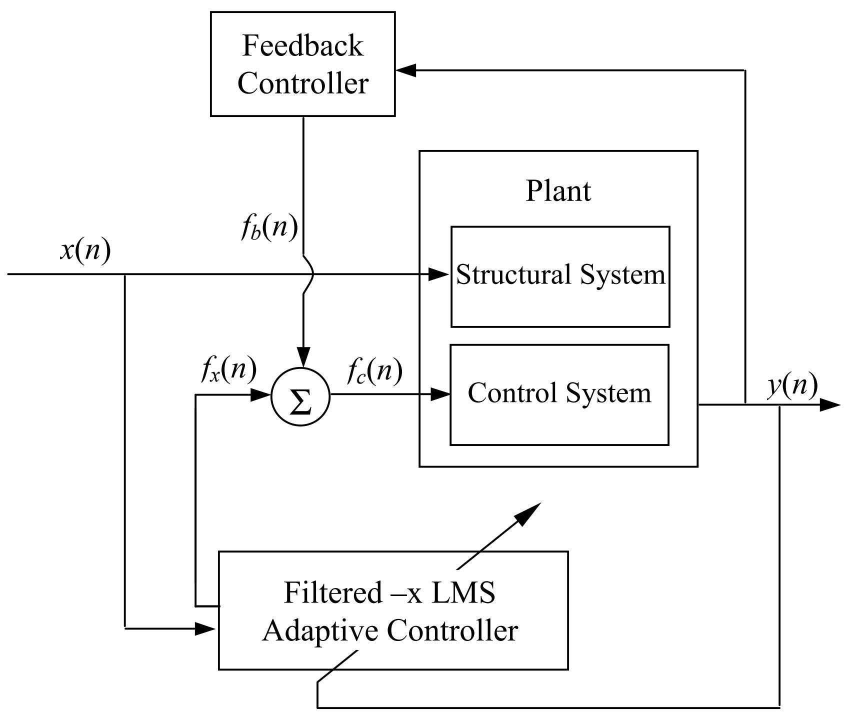

Figure 2.10: Hybrid feedback-LMS control

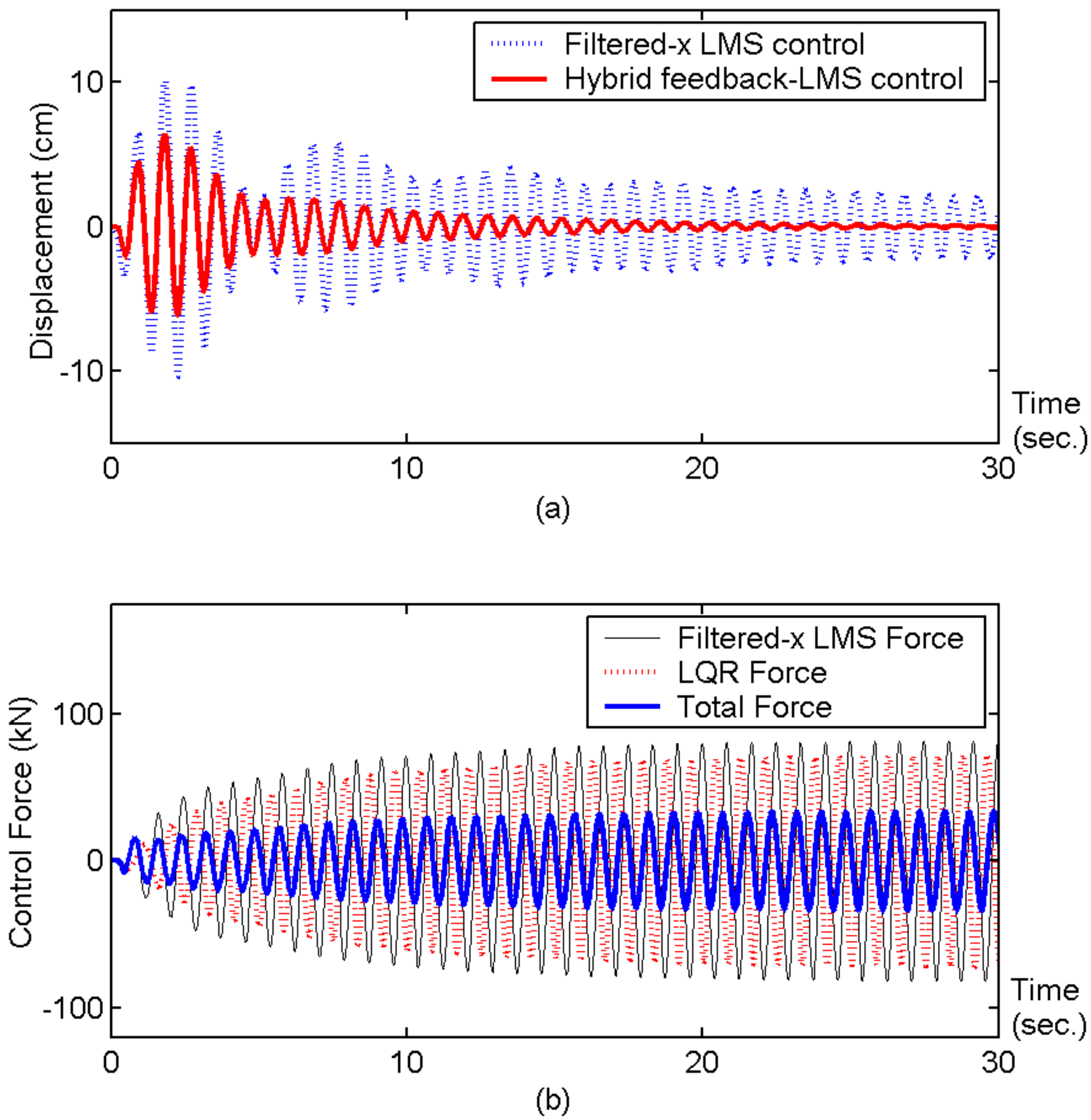

Figure 2.11: Hybrid feedback-LMS control of the ATMD system, $\omega = 1.2\ \omega_n$

Shown in Figure 2.11(a) is the response of the ATMD system subjected to an external disturbance with a frequency equal to 1.2 times the fundamental frequency of the system using the hybrid feedback-LMS control algorithm. The FIR filter of order 10 is used in the control model. In this example, a full-state feedback LQR controller is combined with a filtered-x LMS algorithm where the displacement of the main structure is used as the error signal in Eq. (2.31). The algorithm can be easily modified for velocity- or acceleration-feedback control for more realistic applications. This is demonstrated in the next section where a few selected acceleration responses are used as feedback states for LQG controller as well as error signals to the filtered-x LMS adaptive controller.

The dotted line in Figure 2.11(a) is the results for the filtered-x LMS control algorithm (the same as the solid line in Figure 2.9(b)) and the solid line is the results for the hybrid algorithm. It is observed that the hybrid feedback-LMS control algorithm achieves faster vibration suppression than the filtered-x LMS algorithm. Moreover, responses in earlier stage are similar to those shown in Figure 2.9(a), that is, transient vibrations are controlled by LQR controller and thus more vibration suppressions than the filtered-x LMS algorithm are made. The same conclusion is made from Table 2.2 where response results of the ATMD system for different control algorithms are summarized with reduction ratios presented in parentheses when the disturbance frequency is 1.2 times the fundamental frequency of the ATMD system. While the LQR and filtered-x LMS algorithms can effectively reduce either maximum displacement or RMS displacement, respectively, the hybrid feedback-LMS control algorithm can achieve significant reductions in both maximum and RMS displacements.

The control force for the hybrid feedback-LMS control is presented in Figure 2.11(b). The total control force, $f_c(n)$, is sum of the filtered-x LMS force, $f_x(n)$, plus LQR force, $f_b(n)$. We can see that the envelop of the total control force increases until the displacement of the ATMD system approaches zero, that is, until the filter coefficients updates are stabilized.

Control algorithm	Maximum displacement (cm)	RMS displacement (cm)
No control	10.68	4.46
LQR	8.02 (24.9%)	4.46 (-0.68 %)
Filtered-x LMS	10.4 (2.53 %)	3.04 (31.4%)
Hybrid feedback-LMS	6.36 (40.5%)	1.38 (69.0%)

Table 2.2: Responses of the ATMD system using $\omega = 1.2\ \omega_n$

2.6 Concluding Remarks

Figures 2.12(a) to 2.12(d) show the responses of the ATMD system subjected to an external disturbance with a frequency equal to 1.5 times the fundamental frequency of the system without control, and with LQR, filtered-x LMS, and the new hybrid control algorithms, respectively. These figures show while the LQR control algorithm results in a slight increase of the steady state response, the new control algorithm results in consistent vibration suppression in both transient and steady state responses. This is due to the fact that the external disturbance is a sinusoidal signal with only one frequency component and therefore updating of filter coefficients is not affected by the frequency of the external disturbance by any significant measure

Figure 2.13 shows a comparison of different orders of FIR filters for the ATMD system identification subjected to white noise. White noise has an infinite number of frequencies thus requiring an infinite number of filter coefficients for the *exact* identification. For FIR filters with a smaller number of filter coefficients, larger ripples (errors) are created when the frequency differs more from the natural frequency of the ATMD system.

When the new hybrid feedback-LMS control algorithm is used to control realistic structures against actual destructive environmental forces such as earthquake loads, the adaptation of filter coefficients takes much longer and the required number of filter coefficients becomes large. This is due to the fact that the environmental loads are

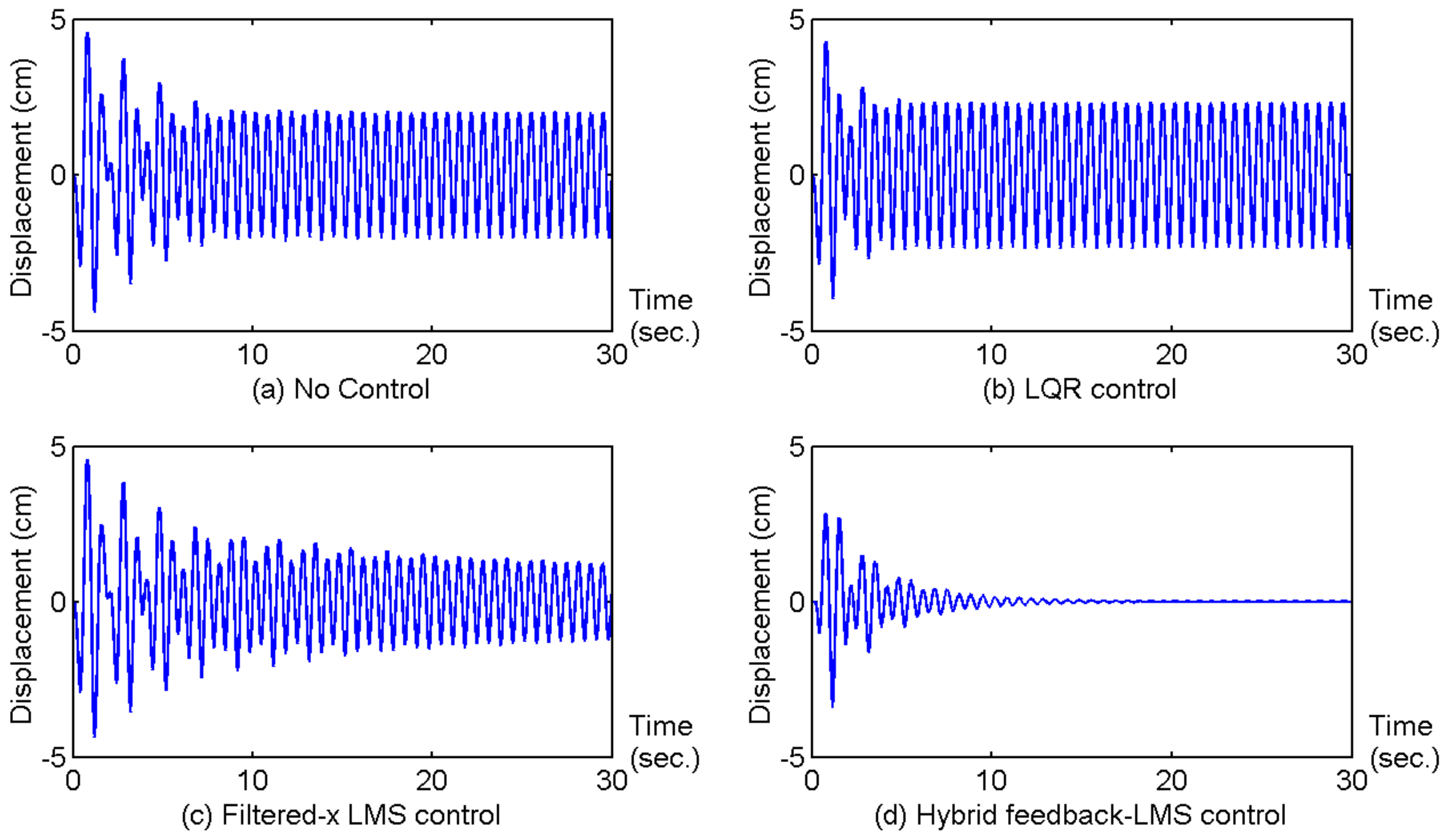

Figure 2.12: Responses of the ATMD system subjected to an external disturbance with a frequency equal to 1.5 times the fundamental frequency of the system

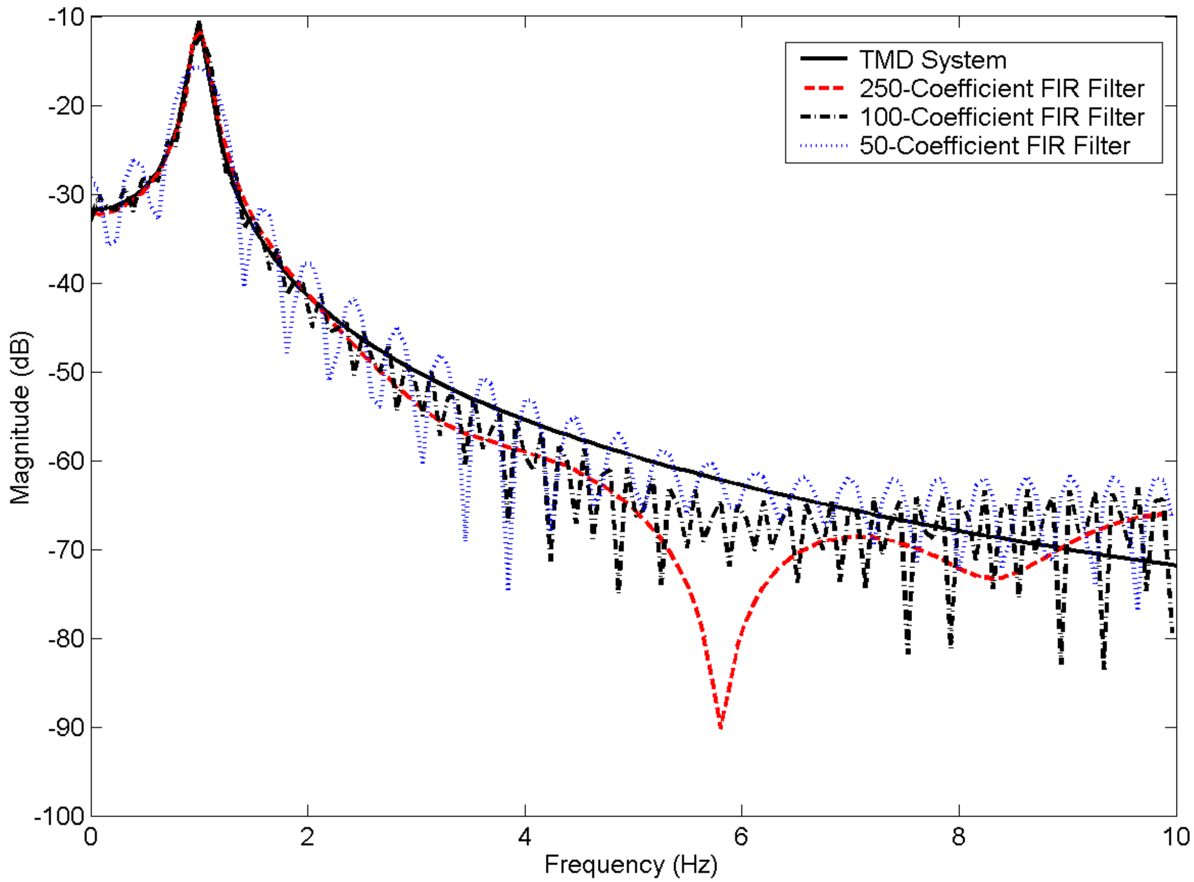

Figure 2.13: Comparison of different coefficient FIR filters for system identification

wideband signals. Moreover, the accurate estimation of the properties of actual structures with FIR filter involves a large number of filter coefficients.

As observed in Figure 2.13 even for a simple system, a large number of filter coefficients is required to achieve a close approximation to the actual frequency response of the system, requiring a significant amount of computational time. Also, note in Figure 2.13 that FIR filters with larger numbers of filter coefficients show poorer approximations in the higher range of frequencies. In a next chapter, the applicability of the hybrid feedback-LMS algorithm presented in this chapter is extended for control of structures subjected to realistic environmental forces through integration with a discrete wavelet low-pass filter.

CHAPTER 3

WAVELET-HYBRID FEEDBACK LMS ALGORITHM FOR ROBUST CONTROL OF STRUCTURES

3. 1 Introduction

An advantage of the adaptive filtered-x LMS control algorithm is that the external excitation is included in the formulation. Further, it can successfully suppress vibrations due to an external disturbance whose frequency differs from the natural frequencies of the structure as demonstrated in Chapter 2. Though the filtered-x LMS control scheme minimizes vibrations over the entire frequency range and thus is less susceptible to modeling errors and inherently more stable, it is not as effective for short transient vibrations such as peaks because it requires adaptation time.

The hybrid feedback-LMS control algorithm, introduced in Chapter 2, is intended to minimize both steady state and transient vibrations by combining the feedback control with a robust adaptive filtered-x LMS algorithm. It is shown that the hybrid feedback-LMS control algorithm achieves faster vibration suppression than the filtered-x LMS algorithm. Further, the algorithm is robust because it takes into account different external disturbances and a large frequency range.

The hybrid feedback-LMS control algorithm, however, cannot be applied directly for control of realistic structures against actual destructive environmental forces such as wind, ocean wave, and earthquake loads. The frequency bandwidths of those environmental forces are much wider than the frequency bandwidth of common structural systems. Moreover, as noted in Chapter 2, in the FIR filter used in the filtered-x LMS algorithm, a large number of filter coefficients are required to achieve a close approximation to the actual frequency response of the system, requiring a significant amount of computational time and making the real time control impractical. Also, FIR filters with larger numbers of filter coefficients show poorer approximations in the higher range of frequencies.

In this Chapter, it is shown that this shortcoming is overcome by integrating a low-pass filter with the filtered-x LMS adaptive controller. A low-pass filter passes all lower frequency signal components with frequencies from zero to the filter cutoff frequency unchanged. Higher frequency components above that cutoff frequency are eliminated, reducing the signal disturbance. Keeping signal components only within certain frequency limit helps the hybrid feedback-LMS control algorithm adapt its coefficients in a more stable fashion by eliminating higher frequency components that obstruct the stabilization of coefficients. This can be effective because the response of most civil structures is not affected by high frequency contents of the external excitations by any significant measure (the exception can be very rigid structures)

Low-pass filtering of signals commonly is made in the Fourier domain. Wang and Wu (1995) use a fourth-order Butterworth dual channel low-pass filter for structural system identification using the LMS method. This filter is often used for low frequency digital signal processing applications, where the sampling frequency (inverse of the discrete time step size) is much higher than the data bandwidth. Though low-pass filters in the Fourier domain are suitable for the system identification where real time implementation is not an issue, they are not appropriate for real time control of structures because of their inordinate computational requirements.

In this Chapter, a wavelet based low-pass filtering is proposed. Considering the fact that the orthogonal wavelet filtering requires only integer operations, real time control of large structures can be achieved with little additional computational efforts due to filtering.

3.2 Wavelet Transform As An Effective Filter For Control Problems

The wavelet transform is a relatively recent mathematical transformation method (Daubechies, 1992; Adeli and Samant, 2000; Adeli and Karim, 2000; Samant and Adeli, 2000 and 2001; Karim and Adeli, 2002a and b; Wu and Adeli 2001). The original signal is transformed into a different domain where a more comprehensive analysis and processing becomes possible. Similar to conventional transform methods such as the Fourier transform, the wavelet transform represents the original signal as a linear combination of basis functions. But, instead of breaking down a signal into a series of basis functions over an infinite range, the original signal is broken down into a series of basis functions that are localized in both time and frequency. Due to locality in both time and frequency domains of its basis function, the wavelet transform provides an effective way of processing signals characterized by time-varying nonstationary frequency contents (Newland, 1993).

If $\psi(t)$ is the basis wavelet function, called a mother wavelet, the members of family are defined as (Rao and Bopardikar, 1998)

$$\psi_{a,b}(t) = \frac{1}{a}\psi\left(\frac{t-b}{a}\right) \tag{3.1}$$

where a and b are real numbers and indicate the scaling and translation of the mother wavelet, respectively. The scaling parameter, a, represents the frequency content of the wavelet. The translation parameter, b, represents the location of wavelet in time. Thus, in contrast to the Fourier transform, the basis function of the wavelet transform retains the time locality as well as frequency locality.

In general, the family of wavelets defined by Eq. (3.1) need not be orthogonal. But, orthogonal wavelets require a substantially fewer number of operations compared with non-orthogonal wavelets, and therefore are used in this study. The wavelet set $\{\psi_{a,b}\}$ forms an orthogonal system if (Daubechies, 1992; Meyer, 1993)

$$\left\langle \psi_{a,b}, \psi_{a,c} \right\rangle = \int \psi_{a,b}(t)\psi_{a,c}(t)dt = 0 \qquad b \neq c \tag{3.2}$$

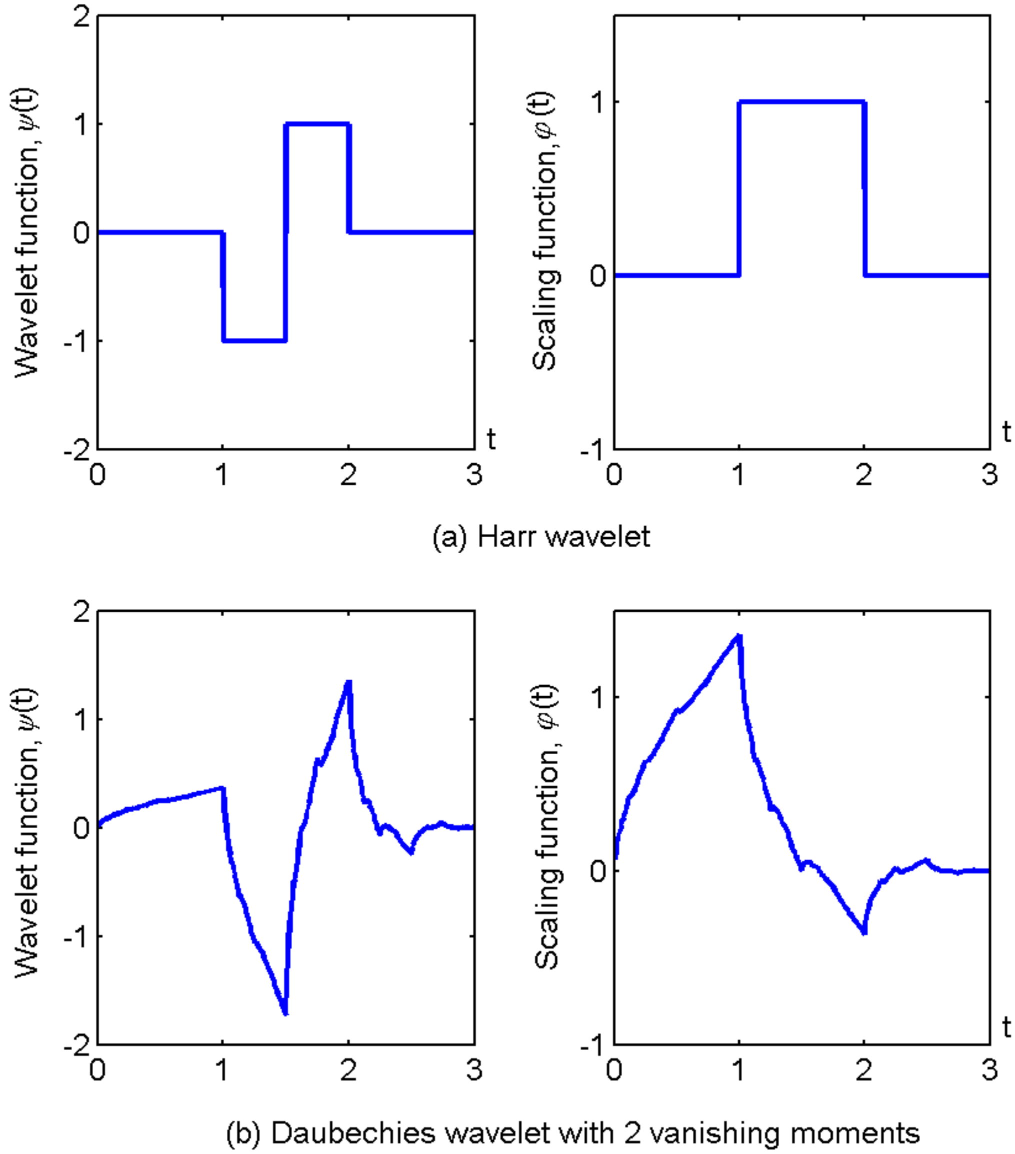

Figure 3.1: Wavelet and scaling functions for Harr wavelet and Daubechies wavelet with 2 vanishing moments

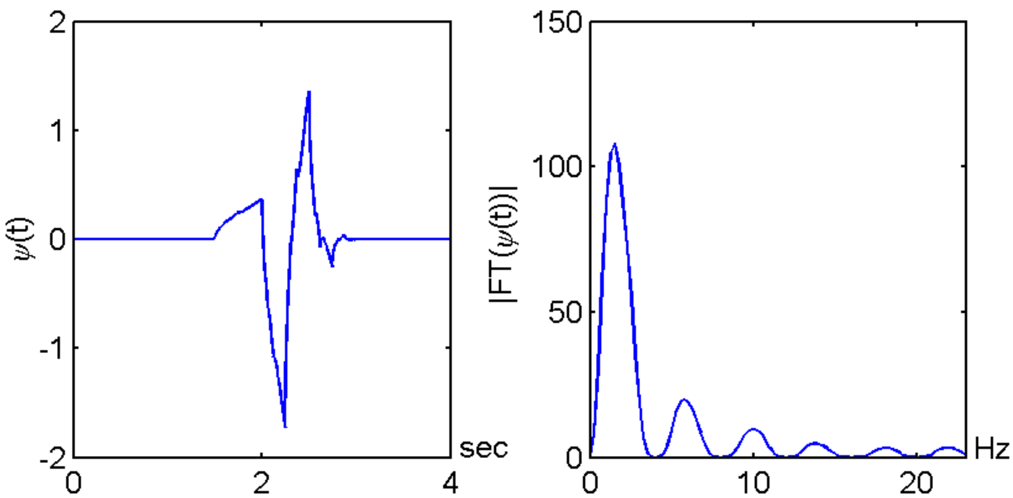

(a) Daubechies wavelet with 2 vanishing moments

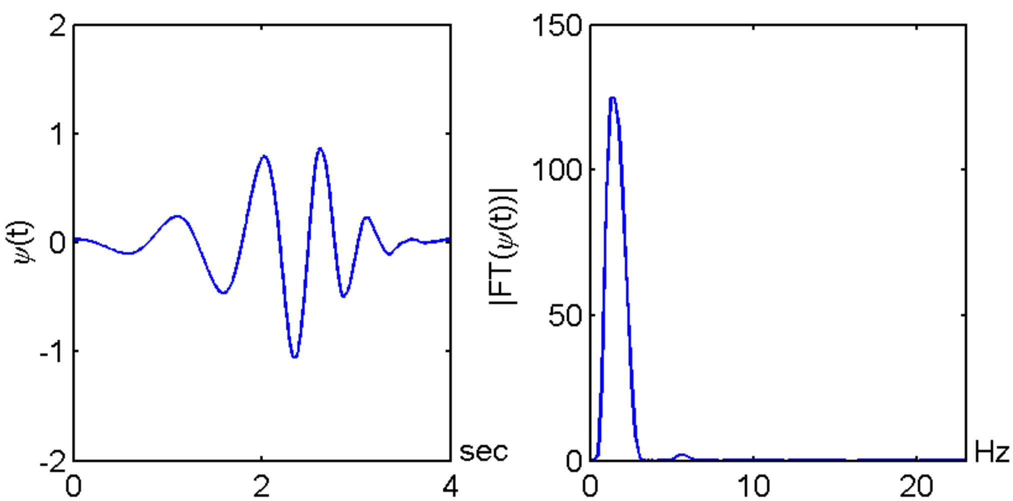

(b) Daubechies wavelet with 9 vanishing moments

Figure 3.2: Daubechies wavelet functions and their Fourier transforms (denoted by FT): (a) with 2 vanishing moments, (b) with 9 vanishing moments

where $\langle \cdot,\cdot \rangle$ represents the inner product. Denoting the number of data to be transformed by N, the wavelet transform using orthogonal wavelets requires only $O(N)$ operations in contrast to $O(N\log N)$ operations needed for the Fast Fourier Transform resulting in much faster transformation (Newland, 1993).

Figure 3.1 shows two examples of orthogonal wavelets; (a) Harr wavelet and (b) Daubechies wavelet with 2 vanishing moments. A wavelet with i-vanishing moments means that "*there exists a certain function θ such that the wavelet can be written as the i^{th} order derivative of θ*" (Mallat, 1989). In this sense, Harr wavelet can be regarded as Daubechies wavelet with 1 vanishing moment.

Figure 3.2 shows Daubechies wavelet functions with 2 and 9 vanishing moments along with their Fourier transforms (FT) which show their frequency contents. The larger the vanishing moments, the more computation is required since there are more coefficients involved. This figure demonstrates clearly that a Daubechies wavelet function with larger vanishing moments provides better frequency locality, whereas a Daubechies wavelet function with smaller vanishing moments shows better time locality. Also, comparing Figures 3.1 and 3.2, it is seen that a wavelet function with larger vanishing moments is smoother than another one with smaller vanishing moments.

If the input is defined in discrete domain and the dyadic dilation is applied, Eq. (3.1) can be expressed as

$$\psi_{j,k}(n) = 2^{-j/2}\psi\left(2^{-j}t - n\right) \tag{3.3}$$

where j, $k \in Z$ and Z indicates the set of integers. In addition to the wavelet function, the family members of the basic scaling function are defined by scaling and translation as

$$\varphi_{j,k}(n) = 2^{-j/2}\varphi\left(2^{-j}n - k\right) \tag{3.4}$$

The relationship between the wavelet function $\psi(n)$ and the scaling functions $\varphi(n)$ are defined such that the set of functions $\psi_{j,k}(n)$ span the difference W_j (wavelet function space) between the scaling function spaces, V_j, while the scaling function spaces are spanned by the various scales of the scaling function as follows:

$$V_j = \underset{k}{\mathrm{Span}}\{\varphi_{j,k}(n)\} \tag{3.5}$$

$$W_j = V_{j+1} \ominus \mathrm{V_j} \tag{3.6}$$

where $\ominus$ represents a direct subtraction.

The wavelet and scaling functions, $\psi(n)$ and $\varphi(n)$, constitute the key elements of the multiresolution analysis (MRA) (Mallat, 1989) which can be employed for filtering purposes. The MRA is formulated with a nesting of the spanned spaces as

$$\cdots \subset V_{-2} \subset V_{-1} \subset V_0 \subset V_1 \subset V_2 \subset \cdots \subset L^2(R) \tag{3.7}$$

where $V_{-\infty} = \{0\}$ (null space) and $V_{\infty} = L^2(R)$ is the space of all square integrable functions. W_j's, $j = -\infty, \ldots, \infty$, are orthogonal to each other because of their definition (Eq. 3.6) and relationships among V_j's, $j = -\infty, \ldots, \infty$ (Eq. 3.7). Based on definition of V_j, we can write the following natural scaling condition for any function $f(n)$:

$$f(n) \in V_j \qquad \leftrightarrow \qquad f(2n) \in V_{j+1} \tag{3.8}$$

If Eqs. (3.5)-(3.8) hold, then there exists a set of functions $\psi_{j,k}$ such that $\psi_{j,k}$ $(k \in Z)$ spans W_j which is the orthogonal complement of the spaces V_j and V_{j+1}. More specifically, if $\{\varphi_{0,k}\}$ spans V_0 then $\{\psi_{0,k}\}$ spans W_0 such that

$$V_1 = V_0 \oplus W_0 \tag{3.9}$$

and

$$L^2(R) = \cdots \oplus W_{-2} \oplus W_{-1} \oplus W_0 \oplus W_1 \oplus W_2 \oplus \cdots \tag{3.10}$$

where ⊕ represents a direct sum. This means that by starting with a representation of a function belonging to a coarse subspace, higher detail or resolution can be obtained by adding spaces spanned by $\psi_{j,k}$ at a higher resolution (i.e. given by the next higher value of j).

A discrete input signal, $x(n)$, can be represented as a combination of wavelet and scaling functions as follows:

$$x(n) = \sum_k c_{j_0,k}\varphi_{j_0,k}(n) + \sum_k \sum_{j=j_0} d_{j,k}\psi_{j,k}(n) \tag{3.11}$$

where the first term is a coarse resolution at scale j_0 and the second term adds details of increasing resolutions. Equation (3.11) can also be viewed as the time-frequency decomposition of $x(n)$ where the second term provides the frequency and time breakdowns of the signal.

From the nesting of the spaces spanned by scaling functions represented by Eq. (3.7) and the relationship between the spaces spanned by wavelet functions and those spanned by scaling functions expressed by Eqs. (3.6) and (3.9), we can write (Mallat, 1989)

$$\varphi(t) = \sum_k h_0[k]\varphi(2t-k) \qquad k \in Z \tag{3.12}$$

$$\psi(t) = \sum_k h_1[k]\varphi(2t-k) \qquad k \in Z \tag{3.13}$$

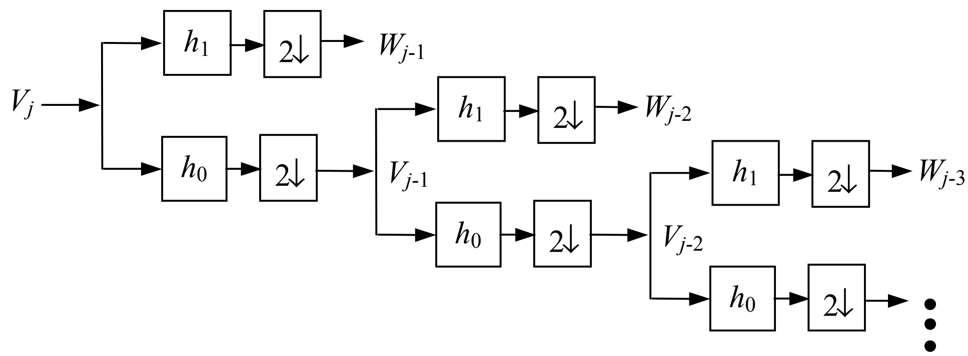

Figure 3.3: A two-band multi-level filter tree

where h_0 and h_1 are filter coefficients. The filter coefficients are obtained by solving Eqs. (3.12) and (3.13). Unique and exact solutions for Eqs. (3.12) and (3.13) exist only when k is equal to 2, 4, and 6 corresponding to the Daubechies wavelet with 1 vanishing moment (or Haar wavelet), 2 vanishing moments (Figure 3.1(b)), and 3 vanishing moments, respectively. For example, the Daubechies wavelet with 2 vanishing moments has the following h_0 coefficients: $(1+\sqrt{3})/4$, $(3+\sqrt{3})/4$, $(3-\sqrt{3})/4$, $(1-\sqrt{3})/4$. The h_1 coefficients can be found by the following equation (Burrus et al., 1998):

$$h_1[n] = (-1)^n h_0[3-n] \tag{3.14}$$

when k is greater than 6, no unique solution exists, and thereby the filter coefficients are obtained numerically by adjusting the coefficients iteratively until the resulting wavelet has desirable decomposition and resolution properties. Illustrative examples on the iterative numerical solution for Eqs. (3.12) and (3.13) can be found in Newland (1993).

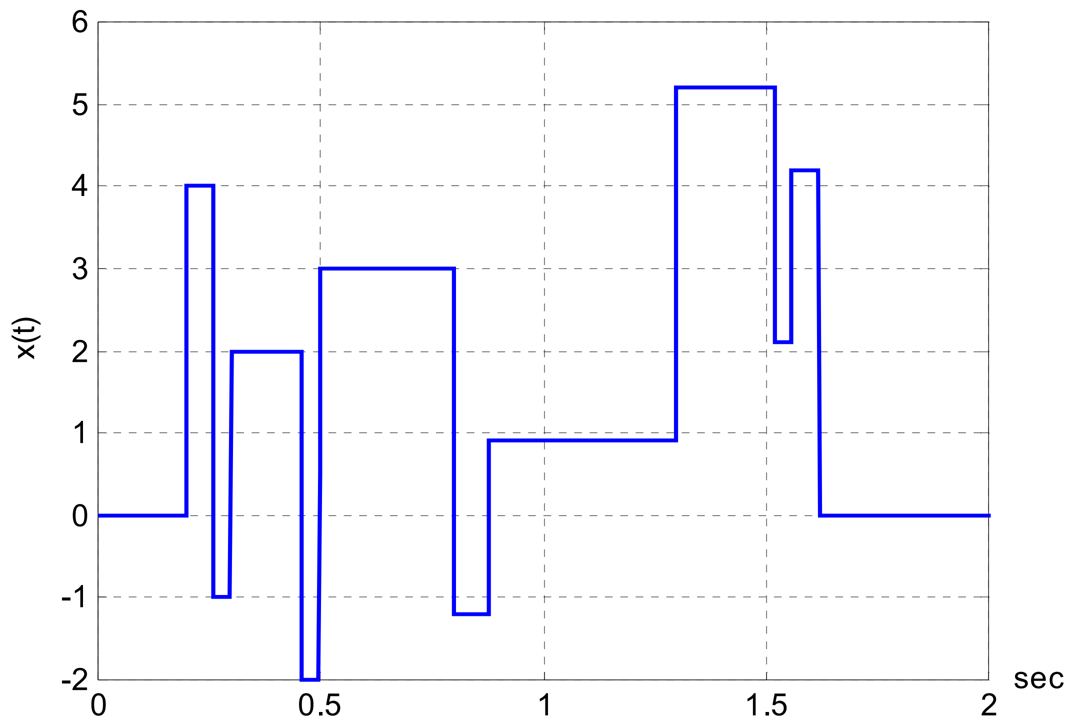

Figure 3.4: An example block signal generated using Matlab

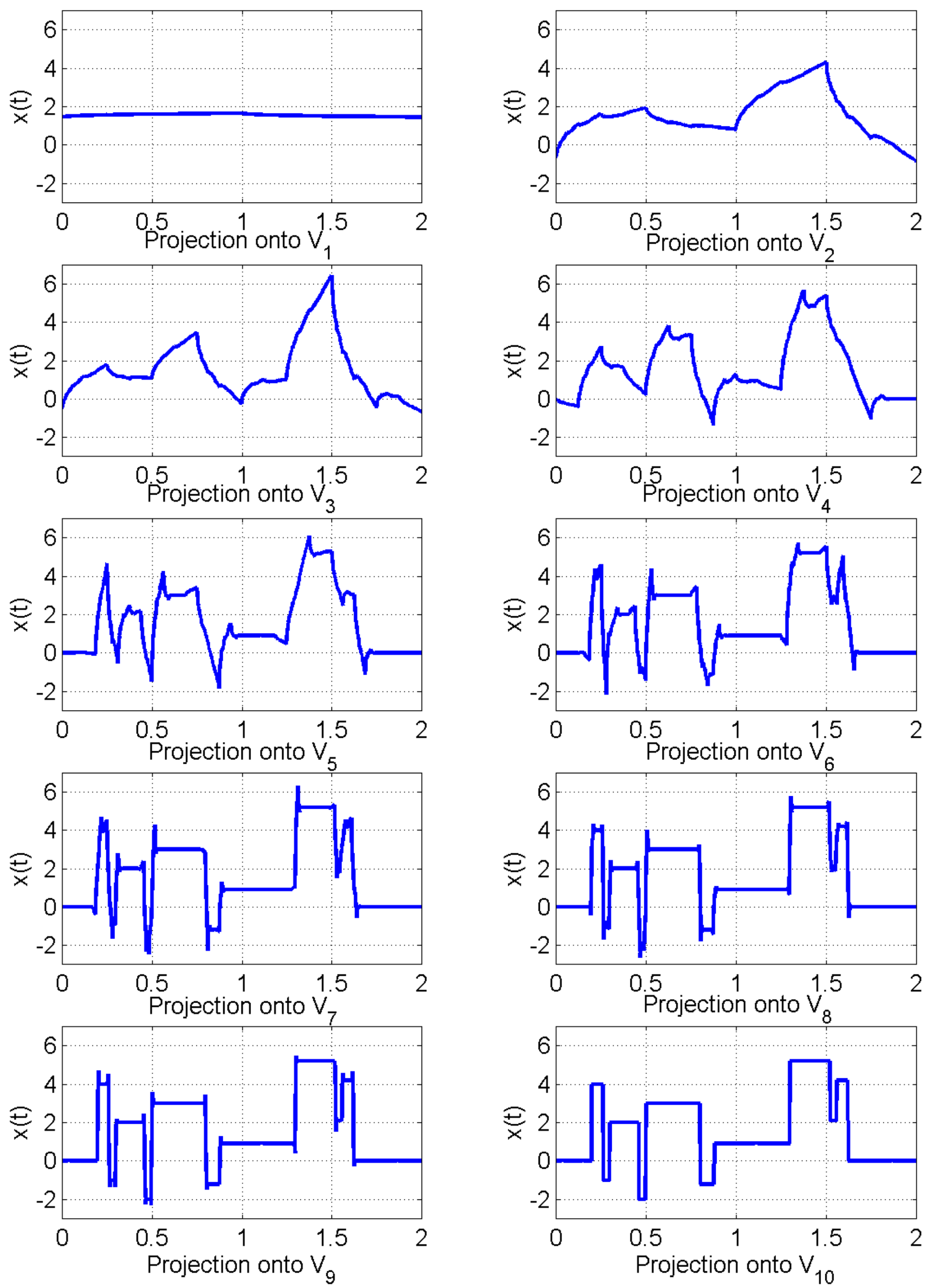

Figure 3.5: Projection of the block signal shown in Figure 3.4 onto V spaces using Daubechies scaling function with 2 vanishing moments

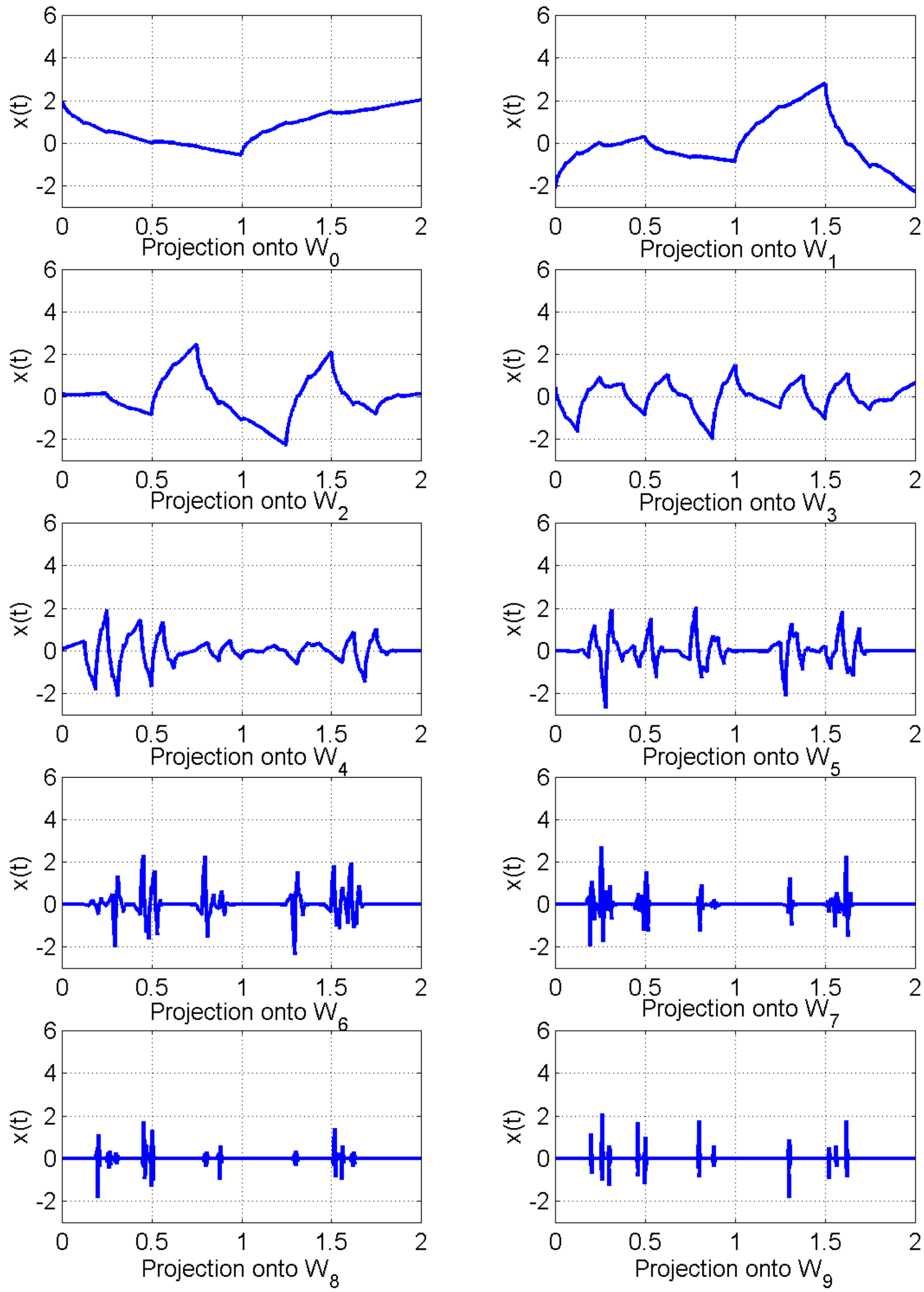

Figure 3.6: Projection of the block signal shown in Figure 3.4 onto W spaces using Daubechies wavelet function with 2 vanishing moments

For a given set of h_0 and h_1 coefficients, the wavelet decomposition can be performed by a two-band filter bank using the time-reversed filters $h_0[-n]$ (low-pass filter) and $h_1[-n]$ (high-pass filter) followed by down-sampling by a factor of 2. The down-sampling by a factor of 2 takes a signal $x(n)$ as input and produces output of $x(2n)$. In practice, this down-sampling is achieved by taking every other term of an input signal. A two-band multi-level filter bank (or filter tree) is shown in Figure 3.3.

Figures 3.5 and 3.6 show an example of multiresolution analysis for an example block signal generated using Matlab (2000) and presented in Figure 3.4. Figure 3.5 shows the approximations of the block signal in various scaling function spaces V_j using Daubechies scaling function with 2 vanishing moments. This figure illustrates how the approximations progress: higher and more accurate resolutions are achieved at spaces with higher scaling functions. The projection of the original block signal onto the highest scaling function space, V_{10}, yields the original signal itself exactly. Figure 3.6 illustrates the individual wavelet decomposition by showing the components of the signal that exist in the wavelet function spaces W_j at different scales j. The relationship between scaling function spaces, V_j, and wavelet function spaces, W_j, represented by Eq. (3.9) can be verified in Figures 3.5 and 3.6. For example, $V_2 = V_1 \oplus W_1$, which in single dimension means the simple addition of projections of the original signal onto spaces V_1 and W_1 yields the projection of the signal onto space V_2. The projection of the original block signal onto the highest wavelet function space W_9, shows the locations of the edges of the original signal quite accurately. In other words, high-frequency content of the signal over the time axis can be represented accurately with the highest wavelet function space. The example presented in Figures 3.4 to 3.6 shows that the wavelet transform provides an effective way of processing signals in time and frequency domains simultaneously.

Based the concept of the filter bank shown in Figure 3.3 and Eqs. (3.12) and (3.13), wavelet transform can be used for low-pass or high-pass filtering depending on the application. An example of wavelet filtering using Daubechies wavelet with 3 vanishing moments is illustrated in Figures 3.7 and 3.8. The original signal shown in Figure 3.7 (a) is a hypothetical ground acceleration signal composed of a sinusoidal signal with a frequency of 1.2 Hz and white noise with standard deviation of 0.2. The sampling frequency is 50 Hz. The original signal in Figure 3.7(a) is low-passed and high-passed up to second level of the filter bank (Figure 3.3). Figures 3.7(b) and 3.7(c) show high-pass and low-pass filtered signals of the original signal shown in Figure 3.7(a). The low-pass filtered signal shown in Figure 3.7(c) approximates the original sinusoidal signal because low-pass filtering reduces the noise in this particular application. The signal in Figure 3.7(b) is the difference between signals in Figures 3.7(a) and 3.7(c) and represents the eliminated noise.

The Fourier transforms of the hypothetical ground acceleration signal shown in Figure 3.7(a) as well as the high-pass and low-pass filtered signals shown in Figures 3.7(b) and 3.7(c) are presented in Figures 3.8(a) to 3.8(c), respectively. As expected, the peak amplitude in Figure 3.8(a) occurs at frequency of 1.2 Hz, the dominant frequency of the original signal shown in Figure 3.7(a). Figure 3.8(b) shows that signals with frequencies roughly below 5 Hz are filtered by the high –pass filtering. Figure 3.8(c)

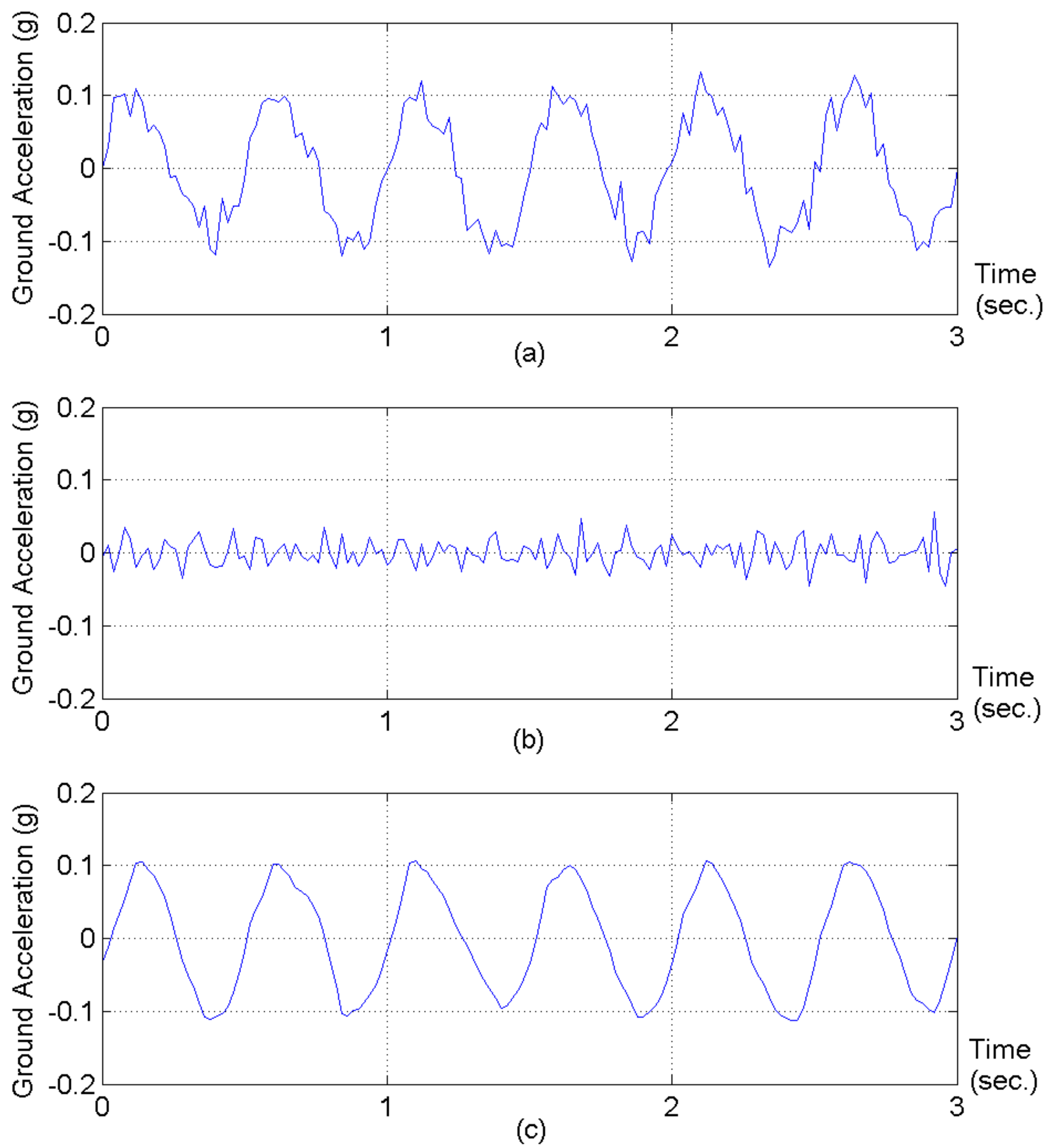

Figure 3.7: Wavelet filtering of signal: (a) original signal, (b) High-pass filtered signal, (c) Low-pass filtered signal

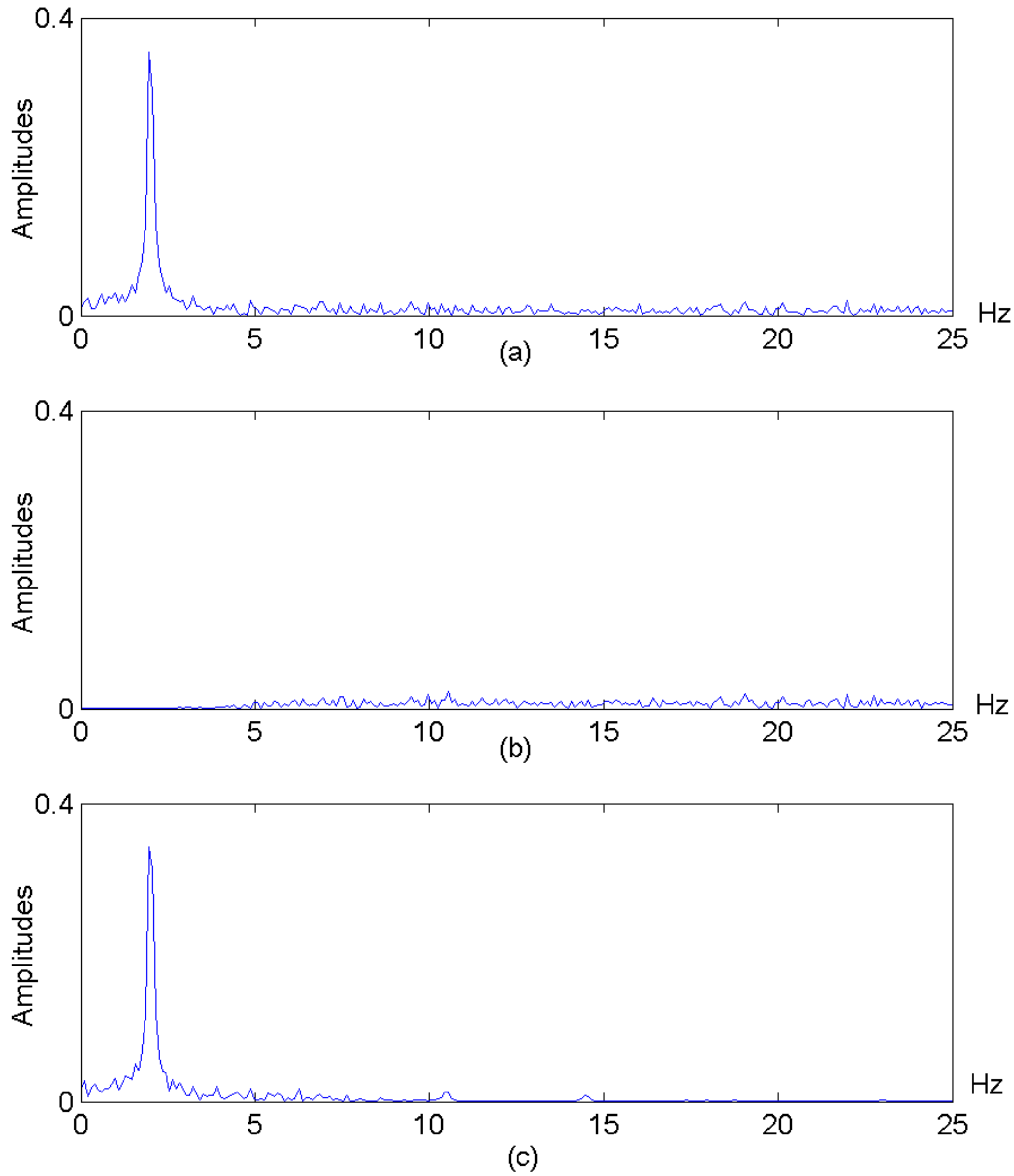

Figure 3.8: Fourier transforms of signals shown in Figure 7: (a) original signal, (b) High-pass filtered signal, (c) Low-pass filtered signal

shows that signals with frequencies roughly above 7 Hz are filtered by the low-pass filtering. For an ideal filter, the cutoff frequency for both high and low-pass filtering should be the same. As for most practical filters, however, the cutoff frequencies of the high-pass and low-pass wavelets filters do not coincide. The difference between the cutoff frequencies depends on the type of the wavelet used.

The need for low-pass filtering for effective control of civil structures subjected to extreme environmental forces was discussed earlier. The examples presented in this section and results displayed in Figures 3.5 to 3.8 indicate that the wavelet transform can be used as an effective filtering scheme for control problems.

3.3 Wavelet-Hybrid Feedback LMS Control Algorithm

Figure 3.9 shows the architecture of the proposed wavelet-hybrid feedback LMS control algorithm. The external disturbance signal, $x(n)$, is simultaneously fed into the structural system without filtering and into the filtered-x LMS adaptive controller after being filtered by the wavelet low-pass filter. Wavelet low-pass filtered signal is fed into the filtered-x LMS adaptive controller to obtain the control force $f_x(n)$. This force is then added to the feedback control force, $f_b(n)$, to yield the total control force, $f_c(n)$, and applied to the structural system to be controlled. The response of structure is then fed back into both feedback controller to obtain the feedback control force, $f_b(n)$, and filtered-x LMS adaptive controller to update the FIR filter coefficients and obtain the control force, $f_x(n)$. It should be noted that in the model presented in Figure 3.9 the wavelet filtering affects only the filtered-x LMS adaptive controller and not the feedback controller. This is because the input to the feedback controller needs to be the response of the structural system subjected to unfiltered signals.

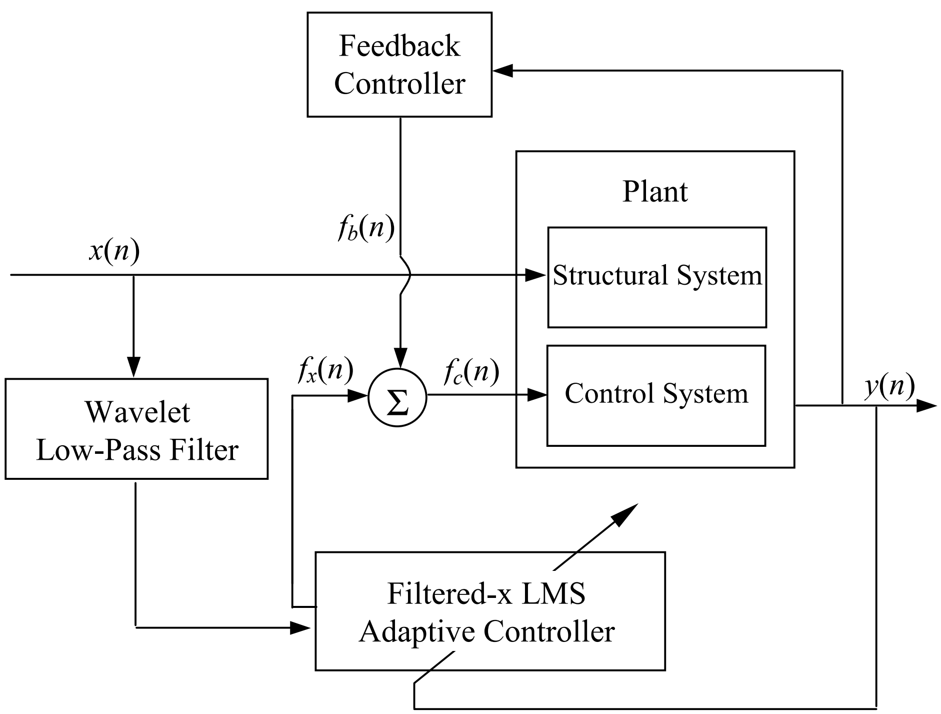

Figure 3.9: Architecture of wavelet-hybrid feedback LMS control model

The choice of the level of low-pass filtering (Figure 3.3) depends on the type of the structure (e.g., rigid versus flexible structures) and the sampling frequency. The level of wavelet low-pass filtering is chosen such that the cutoff frequency is greater than the largest significant natural frequency of the structure. In this study it is found that the cutoff frequency of 1.5 to 2 times the largest significant natural frequency produces the best control results. This is a somewhat large range for cutoff frequencies because these cutoff frequencies of the low-pass wavelet filters can not be specified exactly as they depend on many factors such as sampling frequency, the type of wavelet chosen, and number of vanishing moments.

In the subsequent sections, the effectiveness of the proposed wavelet-hybrid feedback LMS control model is demonstrated by application to two examples. The first example is the active tuned mass damper (ATMD) system described in Chapter 2. The feedback control algorithm used in this example is the LQR algorithm. The second example is the active mass driver (AMD) benchmark problem solved by a number of different investigators (Spencer, et al., 1998). The feedback control algorithm used in this example is the LQG algorithm.

3.3.1 Application to an Active Tuned Mass Damper System

The wavelet-hybrid feedback LMS control algorithm is applied to the ATMD system described in Chapter 2 subjected to the hypothetical ground acceleration signal shown in Figure 3.7(a). For the simulation, the full-state feedback LQR controller is

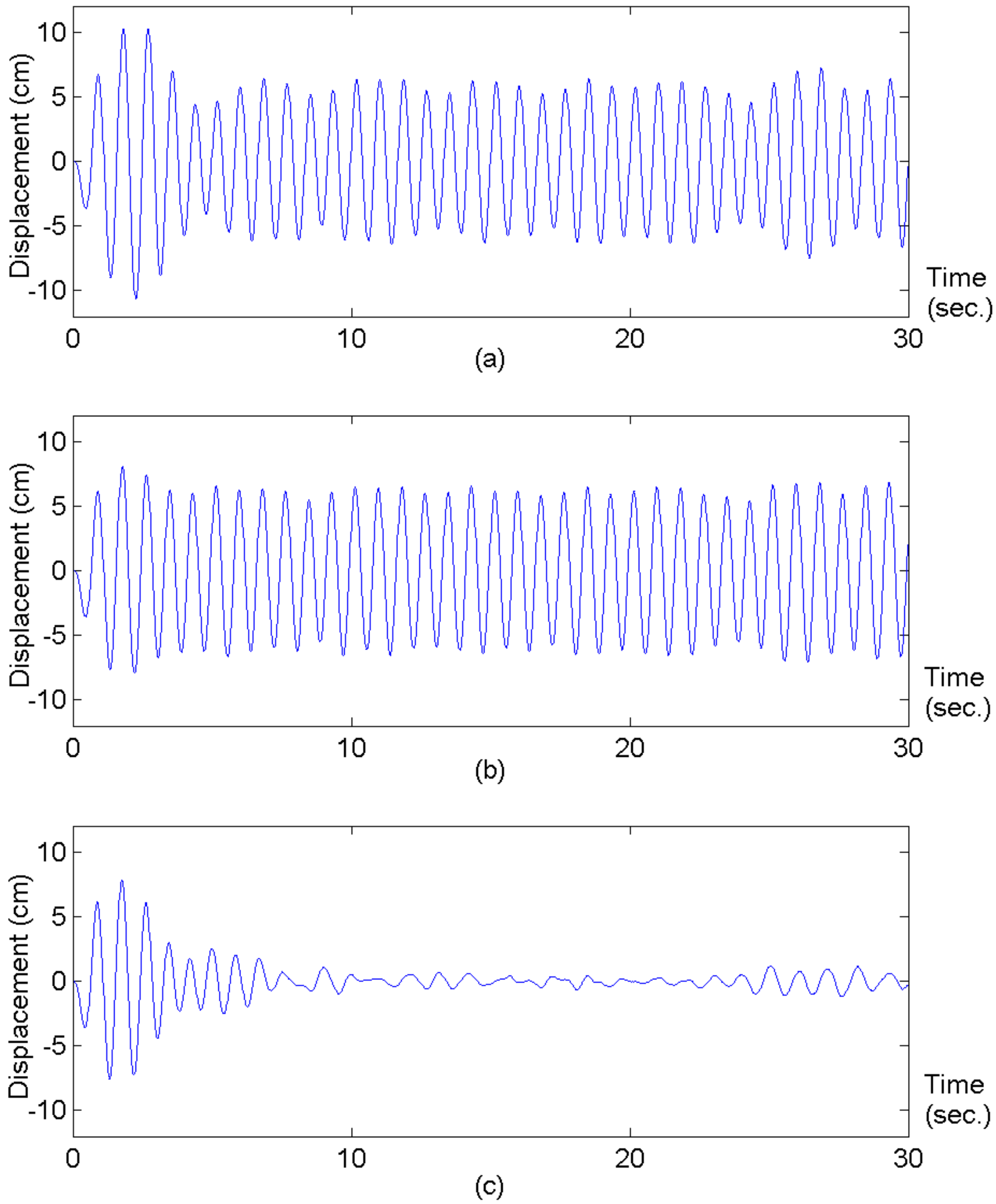

Figure 3.10: Response of the ATMD system: (a) uncontrolled response, (b) response with LQR control, (c) response with wavelet-hybrid feedback LMS control

combined with the filtered-x LMS algorithm where the displacement of the main structure is used as the error signal. Figures 3.10(a) to 3.10(c) show the uncontrolled response, the response with LQR control, and the response with the proposed control model, respectively. The order of the FIR filter coefficients in the control model is set to 50, a relatively low number, to show the effectiveness of the new model even though a 50-coefficient FIR filter does not provide a close approximation of the ATMD system as shown in Figure 2.12. Figure 3.10 demonstrates the superiority of the proposed model to classical LQR feedback control algorithms. It confirms that the proposed control model can effectively minimize the vibrations even when the bandwidth of the external disturbance (25 Hz) is much wider than the natural frequency of the structural system (1 Hz).

3.3.2 Application to an Active Mass Driver Benchmark Example Structure

The proposed control model is applied to the AMD benchmark problem developed by American Society of Civil Engineering (ASCE) Committee on Structural Control (Spencer et al., 1998, also see the web site at http://www.nd.edu/~quake). This structure is a two-dimensional scaled model of the prototype three-story building considered in Chung, et al. (1989) and is subjected to two kinds of one-dimensional ground motion. An AMD is placed on the third floor of the structure to provide a control force to the structure. The AMD consists of a single hydraulic actuator with steel masses attached to the ends of the piston rod. The first three natural frequencies of the 3-story scaled frame are 5.81 Hz, 17.68 Hz, and 28.53 Hz.

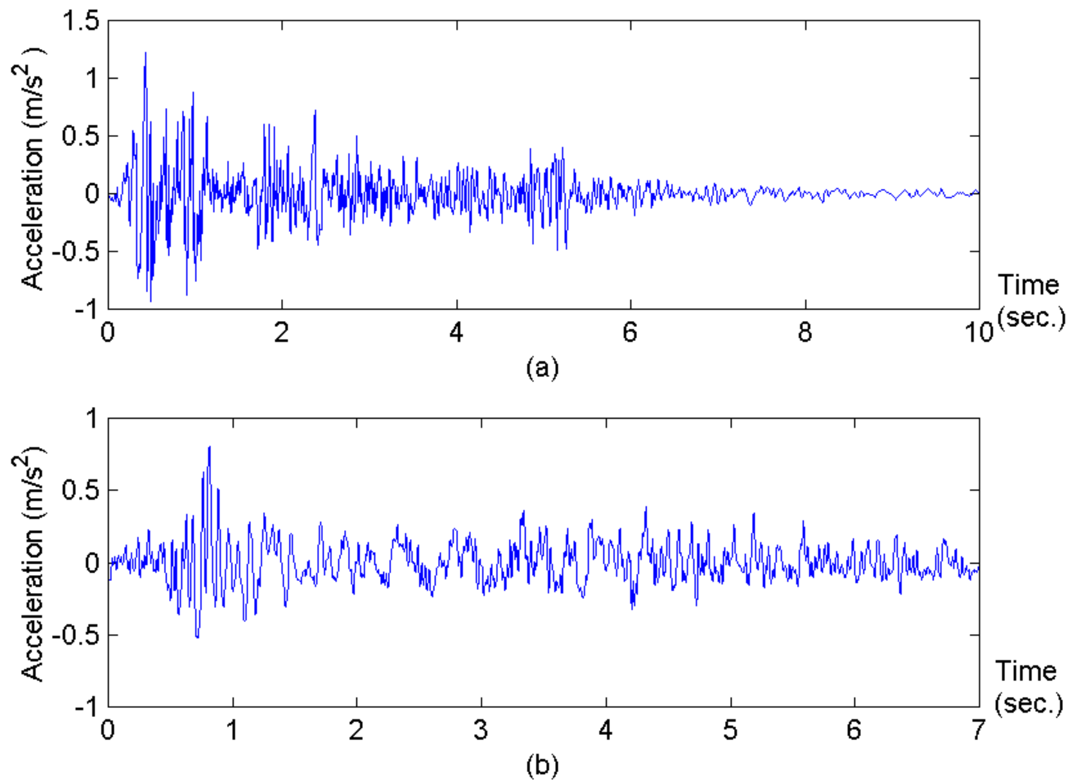

Figure 3.11: Time-scaled time histories used for simulation: (a) NS 1940 El Centro record, (b) NS 1968 Hachinohe record

Ten criteria, denoted by J_1 to J_{10}, are provided to evaluate the control performance. The first five performance measures (J_1 to J_5) are RMS responses of the structure and actuator subjected to an artificial ground acceleration record in the form of a stochastic signal with a spectral density defined by the Kanai-Tajimi spectrum. They are the RMS relative displacement of floors (J_1), the RMS acceleration of floors (J_2), and the RMS displacement, velocity, and acceleration of the actuator (J_3, J_4, and J_5, respectively). Three constraints are included: $\sigma_f \leq 1$ Volt, $\sigma_{am} \leq 2$ g's, and $\sigma_{um} \leq 3$ cm, where σ_f is the RMS actuator input, σ_{am} is the RMS actuator acceleration, σ_{um} is the RMS actuator displacement, and g is the gravitational acceleration.

The next five performance measures (J_6 to J_{10}) are the maximum responses of the structure and actuator subjected to two time-scaled earthquake records, the NS 1940 El Centro record and the NS 1968 Hachinohe record (Figure 3.11). Similar to the first five criteria, they are the maximum relative displacement of floors (J_6), the maximum acceleration of floors (J_7), and the maximum displacement, velocity, and acceleration of the actuator (J_8, J_9, and J_{10}, respectively). Three constraints are included: max $|f| \leq 3$ Volts, max $|u_m| \leq 9$ cm, and max $|a_m| \leq 6$ g's, where f is the actuator input, u_m is the actuator displacement, and a_m is the actuator acceleration.

The performance of the proposed control algorithm for the benchmark problem is demonstrated by numerical simulations using MATLAB SIMILINK (1999). Figure 3.12 shows the SIMULINK diagram for the wavelet-hybrid feedback LMS control model for the benchmark problem subjected to the time-scaled El Centro earthquake. In this diagram, the filtered-x LMS Adaptive controller consists of the 'Filtered-x Signal

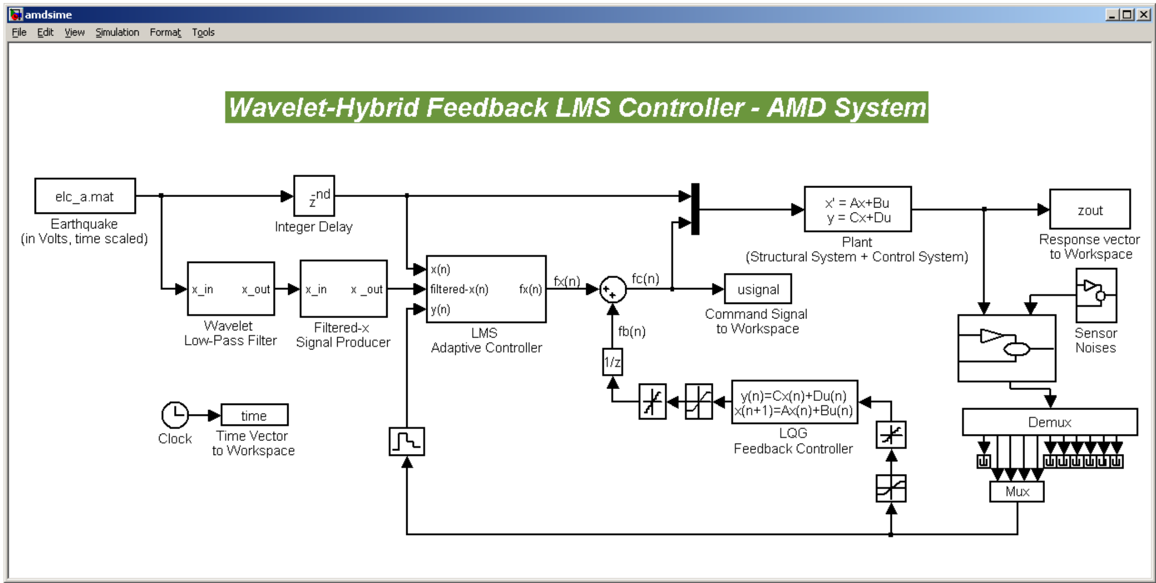

Figure 3.12: SIMULINK diagram for the wavelet-hybrid feedback LMS control model for the benchmark problem subjected to the time-scaled El Centro earthquake

Producer" block and the 'LMS Adaptive Controller' block. As illustrated in Figure 3.9, the control force, $f_x(n)$, produced by the filtered-x LMS controller, and feedback control force, $f_b(n)$, produced by the feedback controller are summed to yield the total control force, $f_c(n)$. A two-level low-pass filter using Daubechies wavelet with 3 vanishing moments is used for this simulation. This two-level wavelet filtering produces a cutoff frequency of about 40 Hz. Thus, the filtered signal covers all three significant natural frequencies of the structural system. Following the sample LQG controller design provided in Spencer et al. (1998), a few selected acceleration responses are used as feedback states for LQG controller as well as error signals to the filtered-x LMS adaptive controller. The order of FIR filter is set to 100. The simulation results indicate that choosing a larger order FIR filter would have an insignificant effect on the performance of the proposed control model, while it requires more calculation time.

The number of vanishing moment does not affect the results significantly, even though they affect the computational time required. Simulations using wavelets with a larger number of vanishing moments produce a slight improvement of results due to their better frequency locality but more CPU requirement, while using wavelets with a fewer number of vanishing moments, for example, Harr wavelet, produces less vibration suppression results due to their poor frequency locality. However, the difference in performance due to different number of vanishing moments is not significant considering the overall performance improvement over the sample LQG controller.

Figure 3.13 shows uncontrolled and controlled third floor displacement and acceleration of the benchmark structure subjected to the time-scaled El Centro earthquake. These responses are compared to responses controlled by the sample LQG controller presented in (Spencer et al. 1998) in Figure 3.14. The values of max $|f|$, max $|u_m|$, and max $|a_m|$ for the El Centro earthquake simulation are 1.061, 3.845, and 5.849, respectively, and satisfy the given constraints.

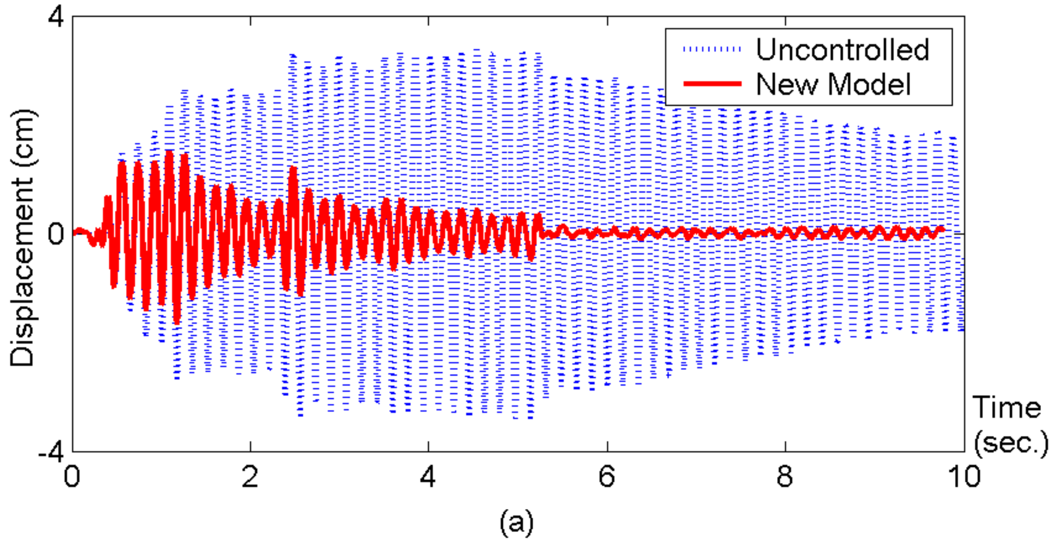

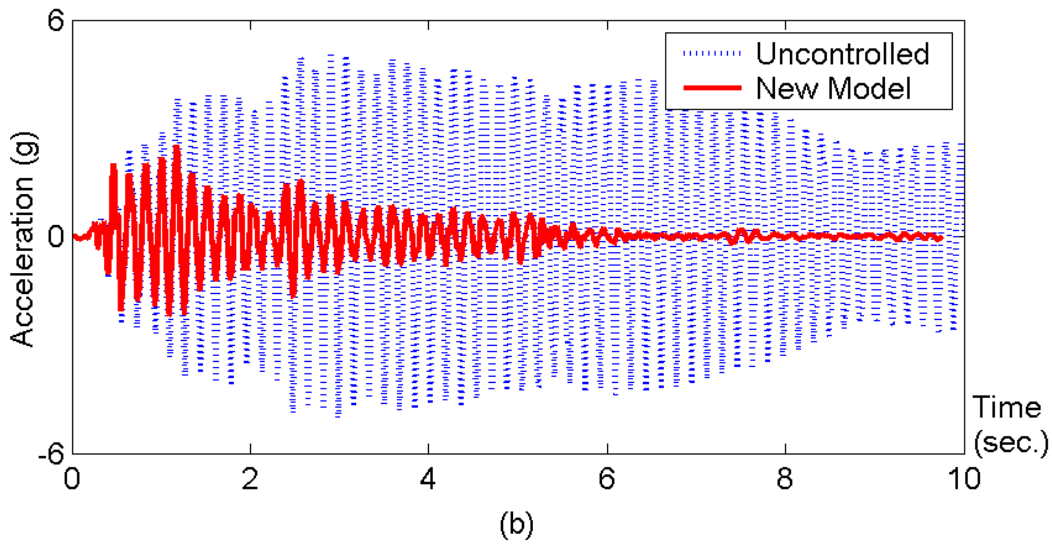

Figure 3.13: Uncontrolled and controlled third floor response time histories of the benchmark structure subjected to the time-scaled El Centro earthquake: (a) displacement, (b) acceleration

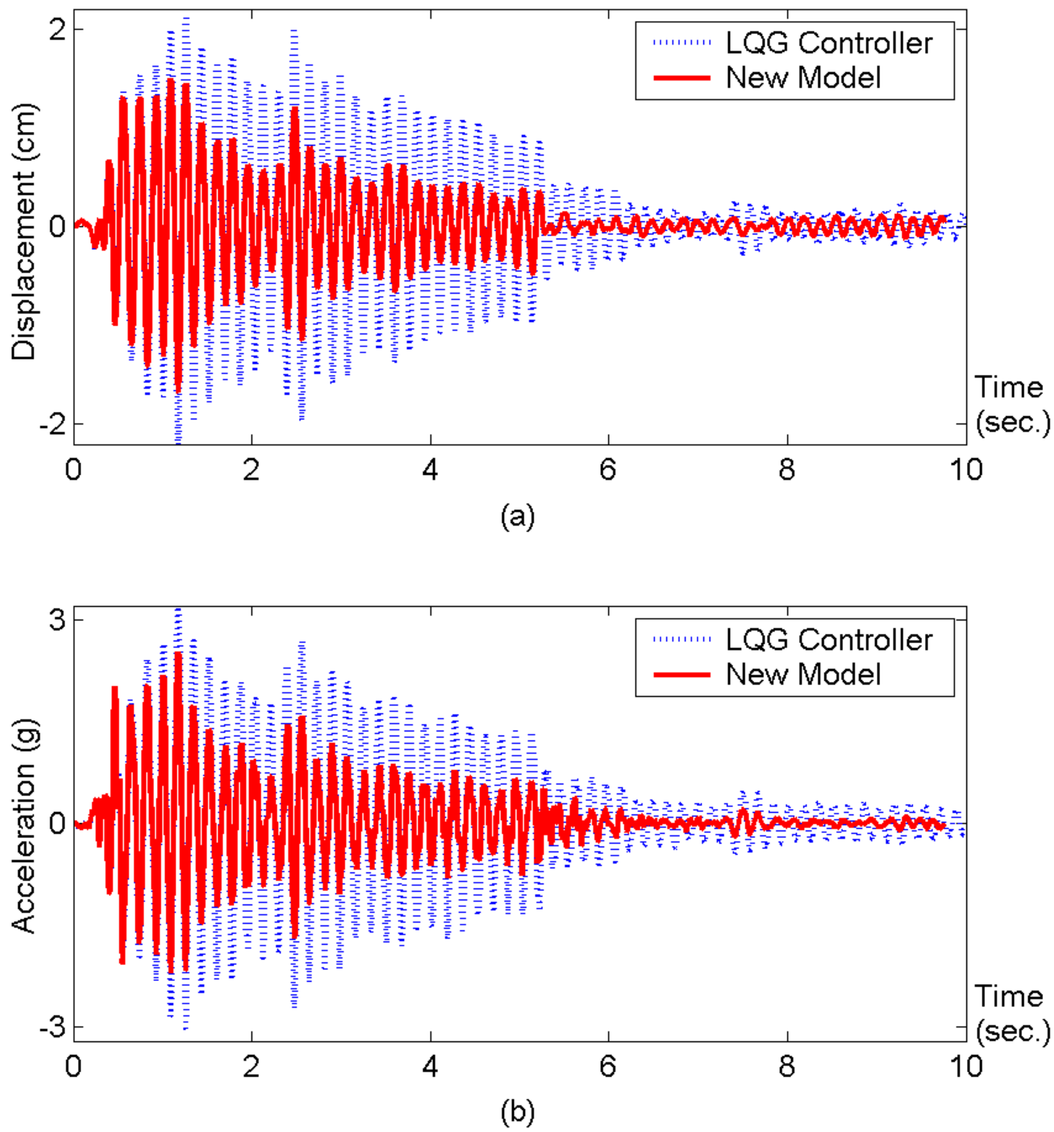

Figure 3.14: Third floor response time histories of the benchmark structure subjected to the time-scaled El Centro earthquake using the new control model and the sample LQG controller: (a) displacement, (b) acceleration

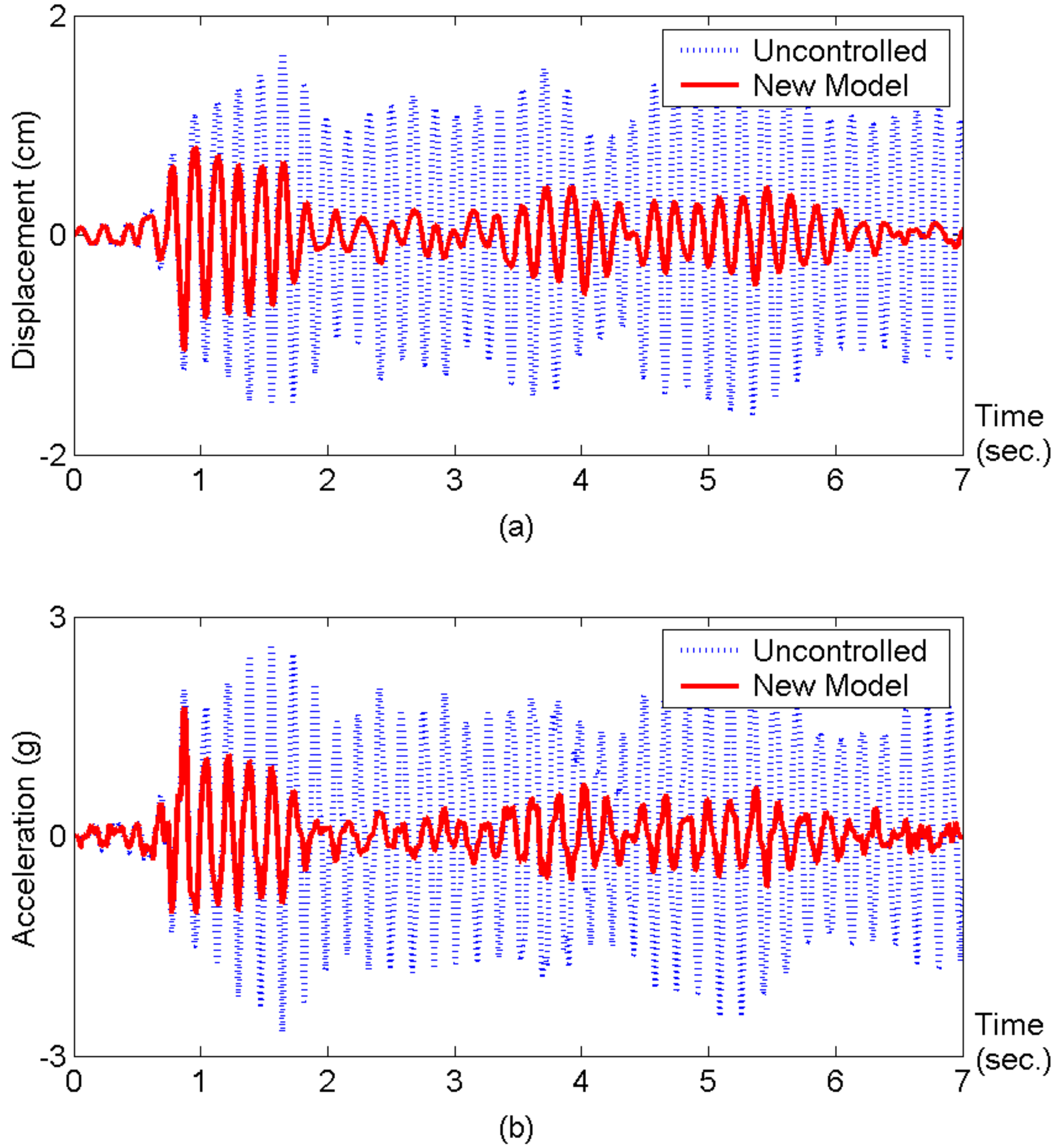

Figure 3.15: Uncontrolled and controlled third floor response time histories of the benchmark structure subjected to the time-scaled Hachinohe earthquake: (a) displacement, (b) acceleration

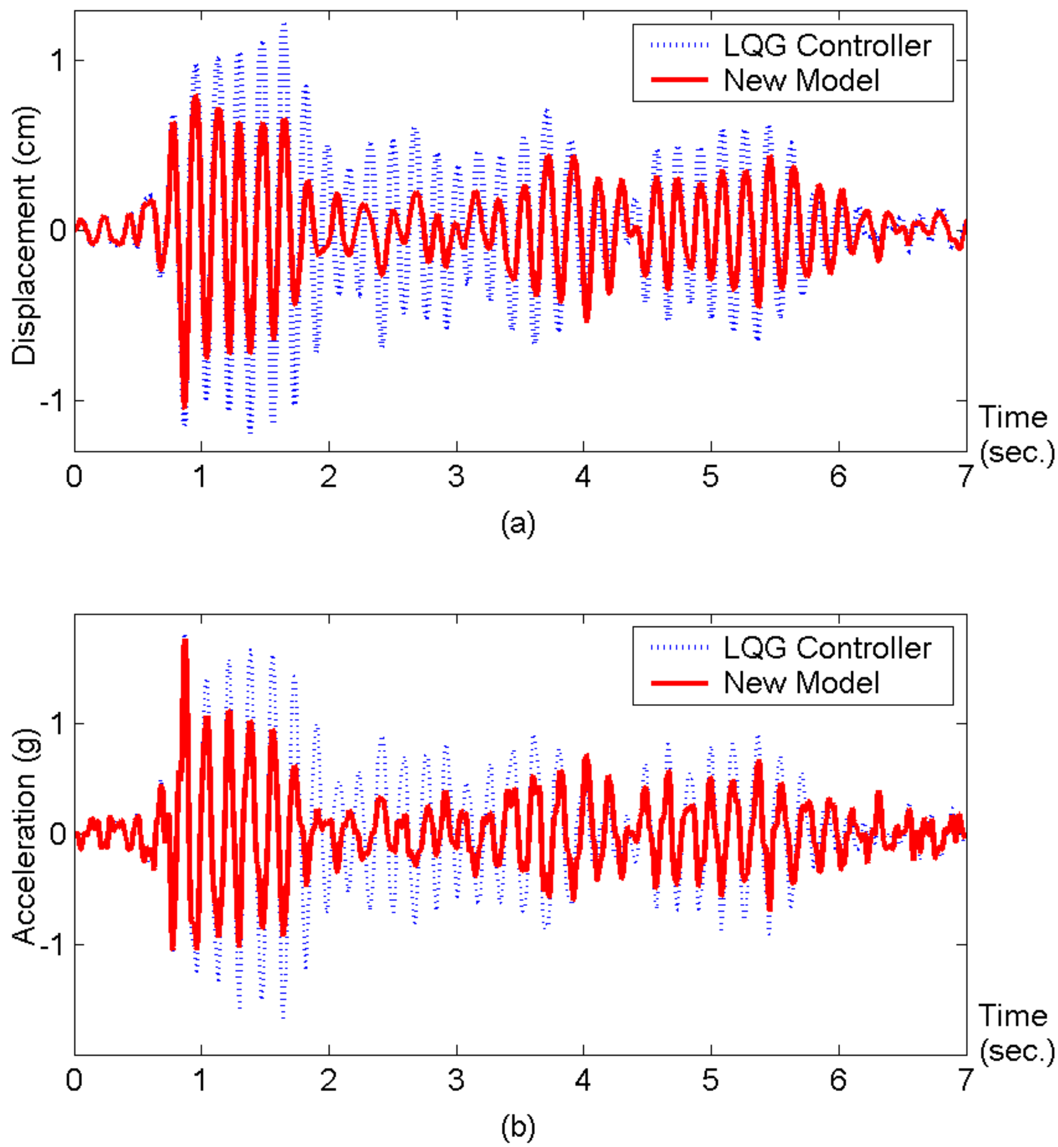

Figure 3.16: Third floor response time histories of the benchmark structure subjected to the time-scaled Hachinohe earthquake using the new control model and the sample LQG controller: (a) displacement, (b) acceleration

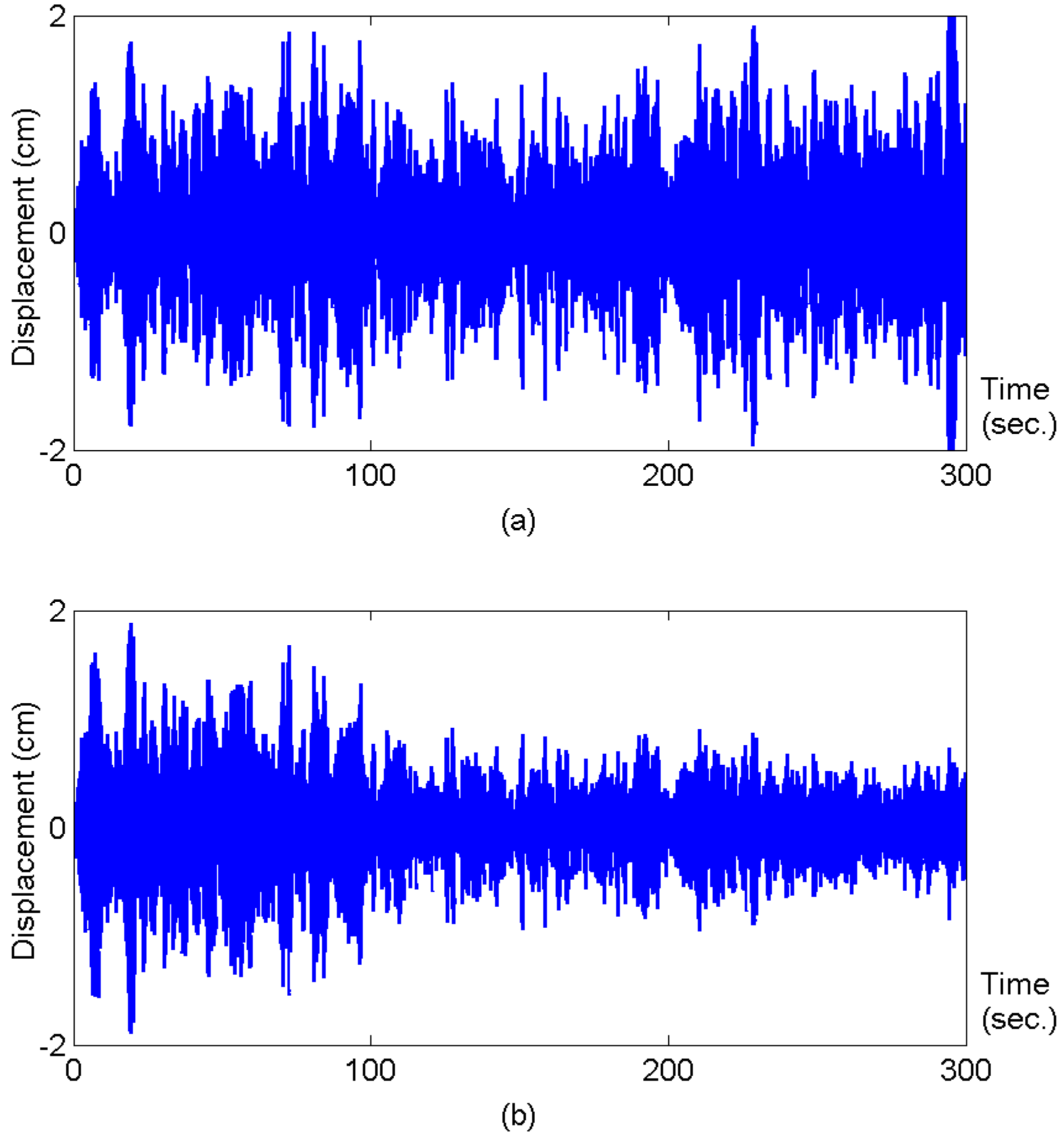

Figure 3.17: Third floor displacement time history of the benchmark structure subjected to the stochastic signal using :(a) sample LQG controller, (b) wavelet-hybrid feedback LMS control

Figure 3.15 shows uncontrolled and controlled third floor displacement and acceleration time history of the benchmark structure subjected to the time-scaled Hachinohe earthquake. And the comparison with the sample LQG controller is presented in Figure 3.16. The values of max $|f|$, max $|u_m|$, and max $|a_m|$ for the Hachinohe earthquake simulation are 1.247, 4.512, and 5.783, respectively.

The simulation using the stochastic signal case (Figure 3.17) with a rather large duration of 300 seconds represents steady state vibrations as opposed to the transient vibration of the time-scaled El Centro earthquake record with duration of 10 seconds (Figures 3.13 and 3.14) and the Hachinohe earthquake record with duration of 7 seconds (Figures 3.15 and 3.16). From Figures 3.17, it can be observed that structural responses controlled by the wavelet-hybrid feedback LMS control algorithm resemble those of the LQG control algorithm in the early stage. But, as time goes on the new control model suppresses the vibrations more effectively. Consequently, it can be concluded that both transient and steady state vibrations are effectively controlled by the new control algorithm. For the stochastic signal, σ_f, σ_{am}, and σ_{um} are 0.388, 1.9910, and 1.442 respectively.

Simulation results for the evaluation criteria J_1 to J_{10} for the stochastic signal and the time-scaled El Centro and Hachinohe earthquake records are summarized in Table 3.1. The RMS values of displacement (J_1) and acceleration (J_2) for the stochastic signal using the new control model are 19% and 21%, respectively, less than the corresponding values using the sample LQG model. The maximum values of displacement (J_6) and acceleration (J_7) for the time-scaled El Centro earthquake using the new control model are 20% and 21%, respectively, less than the corresponding values using the sample LQG model. The corresponding reductions for the time-scaled Hachinohe earthquake are 18% for the maximum displacement and 1% for the maximum acceleration. For the simulation using the time-scaled Hachinohe earthquake, another wavelet, the orthogonal Symmlet wavelet with 3 vanishing moments is applied to show the applicability of other types of orthogonal wavelets. The simulation results presented in Figures 3.15 and 3.16 and Table 3.1 show that the efficacy of the algorithm is not affected noticeably by the choice of wavelets as long as they are orthogonal wavelets.

Quantities	LQG		New Control Model	
(a) Stochastic Signal				
J_1	0.283		0.228	
J_2	0.440		0.346	
J_3	0.510		1.101	
J_4	0.513		1.013	
J_5	0.628		1.112	
(b) Time-scaled Earthquake				
	El Centro	Hachinohe	El Centro	Hachinohe
J_6	0.402	0.456	0.320	0.373
J_7	0.636	0.681	0.500	0.679
J_8	0.593	0.669	0.142	1.689
J_9	0.606	0.771	1.146	1.887
J_{10}	0.940	1.280	1.158	2.073

Table 3.1: Comparison of evaluation criteria for the AMD benchmark problem

The CPU time on an 800 MHz personal computer using the wavelet-hybrid feedback LMS control algorithm for the El Centro earthquake simulation was 8.4 seconds compared with 8.2 seconds for the LQG control algorithm. Thus, the additional computational burden due to the introduction of wavelet filtering and LMS filter coefficient adaptation is negligible.

3.4. Concluding Remarks

As demonstrated in Chapter 2, low-pass filtering of dynamic environmental disturbance signals due to winds, earthquakes, and waves is required when the hybrid feedback-LMS algorithm is used for control of real civil structures, because the frequency bandwidths of such environmental signals are much wider than those of common structural systems. In this chapter, it is shown that the wavelet transform can be effectively used as a low-pass filter for the control of civil structures.

The wavelet-hybrid feedback LMS algorithm proposed in this chapter integrates the wavelet low-pass filter with the hybrid feedback-LMS adaptive controller introduced in Chapter 2. Simulation results demonstrate that the proposed algorithm is effective for control of both steady and transient vibrations without any significant additional computational burden. Both widely used LQR and LQG control algorithms are used for the feedback controller in examples presented. As such, it is concluded that the proposed control model can be used readily to enhance the performance of existing feedback control algorithms.

CHAPTER 4

HYBRID DAMPER-TLCD CONTROL OF STRUCTURES UNDER SEISMIC EXCITATIONS

4. 1 Introduction

In this chapter, a new hybrid control system is presented through judicious integration of a passive supplementary damping system with a semi-active TLCD system. The new hybrid control system utilizes the advantages of both passive and semi-active control systems, thereby improving the overall performance and reliability of the control system. In the following sections, first two semi-active control devices, semi-active damper and semi-active TLCD, along with their original passive devices are presented and their effectiveness in reducing the vibrations of the structures is examined. Then, a new hybrid control system that combines passive supplementary dampers and semi-active TLCD is proposed. The wavelet-hybrid feedback LMS control algorithm presented in Chapter 3 is applied to find optimum control forces. The new hybrid control model is applied to an 8-story shear-building frame and its effectiveness in reducing the vibrations is investigated.

4.2 Supplementary Damper System

4.2.1 Major Types of Supplementary Damper Devices

Supplementary dampers are grouped into two major categories; hysteretic devices and viscoelastic devices (Hanson and Soong, 2001). Hysteretic devices include metallic yielding and friction devices. They rely primarily on relative displacement for their energy dissipation. Energy dissipation of viscoelastic devices, in general, depends on their relative velocity as well as relative displacement. Among the viscoelastic devices, recently developed viscous fluid devices are considered in this study. Typical viscous fluid dampers are cylindrical devices containing incompressible silicon oil, where energy is dissipated as the oil passes through a small orifice. Unlike other viscoelastic devices, the viscous fluid damper does not introduce additional stiffness into the structure. Consequently, its energy dissipation depends only on the relative velocity. Because of this feature as well as simplicity of installation and small size, viscous fluid dampers have recently been applied to a number of real life structural applications (Soong and Constantinou, 1994; Miyamoto and Scholl, 1998). Additional detailed review and valuable information about supplementary damping devices can be found in a recently published book by Hanson and Soong (2001).

4.2.2 Passive Viscous Fluid Dampers

Since the energy dissipation of a viscous fluid device depends only on its relative velocity, its output force can be expressed as a function of its relative velocity, $\dot{u}_v$, as follows:

$$f_v(t) = f_v[\dot{u}_v(t)] \tag{4.1}$$

For the orifice-controlled viscous fluid damper, its output force can be expressed as a power function of the relative velocity (Hanson and Soong, 2001) in the following form:

$$f_v(t) = c_v \left|\dot{u}_v(t)\right|^{\alpha} \operatorname{sgn}(\dot{u}_v(t)) \tag{4.2}$$

where c_v is the generalized damping coefficient, sgn represents the sign function, and α is a coefficient in the range of 0.3 to 2.0. Values of α smaller than 1.0 are effective in reducing vibrations. For structures subjected to earthquake or wind loading, a value of one is often used. The value of $\alpha = 1$ is used in this presentation. In that case, Eq. (4.1) is simplified as

$$f_v(t) = c_v \dot{u}_v \tag{4.3}$$

Then, the governing equation of motion for an m-DOF discrete structural system with multiple supplementary dampers subjected to external excitation becomes

$$\boldsymbol{M\ddot{u}}(t) + \boldsymbol{C\dot{u}}(t) + \boldsymbol{Ku}(t) = \boldsymbol{B_v f_v}(\boldsymbol{\dot{u}_v}(t)) + \boldsymbol{E_e f_e}(t) \tag{4.4}$$

where $\boldsymbol{B_v}$ is the m x l location matrix which define locations of the supplementary damping forces and $\boldsymbol{f_v}(t)$ = l x 1 supplementary damping force vector.

The required damping capacity is determined based on the desired performance level, for example, desired lateral displacement of structures. Generally speaking, dampers with a larger damping coefficient and more dampers result in a more effective response reduction. However, depending on the flexibility/rigidity of a given structure and dynamic characteristics of external disturbance, acceleration and displacement may not always be decreased even when damping is increased. Feng and Shinozuka (1993) report that the increased damping applied to base-isolated bridges results in an increase in the absolute acceleration as well as relative displacements. A similar observation is reported by Sadek and Mohraz (1998) where the authors conclude that increasing damping in flexible structures (with fundamental period longer than 1.5 seconds) increases the acceleration response while decreasing the relative displacements. Therefore, the damping level of supplementary dampers needs to be chosen carefully considering the type of the structure.

In addition to the size of the supplementary damper defining the magnitude of the damping force, the locations and number of dampers need to be selected. In terms of the selection of number and locations, viscous fluid dampers provide great flexibility as one can choose from a range of a relatively large number of low-capacity dampers to a relatively small number of high-capacity dampers. For instance, the Taylor Damper Company provides a list of about 90 bridge and 3- to 67-story building structures, built or designed to be built, where orifice-controlled viscous fluid dampers with capacity ranging from 10 kN to 6700 kN have been used (http://www.taylordevices.com/3seismic.htm).

4.2.3 Semi-Active Viscous Fluid Dampers

Orifice-controlled viscous fluid dampers can be relatively easily modified into semi-active control devices requiring a small power only. This is achieved simply by modulating the size of the opening in the orifice. Developed originally in military, aerospace, and automotive industries, the application of semi-active dampers in civil structures has received the attention of researchers during the past decade (Symans and Constantinou, 1999). Recently, an actual building equipped with semi-active variable dampers was built in Japan (Kurata et al., 1999).

In a semi-active control system, the value of damping coefficient cannot be negative. It is practically bounded in the range of a minimum value, $c_{v\min}$, and a maximum value, $c_{v\max}$. Also, the control forces are constrained to be in the opposite directions of the velocities of the corresponding dampers in order to improve their efficacy. Consequently, the value of damping coefficient for damper i at time t is regulated in accordance with the following constraint:

$$c_v^i(t) = \begin{cases} c_{v\min} & c_v^{i*}(t) < c_{v\min} \text{ or } f_v(t)\dot{u}_v^i(t) \geq 0 \\ c_v^{i*}(t) & \\ c_{v\max} & c_v^{i*}(t) > c_{v\max} \end{cases} \tag{4.5}$$

where $c_v^{i*}(t)$ is the optimal damping coefficient for damper i at time t obtained from the control algorithm adopted.

As in passive damper systems, the effectiveness of the semi-active damper also depends on the flexibility of the structure. Symans and Constantinou (1997) tested a variable semi-active fluid damper for a three-story frame with fundamental frequency of

1.8 Hz analytically and experimentally. They report the same effectiveness for variable semi-active dampers as passive dampers in reducing the structural response. A research on effectiveness of semi-active dampers was also carried by Sadek and Mohraz (1998) for single-degree-of-freedom (SDOF) systems having fundamental period in the range of 0.2 to 3.0 second. They conclude that efficiency of variable semi-active dampers is questionable for rigid structures (with fundamental period less than 1.5 seconds) compared with passive dampers. Even for flexible structures such as base-isolated structures, they report that compared with passive damper systems, semi-active systems improve acceleration response suppression to some extent without any additional suppression of displacement response. In some cases, the displacement is even slightly increased. A similar observation is made by Singh and Matheu (1997) who concluded that semi-active damper systems yield no significant benefit over the passive damper system.

In order to compare the effectiveness of a semi-active viscous fluid damper to that of a passive damper, an 8-story shear-building frame presented in Yang (1982) is examined here (Figure 4.1(a)). This particular structure is chosen because the same example has been used as a test example by a number of other researchers (Yang, 1982; Yang et al., 1987; Soong, 1990; Spencer et al., 1994). The structural properties are: floor mass = 345.6 tons, elastic stiffness of each story = 3.404 x 10^5 KN/m, and internal damping coefficient of each story = 2,937 tons/sec. The damping coefficient corresponds to a 2 percent damping for the fundamental vibration mode of the entire structure.

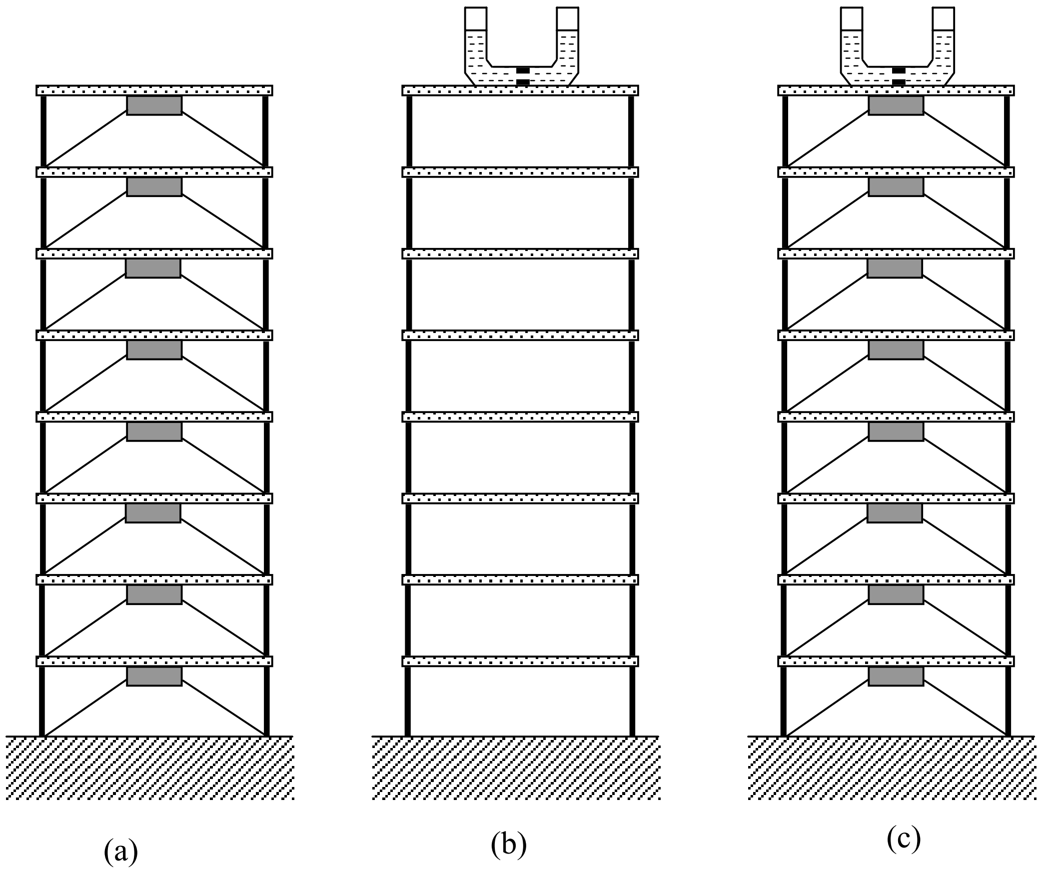

Figure 4.1: Eight-story shear building frame: (a) with passive/semi-active supplementary damper system, (b) with passive/semi-active TLCD system, (c) with hybrid system

Three simulated earthquake ground accelerations used in Yang et al. (1987) and Spencer et al. (1994) are employed (denoted by EQ-I, EQ-II, and EQ-III). They are stochastic signals with a Kanai-Tajimi spectral density defined by

$$S(\omega) = S_0 \left[\frac{4\zeta_g^2 \omega_g^2 \omega^2 + \omega_g^4}{(\omega^2 - \omega_g^2)^2 + 4\zeta_g^2 \omega_g^2 \omega^2} \right] \tag{4.6}$$

where parameters ζ_g, ω_g, and S_0 represent the soil damping property, the dominant frequency of the ground motion, and amplitude intensity of the motion, respectively. The values of these parameters depend on the characteristics and intensity of the ground acceleration in a particular geological location. The values of parameters ζ_g and ω_g for three simulated earthquake ground accelerations are presented in Table 4.1. The value of S_0 is set to be 4.5×10^{-4} m^2/sec^3.

Parameters	EQ-I	EQ-II	EQ-III
ζ_g	0.65	0.064	0.317
ω_g (rad/sec.)	18.85	31.12	10.516

Table 4.1: Parameters of simulated earthquake ground acceleration (Spencer et al. 1994)

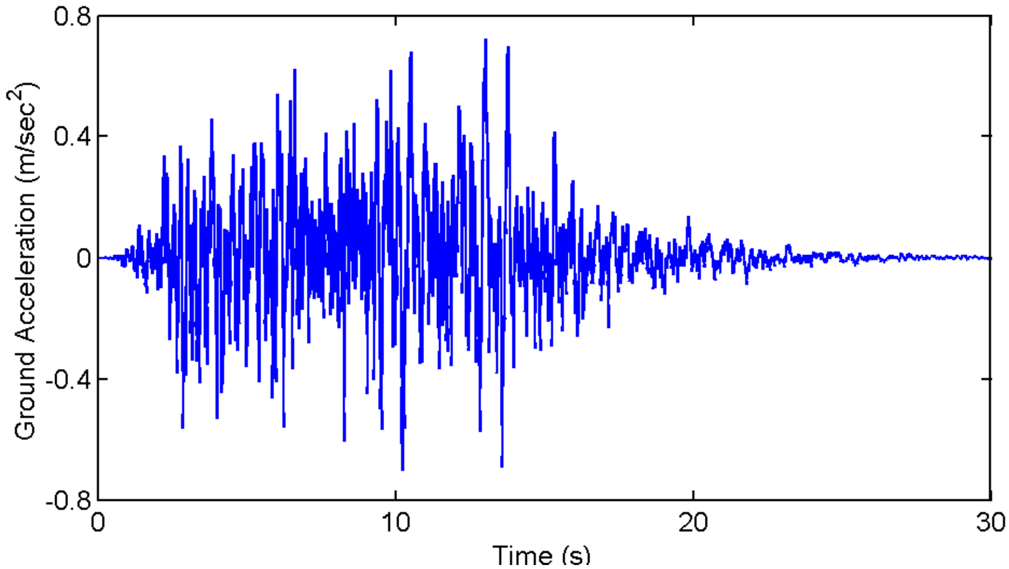

Figure 4.2: Simulated earthquake ground acceleration, EQ-I

For EQ-I, the following time envelope function, $\tau(t)$ is used to specify the shape and duration of the earthquake ground acceleration

$$\tau(t) = \begin{cases} (t/t_1)^2 & 0 \le t < t_1 \\ 1 & \text{for} \quad t_1 \le t < t_2 \\ \exp[-c(t-t_2)] & t > t_2 \end{cases} \tag{4.7}$$

where t_1 = 3 sec, t_2 = 13 sec, and c = 0.26 sec^{-1} are used, following Yang et al. (1987). This particular earthquake ground acceleration, shown in Figure 4.2, is used in this chapter to present the response time histories and the maximum responses of the example structure with various control systems. EQ-II and EQ-III ground accelerations simulate approximately the 1955 San Jose N59E and 1952 Kern County N90E earthquakes, respectively. These earthquake ground accelerations as well as EQ-I are used to measure the RMS responses of the structure.

The same damper is used in every story. The damping coefficient for each supplementary damper (c_v in Eq. 4.3) is chosen such that roughly the same level of reduction of top floor displacement is obtained as the TMD system provided in Yang (1982), resulting in a value of 3,500 kN-sec/m (20 kip-sec/in.), which is well within the practical range of commercially available viscous fluid dampers. This addition of dampers increases the damping in the fundamental mode of the controlled structure to about 5.5 percent.

Figure 4.3 shows time histories of the top floor displacement of the 8-story frame of Figure 4.1(a) for three cases: uncontrolled structure, and passively and semi-actively controlled structure with supplementary dampers subjected to EQ-I. The corresponding maximum accelerations, shear forces, and displacements at different stories are shown in Figure 4.4. In order to find the optimal damping coefficient in Eq. (4.5), the LQR - based semi-active control algorithm provided by Sadek and Mohraz (1998) is used. The value of $c_{v\max}$ used for the semi-active system is 3,500 kN-sec/m (20 kips-sec/in.), the same value used for the damping coefficient of the passive system. The value of $c_{v\min}$ for the semi-active system is set to zero. Results of this investigation and Figures 4.3 and 4.4 indicate that the semi-active viscous fluid damper system provides no noticeable improvement in reducing the displacement and shear force response over the less complicated and less costly passive system while increasing the acceleration responses

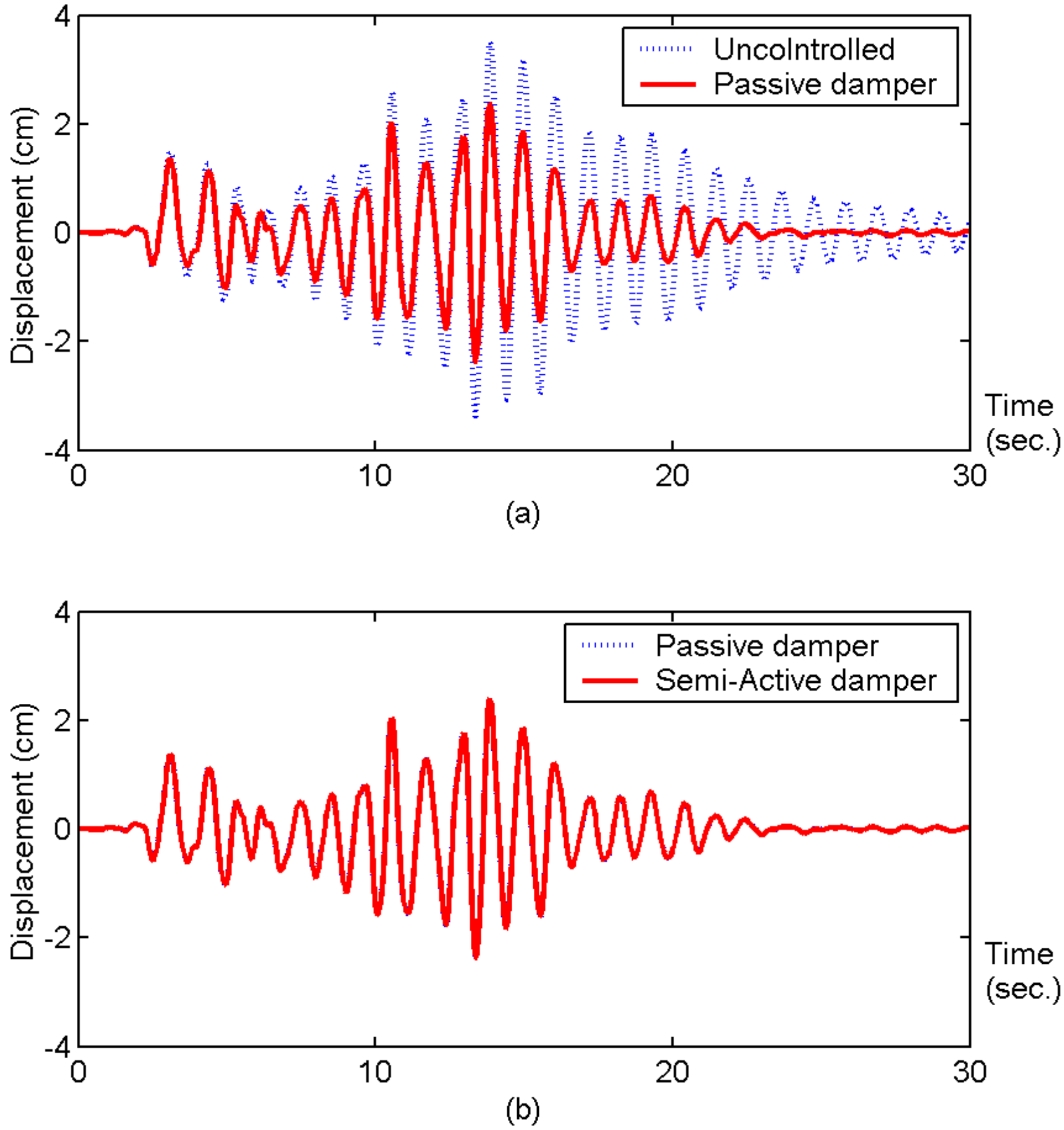

Figure 4.3: Time histories of the top floor displacement of the 8-story frame of Figure 4.1(a) for three cases: uncontrolled structure, and passively and semi-actively controlled structure with supplementary dampers subjected to EQ-I

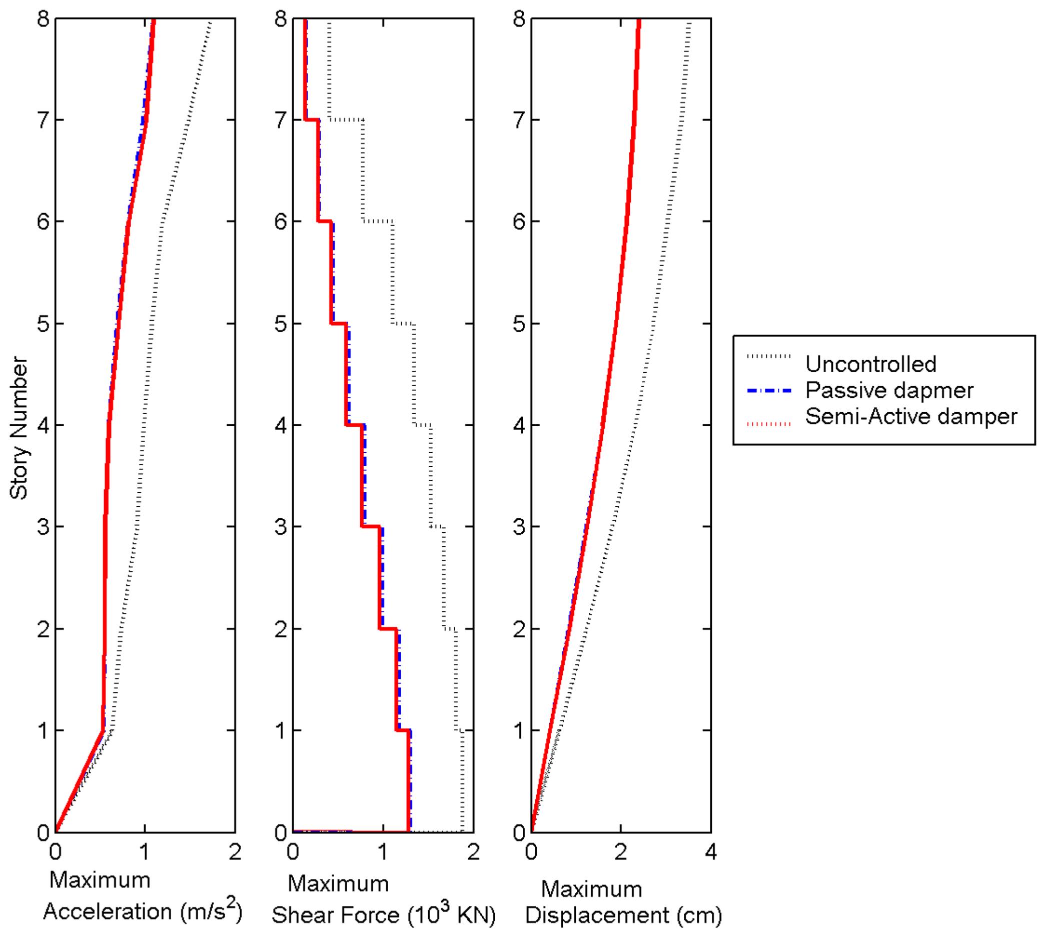

Figure 4.4: Maximum accelerations, shear forces, and displacements for uncontrolled, passively controlled, and semi-actively controlled structure subjected to EQ-I

slightly. Similar observations are found in an experimental study by Symans and Constantinou (1997) using ER (Electrorheological) dampers, and analytical studies by Singh and Matheu (1997) and Sadek and Mohraz (1998) using variable dampers.

4.3 TLCD System

4.3.1 Advantages Over Conventional TMD System

As mentioned in Chapter 1, a TLCD system shown in Figure 4.5 is a special kind of TMD system. In TMD systems, the secondary mass is attached to the main structure through a spring and dashpot. By properly tuning the parameters of mass, spring, and dashpot, the dynamic characteristics of the combined system are altered in order to enhance its effective damping capacity and reduce its response. These parameters are often tuned for the fundamental natural frequency of the system so that the maximum response reduction occurs near that frequency. In other words, a TMD system provides protection for that specific frequency only. A TMD system cannot provide protection for a range of frequencies or bandwidth normally found in a strong ground motion. Moreover, to find the optimal values of parameters for a TMD system, the magnitude of the external excitation must be established *a priori*, which is not practical considering the variable nature of ground motions.

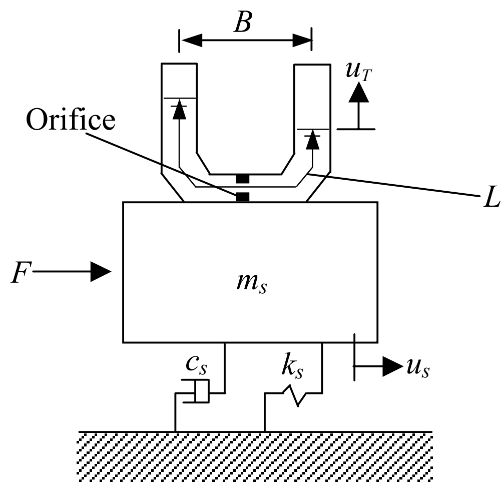

Figure 4.5: A SDOF system with a TLCD system

In a TLCD system the solid mass is replaced by liquid (commonly water) and control forces are based on the motion of a liquid column in a U-tube-like container to counteract the forces acting on the structure (Figure 4.5). The TLCD system exerts a damping force by passage of the liquid through an orifice (Won et al, 1996). It can provide the same level of vibration suppression as a conventional TMD system but with following advantages:

- The required level of damping can be readily achieved and controlled through the orifice/valve, making it suitable not only for passive control systems but also for semi-active control systems
- When there are changes in the dynamic characteristics of the main structure after construction is completed or after the occurrence of an earthquake, the TLCD parameters (frequency and mass) can be easily tuned by adjusting the height of the liquid in the tube.
- The liquid in the system is easily mobilized at all levels of the structural motion, thereby eliminating the activation mechanism required in the conventional TMD system where a certain level of threshold excitation must be set.
- Water contained in the tube can be utilized as a secondary water source for an emergency such as fire.
- It provides configuration and space flexibilities as one can design one large tube or a group of smaller tubes.

4.3.2 Passive TLCD System

Referring to Figure 4.5, when a TLCD system is attached to a SDOF system, the equations of motion are (Sakai et al., 1989)

$$\begin{bmatrix} m_s + m_T & \alpha m_T \\ \alpha m_T & m_T \end{bmatrix} \begin{Bmatrix} \ddot{u}_s(t) \\ \ddot{u}_T(t) \end{Bmatrix} + \begin{bmatrix} c_s & 0 \\ 0 & \dfrac{\rho A \xi(t) |\dot{u}_T(t)|}{2} \end{bmatrix} \begin{Bmatrix} \dot{u}_s(t) \\ \dot{u}_T(t) \end{Bmatrix} + \begin{bmatrix} k_s & 0 \\ 0 & 2\rho A g \end{bmatrix} \begin{Bmatrix} u_s(t) \\ u_T(t) \end{Bmatrix} = \begin{Bmatrix} F(t) \\ 0 \end{Bmatrix} \tag{4.8}$$

where m_s, k_s, and c_s, are mass, stiffness, and damping coefficient of the SDOF primary system, respectively; $m_T = \rho AL$ is the mass of the liquid; $\alpha = B/L$ is the length ratio of the liquid tube; ρ, A, B, and L are the density, the cross-sectional area, the width and the length of the liquid tube, respectively; u_s is the horizontal displacement of the SDOF primary system; u_T is the vertical displacement of the liquid in the liquid column; $\xi(t)$ is the coefficient of head loss determined by the opening ratio (opening percentage) of the orifice at time t; and g is the gravitational acceleration. The second equation in Eq. (4.8) represents the nonlinear equation of the motion of the TLCD. The natural frequency of the TLCD can be obtained as

$$\omega_T = \sqrt{\frac{2\rho Ag}{\rho AL}} = \sqrt{\frac{2g}{L}} \tag{4.9}$$

Equation (4.9) shows that the natural frequency of the TLCD system depends only on the length of the liquid tube. Analogous to TMD systems, tuning ratio, f, and the mass ratio, μ, of a TLCD system relative to the primary system are given by

$$f = \frac{\omega_T}{\omega_s} = \frac{\sqrt{2g/L}}{\omega_s} \tag{4.10}$$

$$\mu = \frac{m_T}{m_s} \tag{4.11}$$

where ω_s is the natural frequency of the primary system. From Eq. (4.8), the equivalent damping ratio $\zeta(t)$ of the TLCD system at time t can be expressed as

$$\zeta(t) = \frac{\xi(t)}{4\sqrt{2gL}}\left|\dot{u}_T(t)\right| \tag{4.12}$$

When the primary system is controlled passively, the head loss coefficient $\xi(t)$ has a constant value. Yet, damping ratio of the TLCD system is also dependent on the velocity of liquid as noted in Eq. (4.12). The relationship between the value of the head loss coefficient and the orifice opening ratio is estimated experimentally (Balendra et al., 1995) and tabulated in the literature (Blevins, 1984).

Equation (4.8) is now expanded for a MDOF attached to a TLCD subjected to an earthquake ground acceleration $\ddot{x}_g$ as follows:

$$\begin{bmatrix} \boldsymbol{M}+\boldsymbol{M'} & \boldsymbol{M}_{ST} \\ \boldsymbol{M}_{TS} & m_T \end{bmatrix} \begin{Bmatrix} \ddot{\boldsymbol{u}}(t) \\ \ddot{u}_T(t) \end{Bmatrix} + \begin{bmatrix} \boldsymbol{C} & [\boldsymbol{0}]_{m\text{x}1} \\ [\boldsymbol{0}]_{1\text{x}m} & c(t) \end{bmatrix} \begin{Bmatrix} \dot{\boldsymbol{u}}(t) \\ \dot{u}_T(t) \end{Bmatrix} + \begin{bmatrix} \boldsymbol{K} & [\boldsymbol{0}]_{m\text{x}1} \\ [\boldsymbol{0}]_{1\text{x}m} & 2\rho Ag \end{bmatrix} \begin{Bmatrix} \boldsymbol{u}(t) \\ u_T(t) \end{Bmatrix}$$

$$= -\begin{Bmatrix} \boldsymbol{MJ} \\ m_T \end{Bmatrix} \ddot{x}_g(t) \tag{4.13}$$

where mass coupling matrices $\boldsymbol{M_{ST}}$ and $\boldsymbol{M}_{TS}$ and the mass contribution of TLCD to the primary system mass matrix represented by $\boldsymbol{M'}$ are

$$\boldsymbol{M}_{ST} = \begin{bmatrix} [\boldsymbol{0}]_{(m-1)\text{x}1} \\ \alpha m_T \end{bmatrix} \tag{4.14}$$

$$\boldsymbol{M}_{TS} = \boldsymbol{M}_{ST}^T \tag{4.15}$$

$$\boldsymbol{M'} = \begin{bmatrix} [\boldsymbol{0}]_{(m-1)\text{x}(m-1)} & [\boldsymbol{0}]_{(m-1)\text{x}1} \\ [\boldsymbol{0}]_{1\text{x}(m-1)} & m_T \end{bmatrix} \tag{4.16}$$

and

$$c(t) = \frac{\rho A \xi(t)}{2} |\dot{u}_T(t)| \tag{4.17}$$

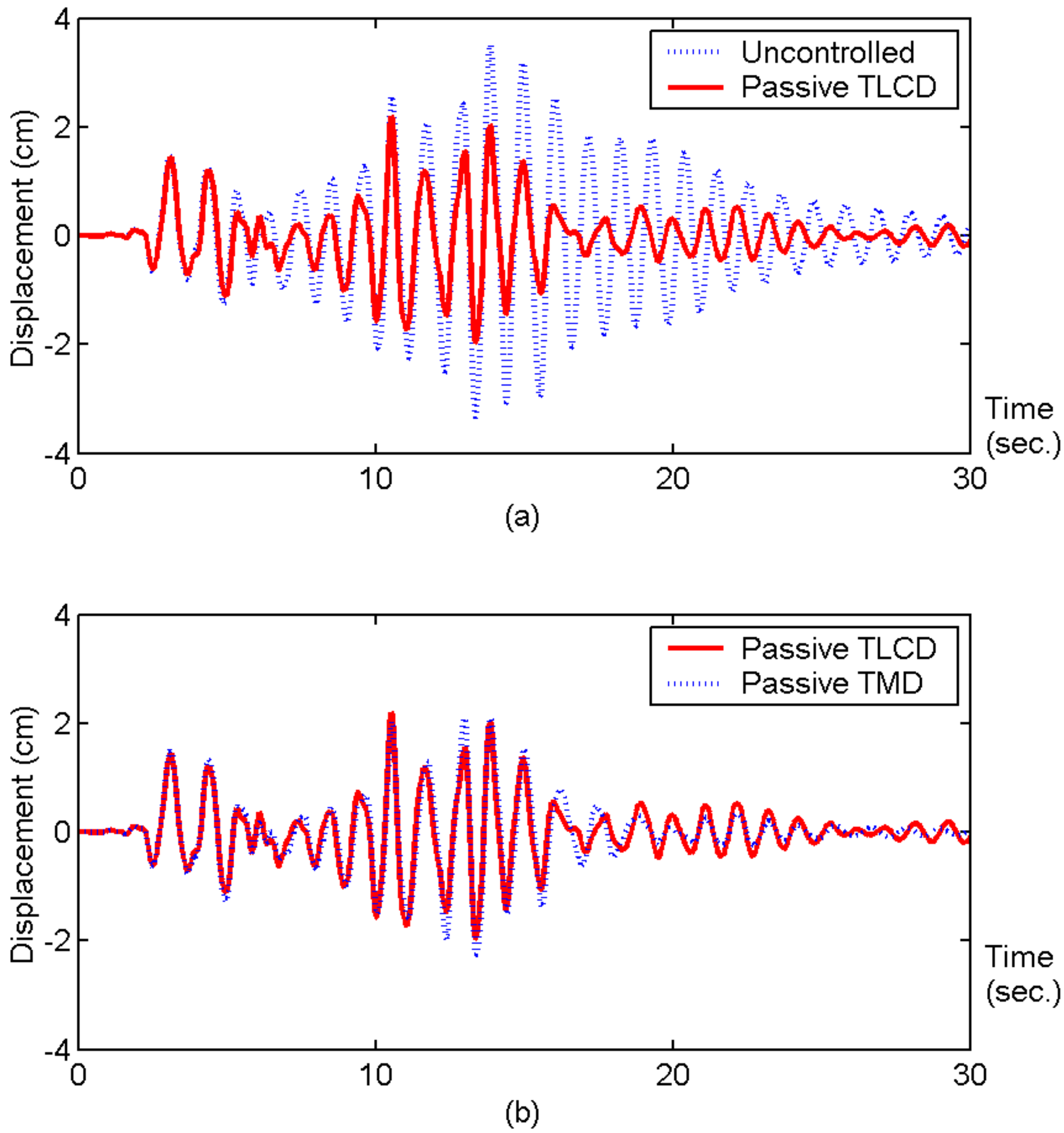

Figure 4.6: Time history of top floor displacement: (a) uncontrolled and passive TLCD controlled responses, (b) passive TMD and passive TLCD controlled responses

in which $\boldsymbol{u}(t) = m\times 1$ is the displacement vector for the primary system; $\boldsymbol{J} = m\times 1$ is a column vector with all elements equal to one.

Figure 4.6 shows time histories of the top floor displacement of the 8-story frame of Figure 4.1(b) for the uncontrolled, and passively controlled TLCD and TMD systems subjected to EQ-I. In order to compare the effectiveness of the TLCD system with that of the TMD system, the same tuning and mass ratios of $f = 0.98$ and $\mu = 0.02$ provided by Yang (1982) for a TMD system are used. The mass ratio, μ, is the ratio of the mass of the TLCD to the generalized mass associated with the first mode of the primary MDOF system. Optimum head loss coefficient of 1.78 is used following Yalla and Kareem (2000). Figure 4.6(b) shows the responses of TLCD and TMD systems in terms of reducing the response are not significantly different when similar design parameters are optimized and used for a given earthquake ground acceleration. Therefore, the TLCD system is preferred over the conventional TMD system because of its practical advantages noted earlier and similar effectiveness.

As in TMD systems, however, the effectiveness of a TLCD system depends on proper tuning of design parameters. Most important design parameters include mass ratio μ, tuning ratio f, and head loss coefficient ξ. These parameters are usually obtained such that the TLCD system minimizes the response in a root mean square sense for a given external excitation. Tuning ratios near but less than one and larger mass ratios generally result in a more effective control of structures. Sadek et al. (1998) and Won et al. (1996) conclude that the optimal head loss coefficient ξ increases as the amplitude of excitation decreases and the mass ratio increases. Like TMD systems, however, optimum values of these parameters are obtained only for any given external excitations with fixed frequency bandwidth and amplitude. In other words, these values are optimal only for the design excitation and not any other external excitation. This shortcoming can be overcome by utilizing semi-active or active control strategies.

4.3.3 Semi-active TLCD System

If the head loss coefficient $\xi(t)$ in Eq. (4.12) can be changed by a controllable orifice, then the passive damping force is transformed into an active force which controls the response of the structure. Equation (4.8) can be re-written as

$$\begin{bmatrix} \boldsymbol{M}+\boldsymbol{M}' & \boldsymbol{M}_{ST} \\ \boldsymbol{M}_{TS} & m_T \end{bmatrix} \begin{Bmatrix} \ddot{\boldsymbol{u}}(t) \\ \ddot{u}_T(t) \end{Bmatrix} + \begin{bmatrix} \boldsymbol{C} & [\boldsymbol{0}]_{m\times 1} \\ [\boldsymbol{0}]_{1\times m} & 0 \end{bmatrix} \begin{Bmatrix} \dot{\boldsymbol{u}}(t) \\ \dot{u}_T(t) \end{Bmatrix} + \begin{bmatrix} \boldsymbol{K} & [\boldsymbol{0}]_{m\times 1} \\ [\boldsymbol{0}]_{1\times m} & 2\rho A g \end{bmatrix} \begin{Bmatrix} \boldsymbol{u}(t) \\ u_T(t) \end{Bmatrix}$$
$$= -\begin{Bmatrix} \boldsymbol{MJ} \\ m_T \end{Bmatrix} \ddot{x}_g(t) + \begin{Bmatrix} \boldsymbol{0} \\ 1 \end{Bmatrix} f_c(t) \tag{4.18}$$

where

$$f_c(t) = -c(t)\dot{u}_T(t) = -\frac{\rho A \xi(t)\left|\dot{u}_T(t)\right|}{2}\dot{u}_T(t) \tag{4.19}$$

Similar to the semi-active damper system, the value of head loss coefficient is regulated in accordance with the semi-active control law expressed as

$$\xi(t) = \begin{cases} \xi_{\min} & \xi^*(t) < \xi_{\min} \text{ or } f_c(t)\dot{u}_T(t) \geq 0 \\ \xi^*(t) & \\ \xi_{\max} & \xi^*(t) > \xi_{\max} \end{cases} \tag{4.20}$$

where ξ_{max} and ξ_{min} are, respectively, the maximum and minimum limits of head loss coefficient and $\xi^*(t)$ is the optimal head loss coefficient at time t obtained from the control algorithm adopted. In practice, the value of ξ_{max} for the semi-active TLCD system is set to be greater than the optimal value of ξ obtained for the passive TLCD system in order to cover a range of amplitude and frequency of excitations. This is because the optimal value of ξ for the passive TLCD is determined in the root mean square sense and design earthquake ground excitation cannot be known *a priori*.

Figure 4.7(a) presents the time histories of top floor displacements for uncontrolled and semi-active TLCD systems shown in Figure 4.1(b) subjected to EQ-I. Figure 4.7(b) presents the time histories of top floor displacements for passive and semi-active TLCD systems subjected to EQ-I. The corresponding maximum accelerations, shear forces, and displacements per story are shown in Figure 4.8. In these numerical simulations of passive and semi-active TLCD systems, a value of 15 is used for ξ_{max}. The value of ξ_{min} is set to be zero because head loss coefficient cannot have a negative value practically. As observed in Figures 4.7 and 4.8, the semi-active TLCD system can yield significant improvement for response reduction over the passive TLCD system unlike semi-active dampers (Figures 4.3 and 4.4).

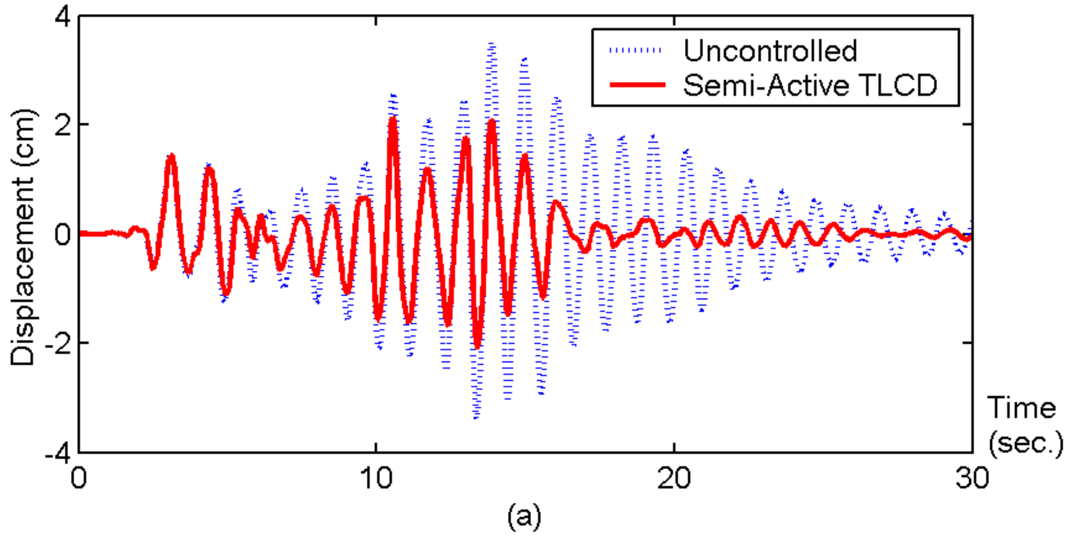

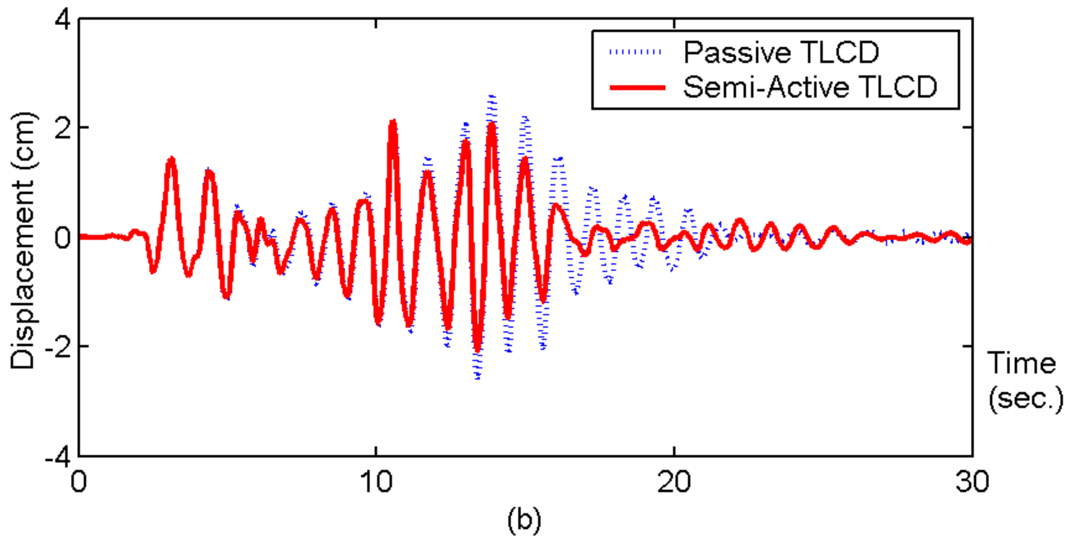

Figure 4.7: Time history of top floor displacements: (a) uncontrolled and semi-active TLCD controlled responses, (b) passive and semi-active TLCD controlled responses

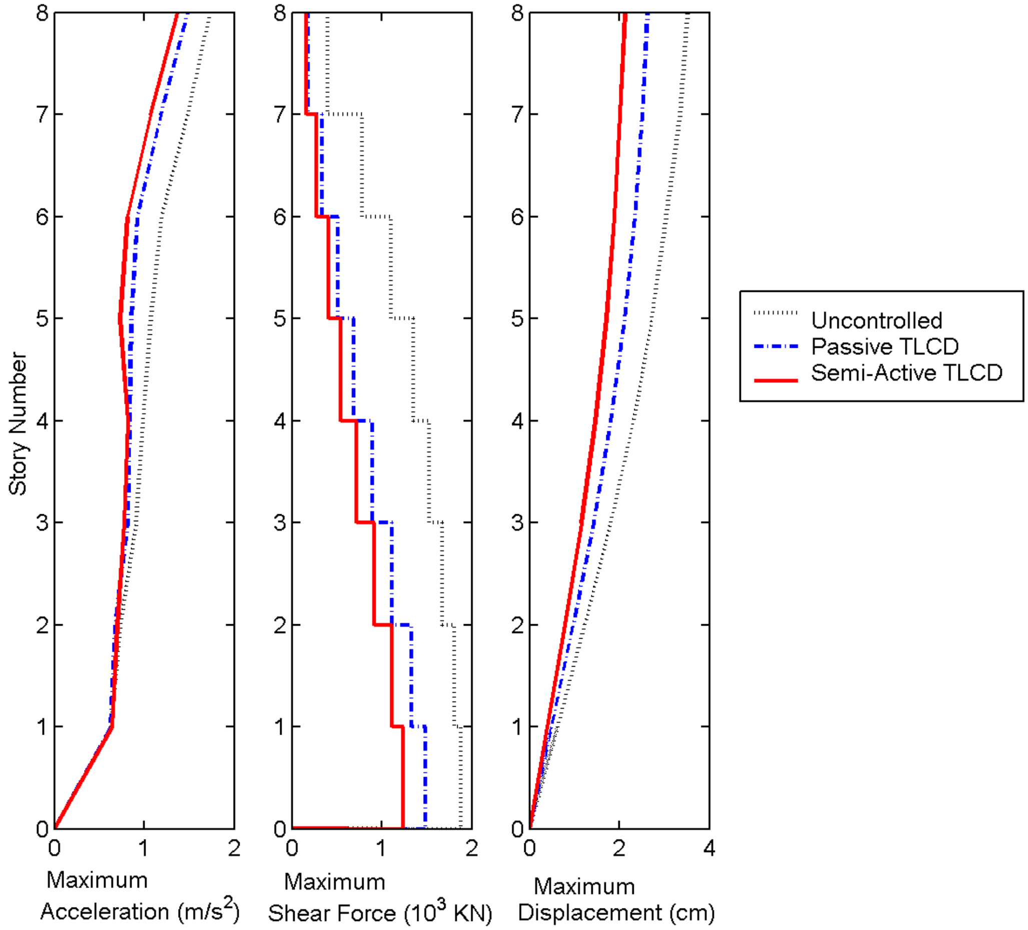

Figure 4.8: Maximum accelerations, shear forces, and displacements per story

4.4 Hybrid Damper-TLCD Control System

In the previous section, the effectiveness of the semi-active TLCD system over the passive TLCD system was demonstrated. By optimally adjusting the head loss coefficient, the semi-active TLCD system can achieve a significant improvement over passive TLCD system. However, performance of either semi-active or passive TLCD system is bounded by mass and tuning ratios of liquid tube. Even though a TLCD system with a larger mass ratio may yield more effective response reductions, the larger mass ratio may increase the stiffness requirement of the primary structure in order to support the larger mass at the top. This may result in an uneconomical design. Also, values of the mass and tuning ratios are limited by the space and length available for the TLCD system.

In this section, the semi-active TLCD system is integrated with passive viscous fluid passive damper devices in order to overcome the shortcomings of the semi-active TLCD system and enhance its reliability and vibration reduction capability. Viscous fluid dampers are used because they do not introduce any additional stiffness and can provide any desired damping force. Moreover, a passive damper system is inherently reliable because it does not depend on an external electric power source. The entire hybrid damper-TLCD control system can operate on very small power, e.g. a battery, without having to rely on a large external electric power. This elimination of the need for a large power requirement makes the proposed hybrid control system more reliable than other hybrid control systems where active and passive systems are combined.

4.4.1 Steps Involved in the Design and Implementation of the Hybrid Damper-TLCD System

The main steps involved in the design and implementation of the proposed hybrid damper-TLCD system are summarized in this section.

1. Determine the design parameters of TLCD: mass ratio μ and tuning ratio f as discussed earlier. These parameters should also be determined based on the trade-off between the desired performance level and practicality. Larger mass ratios may produce more effective response reduction, but the cost, space, and weight of mass may prevent the use of large mass ratios. The tuning ratio depends only on the length of the liquid tube (Eq. 4.3), and the tube may have an irregular shape depending on the required tube length and available space.
2. Select between the continuous and on-off type orifice/valve controller based on cost and practical implementation considerations. In the former which is more effective, the opening ratio of the orifice can be changed continuously. In the latter which is usually less expensive, the opening ratio of the orifice can have just two values, a minimum and a maximum value.
3. Determine the maximum value of the head loss coefficient ξ_{max}. In order to cover a range of excitation amplitude and frequency bandwidth, as a rule of thumb, the value of ξ_{max} for the semi-active system used in the proposed hybrid system should be greater than the value of constant ξ for the passive TLCD system, which is based on

the statistical RMS value computed for a given external excitation. However, very large values of ξ_{max} may not be practical. In the case of a power and/or computer system failure, the opening ratio of the orifice can not be changed and is generally set equal to its minimum or maximum value. This also limits the upper value for ξ_{max}. The power and/or computer system failures most probably are encountered during a strong earthquake when a large value of ξ_{max} may have an adverse effect because larger magnitudes of excitation require smaller values of head loss coefficient when the semi-active TLCD system acts like a passive TLCD system. If the required performance level is not achieved, add passive dampers as described in the next step.

4. Determine the required damping ratios and configuration of supplementary dampers based on performance level requirements. The selection of the damping ratio and damper configuration should be based on the trade-off between the desired response reduction and other factors such as cost, available damper capacity, and architectural considerations.

4.4.2 Evaluation of the Effectiveness of the Hybrid Damper-TLCD System

In order to evaluate the effectiveness of the proposed hybrid damper-TLCD system under various seismic excitations, numerical simulations are performed for the 8-story frame shown in Figure 4.1(c) using the three simulated earthquake ground accelerations discussed earlier in this chapter (Eq. 4.6 and Table 4.1). For the supplementary passive dampers in the hybrid damper-TLCD system, the same uniform damper configuration and damping coefficient are used as those used for the simulation of the passive viscous fluid dampers. Also, the same design parameters used for the semi-active TLCD system are used here in order to compare the effectiveness of the proposed system.

Time histories of top floor displacements for the 8-story frame of Figure 4.1(c) subjected to EQ-I are presented in Figure 4.9. Figure 4.9(a) presents time histories of top floor displacement for the passive damper and hybrid damper-TLCD systems. Figure 4.9(b) presents time histories of top floor displacement for the semi-active TLCD and hybrid damper-TLCD systems. The corresponding maximum accelerations, shear forces, and displacements per story are presented in Figure 4.10.

The maximum responses of the top floor and maximum base shear forces of the structure subjected to EQ-I are summarized in Table 4.2. Maximum top story displacement of the proposed hybrid damper-TLCD system is 25% and 17% less than the corresponding value for the passive damper and semi-active TLCD systems, respectively. Maximum top story acceleration of the hybrid damper-TLCD system is 12% and 30% less than the corresponding value for the passive damper and semi-active TLCD systems, respectively. Maximum shear force (base shear) of the hybrid damper-TLCD system is 22% and 14% less than the corresponding value for the passive damper and semi-active TLCD systems, respectively.

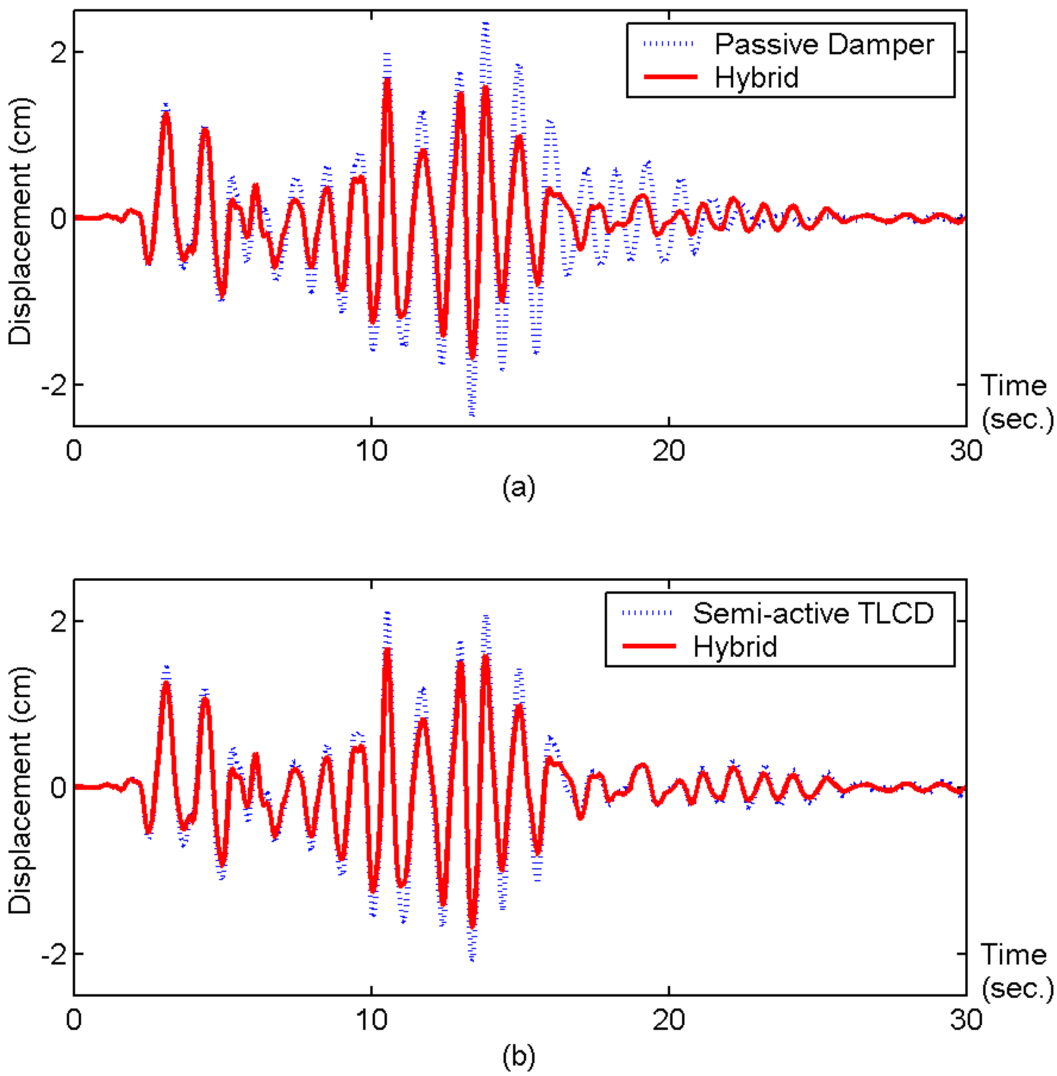

Figure 4.9: Time histories of top floor displacement for the 8-story frame of Figure 4.1(c): (a) passive damper and hybrid system, (b) semi-active TLCD and hybrid system

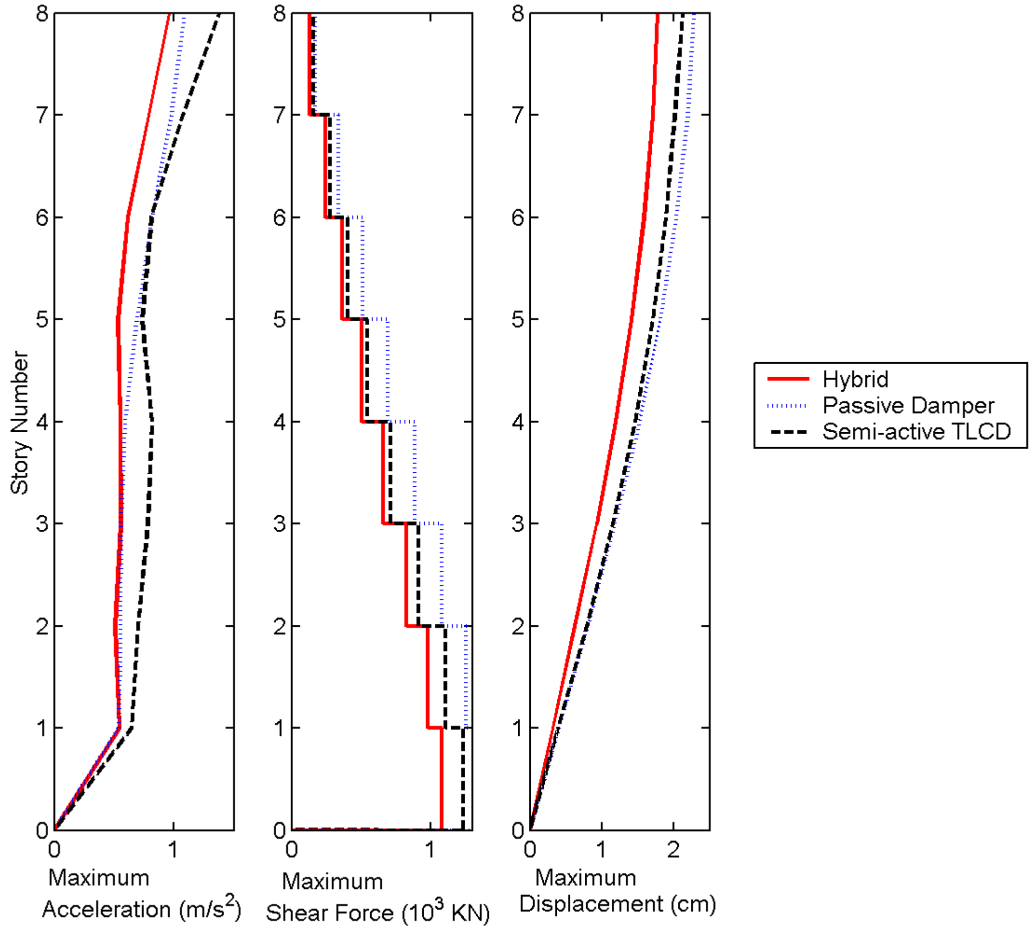

Figure 4.10: Maximum accelerations, shear forces, and displacements per story

Response	Uncontrolled	Passive damper	Semi-active TLCD	Hybrid damper-TLCD
Displacements max$\lvert u_8 \rvert$ (cm)	3.52	2.39	2.13	1.77
Accelerations max$\lvert \ddot{u}_8 \rvert$ (m/sec^2)	1.74	1.09	1.37	0.96
Maximum base shear force (x 10^3 KN)	1.88	1.37	1.24	1.07

u_8= displacement of the 8th (top) floor; $\ddot{u}_8$ = acceleration of the 8th (top) floor

Table 4.2: Maximum responses of top floor and maximum base shear forces of the structure subjected to EQ-I

Table 4.3 presents RMS acceleration and displacement responses of the top floor subjected to all three simulated earthquake ground accelerations, EQ-I, EQ-II, and EQ-III. As for the maximum responses summarized in Table 4.2, RMS responses of the hybrid damper-TLCD system are consistently lower than the corresponding responses of both passive damper and semi-active TLCD systems. From Tables 4.2 and 4.3, it is concluded that the hybrid damper-TLCD system can effectively reduce the responses of structures subjected to different earthquake ground accelerations.

Response	Uncontrolled	Passive damper	Semi-active TLCD	Hybrid damper-TLCD
EQ-I				
RMS(u_8) (cm)	1.12	0.67	0.59	0.49
RMS($\ddot{u}_8$) (m/sec^2)	0.40	0.24	0.25	0.19
EQ-II				
RMS(u_8) (cm)	1.30	0.88	0.86	0.74
RMS($\ddot{u}_8$) (m/sec^2)	0.58	0.34	0.47	0.30
EQ-III				
RMS(u_8) (cm)	1.97	1.45	1.42	1.28
RMS($\ddot{u}_8$) (m/sec^2)	0.76	0.59	0.63	0.57

Table 4.3: RMS responses of top floor of the structure subjected to simulated earthquake ground accelerations, EQ-I, EQ-II, and EQ-III

Figure 4.11 shows the time history of the top floor displacements for the hybrid damper-TLCD system subjected to EQ-I when the semi-active TLCD controller is functioning as a passive system only due to power or computer failure (denoted as TLCD-Off in the figure) along with the response when the hybrid system is functioning in whole. For the TLCD-Off case, the value of head loss coefficient is fixed at $\xi_{\min}$,

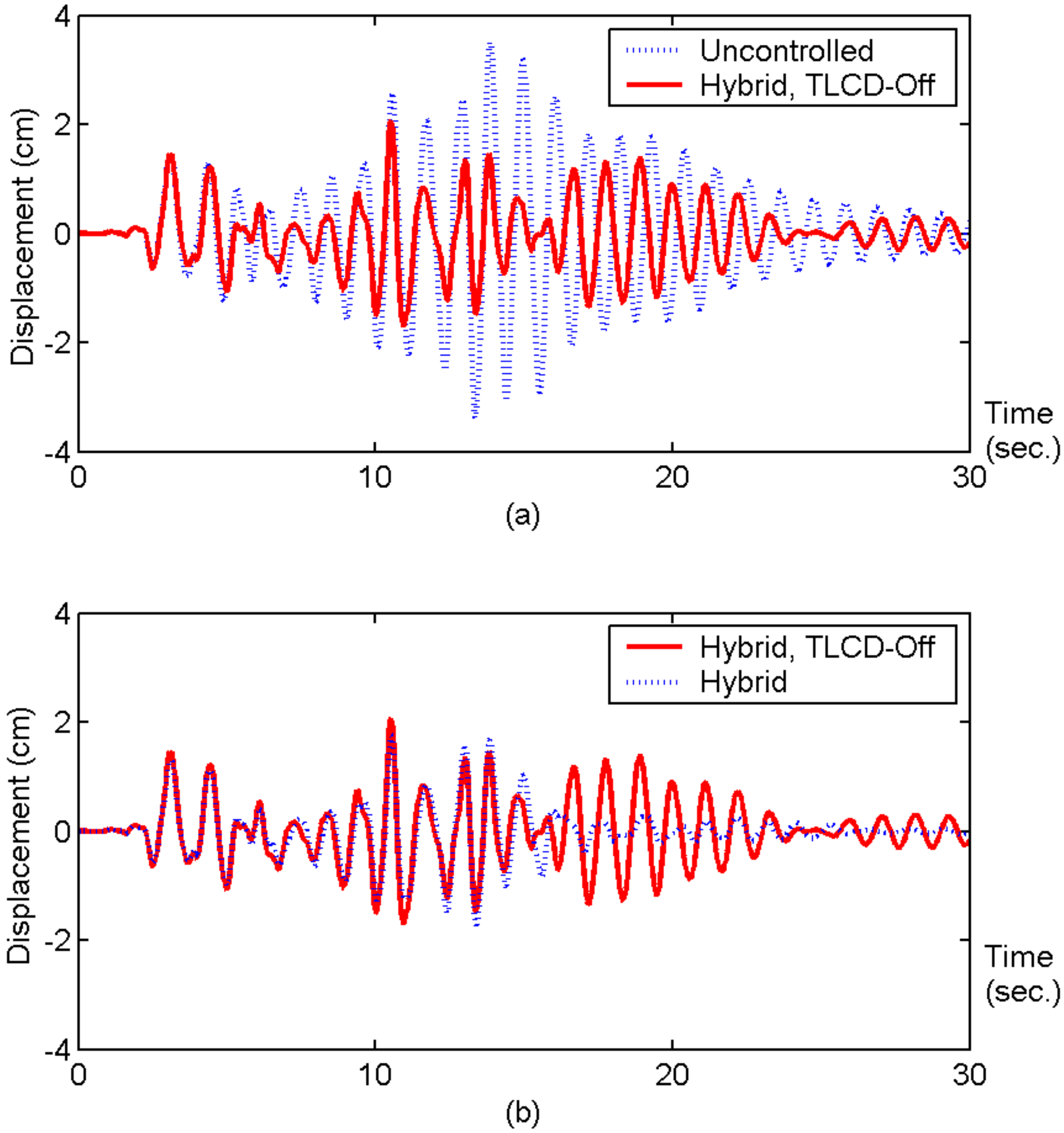

Figure 4.11: Time histories of top floor displacements: (a) uncontrolled system and hybrid system when the semi-active TLCD controller is not functioning fully (TLCD-Off), (b) hybrid controlled system and hybrid system when the semi-active TLCD controller is not functioning fully (TLCD-Off)

assuming a passive rather than a semi-active TLCD system. Even though the performance of the TLCD-Off case dose not match that of the whole hybrid system, especially in the second half of the simulation (Figure 4.11(b)), significant response reduction is still achieved compared with the uncontrolled response (Figure 4.11(a)). Similar results are obtained for the TLCD-Off case with the value of head loss coefficient fixed at $\xi_{\max}$ but are not presented here for the sake of brevity. The results demonstrate that the proposed hybrid damper-TLCD system is stable and robust in terms of power or computer failure.

4.5 Concluding Remarks

For both supplementary damper and TLCD systems, damping is achieved and damping forces are controlled through an orifice/valve, making them suitable not only for passive control systems but also for semi-active control systems. However, it is shown that the performance improvement of semi-active viscous fluid damper systems over the less complicated and less costly passive damper systems is not always guaranteed depending on the flexibility of the structure. On the other hand, a semi-active TLCD system can reduce the response significantly compared with a passive TLCD system. This can be explained by the fact that the head loss coefficients are modified continuously on-line based on the frequency and magnitude of external excitations.

A new hybrid control model is presented by combining supplementary passive damper and semi-active TLCD systems. It is found that the new model is effective in significantly reducing the response of an MDOF system under various seismic excitations. Also, it is shown that the hybrid control system provides increased reliability and maximum operability during normal operations as well as a power or computer failure. The proposed system eliminates the need for a large power requirement, unlike other proposed hybrid control systems where active and passive systems are combined.

CHAPTER 5

HYBRID CONTROL OF 3D IRREGULAR BUILDINGS UNDER SEISMIC EXCITATIONS

5. 1 Introduction

A good number of research articles have been published on active, semi-active, and hybrid control of structures subjected to dynamic excitations in recent years. However, most of these articles deal with two dimensional structures or small 3D structures with symmetrical plans. The two dimensional (2D) analysis of torsionally coupled structures often results in underestimation of coupled lateral and torsional responses.

In this chapter, the hybrid damper-TLCD control model, presented in Chapter 4, is further investigated for control of responses of 3D irregular buildings under various seismic excitations. First, the equations of motion for the combined building and TLCD system are derived for multistory building structures with rigid floors and plan and elevation irregularities. Then, optimal control of 3D irregular buildings equipped with a hybrid damper-TLCD system is described and major steps involved are delineated. The wavelet-hybrid feedback LMS control algorithm, presented in Chapter 3, is applied to find the optimum control forces. Two multistory moment-resisting building structures with vertical and plan irregularities are used to investigate the effectiveness of the new control system in controlling the seismic response of irregular buildings.

5.2 Analytical Model

5.2.1 Coupled Dynamic Responses of 3D Irregular Buildings

The N-story three-dimensional building model considered in this chapter can have both plan and elevation (setback) irregularities. Floor diaphragms are assumed to be rigid. Horizontal loads are transferred to the columns through the rigid floor diaphragms. In general, the center of mass, C_M, does not coincide with the center of resistance, C_R, in each floor (Figure 5.1(a)). The centers of mass and resistance of floors do not have to lie on the same vertical axes (their locations can vary from floor to floor). For such buildings, lateral and torsional motions under seismic excitations are coupled. The structural model has three displacement degrees of freedom at each floor level i: translations in the x- and y-directions, u_i and v_i, respectively, and a rotation about the vertical axis z passing through the center of mass, θ_i (i = 1, 2, …, N). The dynamic equation of motions of the 3D building structure under seismic excitations is written as

$$\boldsymbol{M\ddot{u}} + \boldsymbol{C\dot{u}} + \boldsymbol{Ku} = -\boldsymbol{Mr}_g \ddot{u}_g \tag{5.1}$$

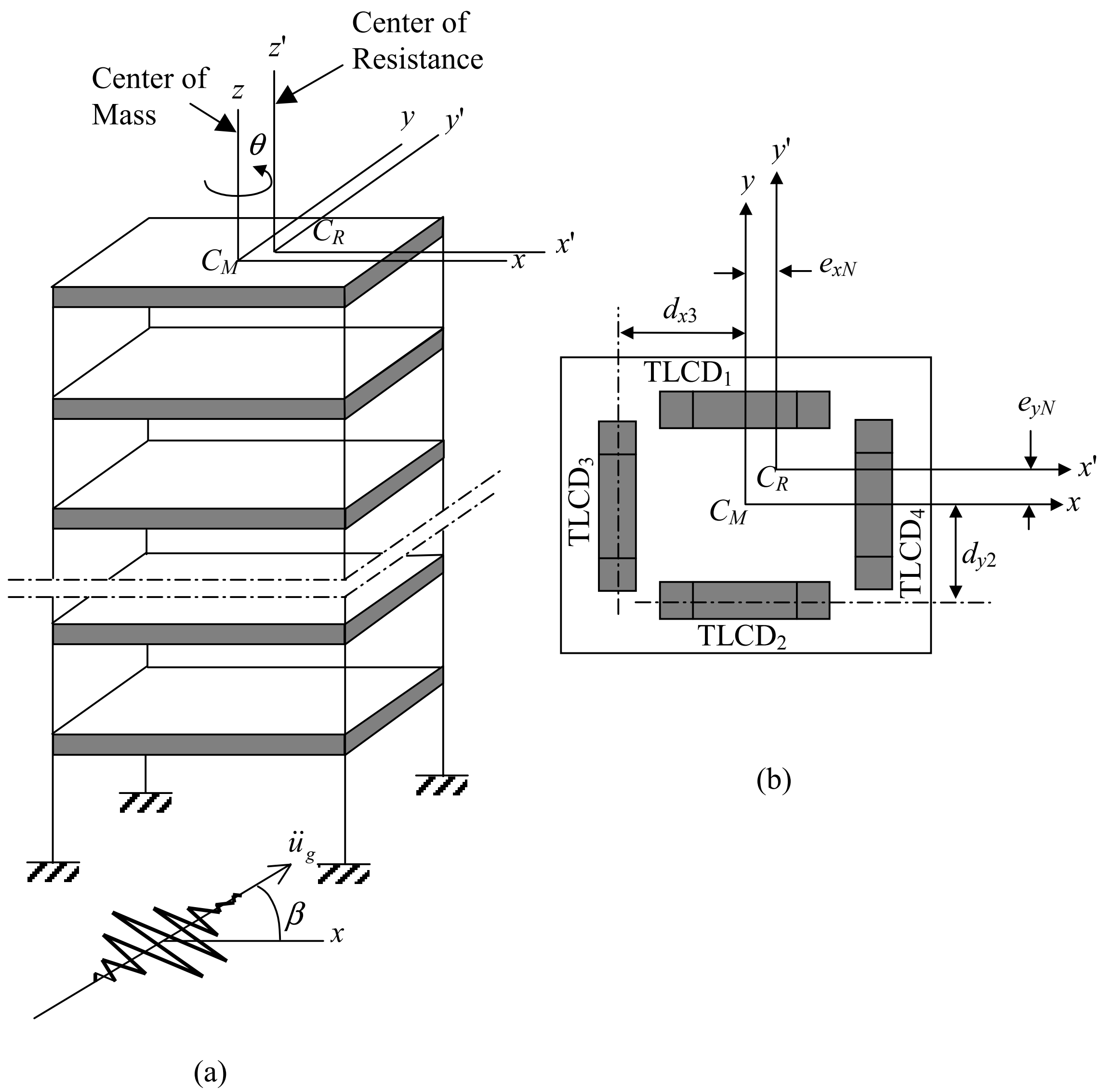

Figure 5.1: Structural model of a 3D building with a multi-TLCD system on the roof subjected to coupled translational and torsional motions

where $\boldsymbol{M}$, $\boldsymbol{C}$, $\boldsymbol{K}$, respectively, are the $3N \times 3N$ mass, damping, and stiffness matrices of the structure and $\ddot{u}_g$ = the ground acceleration. The displacement vector $\boldsymbol{u}$ and the ground influence vector $\boldsymbol{r}_g$ have the forms

$$\boldsymbol{u} = [\boldsymbol{u}_1^{\mathrm{T}}\ \boldsymbol{u}_2^{\mathrm{T}}\ \boldsymbol{u}_3^{\mathrm{T}}\ \ldots\ \boldsymbol{u}_{\mathrm{N}}^{\mathrm{T}}]^{\mathrm{T}} \tag{5.2}$$

$$\boldsymbol{r}_g = [\boldsymbol{r}_{g,1}^{\mathrm{T}}\ \boldsymbol{r}_{g,2}^{\mathrm{T}}\ \boldsymbol{r}_{g,3}^{\mathrm{T}}\ \ldots\ \boldsymbol{r}_{g,\mathrm{N}}^{\mathrm{T}}]^{\mathrm{T}} \tag{5.3}$$

where

$$\boldsymbol{u}_i = \begin{bmatrix} u_i \\ v_i \\ \theta_i \end{bmatrix}, \qquad i = 1, 2, \ldots, N \tag{5.4}$$

$$\boldsymbol{r}_{g,i} = \begin{bmatrix} \cos\beta \\ \sin\beta \\ 0 \end{bmatrix}, \qquad i = 1, 2, \ldots, N \tag{5.5}$$

and β is the direction angle of the incident earthquake motion measured from the x-axis (Figure 5.1(a)).

5.2.2 Dynamic Equation of a TLCD System

In this study, two pairs of TLCDs are installed on the roof of the building, one pair along each principal axis of the building plan (Figure 5.1(b)). This configuration is selected in order to maximize the vibration suppression and to avoid additional undesirable torsional effects. Refering to Figure 4.5, the equations of motion of each

TLCD installed on the roof of the N-story building, in the directions of x- and y-axes are (Liang et al., 2000)

$$m_{x_i}\ddot{x}_i(t)+\frac{\rho A_{x_i}\xi_{x_i}(t)\left|\dot{x}_i(t)\right|}{2}\dot{x}_i(t)+k_{x_i}x_i(t)=-\alpha_{x_i}m_{x_i}\ddot{u}_N(t)+\alpha_{x_i}m_{x_i}d_{y_i}\ddot{\theta}_N(t) \qquad (5.6)$$

$$m_{y_i}\ddot{y}_i(t)+\frac{\rho A_{y_i}\xi_{y_i}(t)\left|\dot{y}_i(t)\right|}{2}\dot{y}_i(t)+k_{y_i}y_i(t)=-\alpha_{y_i}m_{y_i}\ddot{v}_N(t)-\alpha_{y_i}m_{y_i}d_{x_i}\ddot{\theta}_N(t) \qquad (5.7)$$

where the last terms in the right hand side of Eqs. (5.6) and (5.7) represent the torsion contribution. In Eqs. (5.6) and (5.7) m_{x_i} , m_{y_i} , k_{x_i} , k_{y_i} α_{x_i} , and α_{y_i} are, respectively, mass, equivalent stiffness, and width-to-length ratio of the liquid tube of the ith TLCD in x- and y-directions defined by

$$m_{x_i}=\rho A_{x_i}L_{x_i} \qquad m_{y_i}=\rho A_{y_i}L_{y_i} \qquad (5.8)$$

$$k_{x_i}=2\rho g A_{x_i} \qquad k_{y_i}=2\rho g A_{y_i} \qquad (5.9)$$

$$\alpha_{x_i}={}^{B_{x_i}}\!/_{L_{x_i}} \qquad \alpha_{y_i}={}^{B_{y_i}}\!/_{L_{y_i}} \qquad (5.10)$$

and A_{x_i} , A_{y_i} , B_{x_i} , B_{y_i} , L_{x_i} , and L_{y_i} are the cross-sectional area, the width, and the length of the liquid tube of the ith TLCD in the x- and y-directions, respectively; ξ_{x_i} and ξ_{y_i} are the coefficient of head loss determined by the opening ratio of the orifice of the ith TLCD in the x- and y-directions, respectively; x_i is the displacement of the liquid column of the ith TLCD which is parallel to the x-axis; y_i is displacement of the liquid column of the ith TLCD which is parallel to the y-axis, ρ is the density of the liquid; g is the gravitational acceleration; and d_{x_i} and d_{y_i} are the x- and y-coordinates of the center of the ith TLCD in the xy coordinate system with origin at the center of mass, C_M.

5.2.3 Equations of Motion for the Combined Building and TLCD system

Equations of motion for the combined building and TLCD system are obtained by combining Eqs. (5.1), (5.6) and (5.7). The results in matrix notation are

$$\begin{bmatrix} \boldsymbol{M}+\boldsymbol{M}' & \boldsymbol{M}_{DT} \\ \boldsymbol{M}_{TD} & \boldsymbol{M}_T \end{bmatrix} \begin{Bmatrix} \ddot{\boldsymbol{u}} \\ \ddot{\boldsymbol{u}}_T \end{Bmatrix} + \begin{bmatrix} \boldsymbol{C} & [\boldsymbol{0}]_{3N\text{x}4} \\ [\boldsymbol{0}]_{4\text{x}3N} & \boldsymbol{C}_T \end{bmatrix} \begin{Bmatrix} \dot{\boldsymbol{u}} \\ \dot{\boldsymbol{u}}_T \end{Bmatrix}$$
$$+ \begin{bmatrix} \boldsymbol{K} & [\boldsymbol{0}]_{3N\text{x}4} \\ [\boldsymbol{0}]_{4\text{x}3N} & \boldsymbol{K}_T \end{bmatrix} \begin{Bmatrix} \boldsymbol{u} \\ \boldsymbol{u}_T \end{Bmatrix} = -\begin{Bmatrix} \boldsymbol{M}\boldsymbol{r}_g \\ \boldsymbol{M}_T\boldsymbol{r}_T \end{Bmatrix} \ddot{u}_g \tag{5.11}$$

where the matrices

$$\boldsymbol{M}_T = \text{diag}\begin{pmatrix} m_{x_1} & m_{x_2} & m_{y_3} & m_{y_4} \end{pmatrix} \tag{5.12}$$

$$\boldsymbol{C}_T = \text{diag}\begin{pmatrix} \dfrac{\rho A_{x_1}\xi_{x_1}(t)\left|\dot{x}_1(t)\right|}{2} & \dfrac{\rho A_{x_2}\xi_{x_2}(t)\left|\dot{x}_2(t)\right|}{2} & \dfrac{\rho A_{y_3}\xi_{y_3}(t)\left|\dot{y}_3(t)\right|}{2} & \dfrac{\rho A_{y_4}\xi_{y_4}(t)\left|\dot{y}_4(t)\right|}{2} \end{pmatrix} \tag{5.13}$$

$$\boldsymbol{K}_T = \text{diag}\begin{pmatrix} k_{x_1} & k_{x_2} & k_{y_3} & k_{y_4} \end{pmatrix} \tag{5.14}$$

are the mass, equivalent damping, and equivalent stiffness matrices of the TLCD system; $\boldsymbol{u}_T = \begin{bmatrix} x_1 & x_2 & y_3 & y_4 \end{bmatrix}^{\mathrm{T}}$ is the vector containing the vertical displacements of the liquid in the four TLCDs. The ground influence vector associated with TLCDs is represented by $\boldsymbol{r}_T$ as

$$\boldsymbol{r}_T = \begin{bmatrix} \cos\beta & \cos\beta & \sin\beta & \sin\beta \end{bmatrix}^{\mathrm{T}} \tag{5.15}$$

The mass coupling matrices $\boldsymbol{M}_{DT}$ and $\boldsymbol{M}_{TD}$ and the mass contribution of TLCDs to the structural mass matrix represented by $\boldsymbol{M}'$ are

$$\boldsymbol{M}_{DT} = \begin{bmatrix} [\boldsymbol{0}]_{(3N-3)\text{x}4} \\ \begin{bmatrix} \alpha_{x_1} m_{x_1} & \alpha_{x_2} m_{x_2} & 0 & 0 \\ 0 & 0 & \alpha_{y_3} m_{y_3} & \alpha_{y_4} m_{y_4} \\ -\alpha_{x_1} m_{x_1} d_{y_1} & -\alpha_{x_2} m_{x_2} d_{y_2} & \alpha_{y_3} m_{y_3} d_{x_3} & \alpha_{y_4} m_{y_4} d_{x_4} \end{bmatrix}_{3\text{x}4} \end{bmatrix} \tag{5.16}$$

$$\boldsymbol{M}_{TD} = \boldsymbol{M}_{DT}^{T} \tag{5.17}$$

$$\boldsymbol{M'} = \begin{bmatrix} [\boldsymbol{0}]_{(3N-3)\text{x}(3N-3)} & [\boldsymbol{0}]_{(3N-3)\text{x}3} \\ [\boldsymbol{0}]_{3\text{x}(3N-3)} & \begin{bmatrix} M'_{11} & 0 & 0 \\ 0 & M'_{22} & 0 \\ 0 & 0 & M'_{33} \end{bmatrix}_{3\text{x}3} \end{bmatrix} \tag{5.18}$$

where

$$M'_{11} = m_{x_1} + m_{x_2} + m_{y_3} + m_{y_4} \tag{5.19}$$

$$M'_{22} = M'_{11} \tag{5.20}$$

$$M'_{33} = I_{x_1} + I_{x_2} + I_{y_3} + I_{y_4} \tag{5.21}$$

in which I_{x_1} and I_{x_2} are the inertia moments of the liquid in $TCLD_1$ and $TLCD_2$ in the *x*-direction relative to the mass center of the roof floor; and I_{y_3} and I_{y_4} are the inertia moments of the liquid in $TCLD_3$ and $TLCD_4$ in the *y*-direction relative to the mass center of the roof floor (Figure 5.1(b)).

5.3 Optimal Control Of 3D Irregular Buildings Equipped With Hybrid Damper-TLCD System

The wavelet-hybrid feedback LMS control algorithm, presented in Chapter 3, is employed to find optimum control forces. The following presents the major steps involved in the wavelet-based optimal control of 3D irregular buildings equipped with a hybrid damper-TLCD system.

Step 1. Construct a finite element model of the building and obtain the dynamic characteristics of the building structure such as natural frequencies and mode shapes.

Step 2. Determine the design parameters of semi-active TLCD (mass ratio, tuning ratio, and the maximum value of the head loss coefficient) and passive dampers (required damping ratios and configuration). The detailed procedure involved in the determination of the design parameters is summarized in Chapter 4.

Step 3. Design the wavelet-based low-pass filter. This includes the selection of the family of the wavelet, determination of number of vanishing moment for selected wavelet, and the level of filtering. For fast and real time implementation the wavelet needs to be orthogonal. Wavelets with larger numbers of vanishing moments produce better frequency locality and therefore better controllability but require more computer processing power. On the other hand, wavelets with fewer numbers of vanishing moments produce less vibration suppression due to their poor frequency locality. The level of wavelet low-pass filtering is chosen such that the cutoff frequency is greater than the largest significant natural frequency of the structure.

Step 4. Design the feedback controller. For the feedback controller in the control algorithm, either LQR or LQG algorithm (Soong, 1990, Adeli and Saleh, 1997, 1999, Christenson et al., 2003, Connor, 2003) can be used.

Step 5. Integrate the feedback controller (LQR or LQG) with the filtered-x LMS controller and estimate the control force-to-output relationship of the system using the FIR filter in the offline LMS implementation.

Step 6. Construct the optimal controller by integrating the feedback-LMS controller created in Step 5 with the wavelet low-pass filter designed in Step 3. The wavelet low-pass filter must be arranged such that the wavelet filtering of the external excitation affects only the filtered-x LMS adaptive controller and not the feedback controller. This is because the wavelet low-pass filter is primarily used for eliminating higher frequency components of the external excitation which impede the stabilization of the FIR filter coefficients. Further, the input to the feedback controller needs to be the response of the structural system subjected to unfiltered signals.

5.4 Examples

Two multistory moment-resisting building structures are investigated in this chapter, representing two types of irregular building configurations – plan and vertical irregularities – as defined in the International Building Code (IBC, 2000). They are designed according to the American Institute of Steel Construction (AISC) Load and Resistance Factor Design (LRFD) specifications (AISC, 1998) for the combination of static dead and live loads and the lateral loads obtained by the equivalent linear static load procedure described in IBC (2000).

For dynamic analysis, the building structures are modeled with finite elements. Columns and beams are modeled as three-dimensional frame elements with two end nodes. The floor slab is modeled with four-node plane elements. The floor elements are used for generating the floor mass only and their stiffness contributions are ignored due to the rigid diaphragm modeling assumption mentioned earlier. Each node has six (three displacements and three rotations) DOFs. The same three simulated earthquake ground accelerations used in Chapter 4 are employed.

5.4.1 Example 1

This is a 12-story moment-resisting steel frame with a vertical setback on the fifth floor and a height of 54 m as shown in Figure 5.2. The example was first introduced in the literature by Adeli and Saleh (Saleh and Adeli, 1998; Adeli and Saleh, 1999) for study of active control of structures. The same geometry and the static loadings are employed here. The structure has 148 members, 77 nodes, and 462 DOFs prior to applying boundary conditions, rigid diaphragm constraints, and the dynamic condensation. Applying boundary conditions and rigid diaphragm constraints results in

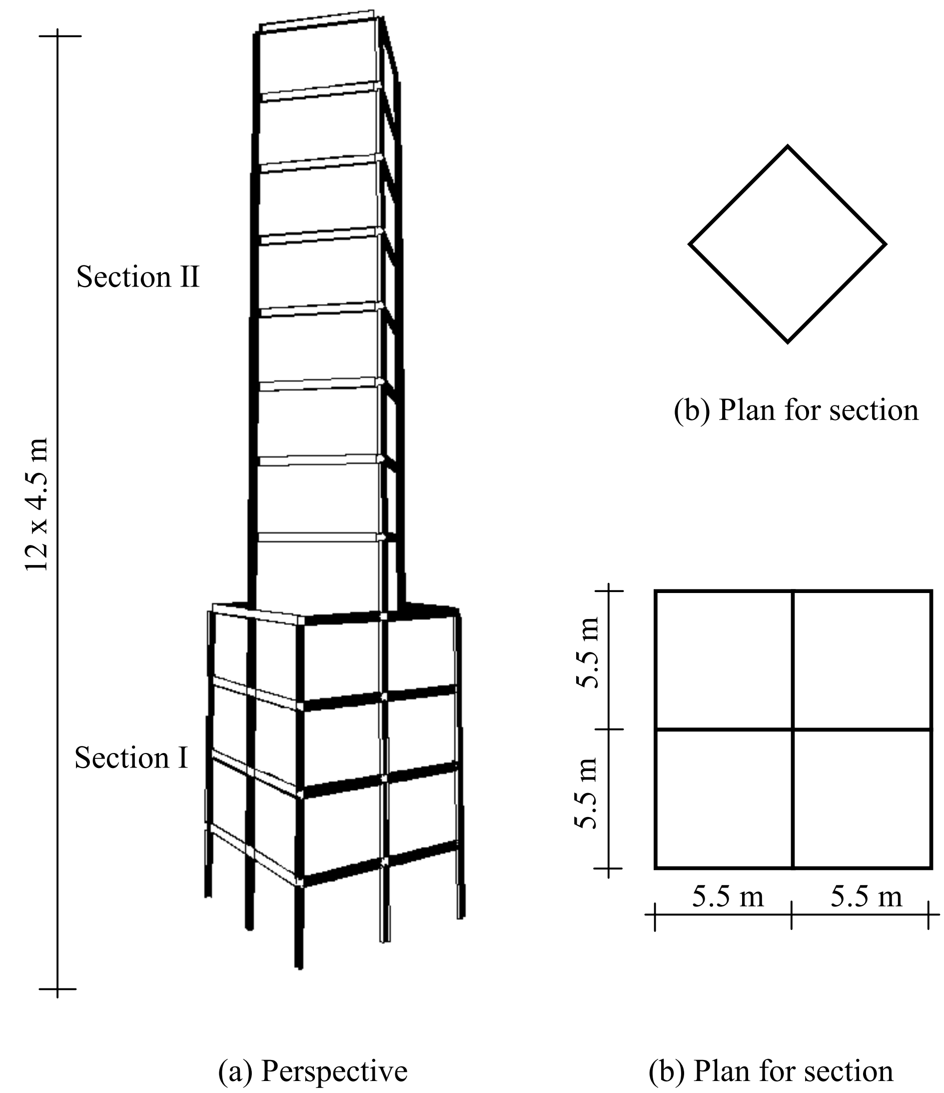

Figure 5.2: Example 1: Twelve-story moment-resisting steel frame with a vertical setback (adapted from Adeli and Saleh, 1999)

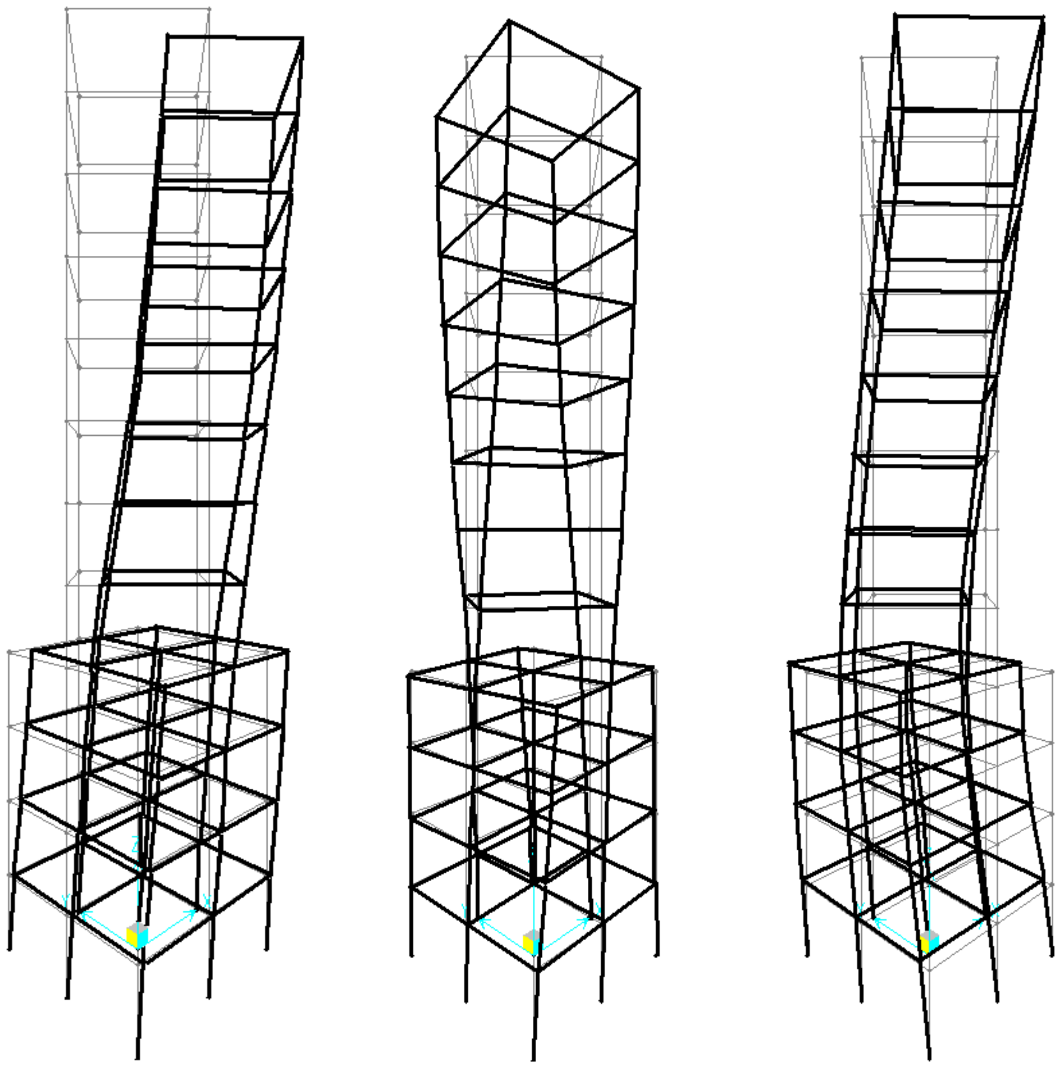

(a) (b) (c)

Figure 5.3: Mode shapes for the twelve-story structure: (a) modes 1 (frequency = 0.564 Hz) and 2 (frequency = 0.583 Hz), (b) mode 3 (frequency = 0.690 Hz), (c) modes 4 (frequency = 1.25 Hz) and 5 (frequency = 1.30 Hz)

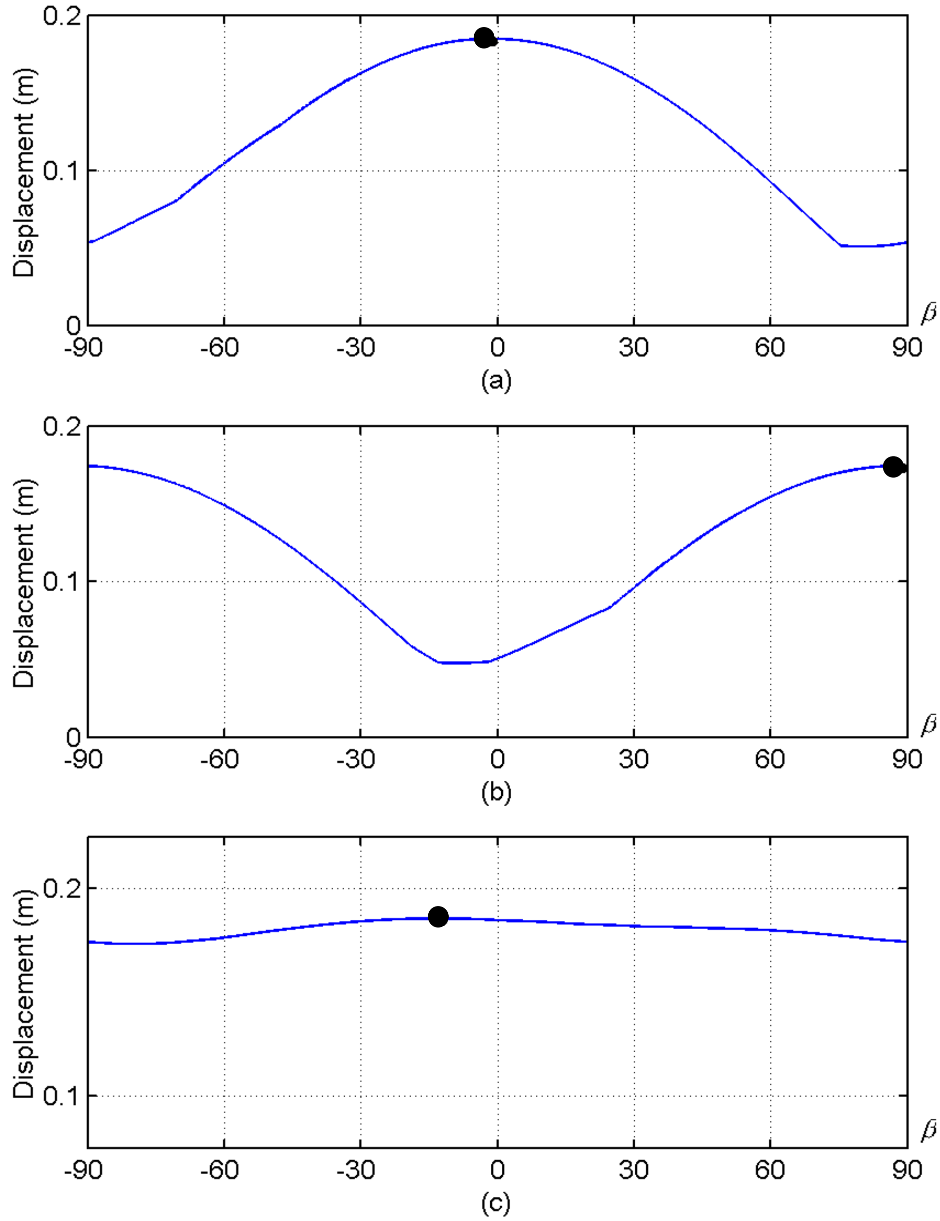

Figure 5.4: Top floor displacements of the 12-story structure subjected to EQ-I as a function of the angle of incidence of the ground acceleration: (a) maximum displacement in *x*-direction, (b) maximum displacement in *y*-direction, (c) the largest RMS value of displacements in *x*- and *y*-directions

240 DOFs. They are further reduced to 36 DOFs by the Guyan reduction of vertical DOFs and rotational DOFs about two horizontal axes (Craig, 1981).

The static loading on the building consists of uniformly distributed floor dead and live loads of 2.88 Kpa (60 psf) and 2.38 Kpa (50 psf), respectively. A total lateral force (base shear) of 243 KN is obtained and distributed over the height of the structure using the equivalent linear static load approach provided by IBC (2000). Each floor shear force is distributed to the nodes in that floor in proportion to nodal masses.

A damping ratio of 2% is used for each mode. The first five mode shapes of this example are presented in Figure 5.3. The shape of the first mode with a frequency of 0.564 Hz is almost identical to the second mode shape with a frequency of 0.583 Hz except for their directions because the building is symmetric in plan. Thus, the first two mode shapes are shown in one figure (Figure 5.3(a)). Similarly, the shapes of the fourth and fifth modes are almost identical except for their directions and therefore presented in one figure (Figure 5.3(c)). Even though the building is symmetric in the plan, the story stiffnesses are different in two principal directions because columns are wide-flange shapes with unequal cross-sectional moments of inertia with respect to their principal axes. Thus, the centers of mass and resistance (or rigidity) in each floor do not coincide, resulting in coupling of torsional and lateral vibrations of the building.

Figure 5.4 shows top floor displacements of the structure subjected to EQ-I as a function of the angle of incidence of the ground acceleration (β) in the range of -90° to 90°. Figures 5.4(a) and 5.4(b) show the maximum displacement in the *x*- and *y*-directions, respectively. Figure 5.4(c) shows the largest RMS value of displacements in the *x*- and *y*-

directions. The coupling effect of lateral and torsional vibrations is observed in Figure 5.4. If there were no coupling the maximum displacements in the x- and y-directions would be at β = 0° and 90°, respectively. However, as noted in Figure 5.4, the maximum displacements in the x- and y-directions occur at β = -1.7° and 88.1°, respectively. These values are near 0° and 90°, respectively, because the structure is symmetric in the plan and centers of mass and resistance are close to each other. The incidence angles that produce the largest displacements are identified with bullets in Figure 5.4. The largest RMS value of the x- and y-displacements of the top floor occurs at β = -13.0° even though the maximum displacements in x- and y-directions occur near 0° and 90°, respectively. The 2D dynamic analysis of this building in x- or y-direction underestimates the maximum response of the structure by up to 4%. Thus, a 3D dynamic analysis needs to be performed in order to obtain more accurate results.

To design a hybrid damper-TLCD control system for a 3D building structure, two parallel sets of TLCDs are used, as noted earlier and shown in Figure 5.1. The same TLCD unit is used in each direction. But, different TLCDs with different parameters are used in perpendicular directions. For the x-direction the following values are used for the TLCD parameters: mass ratio μ = 0.02, tuning ratio f = 0.975, maximum head loss coefficient ξ_{max}, = 30, and liquid tube width-to-length ratio α = 0.9. In this work, viscous fluid dampers are used in the form of diagonal or Chevron bracings but without providing any additional stiffness (Hanson and Soong, 2001). Dampers are chosen such that the damping ratio for the fundamental mode of the structure including its intrinsic damping is increased to 5 percent.

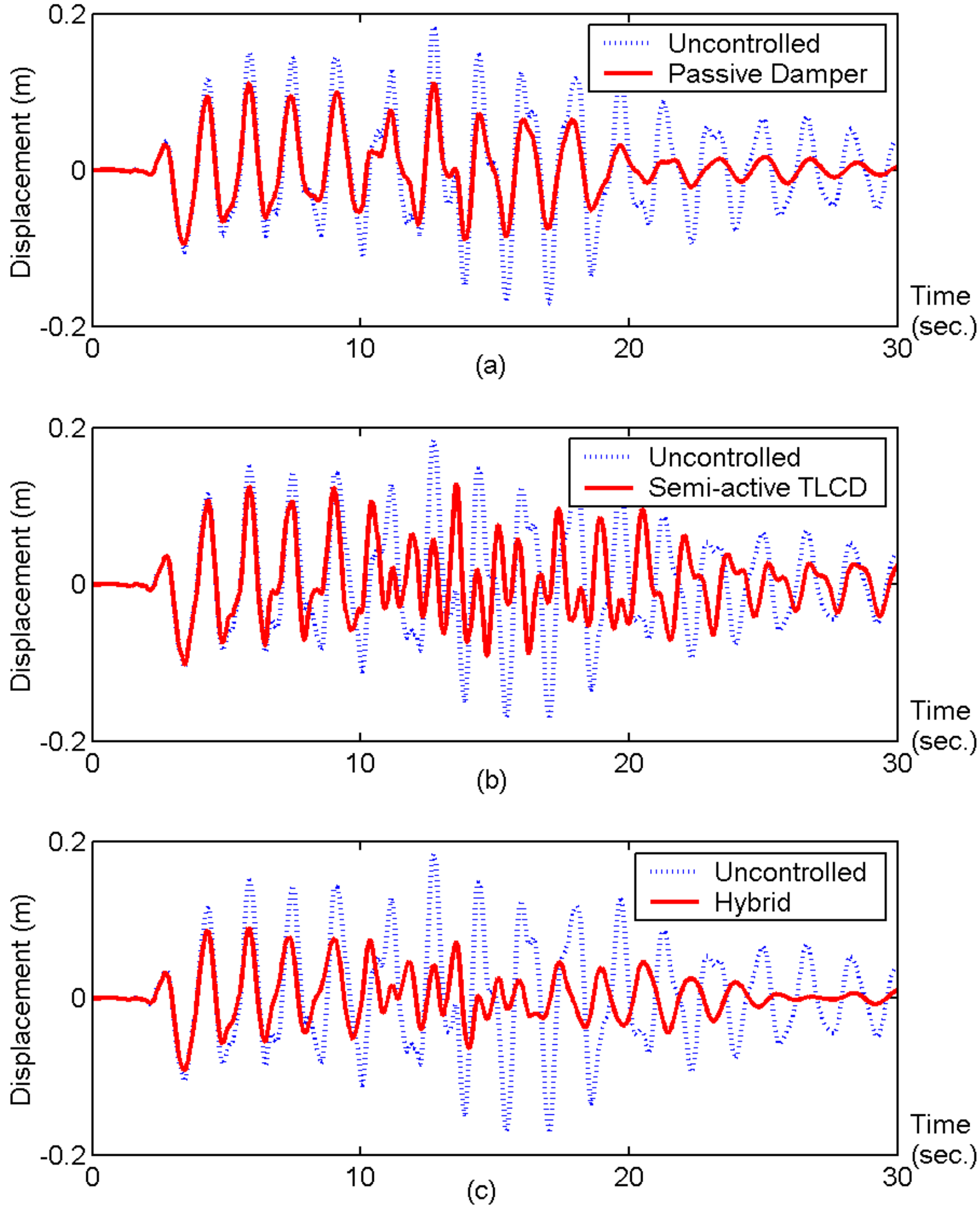

Figure 5.5: Time histories of the top floor displacement of the 12-story structure subjected to EQ-I in *x*-direction using three controlled systems: (a) passive damper system, (b) semi-active TLCD system, (c) hybrid damper-TLCD system

Figure 5.5 shows the time histories of the top floor displacement of the structure subjected to EQ-I in x-direction using three controlled systems: (a) passive damper system, (b) semi-active TLCD system, (c) hybrid damper-TLCD system. These responses are obtained when the earthquake motion is applied in the x-direction (β = 0°) and assuming only the two TLCDs parallel to the x-axis are installed. It is observed from Figure 5.5 that the combination of passive damper and semi-active TLCD systems reduces the response substantially and maximizes the control performance by acting complementary to each other. Further, the integration of a passive supplementary damping system with a semi-active TLCD system provides increased reliability and maximum operability during power failure as described in Chapter 4.

For the 3D control of the structure, values of the damping coefficient for supplementary dampers and the design parameters for the TLCD system in the y-direction are chosen similar to those chosen for the x-direction because the structure is doubly symmetric in the plan. The values of TLCD masses and tuning ratios, however, are chosen slightly differently to take into account the difference in the stiffnesses of the structure in x- and y-directions. The resulting top floor displacement responses of the example structure subjected to EQ-I with β = -13.0° in x- and y-directions using the hybrid damper-TLCD system are presented in Figure 5.6. The earthquake incidence angle of β = -13.0° is used because it produces the largest RMS value of displacements in x- and y- directions in the simulation presented in Figure 5.4. Compared with the uncontrolled system, the hybrid damper-TLCD control system reduces the maximum displacement in x- and y-directions by 53% and 56%, respectively.

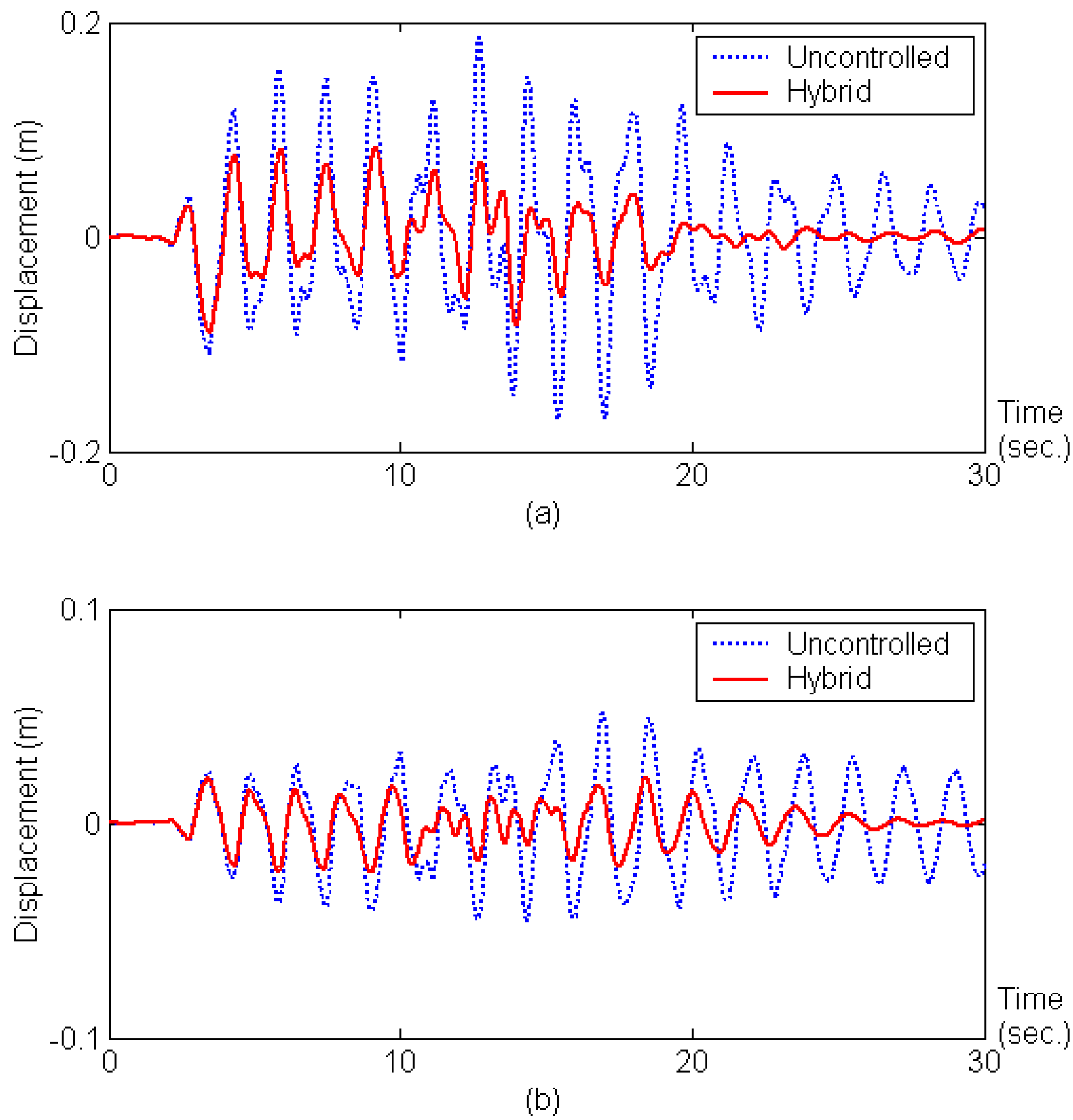

Figure 5.6: Top floor displacement responses of the 12-story structure subjected to EQ-I with β = -13.0° using the hybrid damper-TLCD system: (a) in the *x*-direction, (b) in the *y*-direction

The largest RMS acceleration and displacement responses of the top floor subjected to all three simulated earthquake ground accelerations with β = -13.0° are presented in Table 5.1. Compared with the uncontrolled system, the hybrid damper-TLCD control system reduces the RMS displacement by 46-50 % and RMS acceleration by 61-71%.

Earthquake	Response	Uncontrolled	Hybrid damper-TLCD controlled
EQ-I	Displacement Acceleration	4.18 cm 1.52 m/sec^2	2.10 cm 0.59 m/sec^2
EQ-II	Displacement Acceleration	5.86 cm 2.56 m/sec^2	3.17 cm 0.75 m/sec^2
EQ-III	Displacement Acceleration	7.43 cm 3.83 m/sec^2	3.93 cm 1.33 m/sec^2

Table 5.1: The largest RMS responses of top floor of the 12-story structure subjected to simulated earthquake ground accelerations EQ-I, EQ-II, and EQ-III with β = -13.0°

5.4.2 Example 2

This is an 8-story moment-resisting steel frame with a plan irregularity and a height of 36 m created in this study and shown in Figure 5.7. The structure has 208 members, 99 nodes, and 594 DOFs prior to applying boundary conditions, rigid diaphragm constraints, and the dynamic condensation. Applying boundary conditions and rigid diaphragm constraints results in 288 DOFs. They are further reduced to 24 DOFs by the Guyan reduction of vertical DOFs and rotational DOFs about two horizontal axes.

The static loading on the building consists of uniformly distributed floor dead and live load of 4.78 Kpa (100 psf) and 3.35 Kpa (70 psf), respectively. A total lateral force (base shear) of 963 KN is obtained and distributed over the height of the structure using the equivalent linear static load approach provided by IBC (2000). Each floor shear force is distributed to the nodes in that floor in proportion to nodal masses.

Because of plan irregularity substantially more translational and torsional coupling effect is expected in this example compared with the previous example. Figure 5.8 shows the top floor displacements of the first three modes of vibrations: (a) mode 1 with a frequency of 0.57 Hz, (b) mode 2 with a frequency of 0.72 Hz, (c) mode 3 with a frequency of 0.75 Hz (Displacements in this figure are magnified by 5). Figure 5.9 shows top floor displacements of the structure subjected to EQ-I as a function of the angle of incidence of the ground acceleration (β) in the range of -90° to 90°. Figures 5.9(a) and 5.9(b) show the maximum displacement in the x- and y-directions, respectively. Figure 5.9(c) shows the largest RMS value of displacements in the x- and y- directions.

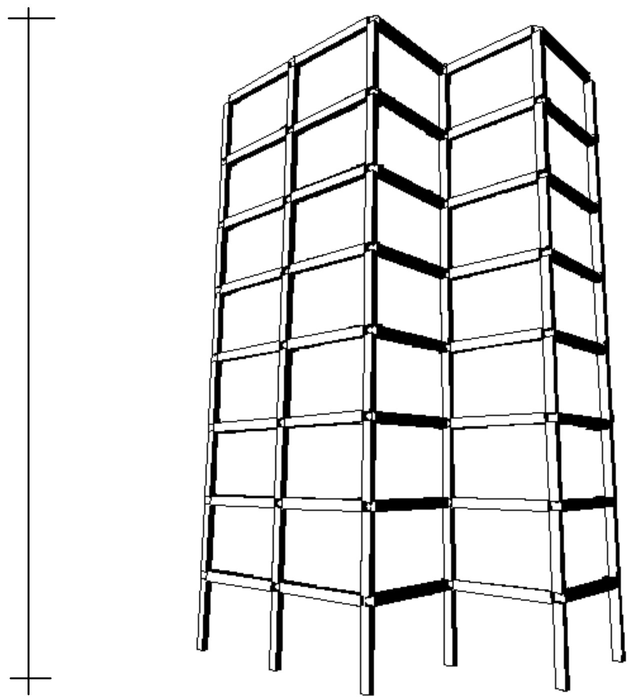

(a) Perspective view

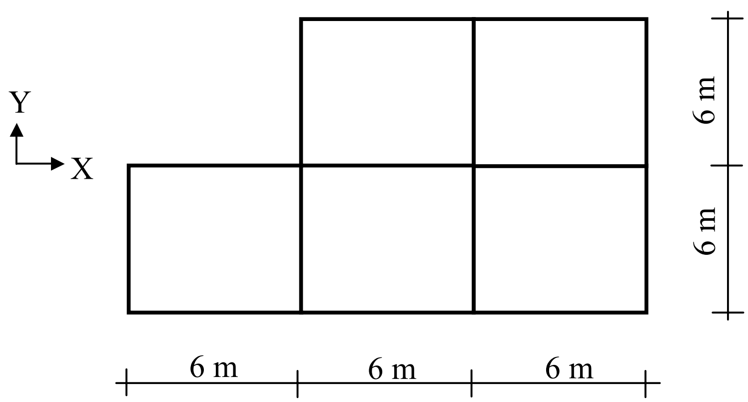

(b) Plan

Figure 5.7: Example 2: Eight-story moment-resisting steel frame with plan irregularity

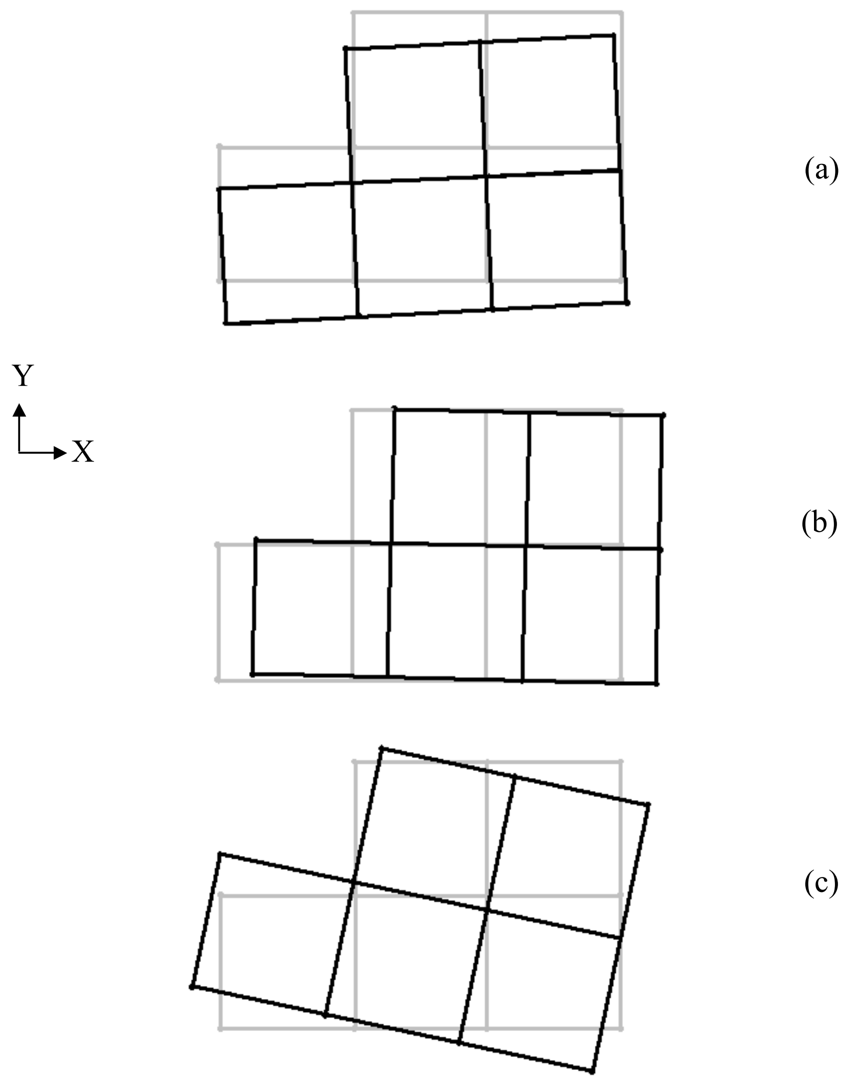

Figure 5.8: Top floor displacements of the first three modes of vibrations for the 8-story structure: (a) mode 1 (frequency = 0.57 Hz), (b) mode 2 (frequency = 0.72 Hz), (c) mode 3 (frequency = 0.75 Hz)

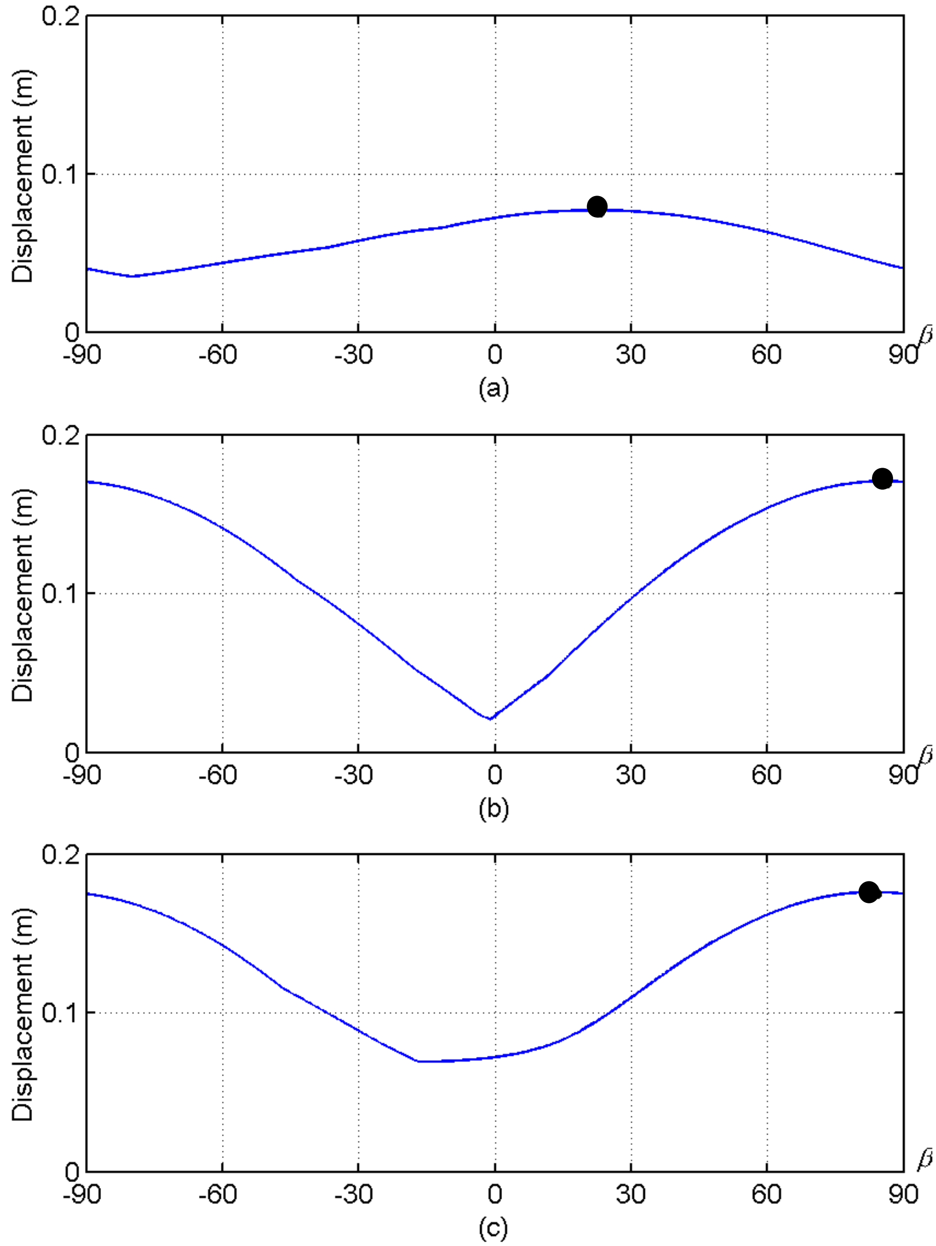

Figure 5.9: Top floor displacements of the 8-story structure subjected to EQ-I as a function of the angle of incidence of the ground acceleration: (a) maximum displacement in *x*-direction, (b) maximum displacement in *y*-direction, (c) the largest RMS value of displacements in *x*- and *y*- directions

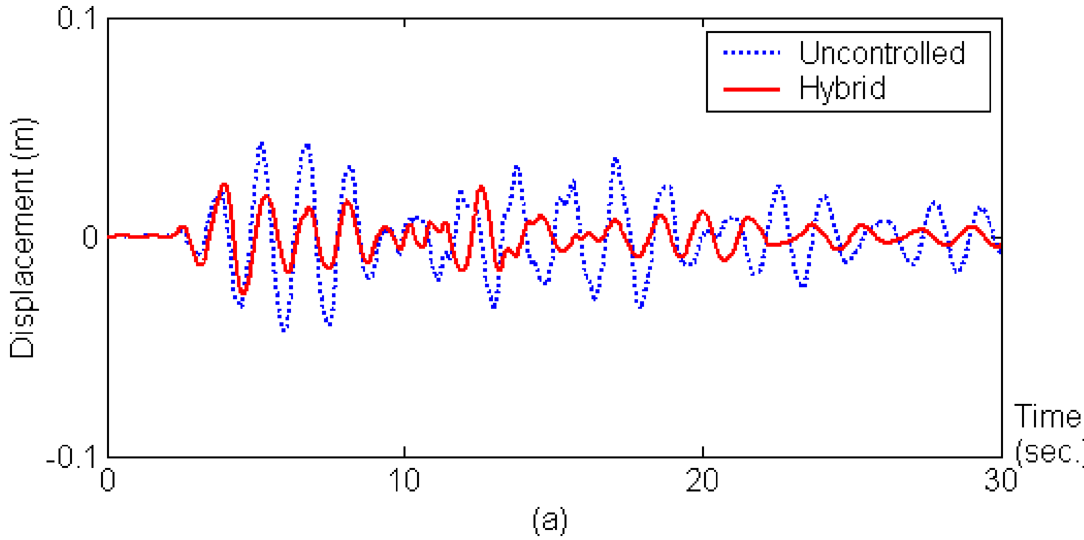

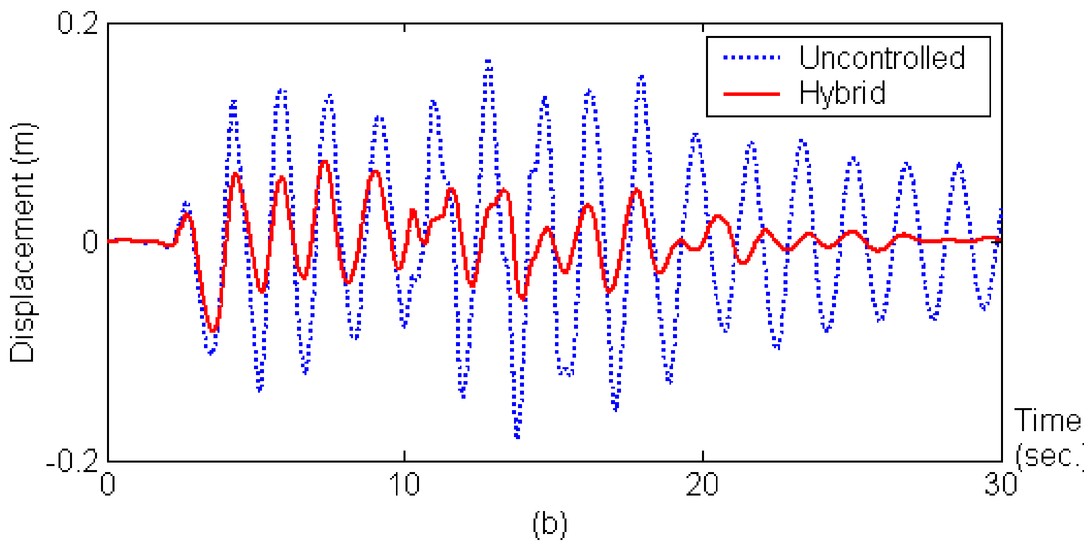

Figure 5.10: Top floor displacement responses of the 8-story structure subjected to EQ-I with $\beta = 83.4°$ using the hybrid damper-TLCD system: (a) in the x-direction, (b) in the y-direction

Substantial coupling effect of lateral and torsional vibrations is observed in Figure 5.9. The incidence angles that produce the largest displacements are identified with bullets. The maximum displacements in *x*- and *y*-directions occur at 22.4° and 85.6°, respectively. The largest RMS value of the *x*- and *y*-displacements of the top floor occurs at $\beta = 83.4°$. The 2D dynamic analysis of this building in *x*- or *y*-direction underestimates the maximum response of the structure by up to 7%. Thus, a 3D dynamic analysis needs to be performed in order to obtain more accurate results.

Earthquake	Response	Uncontrolled	Hybrid damper-TLCD controlled
EQ-I	Displacement Acceleration	4.28 cm 1.18 m/sec^2	1.85 cm 0.34 m/sec^2
EQ-II	Displacement Acceleration	6.98 cm 2.44 m/sec^2	3.11 cm 0.52 m/sec^2
EQ-III	Displacement Acceleration	11.1 cm 7.55 m/sec^2	3.70 cm 1.24 m/sec^2

Table 5.2: The largest RMS responses of top floor of the 8-story structure subjected to simulated earthquake ground accelerations EQ-I, EQ-II, and EQ-III with $\beta = 83.4°$

The top floor displacement responses of the structure subjected to EQ-I with β = 83.4° in the x- and y-directions using the hybrid damper-TLCD system are presented in Figure 5.10. The earthquake incidence angle of with β = 83.4° is used because it produces the largest RMS value of displacements in x- and y-directions in the simulation presented in Figure 5.9. Compared with the uncontrolled system, the hybrid damper-TLCD control system reduces the maximum displacement in x- and y-directions by 38% and 54%, respectively.

The largest RMS acceleration and displacement responses of the top floor subjected to all three simulated earthquake ground accelerations with β = 83.4° are presented in Table 5.2. Compared with the uncontrolled system, the hybrid damper-TLCD control system reduces the RMS displacement by 56-67 % and RMS acceleration by 71-84%.

5.5 Remarks

The hybrid damper-TLCD control system presented in Chapter 4 is further investigated for the control of 3D coupled irregular buildings under various seismic excitations using two multistory moment-resisting building structures with vertical and plan irregularities. The coupled equations of motion for the combined building and TLCD system are derived. Major steps involved in the wavelet-based optimal control of 3D irregular buildings equipped with a hybrid damper-TLCD system are delineated. Two pairs of parallel TLCDs placed along two principal directions of the structural plan are used to control the coupled lateral and torsional response of irregular multistory buildings.

Results of Tables 5.1 and 5.2 and Figures 5.6 and 5.10 clearly indicate that the hybrid damper-TLCD control system can significantly reduce the displacement as well as acceleration responses of 3D irregular buildings subjected to various earthquake ground motions. The same levels of response reduction are achieved for structures with plan and vertical irregularities.

CHAPTER 6

WIND-INDUCED MOTION CONTROL OF 76-STORY BENCHMARK BUILDING USING THE HYBRID DAMPER-TLCD SYSTEM

6.1 Introduction

In this chapter, the effectiveness of both semi-active TLCD system and the hybrid damper-TLCD control system, presented in Chapters 4 and 5, is further investigated for the control of wind-induced motion of high-rise buildings. Simulations are performed on the 76-story building benchmark control problem created by Yang et al. (2000) and described briefly in the next section. To evaluate the effectiveness of the control system against wind loading, wind loads obtained from wind tunnel tests (Yang et al., 2000) and the stochastic wind loads defined by the Davenport's cross-power spectral density matrix (Yang et al. 1998) are used. The performances of semi-active TLCD and hybrid damper-TLCD control systems are compared with that of a sample ATMD system presented in Yang et al. (2000).

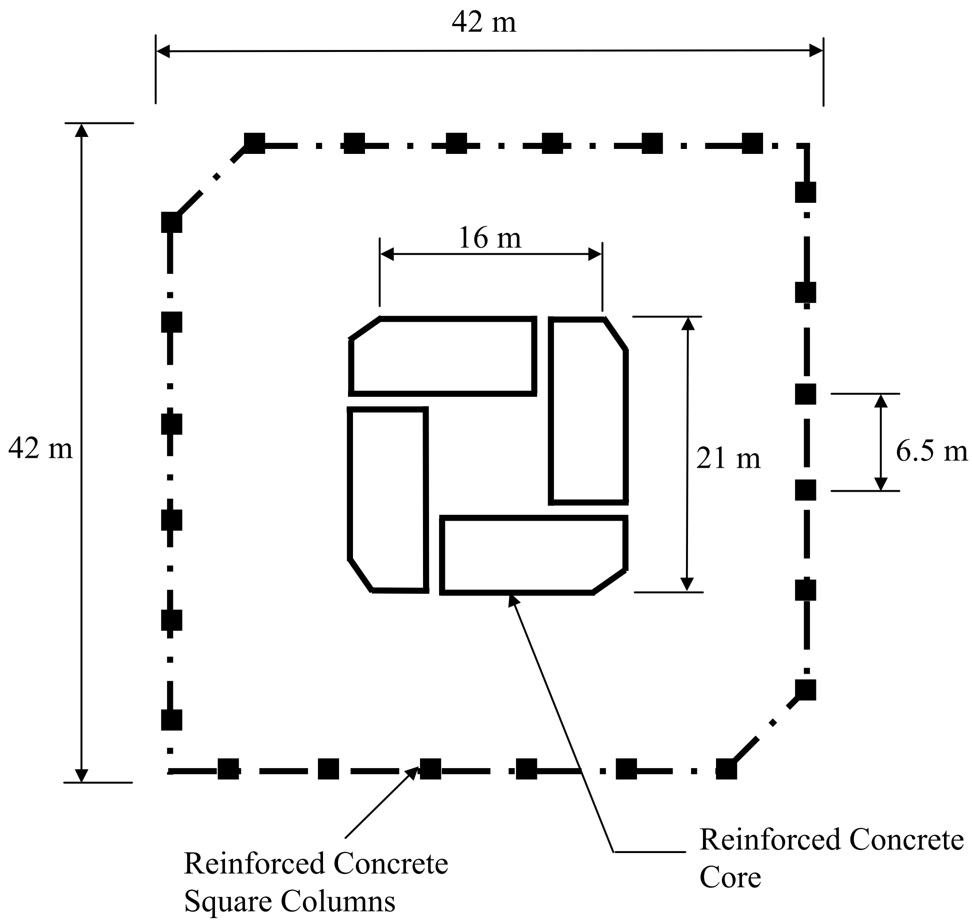

Figure 6.1: The plan sketch of the 76-story benchmark control problem

6.2 Benchmark Problem

The 76-story benchmark building is a 306-m high office tower with a height-to-width ratio of 7.3 proposed for the city of Melbourne, Australia. The plan of the structure is square with two cut corners (Figure 6.1). The building is a reinforced concrete building consisting of a concrete core and an exterior concrete frame. The typical story height is 3.9 m with the exception of the first floor which has a height of 10 m and stories 38 to 40 and 74 to 76 which have a height of 4.5 m. The building has a total mass including heavy machinery in the plant rooms of 153,000 metric tons. Structural analysis is performed in two dimensions based on the symmetric nature of the plan. The first three natural frequencies of the structure based on a two-dimensional structural analysis are 0.16 Hz, 0.765 Hz, and 1.992 Hz.

To evaluate the effectiveness of a control system against wind loading, wind force data obtained from wind tunnel tests are used (Yang et al., 2000). The results of the wind tunnel test are for a building model scale of 400:1 and a velocity scale of 3:1. From the data obtained, the first 900 seconds (15 minutes) of wind pressure data are used for the benchmark problem in this study. Figure 6.2 shows the first 5 minutes time histories of resulting wind loads on 66th and 70th floors, as examples.

As a sample control system, an ATMD system with a mass of 500 metric tons installed on the top floor is used. This represents about 45% of the top floor mass and 0.327% of the total mass of the building. The undamped natural frequency and the damping ratio of ATMD are set to 0.16 Hz and 20%, respectively. Per Yang et al. (2000),

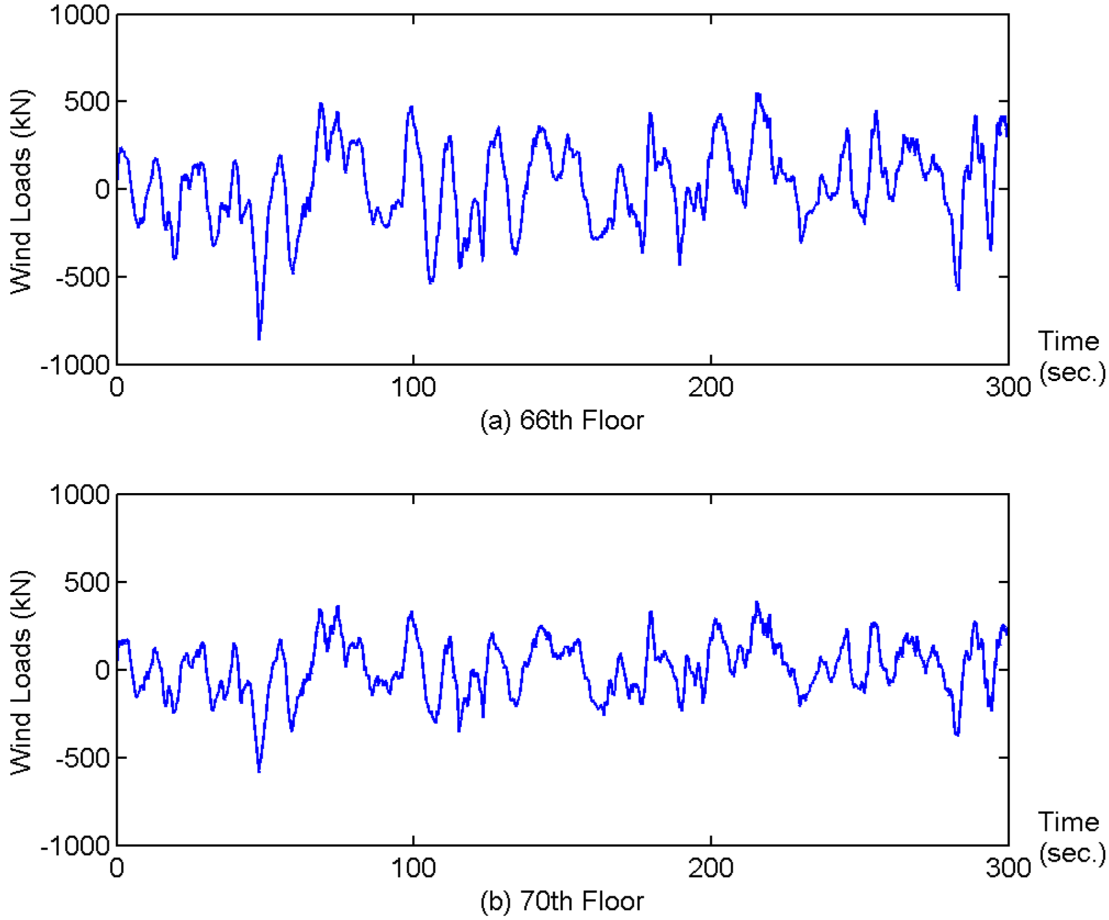

Figure 6.2: Time histories of wind tunnel test loads acting on 66th and 70th floors

the ATMD system is designed such that the peak and RMS (Root Mean Squared) floor accelerations are less than 15 cm/s^2 and 5 cm/s^2, respectively, considered as maximum allowable values for office buildings.

Eight out of twelve criteria proposed by Yang et al. (2000), denoted by J_1 to J_{12}, to evaluate control systems are used in this study. Smaller numbers for each criterion represent a more effective response control performance. The first six performance measures (J_1 to J_6) are RMS responses of the selected floors of the structure and actuator. The next six performance measures (J_7 to J_{12}) are the peak responses of the selected floors of the structure and actuator. Among the twelve criteria, only 8 criteria (J_1 to J_4 and J_7 to J_{10}) are used in this study, because the other four criteria (J_5, J_6, J_{11}, and J_{12}) represent the performance of actuator. Neither semi-active TLCD nor hybrid damper-TLCD system requires any actuator to operate, thus eliminating the need to use the other four criteria.

The first four criteria in terms of RMS responses are

$$J_1 = \max\left(\sigma_{\ddot{x}1},\ \sigma_{\ddot{x}30},\ \sigma_{\ddot{x}50},\ \sigma_{\ddot{x}55},\ \sigma_{\ddot{x}60},\ \sigma_{\ddot{x}65},\ \sigma_{\ddot{x}70},\ \sigma_{\ddot{x}75}\right)/\sigma_{\ddot{x}75\mathrm{o}} \tag{6.1}$$

$$J_2 = \frac{1}{6}\sum_i (\sigma_{\ddot{x}\mathrm{i}}/\sigma_{\ddot{x}\mathrm{io}}) \qquad \text{for } i = 50, 55, 60, 65{,}70 \text{ and } 75 \tag{6.2}$$

$$J_3 = \sigma_{x76}/\sigma_{x76o} \qquad \text{for } i = 50, 55, 60, 65{,}70, 75 \text{ and } 76 \tag{6.3}$$

$$J_4 = \frac{1}{7}\sum_i (\sigma_{xi}/\sigma_{xio}) \qquad \text{for } i = 50, 55, 60, 65{,}70, 75 \text{ and } 76 \tag{6.4}$$

where $\sigma_{\ddot{x}i}$ is the RMS acceleration of the ith floor; $\sigma_{\ddot{x}75o}$ is the RMS acceleration of the 75th floor without control which is equal to $9.142\,\mathrm{cm/sec}^2$; $\sigma_{\ddot{x}io}$ is the RMS acceleration of the ith floor without control; σ_{xi} and σ_{xio} are the RMS displacements of the ith floor with and without control, respectively; σ_{x76o} is the RMS displacement of the 76th floor of the uncontrolled building which is equal to 10.137 cm. The values for RMS responses without control are given in the second and third columns of Table 6.1.

The next four criteria in terms of peak responses are

$$J_7 = \max\left(\ddot{x}_{p1},\ \ddot{x}_{p30},\ \ddot{x}_{p50},\ \ddot{x}_{p55},\ \ddot{x}_{p60},\ \ddot{x}_{p65},\ \ddot{x}_{p70},\ \ddot{x}_{p75}\right) \Big/ \ddot{x}_{p75o} \tag{6.5}$$

$$J_8 = \frac{1}{6}\sum_i (\ddot{x}_{pi} / \ddot{x}_{pio}) \qquad \text{for } i = 50, 55, 60, 65{,}70 \text{ and } 75 \tag{6.6}$$

$$J_9 = x_{p76} / x_{p76o} \tag{6.7}$$

$$J_{10} = \frac{1}{7}\sum_{\mathrm{i}} (x_{pi} / x_{pio}) \qquad \text{for } i = 50, 55, 60, 65{,}70, 75 \text{ and } 76 \tag{6.8}$$

where $\ddot{x}_{pi}$ and $\ddot{x}_{pio}$ are the peak acceleration of ith floor with and without control, respectively; x_{pi} and x_{pio} are the peak displacements of ith floor with and without control, respectively; x_{p76o} is the peak displacement of the 76th floor without control which is equal to 32.30 cm and $\ddot{x}_{p75o}$ is the peak acceleration of the 75th floor without control which is equal to 30.33 cm/sec^2. The values for peak responses without control are given in the second and third columns of Table 6.2.

6.3 Semi-Active TLCD System

When a multi-degree of freedom (MDOF) system with a passive TLCD system (Figure 6.3) is subjected to dynamic wind loading, the equations of motion are

$$\begin{bmatrix} \boldsymbol{M}+\boldsymbol{M}' & \boldsymbol{M}_{ST} \\ \boldsymbol{M}_{TS} & m_T \end{bmatrix} \begin{Bmatrix} \ddot{\boldsymbol{u}}(t) \\ \ddot{u}_T(t) \end{Bmatrix} + \begin{bmatrix} \boldsymbol{C} & [\boldsymbol{0}]_{m\text{x}1} \\ [\boldsymbol{0}]_{1\text{x}m} & c(t) \end{bmatrix} \begin{Bmatrix} \dot{\boldsymbol{u}}(t) \\ \dot{u}_T(t) \end{Bmatrix} + \begin{bmatrix} \boldsymbol{K} & [\boldsymbol{0}]_{m\text{x}1} \\ [\boldsymbol{0}]_{1\text{x}m} & 2\rho A g \end{bmatrix} \begin{Bmatrix} \boldsymbol{u}(t) \\ u_T(t) \end{Bmatrix} = -\begin{Bmatrix} \boldsymbol{F}(t) \\ 0 \end{Bmatrix} \tag{6.9}$$

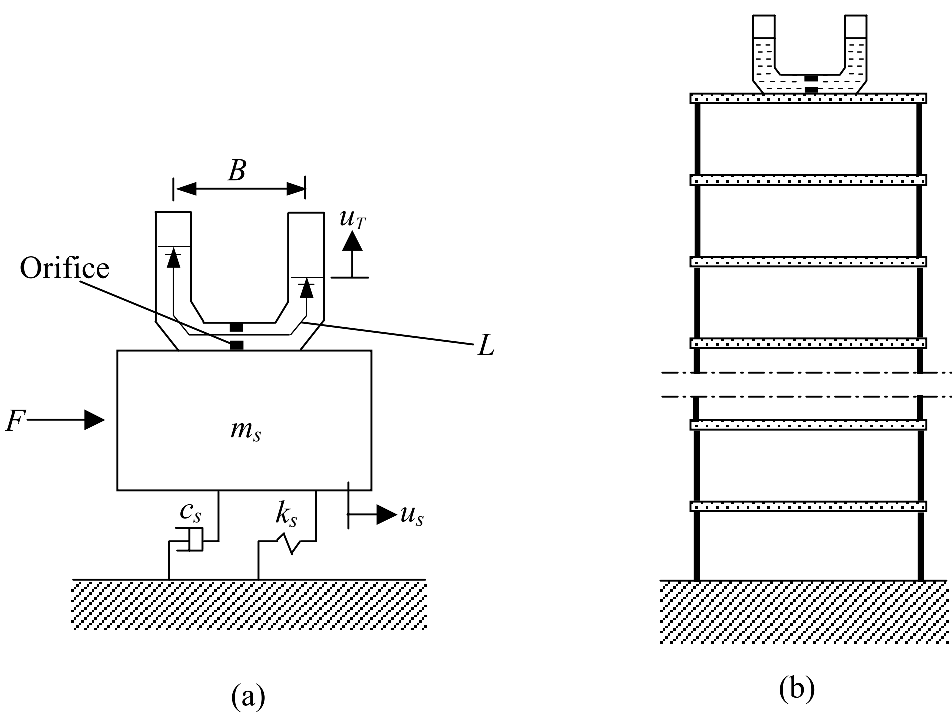

Figure 6.3: TLCD System: a) a SDOF system with a TLCD system b) a TLCD system installed on the roof of a multistory building structure

where mass coupling matrices $\boldsymbol{M}_{ST}$ and $\boldsymbol{M}_{TS}$ and the mass contribution of TLCD to the primary system mass matrix represented by $\boldsymbol{M'}$ are given in Chapter 5.

For a MDOF structure with a semi-active TLCD system subjected to dynamic wind loading, the head loss coefficient $\xi(t)$ in Eq. (6.10) can be changed by a controllable orifice, and Eq. (6.9) can be re-written with an additional term on the right-hand side as

$$\begin{bmatrix} \boldsymbol{M}+\boldsymbol{M'} & \boldsymbol{M}_{ST} \\ \boldsymbol{M}_{TS} & m_T \end{bmatrix} \begin{Bmatrix} \ddot{\boldsymbol{u}}(t) \\ \ddot{u}_T(t) \end{Bmatrix} + \begin{bmatrix} \boldsymbol{C} & [\boldsymbol{0}]_{m\text{x}1} \\ [\boldsymbol{0}]_{1\text{x}m} & 0 \end{bmatrix} \begin{Bmatrix} \dot{\boldsymbol{u}}(t) \\ \dot{u}_T(t) \end{Bmatrix} + \begin{bmatrix} \boldsymbol{K} & [\boldsymbol{0}]_{m\text{x}1} \\ [\boldsymbol{0}]_{1\text{x}m} & 2\rho A g \end{bmatrix} \begin{Bmatrix} \boldsymbol{u}(t) \\ u_T(t) \end{Bmatrix}$$
$$= -\begin{Bmatrix} \boldsymbol{F}(t) \\ 0 \end{Bmatrix} + \begin{Bmatrix} [\boldsymbol{0}]_{m\text{x}1} \\ 1 \end{Bmatrix} f_c(t) \tag{6.10}$$

For the numerical simulation of both passive and semi-active TLCD systems, the same mass of 500 tons as the mass of sample ATMD provided by Yang et al. (2000) is used. The optimum tuning ratio is calculated as 0.974 following Yalla and Kareem (2000). The head loss coefficient ξ of 30 is used for the passive TLCD system, and the values of minimum and maximum head loss coefficients, $\xi_{\min}$ and $\xi_{\max}$, for the semi-active TLCD system is set to be 0 and 50, respectively. The procedure for selection of these numbers is described in Chapter 4 as part of the general model for design of the proposed hybrid damper-TLCD system.

Figure 6.4 shows the comparison of the displacement frequency responses of the 75th floor for the uncontrolled, passive TLCD, and semi-active TLCD systems in the region of the first three natural frequencies of the primary structure. In Figure 6.4, the frequency responses of the uncontrolled and passive TLCD systems near the second and third natural frequencies of the primary system virtually coincide and therefore are indistinguishable. On the other hand, the semi-active TLCD system reduces the responses at every natural frequency. This is because the value of the head loss coefficient is tuned and fixed for the fundamental frequency of the building in the passive TLCD system, while the value varies optimally according to the frequency content of the external force in the semi-active TLCD system.

The RMS displacement and acceleration responses of the selected floors for the sample ATMD and passive and semi-active TLCD systems are presented in Table 6.1 along with the results for the uncontrolled structure. The corresponding peak responses are presented in Table 6.2. It is observed that significant improvement is made when the TLCD system operates semi-actively. While the peak and RMS values of 75th floor accelerations are greater than the maximum allowable values, 15 cm/s^2 and 5 cm/s^2, by 28% and 4%, respectively, for the passive TLCD system, the corresponding values for the semi-active TLCD system are 6% and 18% less than the maximum allowable values, respectively.

The results for the evaluation criteria J_1 to J_4 and J_7 to J_{10} for the sample ATMD and the passive and semi-active TLCD systems are presented in Table 6.3. The results of Table 6.3 indicate that the sample ATMD system produces better results for criteria J_1, J_2, J_7, and J_8. In contrast, the semi-active TLCD system outperforms the sample ATMD system for criteria, J_3, J_4, J_9, and J_{10}. As such, it is concluded that the performance of the semi-active TLCD system is roughly comparable to that of the ATMD system.

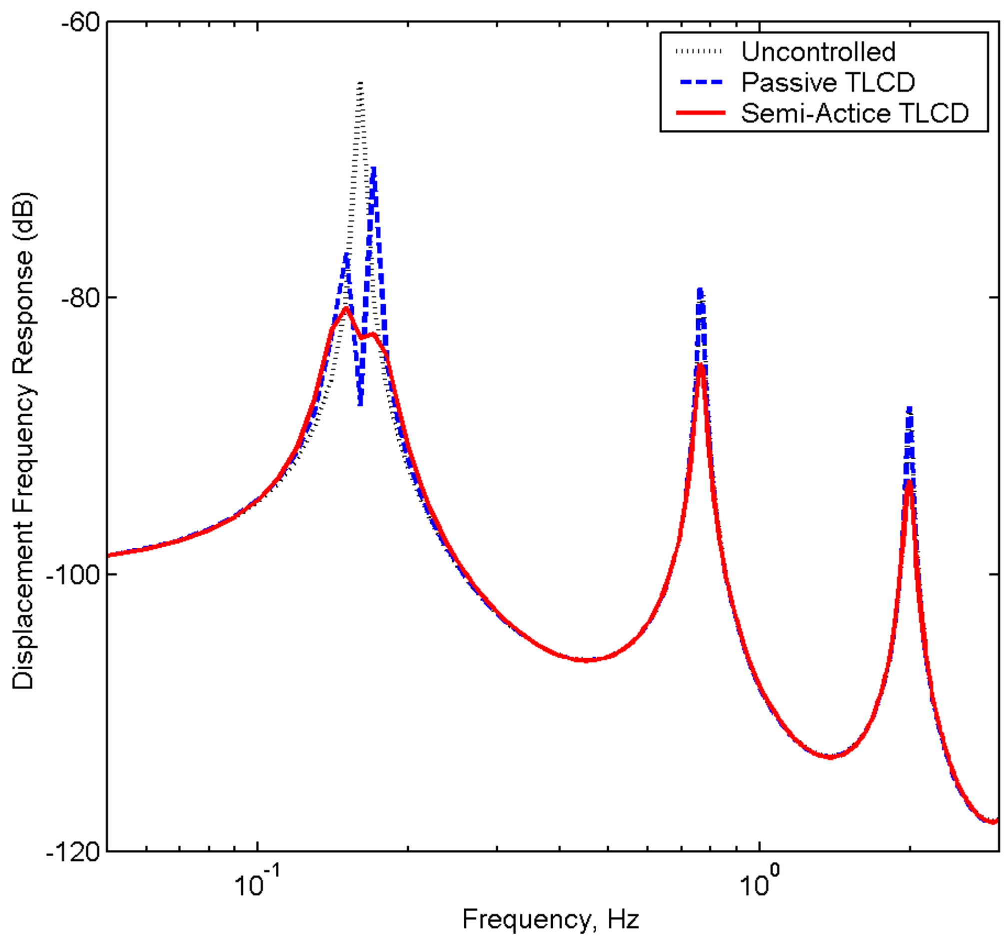

Figure 6.4: Displacement frequency responses of the 75th floor for the uncontrolled, passive TLCD, and semi-active TLCD systems

Floor No.	No control		ATMD		Passive TLCD		Semi-Active TLCD	
	Displacement (cm)	Acceleration (cm/s^2)	Displacement (cm)	Acceleration (cm/s^2)	Displacement (cm)	Acceleration (cm/s^2)	Displacement (cm)	Acceleration (cm/s^2)
1	0.02	0.06	0.01	0.06	0.01	0.06	0.01	0.06
30	2.15	2.02	1.26	0.89	1.39	1.15	1.26	0.97
50	5.22	4.78	3.04	2.03	3.36	2.52	3.03	2.08
55	6.11	5.59	3.55	2.41	3.93	2.90	3.54	2.41
60	7.02	6.42	4.08	2.81	4.51	3.28	4.07	2.73
65	7.97	7.31	4.62	3.16	5.11	3.78	4.61	3.13
70	8.92	8.18	5.17	3.38	5.72	4.31	5.16	3.52
75	9.92	9.14	5.74	3.34	6.36	5.17	5.72	4.11
76	10.14	9.35	5.86	4.70	6.50	4.62	5.85	4.01

Table 6.1: Comparison of RMS displacement and acceleration responses of the 76-story building

Floor No.	No control		ATMD		Passive TLCD		Semi-Active TLCD	
	Displacement (cm)	Acceleration (cm/s^2)	Displacement (cm)	Acceleration (cm/s^2)	Displacement (cm)	Acceleration (cm/s^2)	Displacement (cm)	Acceleration (cm/s^2)
1	0.05	0.22	0.04	0.23	0.04	0.22	0.04	0.23
30	6.84	7.14	5.14	3.38	5.31	4.45	4.93	3.75
50	16.59	14.96	12.22	6.73	12.63	8.24	11.72	7.41
55	19.42	17.48	14.29	8.05	14.71	9.61	13.65	8.48
60	22.34	19.95	16.27	8.93	16.84	11.04	15.63	9.64
65	25.35	22.58	18.36	10.06	19.02	13.01	17.65	11.16
70	28.41	26.04	20.48	10.67	21.22	15.29	19.69	12.43
75	31.59	30.33	22.67	11.56	23.49	19.15	21.80	14.10
76	32.30	31.17	23.15	15.89	24.00	17.15	22.27	14.68

Table 6.2: Comparison of peak displacement and acceleration responses of the 76-story building

RMS Responses				Peak Responses			
Criteria	ATMD	Passive TLCD	Semi-Active TLCD	Criteria	ATMD	Passive TLCD	Semi-Active TLCD
J_1	0.369	0.565	0.449	J_7	0.381	0.631	0.465
J_2	0.417	0.527	0.433	J_8	0.432	0.575	0.483
J_3	0.578	0.641	0.577	J_9	0.717	0.743	0.690
J_4	0.580	0.642	0.579	J_{10}	0.725	0.751	0.700

Table 6.3: Comparison of evaluation criteria for the passive and semi-active TLCD systems

6.4 Hybrid Damper-TLCD System

Agrawal and Yang (1999) present the use of passive dampers for control of the 76-story benchmark building. In their study, a unit damper with capacity of 3.2×10^5 N-sec/m is used, and the optimal distribution of dampers is determined using the Sequential Search Algorithm (SSA) (Zhang and Soong, 1992) and a so-called constrained linear quadratic regulator method. They report that both SSA and the constrained linear quadratic regulator method produce comparable control results. In the SSA method, additional dampers are added and their locations are determined until the responses of a selected floor, 75th floor, in the benchmark example are smaller than pre-defined values.

The responses of the sample ATMD system are used for the pre-defined values, and the wind loads applied to the building are stochastic signals defined by the Davenport's cross-power spectral density matrix (Yang et al., 1998). They conclude that the passive damper system can achieve the same level of performance as the sample ATMD system.

For the numerical simulation of the hybrid damper-TLCD system, the same parameters used for the semi-active TLCD and described in the previous section are employed. A unit viscous fluid damper with capacity of 3.2×10^5 N-sec/m is used and the locations of passive dampers are determined using the SSA method. The RMS acceleration of the 75th floor of the sample ATMD system is used as the pre-defined value for the SSA. The wind loads applied to the building are the same wind tunnel test data described in the previous section. For the proposed hybrid damper-TLCD system the results obtained from the simulation yielded a total of 10 dampers, 4 in the 74th story and 6 in the 75th story. When only passive dampers are used for the control of the structure, a total of 26 dampers are required in the top ten stories to achieve the same level of performance using the same SSA method. It should be noted that the dampers are most effective in the top stories for control of high-rise buildings against wind loading. In contrast, for control of structures against seismic loading, the dampers are generally most effective in the bottom stories.

The comparison of displacement frequency responses of the 75th floor for the uncontrolled, semi-active TLCD, and hybrid damper-TLCD systems is shown in Figure 6.5. This figure shows that the hybrid damper-TLCD system reduces the response of the

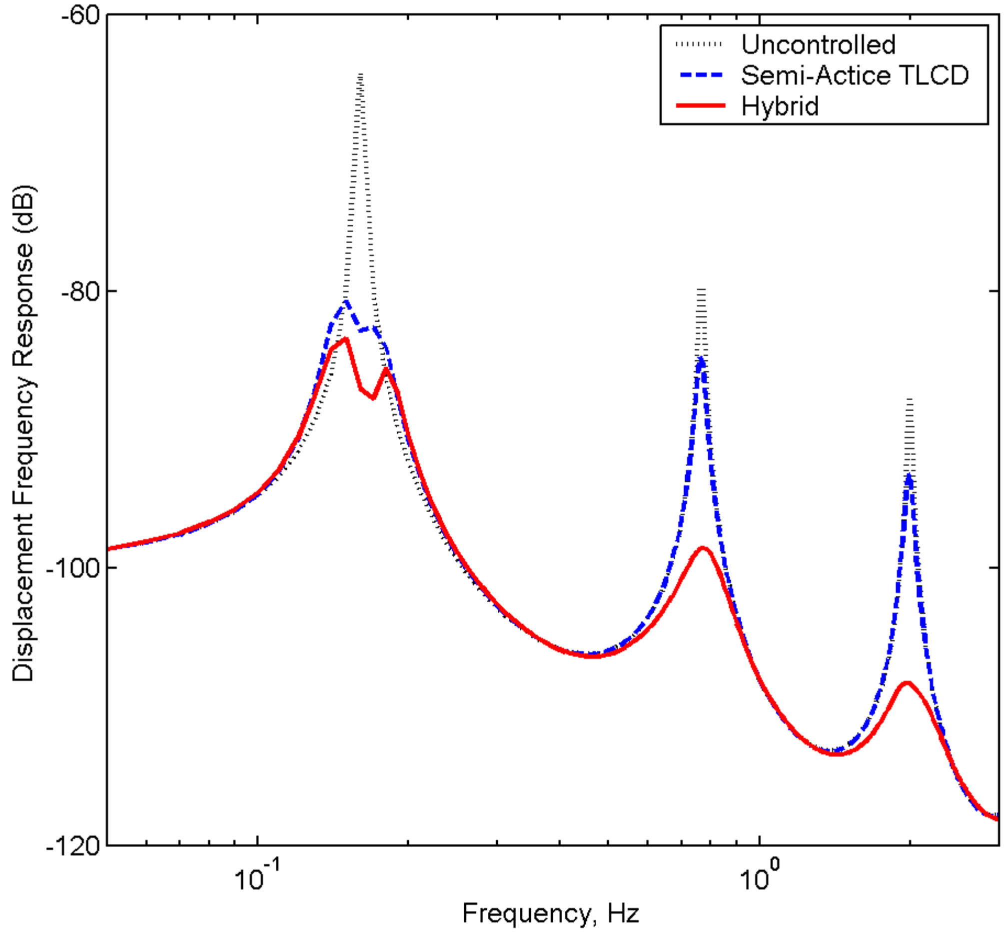

Figure 6.5: Displacement frequency responses of the 75th floor for the uncontrolled, semi-active TLCD, and hybrid damper-TLCD systems

building significantly more than the semi-active TLCD system at every natural frequency of the building (primary structure). The RMS and peak responses of the selected floors of the benchmark building for the hybrid damper-TLCD system are presented in Table 6.4. The corresponding results for the semi-active TLCD system can be found in the last two columns of Tables 6.1 and 6.2. The results of the evaluation criteria for the hybrid damper-TLCD system are presented in Table 6.5. The corresponding results for the semi-active TLCD system can be found in the fourth and eighth columns of Table 6.3. A comparison of results presented in Table 6.5 and the second and sixth columns of Table 6.3 indicates that the hybrid damper-TLCD system outperforms the sample ATMD system in all criteria, except J_7. The performance improvements for the seven criteria J_1 to J_4 and J_8 to J_{10} are, 9%, 19%, 10%, 10%, 1%, 8%, and 8%, respectively. The value of the criterion J_7 for hybrid damper-TLCD system is 7% less than that for the sample ATMD system.

Figure 6.6 shows the displacement response time histories of the 75th floor for both uncontrolled structure and the hybrid damper-TLCD system. Figure 6.7 shows the corresponding results for the acceleration response time histories. These figures as well as Tables 6.2 and 6.4 demonstrate clearly the hybrid damper-TLCD system reduces both displacements and accelerations significantly compared with the uncontrolled structure.

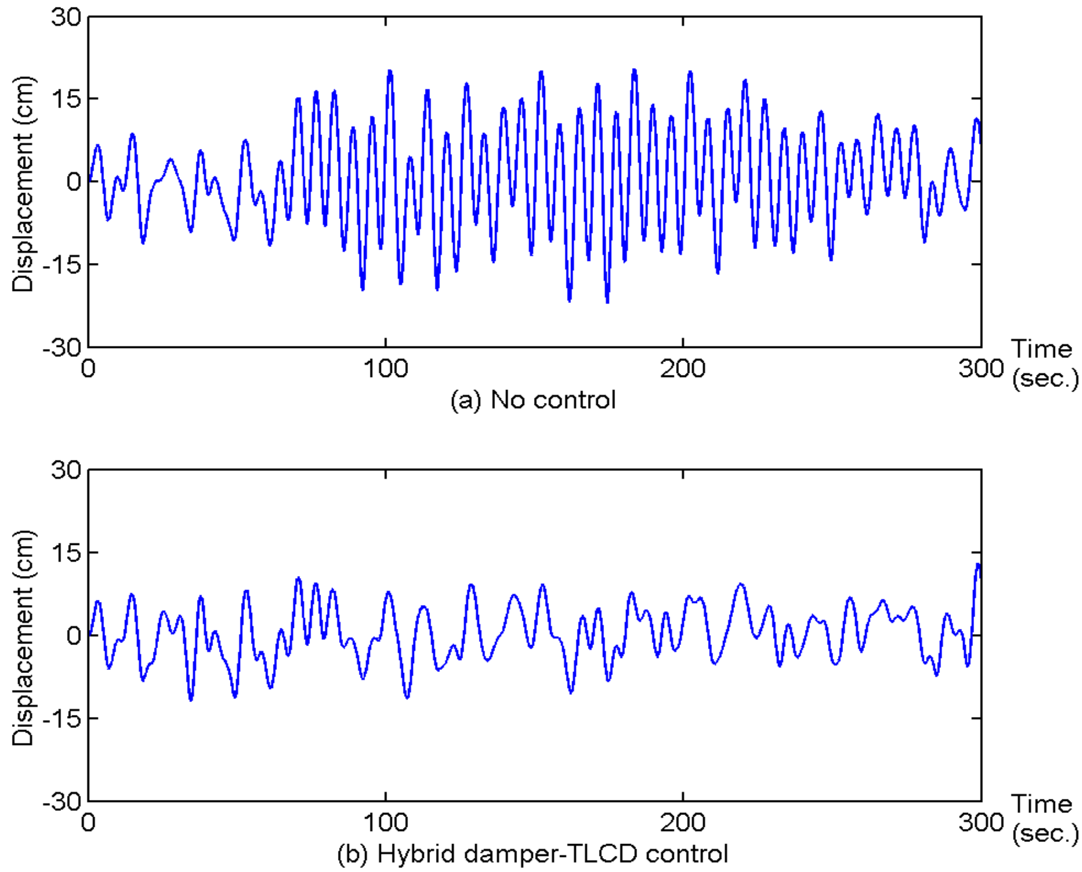

Figure 6.6: Displacement response time histories of the 75th floor subjected to the wind tunnel test loads

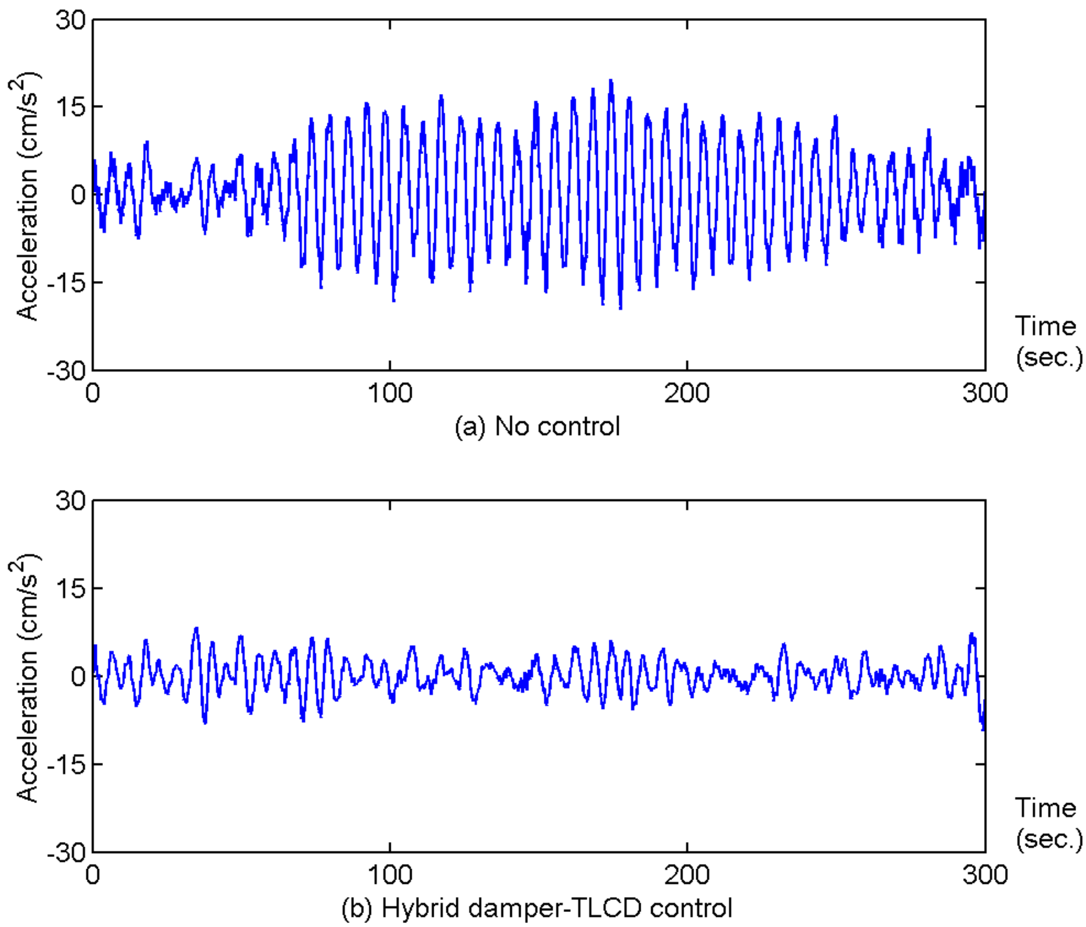

Figure 6.7: Acceleration response time histories of the 75th floor subjected to the wind tunnel test loads

Floor No.	RMS responses		Peak responses	
	Displacement (cm)	Acceleration (cm/s^2)	Displacement (cm)	Acceleration (cm/s^2)
1	0.01	0.06	0.04	0.21
30	1.14	0.69	4.75	2.91
50	2.75	1.63	11.26	6.17
55	3.21	1.90	13.10	8.05
60	3.69	2.16	14.99	8.73
65	4.17	2.49	16.90	9.96
70	4.66	2.77	18.84	11.05
75	5.17	3.07	20.84	12.35
76	5.28	3.53	21.29	12.70

Table 6.4: RMS and peak displacement and acceleration responses of the 76-story building for the hybrid damper-TLCD system

J_1	J_2	J_3	J_4	J_7	J_8	J_9	J_{10}
0.336	0.339	0.521	0.524	0.407	0.431	0.659	0.668

Table 6.5: Evaluation criteria for the hybrid damper-TLCD system

Two additional numerical simulations are carried to evaluate the robustness of the proposed hybrid damper-TLCD system and its sensitivity to modeling errors using the same 76-story building benchmark control problem. The sensitivity analysis is performed in terms of the stiffness of the structure. In one simulation the stiffness of the structure is increased by 15% ($\Delta\boldsymbol{K}$ = +15%) and in another simulation it is decreased by 15% ($\Delta\boldsymbol{K}$ = -15%), as suggested by Yang et al. (2000). The controller configuration obtained for the building with previous value of stiffness is applied to the buildings with $\Delta\boldsymbol{K}$ = ±15% and the same time-history response analyses are carried out.

Floor No.	$\Delta\boldsymbol{K}$ = +15 %		$\Delta\boldsymbol{K}$ = -15 %	
	Displacement (cm)	Acceleration (cm/s^2)	Displacement (cm)	Acceleration (cm/s^2)
1	0.01	0.06	0.01	0.06
30	1.00	0.73	1.43	0.75
50	2.41	1.74	3.44	1.78
55	2.81	2.02	4.02	2.09
60	3.22	2.31	4.61	2.38
65	3.65	2.66	5.22	2.72
70	4.08	2.96	5.84	3.03
75	4.52	3.34	6.48	3.73
76	4.62	3.42	6.63	3.35

Table 6.6: RMS displacement and acceleration responses of the 76-story building for the hybrid control system using the building with uncertainty in stiffness matrix

The resulting RMS and peak displacement and acceleration responses of the selected floors of the benchmark building for the hybrid damper-TLCD systems are presented in Table 6.6 and Table 6.7, respectively. Table 6.8 presents the results for the evaluation criteria. As observed from the results in Tables 6.6-6.8, the hybrid damper-TLCD system is robust in terms of the stiffness modeling error for the control of both displacement and acceleration responses. In particular, the values of RMS and peak accelerations of the 75th floor as well as the top floor (76th floor) of the building with $\Delta\boldsymbol{K}$ = ±15% are all within the allowable maximum values for the floor accelerations, 5 cm/s^2 and 15 cm/s^2, respectively, as mentioned earlier.

Floor No.	$\Delta\boldsymbol{K}$ = +15 %		$\Delta\boldsymbol{K}$ = -15 %	
	Displacement (cm)	Acceleration (cm/s^2)	Displacement (cm)	Acceleration (cm/s^2)
1	0.04	0.20	0.04	0.22
30	4.50	2.79	5.26	2.76
50	10.68	6.98	12.47	6.78
55	12.43	7.95	14.51	8.39
60	14.22	8.57	16.60	9.39
65	16.05	10.02	18.73	11.48
70	17.89	10.89	20.89	12.32
75	19.79	12.44	23.11	13.99
76	20.22	12.16	23.61	13.87

Table 6.7: Peak displacement and acceleration responses of the 76-story building for the hybrid control system using the building with uncertainty in stiffness matrix

RMS Responses			Peak Responses		
Criteria	$\Delta\boldsymbol{K}$ = +15 %	$\Delta\boldsymbol{K}$ = -15 %	Criteria	$\Delta\boldsymbol{K}$ = +15 %	$\Delta\boldsymbol{K}$ = -15 %
J_1	0.365	0.408	J_7	0.410	0.461
J_2	0.362	0.378	J_8	0.437	0.474
J_3	0.456	0.654	J_9	0.626	0.731
J_4	0.458	0.656	J_{10}	0.634	0.740

Table 6.8: Evaluation criteria for the hybrid control system using the building with uncertainty in stiffness matrix

6.5 STOCHASTIC WIND LOADS

To evaluate the effectiveness of the proposed hybrid damper-TLCD control system under various types of wind loads, $\boldsymbol{F}(t)$ in Eqs. (6.9) and (6.10), the stochastic wind loads defined by the Davenport's cross-power spectral density matrix are applied to the benchmark building. The (i, j) element of Davenport's cross-power spectral density matrix defined in the frequency domain, $\boldsymbol{S}_{ww}(\omega)$, is expressed as (Yang et al., 1998)

$$S_{w_i w_j}(\omega) = \frac{8\overline{w}_i \overline{w}_j K_0 V_r^2}{\overline{V}_i \overline{V}_j |\omega|} \frac{(600\omega / \pi V_r)^2}{\left[1 + (600\omega / \pi V_r)^2\right]^{4/3}} \exp\left(-\frac{c_1 |\omega|}{2\pi} \frac{|h_i - h_j|}{V_r} \right) \tag{6.13}$$

where ω is the frequency in radian per second, $\overline{w}_i$ is the average wind force on the ith floor, $\overline{V}_i$ is the mean wind velocity at ith floor, V_r is the reference mean wind velocity in meters per second at 10m above the ground, h_i is the height of the ith floor, K_0 is a constant depending on the surface roughness of the ground, and c_1 is a constant which depends on different factors such as terrain roughness, height above ground, and wind speed. Simiu and Scanlan (1996) present empirical values for this coefficient in terms of the mean wind speed at 10m above the ground in the range 2 to 10. Following Yang et al. (1998), the values of $K_0 = 0.03$, $c_1 = 7.7$, and $V_r = 15$ m/sec are used for the parameters in this study. The first five minutes of time histories of resulting wind loads on 66th and 70th floors are displayed in Figure 6.8.

For the numerical simulation of the hybrid damper-TLCD system using the stochastic wind loads, the same controller configuration obtained previously using the wind tunnel test loads is applied. Figure 6.9 shows the displacement response time histories of the 75th floor for both uncontrolled structure and the hybrid damper-TLCD system subjected to the stochastic wind loads. Figure 6.10 shows the corresponding results for the acceleration response time histories. These figures again show clearly the hybrid damper-TLCD system reduces both displacements and accelerations significantly compared with the uncontrolled structure under the new wind loading.

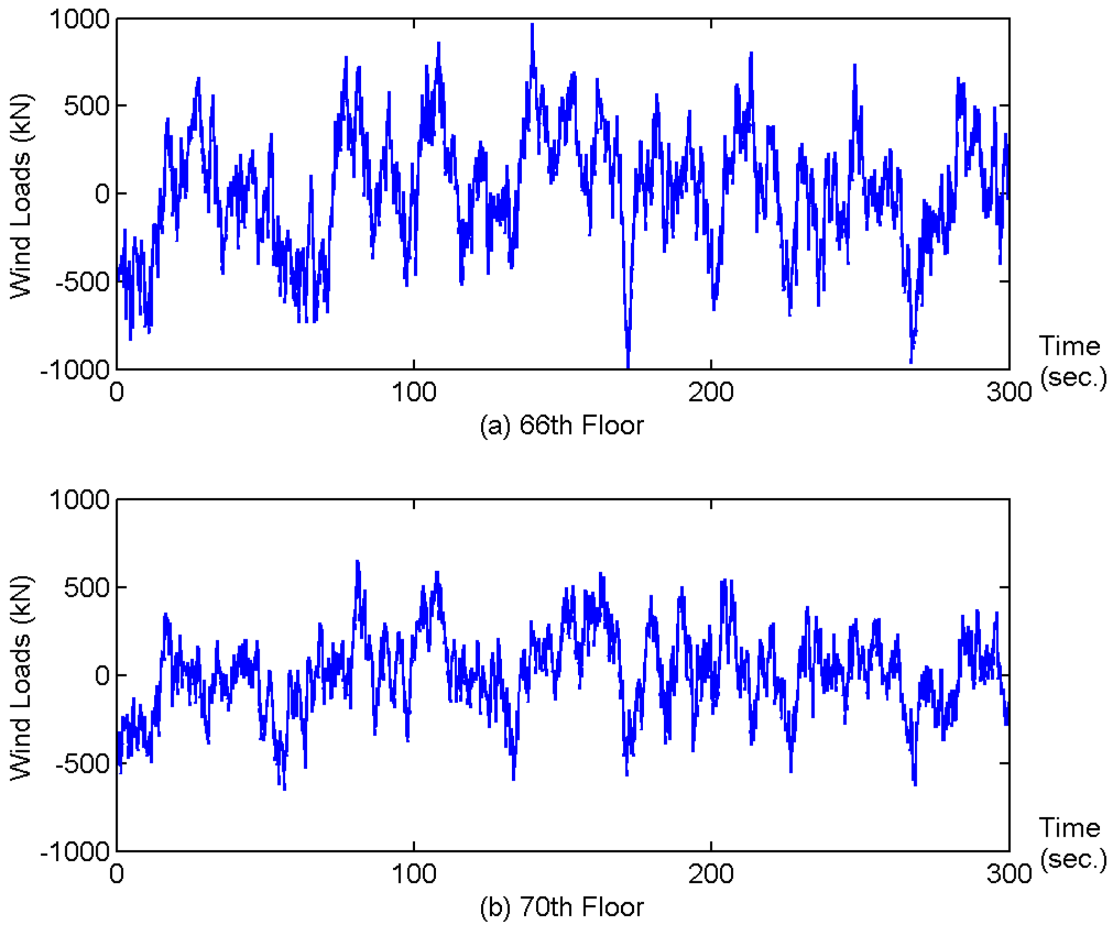

Figure 6.8: Time histories of stochastic wind loads acting on 66th and 70th floors

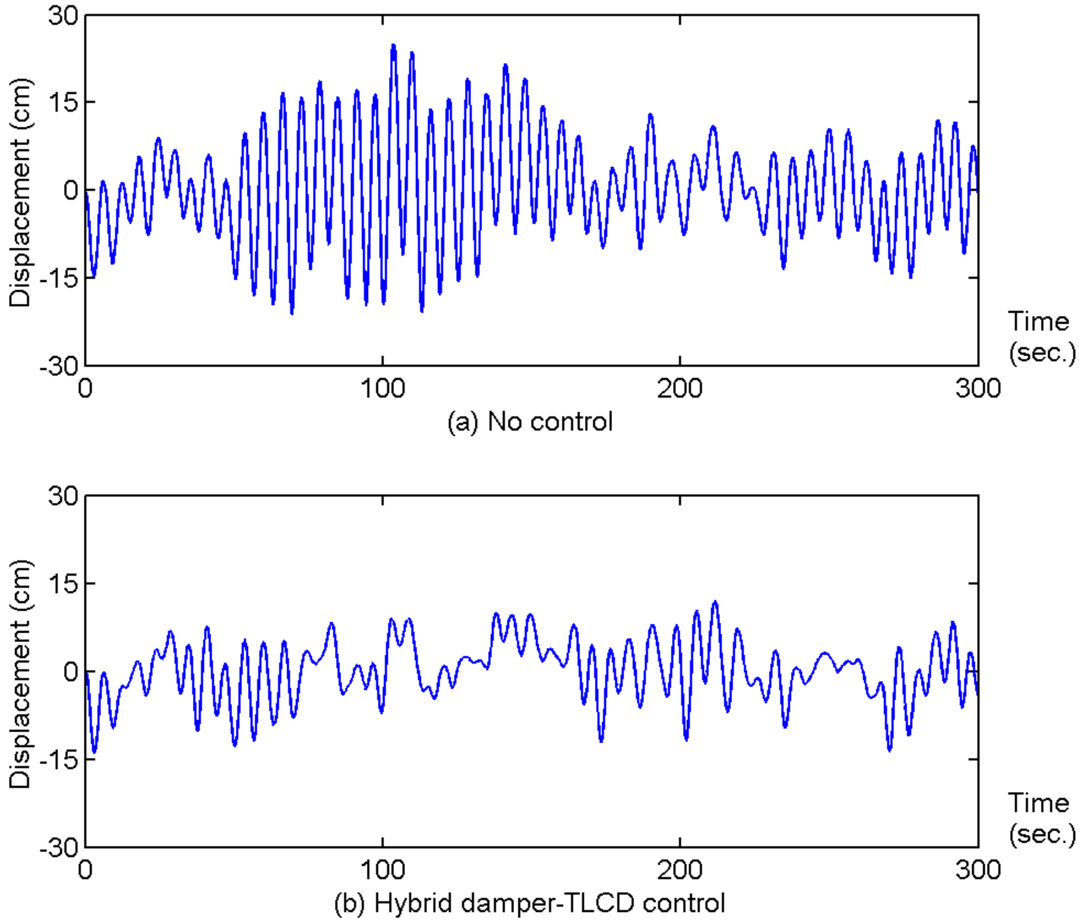

Figure 6.9: Displacement response time histories of the 75th floor subjected to the stochastic wind loads

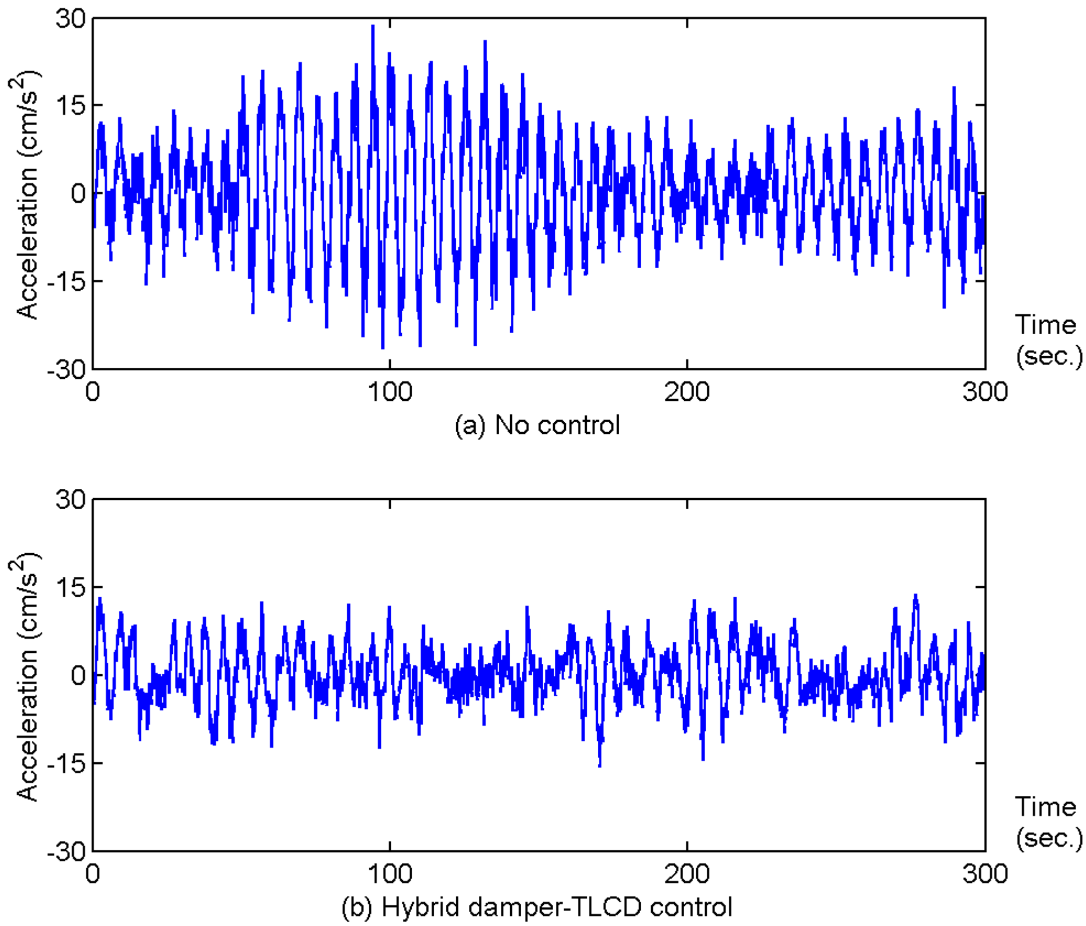

Figure 6.10: Acceleration response time histories of the 75th floor subjected to the stochastic wind loads

6.6. Concluding Remarks

The effectiveness of both a semi-active TLCD system and the hybrid damper-TLCD control system is investigated for control of wind-induced motion of a 76-story benchmark building. It is shown that the semi-active TLCD control system performs comparable to a sample ATMD system. Considering the fact that the semi-active TLCD system does not need any actuator requiring a large electro-mechanic capacity and thus is able to operate with only small power, such as a battery, it is concluded that the semi-active TLCD system is an attractive alternative to the ATMD system. Further, the TLCD system provides many advantages over the TMD system.

By judiciously integrating the semi-active TLCD system with a passive supplementary damper system, the hybrid damper-TLCD system provides reliable and robust control of wind-induced vibrations of high-rise buildings in terms of power or computer failure. It is shown that the hybrid system can reduce the response of the building significantly more than the semi-active TLCD system at every natural frequency of the building. Moreover, the hybrid damper-TLCD system is robust in terms of the stiffness modeling error for the control of both displacement and acceleration responses. Further, the simulation results using stochastic wind loads clearly show that the proposed hybrid control system can perform effectively under various wind loads.

CHAPTER 7

WAVELET-HYBRID FEEDBACK LMS ALGORITHM FOR ROBUST CONTROL OF CABLE-STAYED BRIDGE

7.1 Introduction

Cable-stayed bridges have recently gained increasing popularity due to their economic and aesthetic advantages. These bridges, however, are flexible and control of their vibrations is an important consideration and a challenging problem. It has been recognized that the analysis and control of cable-stayed bridges is a challenging problem with complexities in structural modeling, and control design and implementation. Specially, the geometric nonlinearity of cables due to the change of shape under varying stresses makes the analysis of cable-stayed bridge more complicated compared with other types of bridge structures (Adeli and Zhang, 1995).

Articles on vibration control of cable-stayed bridges have appeared in the literature only recently. Cable stays in such bridges provide relatively small intrinsic damping. Therefore early studies on control of cable-stayed bridge have concentrated on increasing the damping capacity of bridge using passive supplementary dampers. Ali and

Abdel-Ghaffar (1994) discuss the effectiveness, feasibility, and limitations of passive supplementary dampers for cable-stayed bridges analytically. They conclude that when passive damper devices are installed at critical zones, such as between deck and abutment and between deck and tower, the inelastic behavior of cable-stayed bridge can be avoided. A similar experimental study using passive damper devices for control of cable-stayed bridges subjected to seismic loads has been reported by Villaverde and Marin (1995). Tabatabai and Mehrabi (2000) discuss design of mechanical viscous dampers for passive control of cable-stayed bridges under wind induced or galloping vibrations. They present simplified formulations based on the fundamental mode of vibrations for finding the capacities of dampers and their location on the stays.

In addition to passive supplementary dampers, a few studies on active and semi-active control of cable-stayed bridges have also been reported in the literature. Warnitchai et al. (1993) investigate experimentally active tendon control of cable-stayed bridges subjected to a vertical sinusoidal force. Experiments were performed using a simple cable-supported cantilever beam. Schemmann and Smith (1998a and b) investigate the effectiveness of active control of cable-stayed bridges using a LQR feedback control algorithm and discuss issues involved such as geometric nonlinearity and high-order vibration modes. They conclude that control of higher-order modes is critical and actuators located close to the center of bridge span are the most effective for control of the structural response. Bossens and Preumont (2001) present a scheme for active tendon control of cable-stayed bridges subjected to wind and earthquake loading using collocated actuator/sensor pairs and verify it with experimental results on scaled models. He et al. (2001) present semi-active control of a cable-stayed bridge using resetting semi-active stiffness dampers. They show that semi-active control of the bridge reduces the response more significantly than passive supplementary dampers.

In this chapter, the wavelet-hybrid feedback LMS algorithm is used for vibration control of cable-stayed bridges under various seismic excitations. Its effectiveness is investigated through numerical simulation using the benchmark control problem created by Dyke et al. (2000) and described briefly in the next section. The performance of the new algorithm is compared with that of a sample LQG controller. Additional numerical simulations are performed to evaluate the sensitivity of the control model to modeling errors and verify its robustness.

7.2 Cable-Stayed Bridge Benchmark Control Problem

The benchmark control problem used for simulation in this study is based on the Bill Emerson Memorial Bridge, which is under construction in Cape Girardeau, Missouri, USA. The bridge spans the Mississippi river and connects the states of Missouri and Illinois. It consists of a semi-fan type cable-stayed bridge with two main concrete towers and a deck which extends over 12 additional piers in the approach bridge from the Illinois side. In the benchmark control problem, only the cable-stayed part of bridge is used as shown in Figure 7.1.

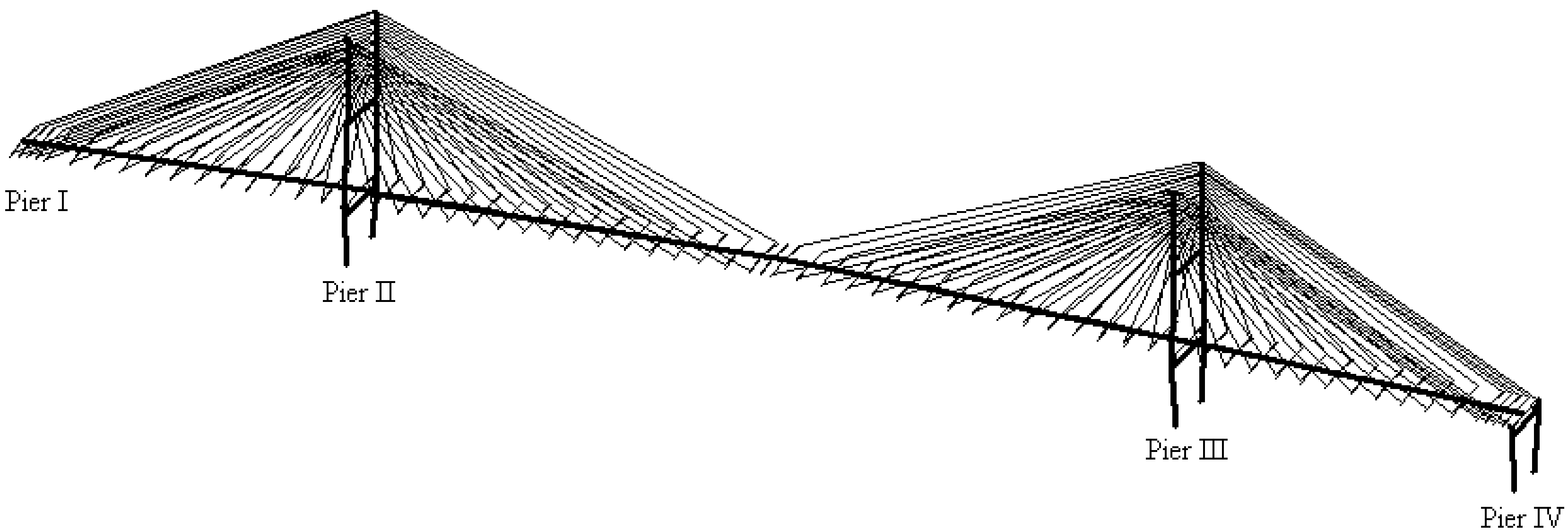

Figure 7.1: 3-D view of the benchmark cable-stayed bridge

In the cable-stayed part of the bridge, the main span has a length of 350.6m and each side span has a length of 142.7m. The heights of H-shaped towers are 100 m at pier II and 105 m at pier III (Figure 7.1). A total of 128 cables, made of high-strength, low relaxation steel, are evenly supported by two towers, that is, 64 cables on each tower. The deck of width 29.3 m is built with prestressed concrete slabs and steel beams.

Dyke et al. (2000) present a benchmark control problem for the cable-stayed bridge. A three-dimensional finite element model of the bridge is created using ABAQUS (1998). Two-node shear beam elements are used to model the beams and two-node linear space truss elements are used to model the cables. Geometric nonlinearity due to cable sag effect is taken into account approximately using an equivalent modulus of elasticity (Adeli and Zhang, 1995). The resulting model has 419 degrees of freedom. The first six natural frequencies of the structure are 0.2889 Hz, 0.3699 Hz, 0.4683 Hz, 0.5158 Hz, 0.5812 Hz, and 0.6490 Hz.

Eighteen criteria, denoted by J_1 to J_{18}, are provided to evaluate the control performance. The first six performance criteria (J_1 to J_6) are non-dimensional ratios of the responses of the controlled bridge to those of the uncontrolled bridge subjected to three earthquakes records, the El Centro (California, 1940), Mexico City (Mexico, 1985), and Gebze (Turkey, 1999) earthquakes, shown in Figure 7.2. They are the maximum values of the base shear and shear at the deck level in the two towers (J_1 and J_2, respectively), the maximum values of the base moment and moment at the deck level in the two towers (J_3 and J_4, respectively), the maximum cable sag or deviation (J_5), and the maximum deck displacement (J_6).

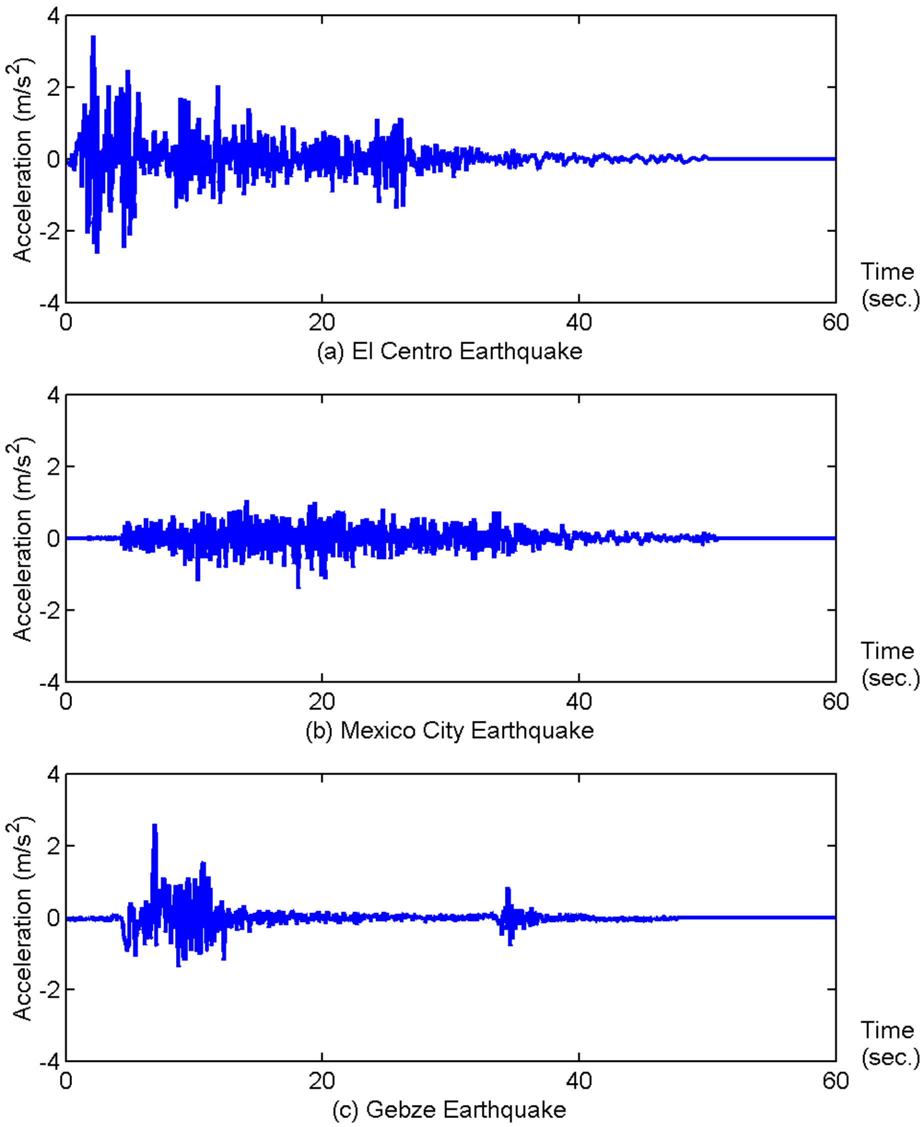

Figure 7.2: Time histories of the El Centro, Mexico City, and Gebze Earthquake acceleration records

The next five performance criteria (J_7 to J_{11}) are non-dimensional ratios of the *normed* responses of the controlled bridge to those of the uncontrolled bridge subjected to the same three earthquakes, where the normed value of a response is defined as

$$\|\bullet\| = \sqrt{\frac{1}{t_f}\int_0^{t_f} (\bullet)^2 \, dt} \qquad (7.1)$$

in which t_f is the time required for the response to attenuate. They are the maximum normed values of the base shear and shear at the deck level in the towers (J_7 and J_8, respectively), the maximum normed values of the base moment and moment at the deck level in the towers (J_9 and J_{10}, respectively), and the maximum normed value of the cable sag or deviation (J_{11}).

The next four performance criteria (J_{12} to J_{15}) are non-dimensional measures of the control device performances. They are the maximum force generated by all the control devices normalized by the weight of bridge superstructure (J_{12}), the maximum stroke of all the control devices normalized by the maximum uncontrolled displacement at the top of the two towers relative to ground (J_{13}), the maximum instantaneous power required to control the bridge normalized by the product of the peak uncontrolled velocity at the top of the two towers relative to ground and the weight of bridge superstructure (J_{14}) where the instantaneous power is given by the absolute value of the product of the velocity and the force generated by the control device, and the integration of instantaneous power over time normalized by the product of the weight of bridge superstructure and the maximum uncontrolled displacement at the top of the two towers relative to ground (J_{15}).

The last three performance criteria are the total number of control devices (J_{16}), the total number of sensors (J_{17}), and the dimension of the discrete time state vector required to implement the control algorithm (J_{18}).

7.3 Numerical Simulations

For the sake of comparison, the same numbers of devices and sensors are used for both new and the sample LQG control algorithms. Also, the same number is used for the dimension of the discrete time state vector required to implement the control algorithm (the last three rows in Table 7.1). Numerical simulation results are displayed in Figures 7.3 to 7.8. Figures 7.3, 7.5, and 7.7 show the uncontrolled and controlled time histories of base shear force and base moment at pier II subjected to El Centro, Mexico City, and Gebze Earthquake records, respectively. Figures 7.4, 7.6, and 7.8 show the time histories of base shear force at pier II subjected to El Centro, Mexico City, and Gebze Earthquake records, respectively, using the sample LQG and the wavelet-hybrid feedback LMS control algorithms. It is clear from the results that the responses of the cable-stayed bridge can be significantly reduced by using the wavelet-hybrid feedback LMS control algorithm. Results also show that the new control algorithm is more effective than the sample LQG controller for all three earthquake records.

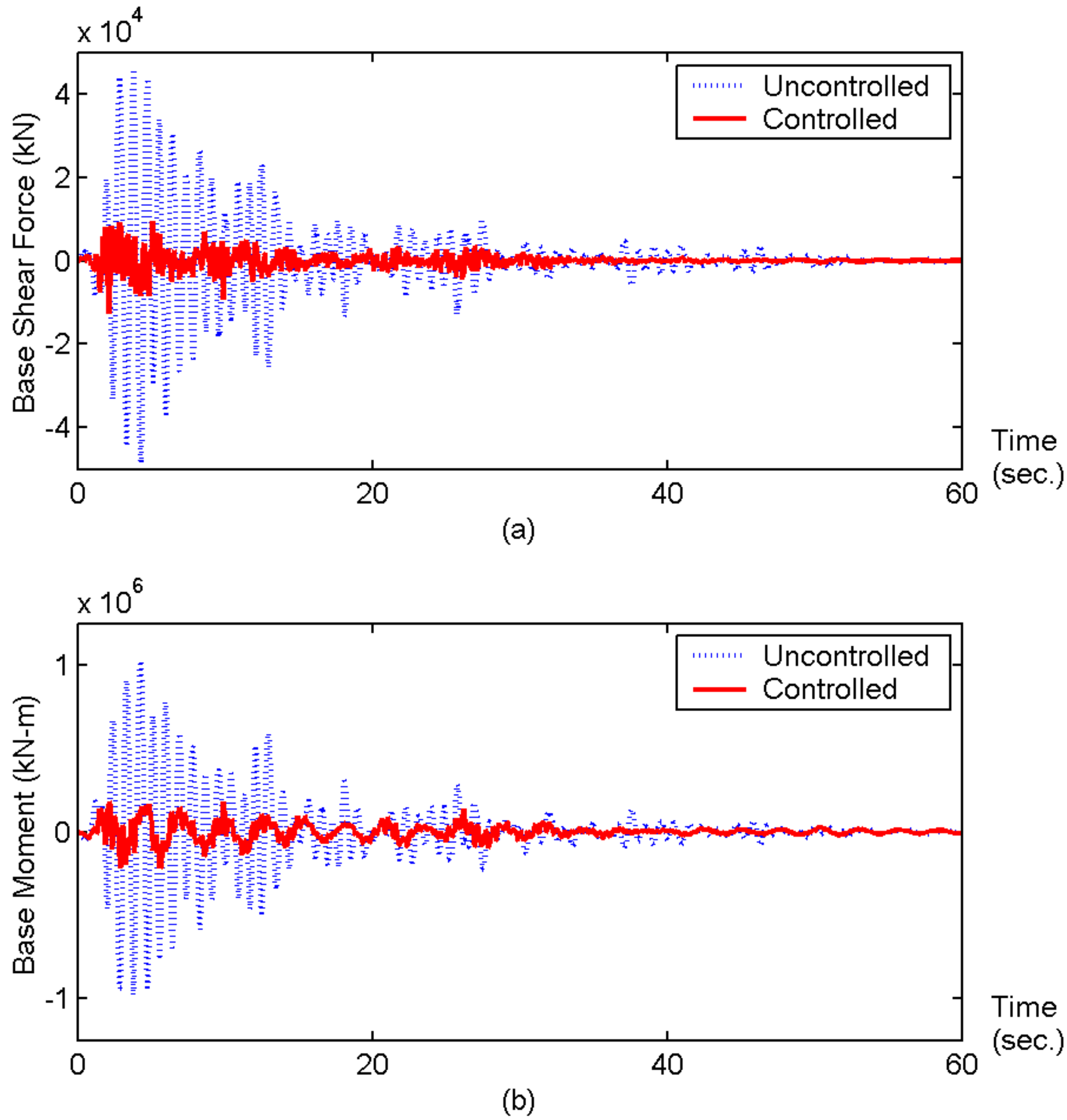

Figure 7.3: Uncontrolled and controlled response time histories of the benchmark bridge subjected to El Centro earthquake record: a) base shear force at pier II, b) base moment at pier II

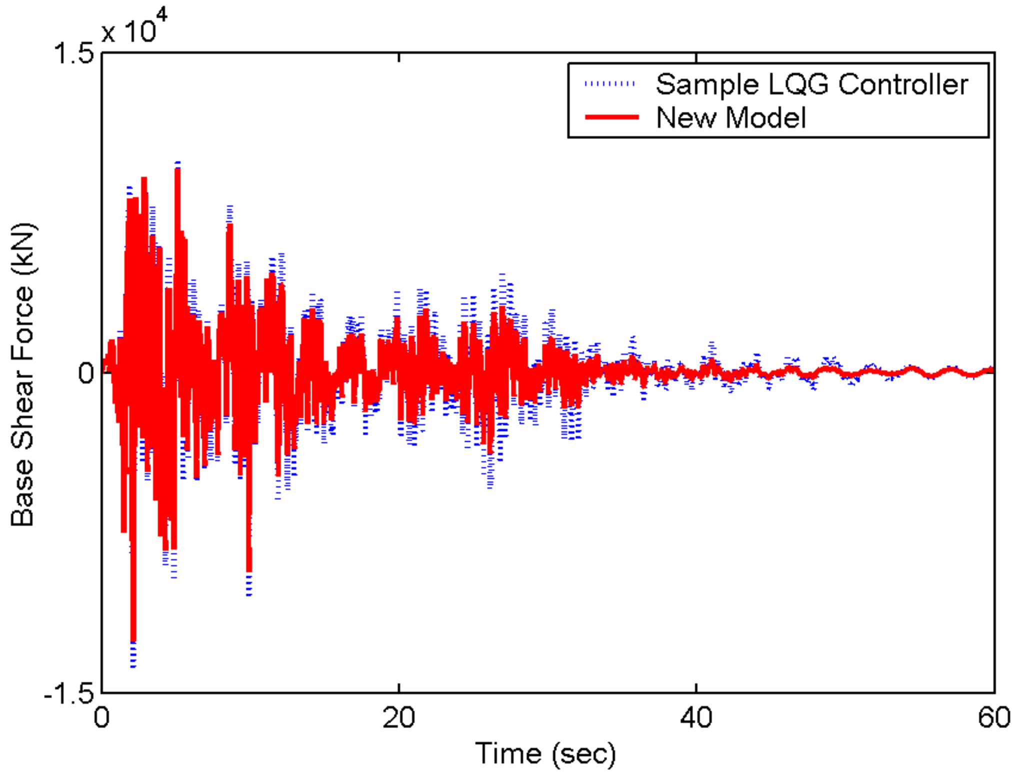

Figure 7.4: Time histories of base shear force at pier II of the benchmark bridge subjected to El Centro earthquake record using the sample LQG and the wavelet-hybrid feedback LMS control algorithms

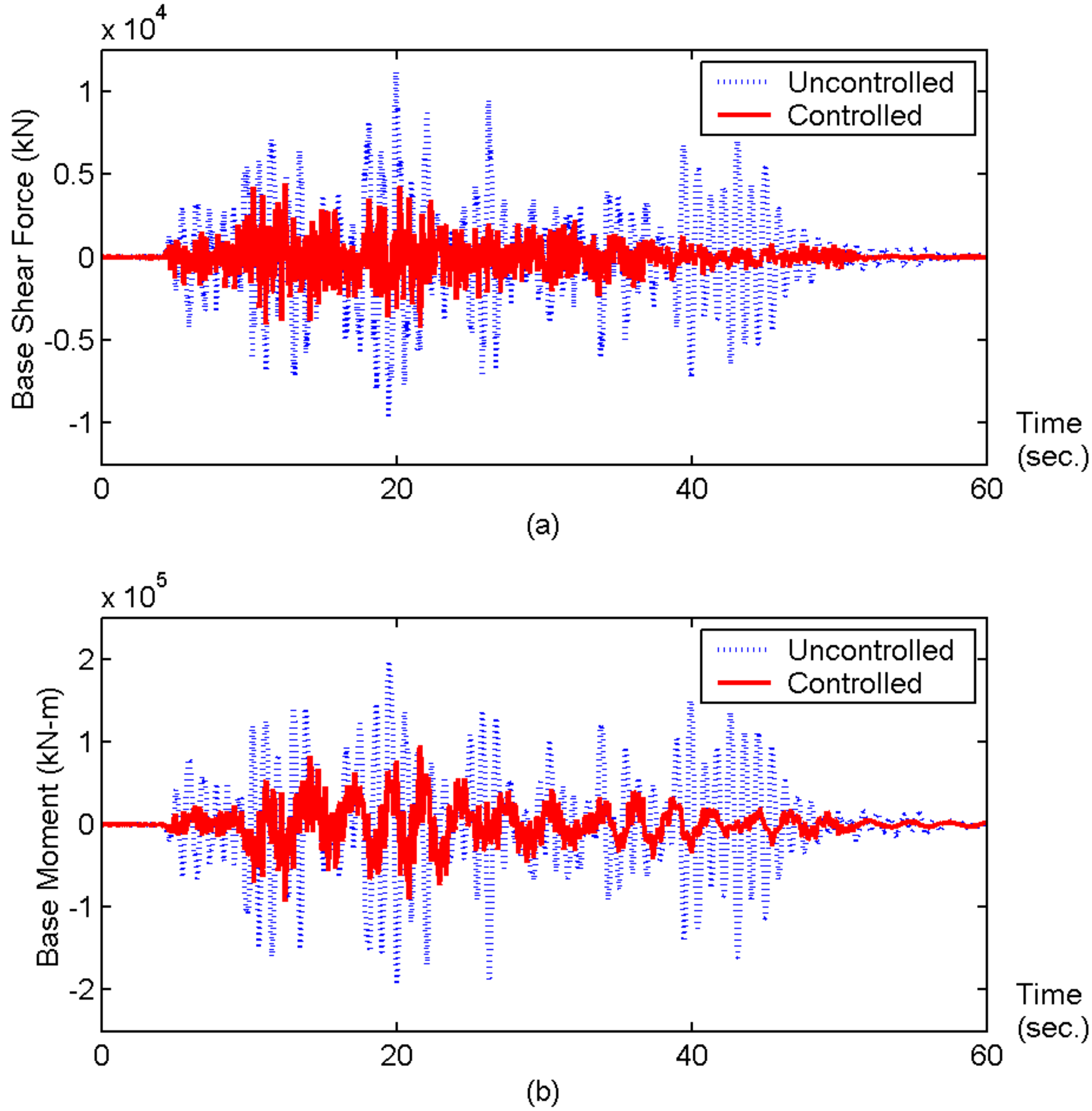

Figure 7.5: Uncontrolled and controlled response time histories of the benchmark bridge subjected to Mexico City earthquake record: a) base shear force at pier II, b) base moment at pier II

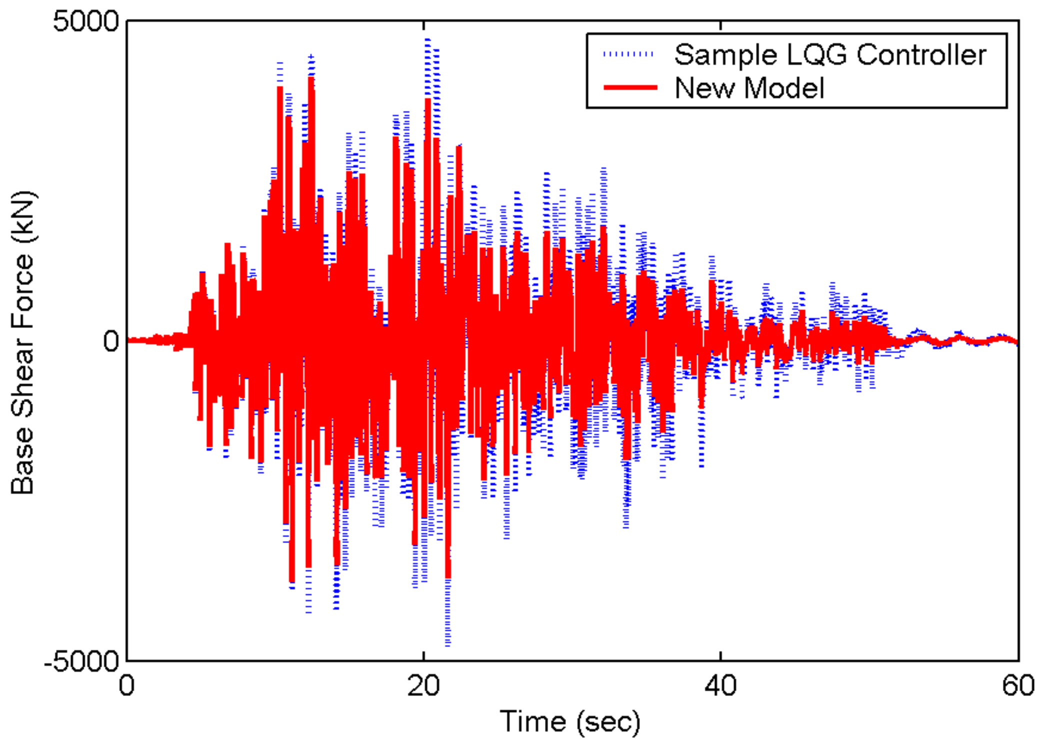

Figure 7.6: Time histories of base shear force at pier II of the benchmark bridge subjected to Mexico City earthquake record using the sample LQG and the wavelet-hybrid feedback LMS control algorithms

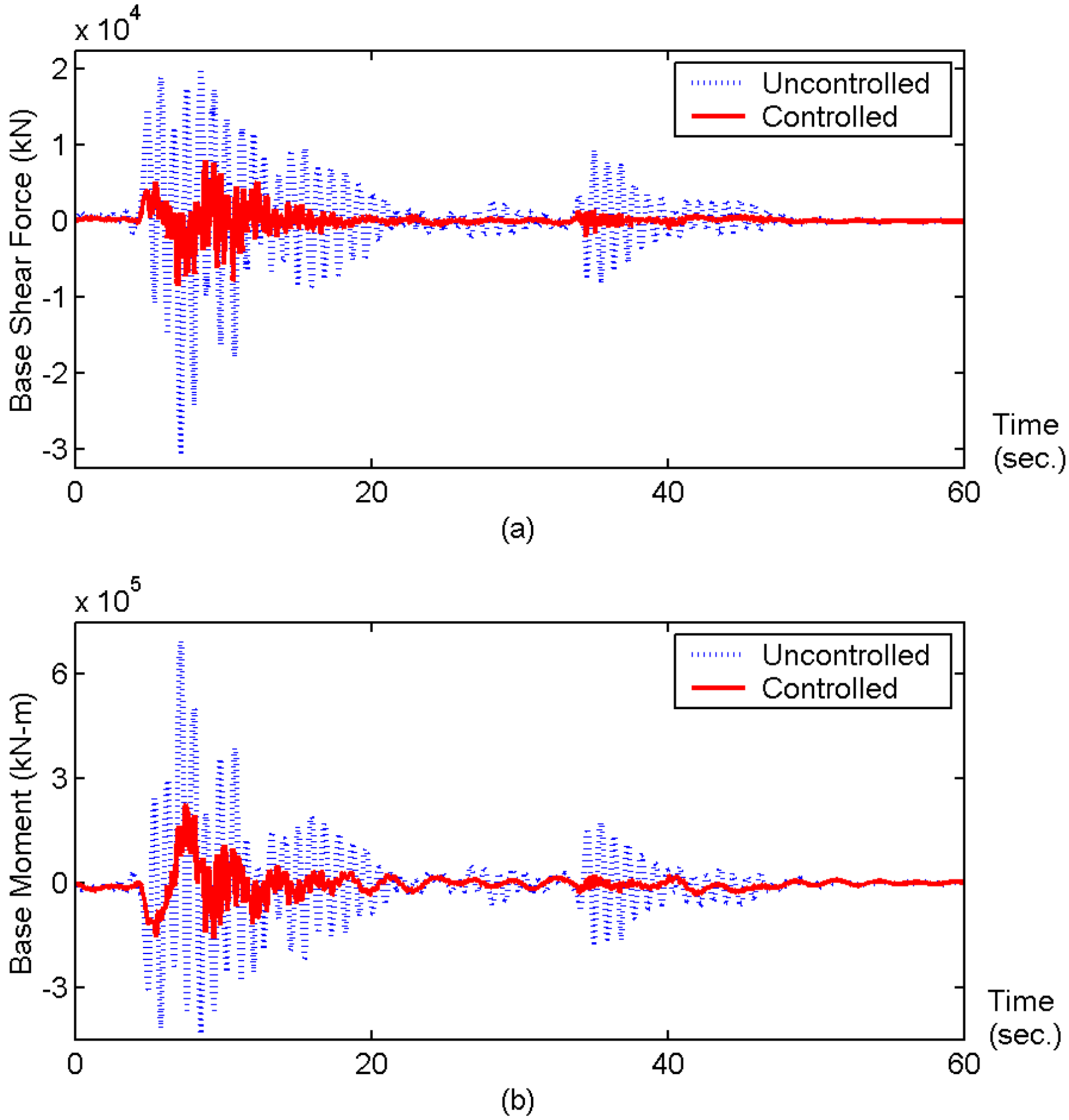

Figure 7.7: Uncontrolled and controlled response time histories of the benchmark bridge subjected to Gebze earthquake record: a) base shear force at pier II, b) base moment at pier II

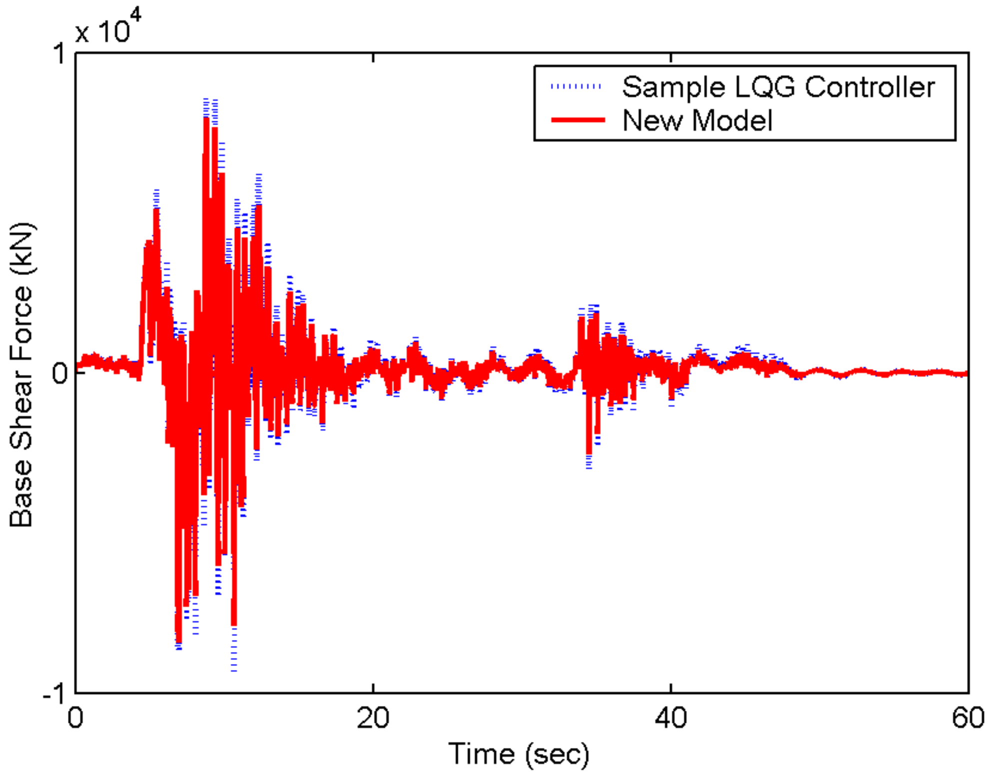

Figure 7.8: Time histories of base shear force at pier II of the benchmark bridge subjected to Gebze earthquake record using the sample LQG and the wavelet-hybrid feedback LMS control algorithms

.

Criterion	Sample LQG Controller			WHFL Controller		
	El Centro	Mexico	Gebze	El Centro	Mexico	Gebze
Max Base Shear (J_1)	0.3970	0.4969	0.4594	0.3344	0.4287	0.4332
Max Deck Shear (J_2)	1.0696	1.2706	1.3775	0.9922	1.0537	1.2300
Max Base Moment (J_3)	0.2943	0.5858	0.4413	0.2742	0.4535	0.3894
Max Deck Moment (J_4)	0.6455	0.6820	1.2234	0.6484	0.4808	0.9533
Max Cable Deviation (J_5)	0.1825	0.0770	0.1501	0.1706	0.0679	0.1238
Max Deck Displacement (J_6)	1.2033	2.3938	3.6042	1.1173	1.6588	2.3374
Norm Base Shear (J_7)	0.2353	0.4554	0.3359	0.2052	0.3481	0.3099
Norm Deck Shear (J_8)	1.2018	1.2566	1.4822	0.9308	0.9433	1.2532
Norm Base Moment (J_9)	0.2703	0.4551	0.4633	0.2229	0.3503	0.3919
Norm Deck Moment (J_{10})	0.8922	1.1251	1.4730	0.6581	0.7815	1.0184
Norm Cable Deviation (J_{11})	2.830E-02	1.043E-02	1.725E-02	2.384E-02	8.939E-03	1.399E-02
Max Control Force (J_{12})	1.961E-03	6.243E-04	1.831E-03	2.161E-03	8.717E-04	1.961E-03
Max Device Stroke (J_{13})	5.834E-06	8.402E-06	2.726E-05	6.417E-06	8.855E-06	2.833E-05
Max Power (J_{14})	3.003E-02	1.043E-02	3.477E-02	3.381E-02	1.476E-02	3.564E-02
Total Power (J_{15})	4.435E-09	1.454E-09	9.594E-09	4.993E-09	2.057E-09	9.835E-09
Number Devices (J_{16})	24	24	24	24	24	24
Number Sensors (J_{17})	9	9	9	9	9	9
Control Resources (J_{18})	30	30	30	30	30	30

Table 7.1: Comparison of evaluation criteria

The results of evaluation criteria are summarized in Table 7.1. The maximum base shear (J_1) in towers using the wavelet-hybrid feedback LMS control model is 16%, 13%, and 6% less than the corresponding values using the sample LQG model when the bridge is subjected to El Centro, Mexico City, and Gebze Earthquake records, respectively. The corresponding normed values (J_7) are 13%, 24% and 8% less than the corresponding values using the sample LQG model, respectively. The maximum shear at deck level (J_2) in towers using the wavelet-hybrid feedback LMS control model is 7%, 17%, and 11% less than the corresponding values using the sample LQG model when the bridge is subjected to El Centro, Mexico City, and Gebze Earthquake records, respectively. The corresponding normed values (J_8) are 23%, 25% and 15% less than the corresponding values using the sample LQG model, respectively. Similar performance improvements are noted for evaluation criteria J_3 to J_6 and J_9 to J_{11}.

In terms of the required control forces and power, criteria J_{12} to J_{15}, the values for the new model are 3-42% greater than those for the sample LQG control algorithm.

7.4 Sensitivity Analysis

Additional numerical simulations are carried to evaluate the robustness of the new wavelet-hybrid feedback LMS algorithm and its sensitivity to modeling errors. Due to geometric nonlinearity, the stiffness of the cable-stayed bridge may change during strong ground motions. Further, the dynamic characteristics of the finite element model may not be identical to those of the real bridge. For the purpose of the sensitivity analysis the following perturbation is introduced in the structural stiffness matrix:

$$\boldsymbol{K}_{\text{pert}} = \boldsymbol{K}(1+\Delta) \tag{7.2}$$

where, Δ is the perturbation ratio, and $\boldsymbol{K}_{\text{pert}}$ is the resulting perturbed structural stiffness matrix.

When the stiffness of the actual structure is greater than that used in the mathematical finite element model, simulation results show no adverse effect on the vibration control of the cable-stayed bridge, as expected. On the other hand, when the stiffness of the actual structure is smaller than that used in the mathematical finite element model simulation results show deterioration in the control performance. Simulations were performed by gradually increasing the magnitude of the perturbation ratio, Δ, in order to investigate the stability of the new control algorithm. Significant vibrations reduction and stable results were obtained with values of perturbation ratio up to -0.07. When Δ = -0.07 the control deterioration is 0.5-12% for El Centro earthquake, 7-40% for Mexico City earthquake, and 2-23% for Gebze earthquake. Consequently, the stability threshold for the perturbation ratio is found to be around -0.07. A similar observation is reported in Turan et al. (2002) where the μ-synthesis feedback control method is used for control of the benchmark cable-stayed bridge.

Figures 7.9 to 7.11 show the uncontrolled and controlled time histories of base shear force and base moment at pier II subjected to three earthquakes used previously when Δ = -0.07. Table 7.2 summarizes the results of evaluation criteria for all three earthquakes. It is observed from the results that no major performance difference in the perturbed system occur, thereby proving the robustness of the new control algorithm.

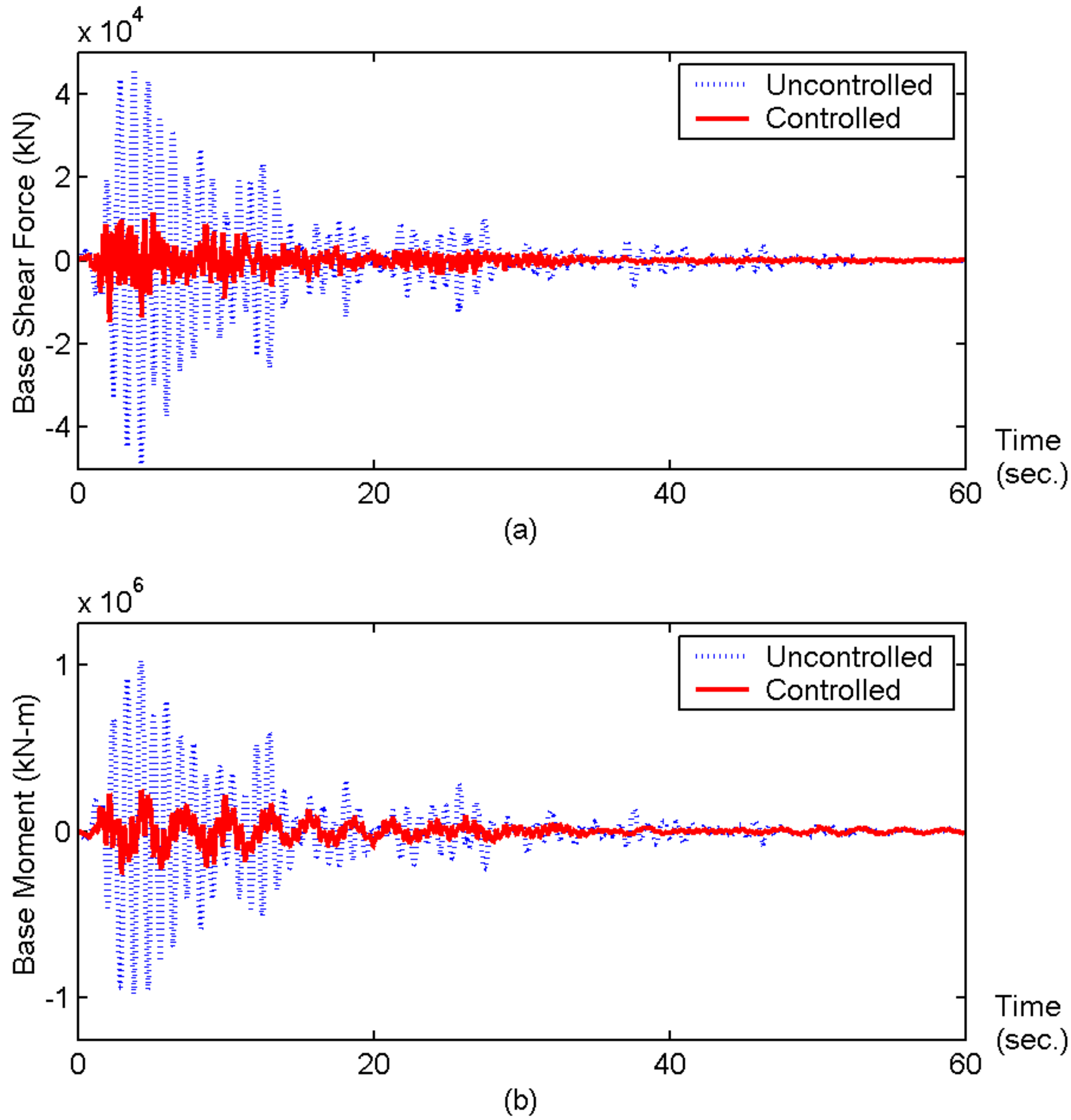

Figure 7.9: Uncontrolled and controlled response time histories of the benchmark bridge with stiffness perturbation, Δ = -0.07, subjected to El Centro earthquake record: a) base shear force at pier II, b) base moment at pier II

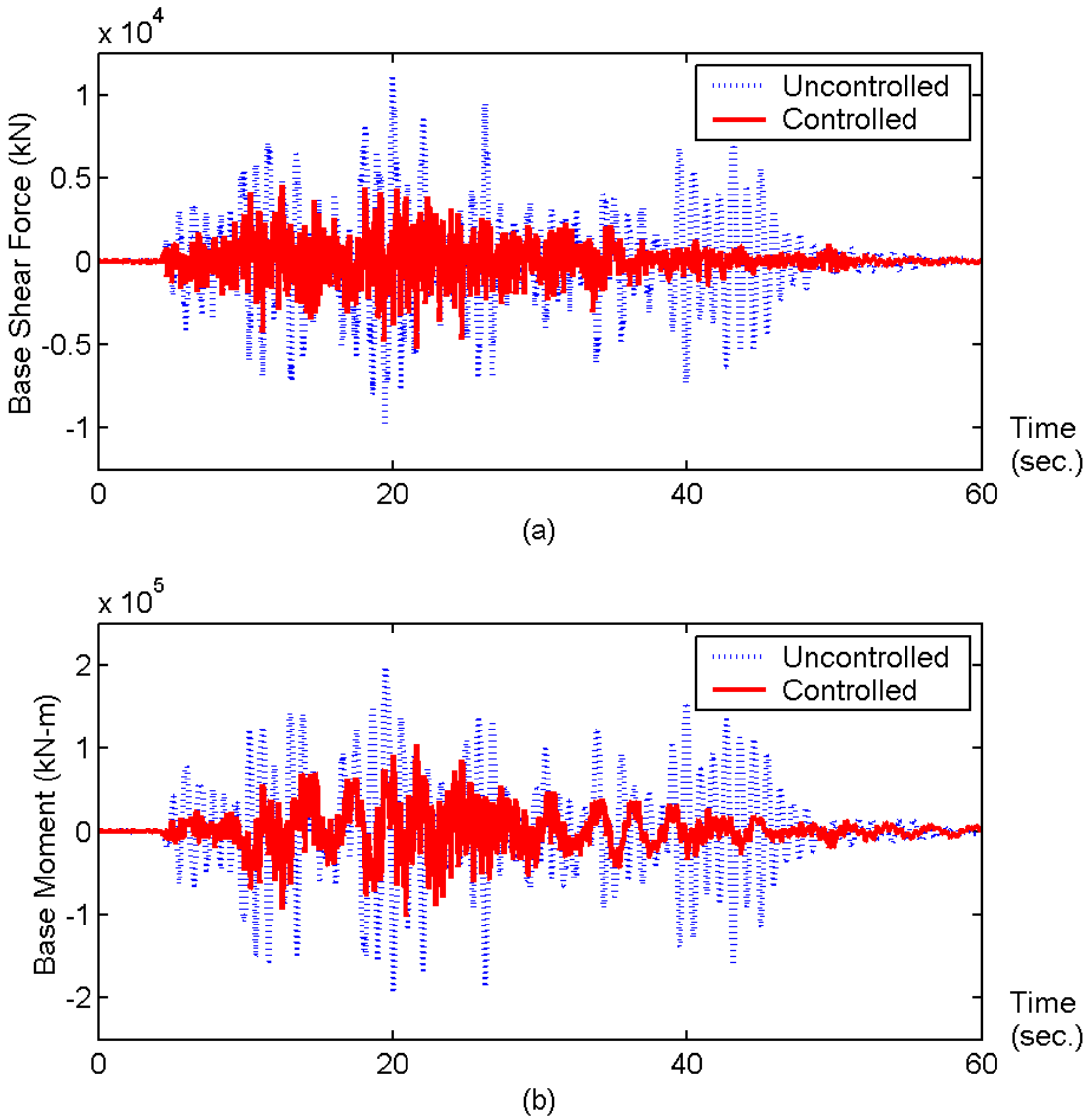

Figure 7.10: Uncontrolled and controlled response time histories of the benchmark bridge with stiffness perturbation, Δ = -0.07, subjected to Mexico City earthquake record: a) base shear force at pier II, b) base moment at pier II

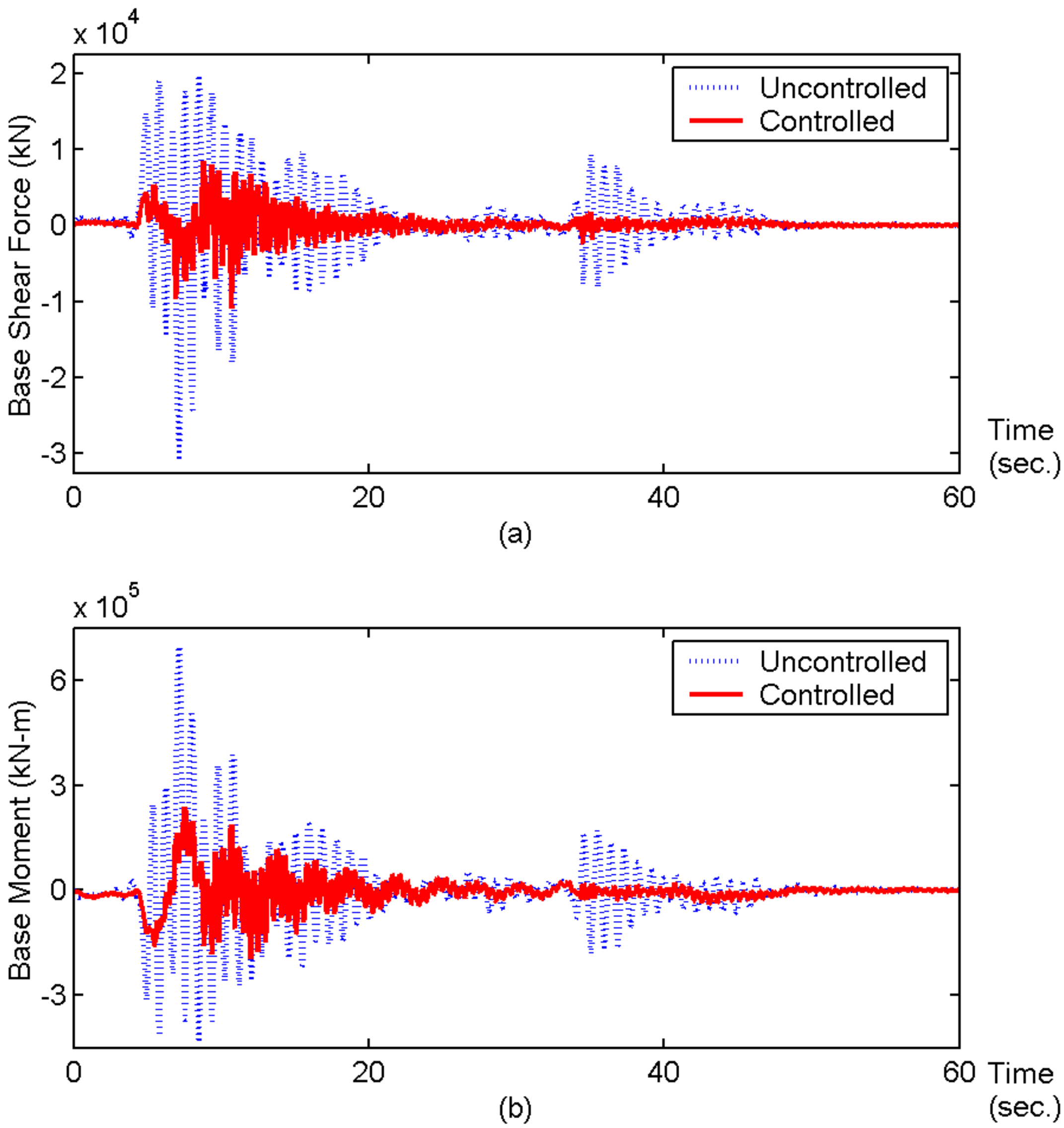

Figure 7.11: Uncontrolled and controlled response time histories of the benchmark bridge with stiffness perturbation, Δ = -0.07, subjected to Gebze earthquake record: a) base shear force at pier II, b) base moment at pier II

Criterion	El Centro	Mexico	Gebze
Max Base Shear (J_1)	0.3583	0.6003	0.4594
Max Deck Shear (J_2)	1.1167	1.3161	1.2689
Max Base Moment (J_3)	0.2784	0.5395	0.4104
Max Deck Moment (J_4)	0.6634	0.5437	0.9711
Max Cable Deviation (J_5)	0.1712	0.0725	0.1527
Max Deck Displacement (J_6)	1.0759	1.9653	2.4250
Norm Base Shear (J_7)	0.2271	0.4545	0.3821
Norm Deck Shear (J_8)	1.1608	1.3495	1.8646
Norm Base Moment (J_9)	0.2437	0.4384	0.4570
Norm Deck Moment (J_{10})	0.7039	0.8967	1.1395
Norm Cable Deviation (J_{11})	2.476E-02	9.494E-03	1.672E-02
Max Control Force (J_{12})	2.161E-03	1.020E-03	1.961E-03
Max Device Stroke (J_{13})	8.216E-06	9.205E-06	2.911E-05
Max Power (J_{14})	3.114E-02	1.377E-02	3.621E-02
Total Power (J_{15})	4.599E-09	1.920E-09	9.991E-09
Number Devices (J_{16})	24	24	24
Number Sensors (J_{17})	9	9	9
Control Resources (J_{18})	30	30	30

Table 7.2: Evaluation criteria results for $\Delta = -0.07$

7.5 Concluding Remarks

The wavelet-hybrid feedback LMS control algorithm is further investigated for vibration control of cable-stayed bridges under various seismic excitations. To evaluate the performance, simulations are performed on a cable-stayed bridge benchmark control problem. Simulation results demonstrate that the new control algorithm is more effective than the sample LQG controller for all three earthquake records consistently.

Moreover, the results of the sensitivity analysis show that the algorithm is stable even when the structural stiffnesses are underestimated by a relatively large value of 7%. This number should be considered in the context of nonlinear behavior of cable-stayed bridges. For control of highrise building structures subjected to wind loading, results provided in Chapter 6 indicate that the control algorithm produces stable results for a much larger value of the perturbation ratio. Consequently, it is concluded that the new control algorithm is robust against the uncertainties existing in modeling structures

CHAPTER 8

CONCLUSIONS AND FUTURE STUDIES

8.1 Summary of Concluding Remarks

A new control algorithm, wavelet-hybrid feedback LMS algorithm, is developed to overcome the shortcomings of the classical feedback control algorithms and the filtered-x LMS control algorithm. The new control algorithm integrates a feedback control algorithm such as the LQR or LQG algorithm with the filtered-x LMS algorithm and utilizes a wavelet multi-resolution analysis for the low-pass filtering of external dynamic excitations. Due to the integration, the total control force is obtained by summing the control force determined by the filtered-x LMS controller and the control force obtained through the feedback controller. Simulation results show that since the control forces determined by the filtered-x LMS algorithm are adapted by updating the FIR filter coefficients at each sampling time until the output error is minimized, the combination of a classical feedback controller with a filtered-x LMS controller results in effective control of both steady-state and transient vibrations. Also, it is shown that the new algorithm is capable of suppressing vibrations over a range of input excitation frequencies unlike the classic feedback control algorithms whose control effectiveness decreases considerably when the frequency of the external disturbance differs from the fundamental frequency of the system. Further, the advantage of the proposed algorithm is that the external excitation is included in the formulation.

The higher frequency contents of external excitations such as earthquakes, winds, and ocean waves, contain noise in nature and thus impede the stabilization of the FIR filter during adaptation. Further, the frequency bandwidths of such environmental signals are much wider than those of common structural systems. Therefore, the use of a low-pass filter that eliminates higher frequency components of the external excitation is crucial in order to apply the algorithm for control of civil structures. This can be effective because the response of most civil structures is not affected by high frequency contents of the external excitations by any significant amount.

A wavelet based low-pass filtering is proposed for stable adaptation of the FIR filter coefficients. Considering the fact that the orthogonal wavelet filtering requires only integer operations, real time control of large structures can be achieved with little additional computational efforts due to filtering. Moreover, the wavelet transform provides an effective way of processing non-stationary signals, to which most environmental signals belong, due to locality of the basis function of wavelet in both time and frequency domains. Simulation results demonstrate the wavelet transform can be effectively used as a low-pass filter for control of civil structures without any significant additional computational burden.

A new hybrid control system, hybrid damper-TLCD system, is proposed, and its performance is evaluated for control of responses of 3D irregular buildings under various seismic excitations and for control of wind-induced motion of high-rise buildings. The new hybrid control system is developed through judicious integration of a passive supplementary damping system with a semi-active TLCD system.

For both supplementary damper and TLCD systems, damping is achieved and damping forces are controlled through an orifice/valve, making them suitable not only for passive control systems but also for semi-active control systems. However, it is shown that the performance improvement of semi-active viscous fluid damper systems over the less complicated and less costly passive damper systems is not always guaranteed depending on the flexibility of the structure, while a semi-active TLCD system can reduce the response significantly compared with a passive TLCD system. As such, by integrating a passive supplementary damping system with a semi-active TLCD system, the new hybrid control system utilizes the advantages of both passive and semi-active control systems along with improving the overall performance significantly. Additionally, the proposed hybrid control system eliminates the need for a large power requirement, unlike other proposed hybrid control systems where active and passive systems are combined.

Simulations performed on irregular 3D building structures and a 76-story building show that the new hybrid control system is effective in significantly reducing the response of structures under seismic excitations as well as wind loads. It is also demonstrated that the hybrid control system provides increased reliability and maximum operability during normal operations as well as a power or computer failure. Further, it is shown that the hybrid damper-TLCD system is robust in terms of the stiffness modeling error for the control of both displacement and acceleration responses.

Finally, the wavelet-hybrid feedback LMS control algorithm is investigated for vibration control of cable-stayed bridge under various seismic excitations. To evaluate the performance, simulations are performed on a cable-stayed bridge benchmark control problem. Simulation results demonstrate that the proposed algorithm is effective for control of cable-stayed bridge. Results also show that the new control algorithm is more effective than the sample LQG controller for all three earthquake records consistently. Moreover, the simulation results at which the structural stiffness matrices are perturbed show that the control algorithm is well performing and robust against the uncertainty existed in the modeling of the bridge.

8.2 Recommendations for Future Research

The semi-active TLCD system described in the dissertation requires a controllable orifice/valve. It is assumed that the valve dynamics is negligible and the headloss coefficient of the orifice (or valve opening ratio) can be ideally changed continuously by applying a command signal. Although useful for design purpose, this ideal model may not accurately describe the nonlinear dynamic behavior of the TLCD system. Therefore, further research can include the valve dynamics in the formulation of the control problem.

Further research is recommended to include the response time of the orifice/valve to the command signal in the formulation. It is also recommended that the modeling of orifice-controlled semi-active TLCD system as well as the effectiveness of the new control algorithm be verified by experiments.

A study on the response time and orifice dynamics of the semi-active Magnetorheological (MR) damper, which also requires a controllable orifice, is performed analytically and experimentally by Yang et al. (2001). They also suggest that the response time and orifice dynamics of the semi-active device be included in the control formulation for more accurate design of control system and show that the pulse width modulation (PWM)-based current driver can be effective in reducing the response time of the MR damper. Since both semi-active TLCD and semi-active MR damper systems utilize similar controllable orifices, the study on the MR damper can be extended to that of semi-active TLCD system.

LIST OF REFERENCES

ABAQUS (1998), Hibbitt, Karlsson & Soresen Inc. Pawtucket, RI.

Abe, M. (1996), "Semi-Active Tuned Mass Dampers for Seismic Protection of Civil Structures", *Earthquake Engineering & Structural Engineering*, Vol. 25, No. 7, pp. 743-749.

Achkire, Y. and Preumont, A. (1996), "Active Tendon Control of Cable-Stayed Bridges", *Earthquake Engineering & Structural Dynamics*, Vol. 25, No. 6, pp. 585-597.

Adeli, H. (2001), "Neural Networks in Civil Engineering: 1989–2000", *Computer-Aided Civil and Infrastructure Engineering*, Vol. 16, No. 2, pp. 126-142.

Adeli, H. and Hung, S. L. (1994), "An Adaptive Conjugate Gradient Learning Algorithm for Effective Training of Multilayer Neural Networks", *Applied Mathematics and Computation*, Vol. 62, No. 1, pp. 81-102.

Adeli, H. and Hung, S. L. (1995), *Machine Learning - Neural Networks, Genetic Algorithms, and Fuzzy Sets*, John Wiley, New York. NY.

Adeli, H. and Karim, A. (2000), "Fuzzy-Wavelet RBF Neural Network Model for Freeway Incident Detection", *Journal of Transportation Engineering*, ASCE, Vol. 126, No. 6, pp. 464-471.

Adeli, H. and Kim, H. (2003), "A Wavelet-Hybrid LMS Algorithm for Robust Control of Structures", *Journal of Structural Engineering*, ASCE, accepted for publication subjected to revisions.

Adeli, H. and Saleh, A. (1997), "Optimal Control of Adaptive/Smart Bridge Structures", *Journal of Structural Engineering*, ASCE, Vol. 123, No. 2, pp. 218-226.

Adeli, H. and Saleh, A. (1999), *Control, Optimization, and Smart Structures - High-Performance Bridges and Buildings of the Future*, John Wiley and Sons, New York.

Adeli, H. and Samant, A. (2000), "An Adaptive Conjugate Gradient Neural Network - Wavelet Model for Traffic Incident Detection", *Computer-Aided Civil and Infrastructure Engineering*, Vol. 13, No. 4, pp. 251-260

Adeli, H. and Zhang, J. (1995), "Fully Nonlinear Analysis of Composite Girder Cable-Stayed Bridges", Computers and Structures, Vol. 54, No. 2, pp. 267-277.

Adeli, H., Zhou, Z., and Dadmehr, N. (2003), "Analysis of EEG Records in an Epileptic Patient using Wavelet Transform", *Journal of Neuroscience Methods*, accepted for publication.

Agrawal, A. K. and Yang, J. N. (1999), "Passive Damper Control of the 76-Story Wind-Excited Benchmark Building", *Proceedings of the Second World Conference on Structural Control*, Chichester, England; New York, Vol. 2, pp. 1481-1490.

AISC (1998), *Manual of Steel Construction - Load and Resistance Factor Design, Vol. I, Structural Members, Specifications, and Codes*, 2nd Ed., 2nd Revision, American Institute of Steel Construction, Chicago, IL.

Ali, H. E. M. and Abdel-Ghaffar, A. M. (1994), "Seismic Energy Dissipation for Cable-Stayed Bridges Using Passive Devices", *Earthquake Engineering & Structural Dynamics*, Vol. 23, No. 8, pp. 877-893.

Arnold, W. F. (1984), "Generalized Eigenproblem Algorithms and Software for Algebraic Riccati Equations", *Proceedings of the IEEE*, Vol. 72, No. 12, pp. 1746-1754.

Bakshi, B. R. and Stephanopoulos, G. (1993), "Wave-Net: a Multiresolution, Hierarchical Neural Network with Localized Learning", *AIChE Journal*, Vol. 39, No.1, pp. 57-81.

Balendra, T., Wang, C. M., and Cheong, H. F. (1995), "Effectiveness of Tuned Liquid Column Dampers for Vibration Control of Towers", "*Engineering Structures*, Vol. 17, No. 9, pp. 668-675.

Blevins, R. D. (1984), *Applied Fluid Dynamics Handbook*, Van Nostrand Reinhold Co., New York, NY.

Bossens, F. and Preumont, A. (2001), "Active Tendon Control of Cable-Stayed Bridges: A Large-Scale Demonstration" *Earthquake Engineering & Structural Dynamics*, Vol. 30, No. 7, pp. 961-979.

Burdisso, R. A., Surarez, L. E. and Fuller, C. R. (1994), “Feasibility Study of Adaptive Control of Structures Under Seismic Excitation”, *Journal of Engineering Mechanics*, ASCE, Vol. 120, No. 3, pp. 580-592.

Burrus, C. S., Gopinath, R. A., and Guo. H, (1998), *Introduction to Wavelets and Wavelet Transforms: a Primer*, Prentice Hall, Upper Saddle River, NJ.

Chen, H. M. Tsai, K. H., Qi, G. Z., Yang, J. C. S. and Amini, F. (1995), “Neural Network for Structure Control”, *Journal of Computing in Civil Engineering*, Vol. 9, No. 2, pp. 168-176.

Christenson, R. E., Spencer, Jr., B. F., Hori, N. and Seto, K. (2003), "Coupled Building Control Using Acceleration Feedback", *Computer-Aided Civil and Infrastructure Engineering*, Vol. 18, No. 1, pp. 3-17.

Chung, L. L., Lin, R. C., Soong, T. T., and Reinhorn, A. M. (1989), “Experiments on Active Control for MDOF Seismic Structures”, *Journal of Engineering Mechanics*, ASCE, Vol. 115, No. 8, pp. 1609-1627.

Connor, J. J. (2003), *Introduction to Structural Motion Control*, Prentice Hall, Upper Saddle River, NJ.

Craig, R. R., (1981), *Structural Dynamics: an Introduction to Computer Methods*, Wiley, New York.

Daubechies, I., (1992), *Ten Lectures on Wavelets*, Society for Industrial and Applied Mathematics, Philadelphia, PA.

Dorato, P., Abdallah, C., and Cerone, V. (1995), *Linear-Quadratic Control: An Introduction*, Prentice Hall, Englewood Cliffs, NJ.

Dyke, S. J., Spencer, B. F. Jr., Quast, P., Kaspari, D. C. Jr. and Sain, M. K. (1996a), “Implementation of an Active Mass Driver using Acceleration Feedback”, *Microcomputers in Civil Engineering*, Vol. 11, No. 5, pp. 305-323.

Dyke, S. J., Spencer, B. F. Jr., Sain, M. K., and Carlson, J. D. (1996b), “Modeling and control of magnetorheological dampers for seismic response reduction”, *Smart Materials and Structures* Vol. 5, No. 5, pp.565-575.

Dyke, S. J., Turan, G., Caicedo, J. M., Bergman, L. A., and Hague, S. (2000), “Benchmark Control Problem for Seismic Response of Cable-Stayed Bridges”, *Proceedings of the Second European Conference on Structural Control*, Also available at http://wusceel.cive.wustl.edu/quake/.

Feng, Q. and Shinozuka, M. (1993), "Control of Seismic Response of Bridge Structures using Variable Dampers", *Journal of Intelligent Material Systems and Structures*, Vol. 4, No. 1, pp. 117-122.

Fortner, B. (2001), "Water Tanks Damp Motion in Vancouver High-Rise", *Civil Engineering*, June, p.18.

Ghaboussi, J. and Joghataie, A. (1995), "Active Control of Structures using Neural Networks", *Journal of Engineering Mechanics*, ASCE, Vol. 121, No. 4, pp. 555-567.

Hanson, R. D. and Soong, T. T. (2001), *Seismic Design with Supplemental Energy Dissipation Devices*, Earthquake Engineering Research Institute (EERI), Oakland, CA.

He, W. L., Agrawal, A. K. and Mahmoud, K. (2001), "Control of Seismically Excited Cable-Stayed Bridge Using Resetting Semiactive Stiffness", *Journal of Bridge Engineering*, Vol. 6, No. 6, pp. 376-384.

Housner, G. W., Bergman, L. A., Caughey, T. K., Chassiakos, A. G., Claus, R. O., Masri, S. F., Skelton, R. E., Soong, T. T., Spencer, B. F., and Yao, J. T. P. (1997), "Structural Control: Past, Present, and Future", *Journal of Engineering Mechanics*, ASCE, Vol. 123, No.9, Special Issue, pp. 897-971.

Hovat, D., Barak, P., and Rabins, M. (1983), "Semi-Active Versus Passive of Active Tuned Mass Dampers for Structural Control", *Journal of Engineering Mechanics*, ASCE, Vol. 109, No. 3, pp. 691-705.

IBC (2000), *International Building Code 2000*, International Code Council, Falls Church, Virginia.

Kareem, A. (1994), "The Next Generation of Tuned Liquid Dampers", *Proceedings of First World Conference on Structural Control*, Los Angeles, California, USA, pp. FP5-19-FP5-28.

Kareem, A. and Kline, S. (1995), "Performance of Multiple Mass Dampers under Random Loading", *Journal of Structural Engineering*, Vol. 121, No. 2, pp.348-361.

Karim, A. and Adeli, H. (2002a), "Comparison of the Fuzzy – Wavelet RBFNN Freeway Incident Detection Model with the California Algorithm", *Journal of Transportation Engineering*, ASCE, Vol. 128, No. 1, pp. 21-30.

Karim, A. and Adeli, H. (2002b), "Incident Detection Algorithm Using Wavelet Energy Representation of Traffic Patterns", *Journal of Transportation Engineering*, ASCE, Vol. 128, No. 3, pp. 232-242.

Kim, H. and Adeli, H, (2003a), "Hybrid Feedback-LMS Algorithm for Structural Control", *Journal of Structural Engineering*, ASCE, accepted for publication subjected to revisions.

Kim, H. and Adeli, H, (2003b), "Hybrid Damper-TLCD Control of Structures under Seismic Excitations using a Wavelet-Based Algorithm", *Journal of Structural Engineering*, ASCE, submitted.

Kim, H. and Adeli, H, (2003c), "Wavelet-Based Hybrid Control of 3D Irregular Buildings under Seismic Excitations", submitted.

Kim, H. and Adeli, H, (2003d), "Wind-Induced Motion Control of 76-Story Benchmark Building using the Hybrid Damper-TLCD System", submitted.

Kim, H. and Adeli, H. (2003e), "Wavelet-Hybrid Feedback LMS Algorithm for Robust Control of Cable-Stayed Bridges", submitted.

Kurata, N., Kobori, T, Takahashi, M, Niwa, N. and Midorikawa, M. (1999), "Actual Seismic Response Controlled Building with Semi-Active Damper System", *Earthquake Engineering & Structural Engineering*, Vol. 28, No. 11, pp. 1427-1447.

Lee-Glauser, G. J., Ahmadi, G., and Horta, L. G. (1997), "Integrated Passive/Active Vibration Absorber for Multistory Buildings", *Journal of Structural Engineering*, ASCE, Vol. 123, No. 4, pp. 499-504.

Lewis, F. L. and Syrmos, V. L. (1995), *Optimal Control*, Wiley, New York, NY.

Liang, S., Li, Q., and Qu, W., (2000), "Control of 3-D Coupled Responses of Wind-Excited Tall Buildings by a Spatially Placed TLCD System", *Wind & Structures*, Vol. 3, No. 3, pp. 193-207.

Mallat, S. G. (1989), "A Theory for Multiresolution Signal Decomposition: The Wavelet Representation", *IEEE Transactions on Pattern Analysis and Machine Intelligence*, Vol. 11, No. 7, pp.674-693.

Matlab (1999), *SIMULINK: Dynamic System Simulation for Matlab*, Mathworks Inc, Natick, MA.

Matlab (2000), *Control system toolbox for use with Matlab*, Mathworks Inc, Natick, MA.

Meyer, Y. (1993), *Wavelets: Algorithms & Applications*, Society for Industrial and Applied Mathematics, Philadelphia, PA.

Miyamoto, H. K. and Scholl, R. E. (1998), "Steel Pyramid", *Modern Steel Construction*, November, pp. 42-28.

Mokha, A. S., Amin, N., Constantinou, M. C., and Zayas, V. (1996), “Seismic Isolation Retrofit of Large Historic Building”, *Journal of Structural Engineering*, Vol. 122, No. 3, pp.298-308.

Newland, D. E. (1993), *An Introduction to Random Vibrations, Spectral and Wavelet Analysis*, Wiley, New York, NY.

Prakah-Asante, K. O. and Craig, K. C. (1994), “The Application of Multi-Channel Design Methods for Vibration Control of an Active Structure”, *Smart Material and Structures*, Vol. 3, No. 3, pp. 329-343.

Rao, R. M. and Bopardikar, A. S. (1998), *Wavelet Transforms: Introduction to Theory and Applications*, Addison-Wesley, Reading, MA.

Sadek, F. and Mohraz, B. (1998), “Semiactive Control Algorithms for Structures with Variable Dampers”, *Journal of Engineering Mechanics*, ASCE, Vol. 124, No. 9, pp. 981-990.

Sadek, F., Mohraz, B. and Lew, H. S. (1998), “Single- and Multiple-Tune Liquid Column Dampers for Seismic Applications”, *Earthquake Engineering & Structural Dynamics*, Vol. 27, No. 5, pp. 439-463.

Sakai, F., Takaeda, S., and Tamaki, T. (1989), “Tuned Liquid Column Damper – New Type Device for Suppression of Building Vibrations”, *Proceedings of International Conference on Highrise Buildings*, Nanjing, China, pp. 926-931.

Sakai, F., Takaeda, S., and Tamaki, T. (1991), "Tuned liquid damper (TLCD) for Cable-Stayed Bridges", *Proceedings of Specialty Conf. Invitation in Cable-Stayed Bridges*, Fukuoka, Japan, pp. 197-205.

Saleh, A. and Adeli, H. (1997), "Robust Parallel Algorithms for Solution of the Riccati Equation", *Journal of Aerospace Engineering*, ASCE, Vol. 10, No. 3, pp. 126-133.

Saleh, A. and Adeli, H. (1998), “Optimal Control of Adaptive/Smart Multistory Building Structures”, *Computer-Aided Civil and Infrastructure Engineering*, Vol. 13, No. 6, pp. 389-403.

Samali, B., Kwok, K., and Gao, H. (1998), “Wind Induced Motion Control of a 76 Storey Building By Liquid Dampers” *Proceedings Of Second World Conference on Structural Control*, Vol. 2, pp. 1473-1480, John Wiley & Sons, New York, NY.

Samant, A. and Adeli, H. (2000), "Feature Extraction for Traffic Incident Detection using Wavelet Transform and Linear Discriminant Analysis", *Computer-Aided Civil and Infrastructure Engineering*, Vol. 15, No. 4, pp. 241-250.

Samant, A. and Adeli, H. (2001), “Enhancing Neural Network Incident Detection Algorithms using Wavelets”, *Computer-Aided Civil and Infrastructure Engineering*, Vol. 16, No. 4, pp. 239-245.

Schemmann, A. G. and Smith, H. A. (1998a), “Vibration Control of Cable-Stayed Bridges, Part 1: Modeling Issues”, *Earthquake Engineering & Structural Dynamics*, Vol. 27, No. 8, pp. 811-824.

Schemmann, A. G. and Smith, H. A. (1998b), “Vibration Control of Cable-Stayed Bridges, Part 2: Control Analyses”, *Earthquake Engineering & Structural Dynamics*, Vol. 27, No. 8, pp. 825-843.

Simiu, E. and Scanlan, R. H. (1996), *Wind Effects on Structures: Fundamentals and Applications to Design*, John Wiley, New York, NY.

Singh, M. P. and Matheu, E. E. (1997), “Active and Semi-active Control of Structures under Seismic Excitation”, *Earthquake Engineering & Structural Dynamics*, Vol. 26, No. 2, pp. 193-213.

Skelton, R. E. (1988), *Dynamic Systems Control: Linear Systems Analysis and Synthesis*, Wiley, New York, NY.

Soong, T. T. (1990), *Active Structural Control: Theory and Practice*, Wiley, New York, NY.

Soong, T. T. and Constantinou, C. (Eds.) (1994), *Passive and Active Structural Vibration Control in Civil Engineering*, Springer-Verlag, New York, NY.

Soong, T. T. and Reinhorn, A. M. (1993), “An Overview of Active and Hybrid Structural Control Research in the U.S.”, *Structural Design of Tall Buildings*, Vol. 2, No. 3, pp. 192-209.

Spencer, B. F. Jr., Dyke, S. J. and Deoskar, H. S. (1998), “Benchmark Problems in Structural Control: Part I - Active Mass Driver System”, *Earthquake Engineering & Structural Engineering*, Vol. 27, No. 11, pp. 1127-1139.

Spencer, B. F. Jr., Suhardjo, J., and Sain, M. K. (1994), “Frequency Domain Optimal Control Strategies for Aseismic Protection”, *Journal of Engineering Mechanics*, ASCE, Vol. 120, No. 1, pp. 135-158.

Stein, G. and Athans, M. (1987), “The LQG/LTR Procedure for Multivariable Feedback Control Design”, *IEEE Transactions On Automatic Control*, Vol. AC32, No. 2, pp. 105-114.

Suhardjo, J., Spencer, B. F. Jr., and Kareem, A. (1992), "Frequency Domain Optimal Control of Wind-Excited Buildings", *Journal of Engineering Mechanics*, ASCE, Vol. 118, No. 12, pp. 2463-2481.

Symans, M. D. and Constantinou, C. (1997), "Seismic Testing of a Building Structure with a Semi-Active Fluid Damper Control System", *Earthquake Engineering & Structural Dynamics*, Vol. 26, No. 7, pp. 759-777.

Symans, M. D. and Constantinou, C. (1999), "Semi-active Control Systems for Seismic Protection of Structures: A State-of-the-art Review", *Engineering Structures*, Vol. 21, No. 6, pp.469-487.

Tabatabai, B. and Mehrabi, A.B. (2000), "Design of Mechanical Viscous Dampers for Stay Cables", *Journal of Bridge Engineering*, Vol. 5, No. 2, pp.114-123

Tarrab, M. and Feuer, A. (1988), "Convergence and Performance Analysis of the Normalized LMS Algorithm with Uncorrelated Gaussian Data", *IEEE Transactions on Information Theory*, Vol. 34, No. 4, pp. 680-691.

Teramura, A. and Yoshida, O. (1996), "Development of Vibration Control System Using U-shaped Water Tank", *Proceedings of the Eleventh World Conference on Earthquake Engineering*, Pergamon, Paper No. 1343.

Turan, G., Voulgaris, P., and Bergman, L. (2002), "µ-Synthesis Control of a Cable-Stayed Bridge Against Earthquake Excitation", *Proceedings of the Third World Conference in Structural Control*, Coma, Italy. Also available at http://wusceel.cive.wustl.edu/quake

Villaverde, R. and Marin, S. C. (1995), "Passive Seismic Control of Cable-Stayed Bridges with Damped Resonant Appendages", *Earthquake Engineering & Structural Dynamics*, Vol. 24, No. 2, pp. 233-246.

Wang, M. L. and Wu, F. (1995), "Structural System Identification using Least Mean Square (LMS) Adaptive Technique", *Soil Dynamics and Earthquake Engineering*, Vol. 14, No. 6, pp. 409-418.

Warnitchai, P., Fujino, Y., Pacheco, B. M. and Agret, R. (1993), "Experimental Study on Active Tendon Control of Cable-Stayed Bridges *Earthquake Engineering & Structural Dynamics*, Vol. 22, No. 2, pp. 93-111.

Widrow, B. J. and Stearns, S. D. (1985), *Adaptive Signal Processing*, Prentice-Hall, Englewood Cliffs, NJ.

Won, A. Y. J., Pires, J. A., and Haroun, M. A. (1996), "Stochastic Seismic Performance Evaluation of Tuned Liquid Column Dampers", *Earthquake Engineering & Structural Dynamics*, Vol. 25, No. 11, pp.1259-1274.

Wu, M. and Adeli, H. (2001), "Wavelet-Neural Network Model for Automatic Traffic Incident Detection," *Mathematical and Computational Applications*, Vol. 6, No. 2, pp. 85-96.

Yalla, S. K., and Kareem, A. (2000), "Optimum Absorber Parameters for Tuned Liquid Column Dampers", *Journal of Structural Engineering*, Vol. 126, No. 8, pp.906-915.

Yalla, S. K., Kareem, A., and Kantor, J. C. (2001), "Semi-active Tuned Liquid Column Dampers for Vibration Control of Structures", *Engineering Structures*, Vol. 23, No. 11, pp. 1469-1479.

Yang, G. and Satoh Y. (2001), *Java-Powered Simulator for Structural Vibration Control*, http://www.nd.edu/~quake/java/sin.html.

Yang, G., Jung, H. J. and Spencer, B. F. Jr. (2001) "Dynamic Modeling of Full-Scale MR Dampers for Civil Engineering Applications," *US-Japan Workshop on Smart Structures for Improved Seismic Performance in Urban Region*, Seattle, WA, Aug. pp. 14–16,.

Yang, J. N. (1982), "Control of Tall Building under Earthquake Excitation", *Journal of Engineering Mechanics Division*, ASCE, Vol. 108, No. EM5, pp. 833-849.

Yang, J. N. and Li, Z. (1991), "Instantaneous Optimal Control of Linear and Nonlinear Structures – Stable Controller", *Technical Report, NCEER-TR-91-0026*, National Center for Earthquake Engineering Research, Buffalo, NY.

Yang, J. N., Agrawal, A. K., Samali, B., and Wu, J. C. (2000), "A Benchmark Problem for Response Control of Wind-Excited Tall Buildings" *Proceedings of Fourteenth Engineering Mechanics Conference*, ASCE, Austin, Texas, 8p., Also available at: http://www-ce.engr.ccny.cuny.edu/people/faculty/agrawal/benchmark.html.

Yang, J. N., Akbrapour, A. and Ghaemmaghami, P. (1987), "New Optimal Control Algorithms for Structural Control", *Journal of Engineering Mechanics*, ASCE, Vol. 113, No. 9, pp. 1369-1386.

Yang, J. N., Wu, J. C., Samali, B., and Agrawal, A. K. (1998), "A Benchmark Problem for Response Control of Wind-Excited Tall Buildings" *Proceedings Of Second World Conference on Structural Control*, Vol. 2, pp. 1407-1416, John Wiley & Sons, New York, NY.

Yao, J. T. P. (1972), "Concept of Structural Control", *Journal of Structural Division*, ASCE, Vol. 98, No. ST7, pp. 1567-1574.

Youssef, N., Nuttall, B., Hata, O., Tahtakran, O., and Hart, G. C. (2000), "Los Angeles City Hall", *Structural Design of Tall Buildings*, Vol. 9, No. 1, pp. 3-24.

Zhang, R.H. and Soong, T. T. (1992), “Seismic Design of Viscoelastic Dampers for Structural Applications”, *Journal of Structural Engineering*, ASCE, Vol. 118, No. 5, 1992, pp. 1375-1392.

Zhou, Z. and Adeli, H. (2003), "Time-frequency Signal Analysis of Earthquake Records using Mexican Hat Wavelets", *Computer-Aided Civil and Infrastructure Engineering*, Vol. 18, No. 5.

APPENDIX A

STRUCTURAL PROPERTIES OF THE ATMD SYSTEM

USED IN CHAPTERS 2 AND 3

$$\boldsymbol{M} = \begin{bmatrix} 100 & 0 \\ 0 & 1 \end{bmatrix} \times 10^3 \, kg$$

$$\boldsymbol{C} = \begin{bmatrix} 1.3495 & -0.0928 \\ -0.0928 & 0.0928 \end{bmatrix} \times 10^4 \, \mathrm{N \cdot s/m}$$

$$\boldsymbol{K} = \begin{bmatrix} 3.9861 & -0.0383 \\ -0.0383 & 0.0383 \end{bmatrix} \times 10^6 \, \mathrm{N/m}$$

$$\boldsymbol{Q} = diag\begin{bmatrix} 5000 & 10 & 0 & 0 \end{bmatrix}$$

$$\boldsymbol{R} = [1]$$

APPENDIX B

PROGRAMMING CODES FOR THE WAVELET-HYBRID FEEDBACK LMS ALGORITHM USING MATLAB

B.1 Program to draw the frequency response function of the ATMD system with and without

```
clear;

% ... Structural properties
m1 = 100000; % kg
fs = 1; % frequency, Hz
zeta_s = 0.01; % damping ratio

% ...ATMD properties
massRatio = 0.01;
fd = 0.985; % Hz
zeta_d =0.075; %
k0 =10000;

% ...Construct necessary parameters
m2 = m1*massRatio;
k1 = (2*pi*fs)^2*m1;
c1 = 4*pi*zeta_s*fs*m1;
k2 = (2*pi*fd)^2*m2;
c2 = 4*pi*zeta_d*fd*m2;

M = [m1 0;0 m2];
K = [k1+k2 -k2;-k2 k2];
Damping = [c1+c2 -c2;-c2 c2];

% …Construct the state space form
A = [zeros(length(M)) eye(length(M));-inv(M)*K -inv(M)*Damping];
```

```
C = [1 0 0 0];
D = 0;
E = [0;0;-1;-1];
B = [zeros(length(M),1);-1/m1; 1/m2]*k0;

% ...Weight Matrices
Q = diag([5000;10;0;0]);
R = 1;

% … Get the gain matrix
[G,S,e] = lqr(A,B,Q,R);
AG = A - B*G;

w=2*pi*[0:0.1:3];
[m,p,w]=bode(A,E,C,D,1,w);
[mc,pc,w]=bode(AG,E,C,D,1,w);

figure,plot(w/2/pi,20*log10(m),'k',w/2/pi,20*log10(mc),'k--');
axis([0 3 -50 0])
xlabel('Frequency (Hz)'),ylabel('Magnitude (dB)')
legend('without control','with LQR control')
```

B.2 Program to run LMS algorithm for the ATMD system

```
clear;

% ...Structural properties
m1 = 100000; % kg
fs = 1; % frequency, Hz
zeta_s = 0.01; % damping ratio

% ...ATMD  properties
massRatio = 0.01;
fd = 0.985; % Hz
zeta_d =0.075; %
k0 =10000;

% ...Construct necessary parameters
m2 = m1*massRatio;
k1 = (2*pi*fs)^2*m1;
c1 = 4*pi*zeta_s*fs*m1;
k2 = (2*pi*fd)^2*m2;
c2 = 4*pi*zeta_d*fd*m2;
```

```
M = [m1 0;0 m2];
K = [k1+k2 -k2;-k2 k2];
Damping = [c1+c2 -c2;-c2 c2];

A = [zeros(length(M)) eye(length(M));-inv(M)*K -inv(M)*Damping];
C = [1 0 0 0];
Dc = [0 0];
B = [zeros(length(M),1);-1/m1; 1/m2]*k0;
E = [0;0;-1;-1];
Bc = [E B];

% ...loads
Ts=1/50;
freq=1.2;
t=[0:Ts:40];
Tf = t(length(t));
u=100*sin(2*pi*freq*t);
N=size(t,2);

[Ad,Bd,Cd,Dd]= C2DM(A,Bc,C,Dc,Ts,'tustin');
[d,x]=dlsim(Ad,Bd(:,2),Cd,Dd(:,2),u);

N_coeff = 2;
w1=zeros(N_coeff,size(d,1));
e=zeros(size(d));
y=zeros(size(d));

% ...RUN SIMULINK MODEL
sim('fig67sim')

subplot(2,1,1),plot(t,d)
xlabel('time (sec.)')
ylabel('Disp. (cm)')
subplot(2,1,2),plot(tout,err)
xlabel('time (sec)')
ylabel('Error Signal (cm)')

figure,plot(tout,W(:,1),t,W(:,2))
xlabel('time (sec.)')
ylabel('Filter Coefficients')
```

B.3 Program to run Filtered-x LMS algorithm using the ATMD system

```
clear;

% ...Structural properties
m1 = 100000; % kg
fs = 1; % frequency, Hz
zeta_s = 0.01; % damping ratio

% ...ATMD properties
massRatio = 0.01;
fd = 0.985;
zeta_d =0.075;
k0 =10000;

% ... Construct necessary parameters
m2 = m1*massRatio;
k1 = (2*pi*fs)^2*m1;
c1 = 4*pi*zeta_s*fs*m1;
k2 = (2*pi*fd)^2*m2;
c2 = 4*pi*zeta_d*fd*m2;

M = [m1 0;0 m2];
K = [k1+k2 -k2;-k2 k2];
Damping = [c1+c2 -c2;-c2 c2];

A = [zeros(length(M)) eye(length(M));-inv(M)*K -inv(M)*Damping];
C = [1 0 0 0];
D = 0;
E = [0;0;-1;-1];
B = [zeros(length(M),1);-1/m1; 1/m2]*k0;

Bc = [E B];
Dc = [D D];

%  OFF-LINE
Ts = 1/50;
[Ad,Bd,Cd,Dd]= C2DM(A,Bc,C,Dc,Ts,'tustin');
[num,den] = ss2tf(Ad,Bd(:,2),Cd,Dd(:,2));

%  ON-LINE
freq = 1.2
N_coeff = 2;
Tf = 30;
```

```
t=[0:Ts:Tf];
u=100*sin(2*pi*freq*t);

sim('fig9sim')

% ...LQR control
Q = diag([5000;10;0;0]);
R = 1;
 [G,S,e1] = lqr(A,B,Q,R);
AG = (A-B*G);
[Ad,Bd,Cd,Dd] = C2DM(AG,Bc,C,Dc,Ts,'tustin');
 [X4 Y] = lsim(AG,Bc(:,1),C,Dc(:,1),u(1:length(u)),t);
[X44 Y] = lsim(A,Bc(:,1),C,Dc(:,1),u(1:length(u)),t);

%figure
subplot(2,1,1),plot(t,X44,'k:',t,X4,'k')
legend('without control','LQR control')
ylabel('Displacement (cm)')

subplot(2,1,2),plot(t,X44,'k:',t,zout,'k')
legend('without control','Filtered-x LMS control')
ylabel('Displacement (cm)')
xlabel('Time(sec.)')
```

B.4Program to run Hybrid feedback-LMS algorithm using the ATMD system

```
clear;

% ...Structural properties
m1 = 100000; % kg
fs = 1; % frequency, Hz
zeta_s = 0.01; % damping ratio

% ...ATMD/HMD properties
massRatio = 0.01;
fd = 0.985; % Hz
zeta_d =0.075;
k0 =10000;

% ...Construct necessary parameters
m2 = m1*massRatio;
k1 = (2*pi*fs)^2*m1;
c1 = 4*pi*zeta_s*fs*m1;
```

```
k2 = (2*pi*fd)^2*m2;
c2 = 4*pi*zeta_d*fd*m2;

M = [m1 0;0 m2];
K = [k1+k2 -k2;-k2 k2];
Damping = [c1+c2 -c2;-c2 c2];

A = [zeros(length(M)) eye(length(M));-inv(M)*K -inv(M)*Damping];
C = eye(4);
D = zeros(4,1);
Dc = [D D];
B = [zeros(length(M),1);-1/m1; 1/m2]*k0;
E = [0;0;-1;-1];
Bc = [E B];


% ...loading
Ts=1/50;
freq=1.2;
t=[0:Ts:30];
u=100*sin(2*pi*freq*t);

[At] = [A];
[Bt] = [E B];
[Ct] = [C];
[Dt] = [D D];
[Atd,Btd,Ctd,Dtd] = C2DM(At,Bt,Ct,Dt,Ts,'tustin');

% LQR
Q = diag([5000;10;0;0]); %Q = diag([k1;0;0;0]);
R = 1;
[G,S,e1] = lqr(A,B,Q,R);
AG = (A-B*G);
[Ad,Bd,Cd,Dd] = C2DM(AG,Bc,C,Dc,Ts,'tustin');
Gd = inv((Bd(:,2)'*Bd(:,2)))*Bd(:,2)'*(Atd-Ad);

% ...offline estimation
 [num,den] = ss2tf(Ad,Bd(:,2),Cd,Dd(:,2));
rhat_K=filter(num(1,:),den,u);

stepsize=8e-3;
N_coeff = 10;
Tf = 30;
sim('fig10_2sim')
```

```
w=zeros(N_coeff,size(t,2)+1);
uc=zeros(1,size(t,2)+1);
zd=zeros(size(Ad,1),size(t,2)+1);
z3d=zeros(size(Ad,1),size(t,2)+1);

a=1.0e-10;
for k=N_coeff+1:size(t,2)
    ref = u(k:-1:k-N_coeff+1);
    uc_LMS(k) = w(1:N_coeff,k)' *  ref';
    uc_LQR(k) = -Gd*zd(:,k);
    uc(k)=uc_LMS(k)+uc_LQR(k);

    zd(:,k+1) = Atd*zd(:,k) + Btd*[u(k);uc(k)];
    err(:,k) = Ctd*zd(:,k) + Dtd*[u(k);uc(k)];
    rhat=rhat_K(k:-1:k-N_coeff+1);

    % ...calculate update of control for time k+1
    for jj=1:N_coeff
        w(jj,k+1) = w(jj,k) - stepsize/(rhat*rhat'+a)* rhat(jj) * err(1,k);
    end
end

%... check result
for k=N_coeff+1:size(t,2)
    z(:,k+1) = Atd*zd(:,k) + Btd*[u(k);uc(k)];
    err2(:,k) = Ctd*zd(:,k) + Dtd*[u(k);uc(k)];
end

% ... response of Filter-x control
load filtxlms12.mat

% ...LQR
[X0 Y] = dlsim(Ad,Bd(:,1),Cd,Dd(:,1),u);
% ... No control
[X Y] = dlsim(Atd,Btd(:,1),Ctd,Dtd(:,1),u);

% Draw Figures
clf;
set(gcf,'defaultaxeslinewidth',1);      % Change axes line thickness
set(gcf,'defaultlinelinewidth',2);      % Change curve line thickness
set(gcf,'defaulttextfontsize',12);      % Change fontsize
set(gcf,'defaultaxesfontsize',12);
```

```
subplot(2,1,1),plot(t,filtxd,'k:',t,err2(1,:))
set(gca,'ytick',[-10 0 10 ])
set(gca,'xtick',[0 10 20 30])
xlabel('(a)')
ylabel('Displacement (cm)')
legend('Filtered-x LMS control','Hybrid feedback-LMS control')

subplot(2,1,2),plot(t,uc_LMS/10,'k:',t,uc_LQR/10,'r-.',t,uc(1:1501)/10)
axis([0 30 -120 175])
set(gca,'ytick',[-100 0 100 ])
set(gca,'xtick',[0 10 20 30])
xlabel('(b)')
ylabel('Control Force (kN)')
legend('Filtered-x LMS Force','LQR Force', 'Total Force')
```

B.5 Program to draw wavelet and scaling functions for Harr and Daubechies wavelet with 2 vanishing moments

```
% Needs Wavelab toolbox

clear all;

% ... set graph parameters
clf;
set(gcf,'defaultaxeslinewidth',1);     % Change axes line thickness
set(gcf,'defaultlinelinewidth',2);     % Change curve line thickness
set(gcf,'defaulttextfontsize',12);     % Change fontsize
set(gcf,'defaultaxesfontsize',12);

n = 1024;
J = log2(n);

% D4 (Daubechies wavelet with 2 vanishing moments)
j = 7;
p = 4;
k = 2^(J-j-1);
m = MakeWavelet(J-j,k,'Daubechies',p,'Mother',n ).*2^(j/2);
supp = find(abs(m) >0.0000001);
mins = min(supp);
maxs = max(supp);
i = (((1:n)-n/2)./2^j)+1;
subplot(223)
plot(i(mins:maxs),m(mins:maxs))
axis([0 3 -2 2])
```

```
ylabel('Wavelet function,')
set(gca,'xtick',[0 1 2 3])
set(gca,'ytick',[-2 -1 0 1 2])

str(1)={'\it\psi\rm(t)'};
text(-0.66,1.6,str,'rotation',90)

j = 7;
p = 4;
k = 2^(J-j-1);
m = MakeWavelet(J-j,k,'Daubechies',p,'Father',n ).*2^(j/2);
supp = find(abs(m) >0.0000001);
mins = min(supp);
maxs = max(supp);
i = (((1:n)-n/2)./2^j)+1;
subplot(224)
plot(i(mins:maxs),m(mins:maxs))
axis([0 3 -1 1.5])
set(gca,'ytick',[-1 0 1])

ylabel('Scaling function,')
xlabel('(b) Daubechies wavelet with 2 vanishing moments','Fontsize',12)
text(-0.66,1.3,'j','rotation',90) % need to change font to 'symbol'
text(-0.66,1.45,'(t)','rotation',90)
text(3.1,-0.9,'t')

% Harr
t = linspace(0,3,3000);
scale = zeros(1,3000);
scale(1000:2000) = 1.0;

subplot(222), plot(t,scale)
axis([0 3 -1 1.5])
set(gca,'ytick',[-1 0 1])

ylabel('Scaling function,')
xlabel('(a) Harr wavelet','Fontsize',12)
text(-0.66,1.3,'j','rotation',90) % need to change font to 'symbol'
text(-0.66,1.45,'(t)','rotation',90)
text(3.1,-0.9,'t')

wavelet = zeros(1,3000);
wavelet(1000:1500) = -1.0;
wavelet(1501:2000)= 1.0;
```

```
subplot(221), plot(t,wavelet)
axis([0 3 -2 2]);
ylabel('Wavelet function,')

str(1)={'\it\psi\rm(t)'};
text(-0.66,1.6,str,'rotation',90)
text(3.1,-1.9,'t')
set(gca,'xtick',[0 1 2 3])
set(gca,'ytick',[-2 -1 0 1 2])
```

B.6 Program to obtain Fourier Transform of wavelet functions

```
% Needs Wavelab toolbox

clear;

% ... set graph parameters
clf;
set(gcf,'defaultaxeslinewidth',1);      % Change axes line thickness
set(gcf,'defaultlinelinewidth',1);      % Change curve line thickness

n = 1024;
J = log2(n);
j =7;

dt = 4/n; % time
dw = 1/(n*dt); % frequency
t=0.0:dt:(n-1)*dt;  %t = t-1;
w=0.0:dw:(n-1)*dw;

% FFT D4, Daubechies wavelet with 2 vanishing moments
p = 4;
k = 2^(J-j-1);
m4 = MakeWavelet(J-j,k,'Daubechies',p,'Mother',n).*2^(j/2);

M4 = fft(m4);
mag_4 = abs(M4);

subplot(221), plot(t,m4)
axis([0 4 -2 2]);
set(gca,'ytick',[-2 -1 0 1 2])

text(4.1,-1.9,'sec')
ylabel('\it\psi\rm(t)')
```

```
xlabel('(a) Daubechies wavelet with 2 vanishing moments','Fontsize',12)


subplot(222),plot(w(1:100),mag_4(1:100))
axis([0 23 0 150]);
ylabel('|FT(\it\psi\rm(t))|')
text(23.5,3.1,'Hz')
set(gca,'xtick',[0 10 20])

% FFT D18, Daubechies wavelet with 9 vanishing moments
p = 18;
k = 2^(J-j-1);
m = MakeWavelet(J-j,k,'Daubechies',p,'Mother',n).*2^(j/2);

M18 = fft(m);
mag_18 = abs(M18);
subplot(223), plot(t,-m)
axis([0 4 -2 2]);
set(gca,'ytick',[-2 -1 0 1 2])

text(4.1,-1.9,'sec')
ylabel('\it\psi\rm(t)')
xlabel('(b) Daubechies wavelet with 9 vanishing moments','Fontsize',12)

subplot(224),plot(w(1:100),mag_18(1:100))
axis([0 23 0 150]);
ylabel('|FT(\it\psi\rm(t))|')
text(23.5,3.1,'Hz')
set(gca,'xtick',[0 10 20])
```

B.7 Program for the MultiResoultion Analysis (MRA) of wavelet transforms

```
clear;

n=1024;
dt = 2/n;
t=0.0:dt:(n-1)*dt;

sig = makesignal('Blocks',n);
type = 'Daubechies';
par = 4;
L = 1;
qmf=makeonfilter(type, par);
```

```
wc=fwt_po(sig, L, qmf);

% ... set graph parameters
set(gcf,'defaultlinelinewidth',2);
set(gcf,'defaulttextfontsize',13);
set(gcf,'defaultaxesfontsize',13);

%%%%%%%%%%%%%%%%%%%%%%%
% Analysis
%%%%%%%%%%%%%%%%%%%%%%%%
wcvL=zeros(1,n);

%figure;
clf;
wcvL((2^(9))+1:2^(10))=wc((2^(9))+1:2^(10));
vL=iwt_po(wcvL, L, qmf);
subplot(5,2,10);
plot(t, vL), grid on;
xlabel('Projection onto W_9','Fontsize',13)
ylabel('x(t)','Fontsize',13)
axis([0 2 -3 6]);

wcvL=zeros(1,n);
wcvL((2^(8))+1:2^(9))=wc((2^(8))+1:2^(9));
vL=iwt_po(wcvL, L, qmf);
subplot(5,2,9);
plot(t, vL), grid on;
xlabel('Projection onto W_8','Fontsize',13)
ylabel('x(t)','Fontsize',13)
axis([0 2 -3 6]);

wcvL=zeros(1,n);
wcvL((2^(7))+1:2^(8))=wc((2^(7))+1:2^(8));
vL=iwt_po(wcvL, L, qmf);
subplot(5,2,8);
plot(t, vL), grid on;
xlabel('Projection onto W_7','Fontsize',13)
ylabel('x(t)','Fontsize',13)
axis([0 2 -3 6]);

wcvL=zeros(1,n);
wcvL((2^(6))+1:2^(7))=wc((2^(6))+1:2^(7));
vL=iwt_po(wcvL, L, qmf);
subplot(5,2,7);
```

```
plot(t, vL), grid on;
xlabel('Projection onto W_6','Fontsize',13)
ylabel('x(t)','Fontsize',13)
axis([0 2 -3 6]);

wcvL=zeros(1,n);
wcvL((2^(5))+1:2^(6))=wc((2^(5))+1:2^(6));
vL=iwt_po(wcvL, L, qmf);
subplot(5,2,6);
plot(t, vL), grid on;
xlabel('Projection onto W_5','Fontsize',13)
ylabel('x(t)','Fontsize',13)
axis([0 2 -3 6]);

wcvL=zeros(1,n);
wcvL((2^(4))+1:2^(5))=wc((2^(4))+1:2^(5));
vL=iwt_po(wcvL, L, qmf);
subplot(5,2,5);
plot(t, vL), grid on;
xlabel('Projection onto W_4','Fontsize',13)
ylabel('x(t)','Fontsize',13)
axis([0 2 -3 6]);

wcvL=zeros(1,n);
wcvL((2^(3))+1:2^(4))=wc((2^(3))+1:2^(4));
vL=iwt_po(wcvL, L, qmf);
subplot(5,2,4);
plot(t, vL), grid on;
xlabel('Projection onto W_3','Fontsize',13)
ylabel('x(t)','Fontsize',13)
axis([0 2 -3 6]);

wcvL=zeros(1,n);
wcvL((2^(2))+1:2^(3))=wc((2^(2))+1:2^(3));
vL=iwt_po(wcvL, L, qmf);
subplot(5,2,3);
plot(t, vL), grid on;
xlabel('Projection onto W_2','Fontsize',13)
ylabel('x(t)','Fontsize',13)
axis([0 2 -3 6]);

wcvL=zeros(1,n);
wcvL((2^(1))+1:2^(2))=wc((2^(1))+1:2^(2));
vL=iwt_po(wcvL, L, qmf);
```

```
subplot(5,2,2);
plot(t, vL), grid on;
xlabel('Projection onto W_1','Fontsize',13)
ylabel('x(t)','Fontsize',13)
axis([0 2 -3 6]);

wcvL=zeros(1,n);
wcvL((2^(0))+1:2^(1))=wc((2^(0))+1:2^(1));
vL=iwt_po(wcvL, L, qmf);
subplot(5,2,1);
plot(t, vL), grid on;
xlabel('Projection onto W_0','Fontsize',13)
ylabel('x(t)','Fontsize',13)
axis([0 2 -3 6]);

%%%%%%%%%%%%%%%%%%%%%%%
% Reconstruction
%%%%%%%%%%%%%%%%%%%%%%%%
% ... V0
%figure
clf;
wcvL=zeros(1,n);
wcvL(2^(0))=wc(2^(0));
vL=iwt_po(wcvL, L, qmf);
plot(t, vL), grid on;

%figure;
clf;
wcvL=zeros(1,n);
wcvL((2^(0)):2^(1))=wc((2^(0)):2^(1));
vL=iwt_po(wcvL, L, qmf);
subplot(5,2,1);
plot(t, vL), grid on;
xlabel('Projection onto V_1','Fontsize',13)
ylabel('x(t)','Fontsize',13)
axis([0 2 -3 7]);
%set(gca,'xtick',[0 1 2])

wcvL((2^(1))+1:2^(2))=wc((2^(1))+1:2^(2));
vL=iwt_po(wcvL, L, qmf);
subplot(5,2,2);
plot(t, vL), grid on;
xlabel('Projection onto V_2','Fontsize',13)
ylabel('x(t)','Fontsize',13)
```

```
axis([0 2 -3 7]);

wcvL((2^(2))+1:2^(3))=wc((2^(2))+1:2^(3));
vL=iwt_po(wcvL, L, qmf);
subplot(5,2,3);
plot(t, vL), grid on;
xlabel('Projection onto V_3','Fontsize',13)
ylabel('x(t)','Fontsize',13)
axis([0 2 -3 7]);

wcvL((2^(3))+1:2^(4))=wc((2^(3))+1:2^(4));
vL=iwt_po(wcvL, L, qmf);
subplot(5,2,4);
plot(t, vL), grid on;
xlabel('Projection onto V_4','Fontsize',13)
ylabel('x(t)','Fontsize',13)
axis([0 2 -3 7]);

wcvL((2^(4))+1:2^(5))=wc((2^(4))+1:2^(5));
vL=iwt_po(wcvL, L, qmf);
subplot(5,2,5);
plot(t, vL), grid on;
xlabel('Projection onto V_5','Fontsize',13)
ylabel('x(t)','Fontsize',13)
axis([0 2 -3 7]);

wcvL((2^(5))+1:2^(6))=wc((2^(5))+1:2^(6));
vL=iwt_po(wcvL, L, qmf);
subplot(5,2,6);
plot(t, vL), grid on;
xlabel('Projection onto V_6','Fontsize',13)
ylabel('x(t)','Fontsize',13)
axis([0 2 -3 7]);

wcvL((2^(6))+1:2^(7))=wc((2^(6))+1:2^(7));
vL=iwt_po(wcvL, L, qmf);
subplot(5,2,7);
plot(t, vL), grid on;
xlabel('Projection onto V_7','Fontsize',13)
ylabel('x(t)','Fontsize',13)
axis([0 2 -3 7]);

wcvL((2^(7))+1:2^(8))=wc((2^(7))+1:2^(8));
vL=iwt_po(wcvL, L, qmf);
```

```
subplot(5,2,8);
plot(t, vL), grid on;
xlabel('Projection onto V_8','Fontsize',13)
ylabel('x(t)','Fontsize',13)
axis([0 2 -3 7]);

wcvL((2^(8))+1:2^(9))=wc((2^(8))+1:2^(9));
vL=iwt_po(wcvL, L, qmf);
subplot(5,2,9);
plot(t, vL), grid on;
xlabel('Projection onto V_9','Fontsize',13)
ylabel('x(t)','Fontsize',13)
axis([0 2 -3 7]);

wcvL((2^(9))+1:2^(10))=wc((2^(9))+1:2^(10));
vL=iwt_po(wcvL, L, qmf);
subplot(5,2,10);
plot(t, vL), grid on;
xlabel('Projection onto V_1_0','Fontsize',13)
ylabel('x(t)','Fontsize',13)
axis([0 2 -3 7]);

% check
vL=iwt_po(wc, L, qmf);
temp = wc-wcvL;
%figure;
%subplot(211),plot(t, vL), grid on;
%subplot(212),plot(t, temp), grid on;
```

B.8 Program to perform the wavelet low- and high-pass filtering

```
clear;

% obtain wavelet filters
type='Db3';
[lod,hid,lor,hir] = wfilters(type);

Ts=1/50;
freq=2;
Tf =100;
t=[Ts:Ts:Tf];
sig = 0.2;
uless=sin(2*pi*freq*t);
```

```
noise=sig*randn(1,size(t,2));
noisysine = 100/981*(uless+noise);

% run simulink model
sim('fig7simlev2')

x=0:Ts:20.47;

subplot(3,1,1);
plot(x(1:3/Ts+1), noisysine (3/Ts:6/Ts)), grid on;
ylabel('Ground Acc. (g)')
xlabel('(a)')

subplot(3,1,2);
plot(x(1:3/Ts+1), hpfsignal(3/Ts-intdelay:6/Ts-intdelay)),axis([0 3 -0.2 0.2]), grid on;
ylabel('Ground Acc.(g)')
xlabel('(b)')

subplot(3,1,3);
plot(x(1:3/Ts+1), lpfsignal(3/Ts-intdelay:6/Ts-intdelay)),axis([0 3 -0.2 0.2]), grid on;
ylabel('Ground Acc. (g)')
xlabel('(c)')

u = noisysine(989:1500);
hisig = hpfsignal(990:1501);
losig = lpfsignal(990:1501);
N=512;
Dt = Ts;
fs = 1/Dt;
X1 = fft(u,N);
X2 = fft(hisig,N);
X3 = fft(losig,N);
C1 = abs(X1(1:N/2+1)*Dt);
C2 = abs(X2(1:N/2+1)*Dt);
C3 = abs(X3(1:N/2+1)*Dt);
freq = fs*(0:N/2)/N;

figure
subplot(3,1,1),plot(freq,C1)
xlabel('(a)')
yLabel('Fourier Amplitudes');
subplot(3,1,2),plot(freq,C2)
xlabel('(b)')
yLabel('Fourier Amplitudes');
```

```
subplot(3,1,3),plot(freq,C3)
xlabel('(c)')
yLabel('Fourier Amplitudes');
```

B.9 Program to perform the wavelet-hybrid feedback LMS algorithm with sinusoidal force

```
clear;

% ...Structural properties
m1 = 100000; % kg
fs = 1; % frequency, Hz
zeta_s = 0.01; % 0.01 damping ration

% ...ATMD/HMD properties
massRatio = 0.01;
fd = 0.985; % Hz
zeta_d =0.075;
k0 =10000;

% ...Construct necessary parameters
m2 = m1*massRatio;
k1 = (2*pi*fs)^2*m1;
c1 = 4*pi*zeta_s*fs*m1;
k2 = (2*pi*fd)^2*m2;
c2 = 4*pi*zeta_d*fd*m2;

M = [m1 0;0 m2];
K = [k1+k2 -k2;-k2 k2];
Damping = [c1+c2 -c2;-c2 c2];

A = [zeros(length(M)) eye(length(M));-inv(M)*K -inv(M)*Damping];
C = [1 0 0 0];
D = 0;
Dc = [D D];
B = [zeros(length(M),1);-1/m1; 1/m2]*k0;
E = [0;0;-1;-1];
Bc = [E B];

% ...Loads, with 0.2 standard deviation
freq=1.2;
Ts = 1/50;
Tf = 40;
```

```
t=[0:Ts:Tf];
sig = 0.2;
uless=sin(2*pi*freq*t);
noise=sig*randn(1,size(t,2));
u = uless+noise;
noisysine = 100*u;

% ...Response w/o control
[Ad,Ed,Cd,Dd]= C2DM(A,E,C,D,Ts,'tustin');
[d1,x]=dlsim(Ad,Ed,Cd,Dd,noisysine);

% ...Response w/ LQR control
Q = diag([5000;10;0;0]);
R = 1;
[G,S,e] = lqr(A,B,Q,R);
AG = A - B*G;
[Ad,Bd,Cd,Dd]= C2DM(AG,Bc,C,Dc,Ts,'tustin');
[d2 Y] = dlsim(Ad,Bd(:,1),Cd,Dd(:,1),noisysine);

%~~~~~~~~~~~~~~~~~~~~~~~~~~~~~~~~~~~~~~~~~~~~~~~~~~~~~~~~~~~~
% ...Wavelet-Hybrid LMS control
%~~~~~~~~~~~~~~~~~~~~~~~~~~~~~~~~~~~~~~~~~~~~~~~~~~~~~~~~~~~~
Bc = [E B];
Dc = [D D];
[Ad,Bd,Cd,Dd]= C2DM(AG,Bc,C,Dc,Ts,'tustin');

% ...offline iir filters
[num den] = ss2tf(Ad,Bd,Cd,Dd,2);

% ...obtain wavelet filters
type='db3';  % Daubechies wavelet with 3 vanishing moments
[lod,hid,lor,hir] = wfilters(type);

% integer delay (latency)
nd = 10; %7*(length(lod)-1)+16;
N_coeff = 50;
sim('fig11sim');

zwhlcontrled = zout(nd+1+1:length(zout));
subplot(3,1,1),plot(t,d1); %axis([0 20 -13 13]);
axis([0 30 -12 12])
set(gca,'ytick',[-10 0 10])
set(gca,'xtick',[0 10 20 30])
xlabel('(a)')
```

```
ylabel('Displacement (cm)')

subplot(3,1,2),plot(t,d2);
xlabel('(b)');
ylabel('Displacement (cm)')
axis([0 30 -12 12])
set(gca,'ytick',[-10 0 10])
set(gca,'xtick',[0 10 20 30])

subplot(3,1,3),plot(t(1:length(zwhlcontrled)),zwhlcontrled);
xlabel('(c)')
ylabel('Displacement (cm)')
axis([0 30 -12 12])
set(gca,'ytick',[-10 0 10])
set(gca,'xtick',[0 10 20 30])
```

B.10 Program to perform the Wavelet-hybrid feedback LMS algorithm for ATMD system

```
clear;

load elc_a
elcentro = e(2,:);
Ts = 0.001;

% ...build model
[At,Bt,Ct,Dt,Acd,Bcd,Ccd,Dcd] = build_mod(Ts);

% ... Response w/o control
[XNONE,Y]=lsim(At,Bt(:,1),Ct,Dt(:,1),e(2,:),e(1,:));

%  ...Off line Filtered-x LMS
load widoffamd;

% SIMULATION PARAMETERS
dtint   = 0.0001;                % integration step
dts = 0.004;                     % time increment for saving data
n       = 1e7;                   % number of samples saved
tol     = 1e-6;                  % tolerance
qint    = 6/(2^12);              % quantizer interval

%  ...ON-LINE
N_coeff = 100;
```

```
% ...obtain wavelet filters
type='db3';  % Daubechies wavelet with 3 vanishing moments
[lod,hid,lor,hir] = wfilters(type);

nd = 80;
Tf = 10+nd*Ts;
sim('amdsime')

[Eu_max,Exm_max,Exdotdotam_max,EJ6,EJ7,EJ8,EJ9,EJ10] = eval_e(zout,usignal);
EJ_WHL =[Eu_max,Exm_max,Exdotdotam_max,EJ6,EJ7,EJ8,EJ9,EJ10]
zoutWHL=zout;

% ...LQG Control
sim('amdLQG')
[Eu_max,Exm_max,Exdotdotam_max,EJ6,EJ7,EJ8,EJ9,EJ10] = …
        eval_e(zoutLQG,usignalLQG);
EJ_LQG =[Eu_max,Exm_max,Exdotdotam_max,EJ6,EJ7,EJ8,EJ9,EJ10];

% Draw figures
set(gcf,'defaultlinelinewidth',1);      % Change curve line thickness
set(gcf,'defaulttextfontsize',12);      % Change fontsize
set(gcf,'defaultaxesfontsize',12);
clf;

t=[0:0.004:Tf];
t=t-nd*0.004;

Time = [0:0.004:10];
subplot(2,1,1),
plot(Time,XNONE(:,3)/0.51,'b:',t,zoutWHL(:,3)/0.51,'k-')
axis([0 10 -4 4]);
set(gca,'ytick',[-4 0 4])
xlabel('(a)')
ylabel('Displacement (cm)')
legend('Uncontrolled','New Model')
str(1)={'Time'};
str(2)={'(sec.)'};
text(10.1,-3.5,str)

subplot(2,1,2),
plot(Time,XNONE(:,11),'b:',t,zoutWHL(:,11),'k-')
axis([0 10 -6 6]);
set(gca,'ytick',[-6 0 6])
xlabel('(b)')
```

```
ylabel('Acceleration (g)')
legend('Uncontrolled','New Model')
str(1)={'Time'};
str(2)={'(sec.)'};
text(10.1,-5.2,str)

figure;
Time = [0:0.005:10];
subplot(2,1,1),plot(Time,zout(:,3)/0.51,'b:',t,zoutWHL(:,3)/0.51,'k-')
axis([0 10 -2.2 2.2]);
set(gca,'ytick',[-2. 0 2.])
set(gca,'xtick',[0 2 4 6 8 10])
xlabel('(a)')
ylabel('Displacement (cm)')
legend('LQG Controller','New Model')
str(1)={'Time'};
str(2)={'(sec.)'};
text(10.1,-1.8,str)

subplot(2,1,2),plot(Time,zout(:,11),'b:',t,zoutWHL(:,11),'k-')
axis([0 10 -3.2 3.2]);
set(gca,'ytick',[-3. 0 3.])
set(gca,'xtick',[0 2 4 6 8 10])
xlabel('(b)')
ylabel('Acceleration (g)')
legend('LQG Controller','New Model')
str(1)={'Time'};
str(2)={'(sec.)'};
text(10.1,-2.8,str)
```

B.11 Program to read the nodal data & element data of SAP2000 s2k file

```
%   All data will be saved in OOOO_s2k.mat (OOOO: name of structure)
%
% Reading data:
%       Nodal data:
%               Node # and nodal coodinates (x-coordinate, y-coord, and z-coord)
%       Element data:
%               Element #, node_i and node_j (end nodes) of the corresponding
%               element, material_no (SEC), and beta_ang
%       Nodal Mass
%               Node # and nodal mass (6 mass components for each node)
%
% Note:
```

```
%   Common:
%       1. Total node number and total element number need to be set before reading
%          copied s2k data files.
%   Nodal Data:
%       1. Create a separate file (OOOO_node.txt) containing the node data of s2k file
%       2. SAP2000 s2k file may contain very small number which should be "0"
%       Thus, if numbers are less than the given tolerance, numbers are set to be 0
%       Tolerance is set to 10^-10;
%   Element Data:
%       1. Create a separate file (OOOO_elem.txt) containing the section data of s2k file
%       2. Section data (SEC) of s2k file need to be converted to material_no
%               of Matlab Frame3D code before data are read
%               (using the "Edit->Replace" function).
%   Nodal Mass
%       1. Create a separate file (OOOO_mass.txt) containing the Masss data of s2k file
%       2. Unit (N-m or lb-in) needs to be carefully checked
%
clear;

total_node_no = 77;
total_elem_no = 148;

file_name_node='bldg12_node.txt';   % file containing nodal data
file_name_elem='bldg12_elem.txt';   % file containing element data
file_name_mass='bldg12_mass.txt';   % file containing element data

fid_node=fopen(file_name_node,'r');
fid_elem=fopen(file_name_elem,'r');
fid_mass=fopen(file_name_mass,'r');  % unit: N-m

% ~~~~~~~~~~~~~~~~~~~~~~~~~~~~~~~~~~~~~~~~~~~~~~~~~~~~~~~~~~~~~~~~~~~~~
%  I. Read the node (JOINT) data
% ~~~~~~~~~~~~~~~~~~~~~~~~~~~~~~~~~~~~~~~~~~~~~~~~~~~~~~~~~~~~~~~~~~~~~
tolerance=10^-10;

node_no=zeros(total_node_no,1);
x_coord=zeros(total_node_no,1);
y_coord=zeros(total_node_no,1);
z_coord=zeros(total_node_no,1);

%while feof(fid)==0
for jj=1:total_node_no
  line=fgetl(fid_node);
  spaceCheck=isspace(line); % 0: not space, 1: space
```

```
char_double=double(line); % conversion of character to numeric value

% ... 1) get element #
node_char=char('');
number_met=0;
for kk=1:length(line)
  if(spaceCheck(kk)~=1)
    % only first non-space is of concern
    number_met=1;
    node_char = [node_char line(kk)];
  elseif((number_met==1)&(spaceCheck(kk)==1))
    break;
  end
end
node_no(jj)=str2num(node_char);

% ... 2) get x_coord
% double('X')=88, only one X exists
x_char=char('');
X_met=0;
for kk=1:length(line)
  if(char_double(kk)==88)
    X_met=1;
    for mm=kk+2:length(line)
      if(spaceCheck(mm)~=1)
        x_char = [x_char line(mm)];
      elseif((X_met==1)&(spaceCheck(mm)==1))
        break;
      end
              end
  end
end
x_coord(jj)=str2num(x_char);
if(abs(x_coord(jj))<tolerance)
  x_coord(jj) = 0;
end

% ... 3) get y_coord
% double('Y')=89, only one Y exists
y_char=char('');
Y_met=0;
for kk=1:length(line)
  if(char_double(kk)==89)
    Y_met=1;
```

```
      for mm=kk+2:length(line)
        if(spaceCheck(mm)~=1)
          y_char = [y_char line(mm)];
        elseif((Y_met==1)&(spaceCheck(mm)==1))
          break;
        end
                end
    end
  end
  y_coord(jj)=str2num(y_char);
  if(abs(y_coord(jj))<tolerance)
    y_coord(jj) = 0;
  end

  % ... 4) get zcoord
  % double('Z')=90, only one Z exists,
  % z_coord: after '=' upto "end of line"
  z_char=char('');
  for kk=1:length(line)
    if(char_double(kk)==90)
      z_char = [z_char line(kk+2:length(line))];
      break;
    end
  end
  z_coord(jj)=str2num(z_char);
  if(abs(z_coord(jj))<tolerance)
    z_coord(jj) = 0;
  end
end
node_no(1:jj);
x_coord(1:jj);
y_coord(1:jj);
z_coord(1:jj);

% ~~~~~~~~~~~~~~~~~~~~~~~~~~~~~~~~~~~~~~~~~~~~~~~~~~~~~~~~~~~~~~~~~~~~~~~~~
%  II. Read the element (SECTION) data
% ~~~~~~~~~~~~~~~~~~~~~~~~~~~~~~~~~~~~~~~~~~~~~~~~~~~~~~~~~~~~~~~~~~~~~~~~~
elem_no=zeros(total_elem_no,1);
elem_ij=zeros(total_elem_no,2);
material=zeros(total_elem_no,1);
ang=zeros(total_elem_no,1);

for jj=1:total_elem_no
  line=fgetl(fid_elem);
```

```
spaceCheck=isspace(line); % 0: not space, 1: space
char_double=double(line); % conversion of character to numeric value

% ... 1) get element #
el_char=char('');
number_met=0;
for kk=1:length(line)
  if(spaceCheck(kk)~=1)
    % only first non-space is of concern
    number_met=1;
    el_char = [el_char line(kk)];
  elseif((number_met==1)&(spaceCheck(kk)==1))
    break;
  end
end
elem_no(jj)=str2num(el_char);

% ... 2) get node_i & node_j
%                      double('J')=74
node_char=char('');
J_met=0;
for kk=1:length(line)
  if(char_double(kk)==74)
    J_met=1;
    for mm=kk+2:length(line)
      if(spaceCheck(mm)~=1)
        node_char = [node_char line(mm)];
      elseif((J_met==1)&(spaceCheck(mm)==1))
        break;
      end
    end

    % ... get node_i
    % double(',')=44
    i_char=('');
    comma_loc=0;
    double_node=double(node_char);
    for mm=1:length(node_char)
      if(double_node(mm)~=44)
        i_char=[i_char node_char(mm)];
      else
        comma_loc=mm;
        break;
      end
```

```
        end
        j_char=node_char(comma_loc+1:length(node_char));
        break;
      end
    end
    elem_ij(jj,1)=str2num(i_char);
      elem_ij(jj,2)=str2num(j_char);

    % ... 3) get material_no
    % double('C')=67, only one C exists
    sec_char=char('');
    C_met=0;
    for kk=1:length(line)
      if(char_double(kk)==67)
        C_met=1;
        for mm=kk+2:length(line)
          if(spaceCheck(mm)~=1)
            sec_char = [sec_char line(mm)];
          elseif((C_met==1)&(spaceCheck(mm)==1))
            break;
          end
          end
      end
    end
    material(jj)=str2num(sec_char);

    % ... 4) get angle
    % double('A')=65, only one A exists
    % ang: after '=' upto "end of line"
    angle_char=char('');
    for kk=1:length(line)
      if(char_double(kk)==65)
        angle_char = [angle_char line(kk+4:length(line))];
        break;
      end
    end
    ang(jj)=str2num(angle_char);


    %line=fscanf(fid,'%s',[148,1])
  end
  elem_no(1:jj);
  ang(1:jj);
  elem_ij(1:jj,:);
```

```
material(1:jj);

% ~~~~~~~~~~~~~~~~~~~~~~~~~~~~~~~~~~~~~~~~~~~~~~~~~~~~~~~~~~~~~~~~~~~~~~~~~~~~~~~~
%   III. Read the nodal mass (Mass) data
% ~~~~~~~~~~~~~~~~~~~~~~~~~~~~~~~~~~~~~~~~~~~~~~~~~~~~~~~~~~~~~~~~~~~~~~~~~~~~~~~~
ux_mass=zeros(total_node_no,1);
uy_mass=zeros(total_node_no,1);
uz_mass=zeros(total_node_no,1);
rx_mass=zeros(total_node_no,1);
ry_mass=zeros(total_node_no,1);
rz_mass=zeros(total_node_no,1);

%for jj=1:1
while feof(fid_mass)==0
  line=fgetl(fid_mass);
  spaceCheck=isspace(line); % 0: not space, 1: space
  char_double=double(line); % conversion of charater to numeric value

  % ... 1) get element #
  % double('A')=65, only one A exists
    node_char=char('');
  A_met=0;
  for kk=1:length(line)
    if(char_double(kk)==65)
      % only first non-space is of concern
      A_met=1;
        for mm=kk+4:length(line)
        if(spaceCheck(mm)~=1)
          node_char = [node_char line(mm)];
        elseif((A_met==1)&(spaceCheck(mm)==1))
          break;
        end
        end
    end
  end
  node_index=str2num(node_char);

  % ... 2) get ux_mass
  % double('U')=85, doubel('1')=49
  ux_char=char('');
  U1_met=0;
  for kk=1:length(line)
    if((char_double(kk)==85)&(char_double(kk+1)==49))
      U1_met=1;
```

```
      for mm=kk+3:length(line)
        if(spaceCheck(mm)~=1)
          ux_char = [ux_char line(mm)];
        elseif((U1_met==1)&(spaceCheck(mm)==1))
          break;
        end
        end
    end
  end
  ux_mass(node_index)=str2num(ux_char);

  % ... 3) get uy_mass
  % double('U')=85, doubel('2')=50
  uy_char=char('');
  U2_met=0;
  for kk=1:length(line)
    if((char_double(kk)==85)&(char_double(kk+1)==50))
      U2_met=1;
      for mm=kk+3:length(line)
        if(spaceCheck(mm)~=1)
          uy_char = [uy_char line(mm)];
        elseif((U2_met==1)&(spaceCheck(mm)==1))
          break;
        end
        end
    end
  end
  uy_mass(node_index)=str2num(uy_char);

  % ... 3) get uz_mass
  % double('U')=85, doubel('3')=51
  uz_char=char('');
  for kk=1:length(line)
    if((char_double(kk)==85)&(char_double(kk+1)==51))
      uz_char = [uz_char line(kk+3:length(line))];
      break;
    end
  end
  uz_mass(node_index)=str2num(uz_char);
end
%mass=[ux_mass uy_mass uz_mass]

% ~~~~~~~~~~~~~~~~~~~~~~~~~~~~~~~~~~~~~~~~~~~~~~~~~~~~~~~~~~~~~~~~~~~~~~~~~~
%  IV. Save all data
```

```
% ~~~~~~~~~~~~~~~~~~~~~~~~~~~~~~~~~~~~~~~~~~~~~~~~~~~~~~~~~~~~~~~~~~~~~~
save bldg12_s2k node_no x_coord y_coord z_coord elem_no elem_ij material ang ...
                              ux_mass uy_mass uz_mass rx_mass ry_mass rz_mass

status=fclose('all');
```

B.12 Program to generate M,C, & K matrices of a 3D frame structure

```
%
% Note:
%       1. These matrices are saved in MCK_OOOO.mat
%                     where OOOO is the name of the structure to be analyzed
%       2. Accordingly, input file name must be in the form of OOOO_input.m
%       3. Damping in each node is assumed to be proportional for the mode's
%                     associated frequency.
%
% Input to be provided
%       1. Input file name
%       2. Mass type (1: Lumped mass, 2: Consistent mass, 3: Nodal mass)
%       3. The damping in the first node and the max. damping (ratio of critical damping)
%

clear;

% ~~~~~~~~~~~~~~~~~~~~~~~~~~~~~~~~~~~~~~~~~~~~~~~~~~~~~~~~~~~~~~
% Input (bldg12)
%       Saleh's Example 3, 12-story steel frame building
%       "Optimal Control of Adaptive/Samrt Multistory Building Structures"
%       Saleh and Adeli, (1998), CACAIE, pp.389-403
% ~~~~~~~~~~~~~~~~~~~~~~~~~~~~~~~~~~~~~~~~~~~~~~~~~~~~~~~~~~~~~~
structure = 'bldg12';
mass_type=3; % nodal mass
zeta_1=0.02; % damping in the first mode, 2%
zeta_max = 0.1; % 10%, max damping

% ~~~~~~~~~~~~~~~~~~~~~~~~~~~~~~~~~~~~~~~~~~~~~~~~~~~~~~~~~~~~~~
% ... Open input file
% ~~~~~~~~~~~~~~~~~~~~~~~~~~~~~~~~~~~~~~~~~~~~~~~~~~~~~~~~~~~~~~
input_file = [structure '_input'];
eval(input_file);

% ~~~~~~~~~~~~~~~~~~~~~~~~~~~~~~~~~~~~~~~~~~~~~~~~~~~~~~~~~~~~~~
% ... Generate K and M matrices of a 3D Frame
% ~~~~~~~~~~~~~~~~~~~~~~~~~~~~~~~~~~~~~~~~~~~~~~~~~~~~~~~~~~~~~~
Frame3D
```

```
%K=0.9*K;
% ... check natural frequencies
[evecs,evals] = eig(K,M);
[omeg,w_order]= sort(sqrt(diag(evals)));
wn=omeg(1:10);
fn=omeg(1:10)/2/pi;
T=1./fn

% ~~~~~~~~~~~~~~~~~~~~~~~~~~~~~~~~~~~~~~~~~~~~~~~~~~~~~~~~~~~~~~~~
% Generate Damping (C) matrix
%       Refer to BLD_MOD.m of 2nd benchmark problem
% ~~~~~~~~~~~~~~~~~~~~~~~~~~~~~~~~~~~~~~~~~~~~~~~~~~~~~~~~~~~~~~~~
% ... Re-arrange the mode shapes
Evecs       = evecs(:,w_order);

% ... Generate the modal damping matrix, Cbar
zeta        = zeta_1; %zeta_1/omeg(1)*omeg;
zeta        = min(zeta,zeta_max);
Cbar        = diag(2*zeta.*omeg);

% ... Generate the damping matrix, C
C       = M*Evecs*Cbar*inv(Evecs);

% ... Check damping ratios
M_factor = transpose(Evecs)*M*Evecs;
for jj=1:length(M)
  Evecs2(:,jj) = Evecs(:,jj)/sqrt(M_factor(jj,jj));
end
Mnorm = transpose(Evecs2)*M*Evecs2; % must be Identity matrix
Knorm = transpose(Evecs2)*K*Evecs2; % must be diag(omega_i^2)
Cnorm = transpose(Evecs2)*C*Evecs2; % must be diag(2*zeta_i*omega_i)
zeta2 = diag(Cnorm)/2 ./sqrt(diag(Knorm));

% ~~~~~~~~~~~~~~~~~~~~~~~~~~~~~~~~~~~~~~~~~~~~~~~~~~~~~~~~~~~~~~~~
% Save M, C, K matrices and other required infos
%       i.e. ID arrays and active_dofs
% ~~~~~~~~~~~~~~~~~~~~~~~~~~~~~~~~~~~~~~~~~~~~~~~~~~~~~~~~~~~~~~~~
save MCK_bldg12 M C K ID_F ID_FD2 active_dofs Ng
```

B.13 Program to generate K & M matrices of a 3D frame

```
% Euler-Bernoulli beam model is used for the frame elements
%
% References
```

```
%   1. "Finite Element Programs in Structural Engineering &
%                  Continum Mechanics", Carl T. F. Ross, (1996)
%   2. "Matrix Analysis of Structure" (Korean version), R. E. Sennet, (1994)
%   3. "Computer Analysis of Structural Frameworks", James A.D. Balfour
%                  (1992)
%   4. "Structural Dynamics: Theory and Computation", M. Paz, (1980)
%   5. "SAP2000 Basic Analysis Manual"
%   6. "Benchmark Control Problems for Seismically Excited Nonlinear Buildings"
%                  R.E. Christenson, B.F. Spencer Jr., and S.J. Dyke

%
%   Note on GCS (Global Coordinate System) and the beta angle
%        Frame3D.m uses the same global X-Y-Z axes of SAP2000, and same beta angle.
%        beta_angle: angle through which the element must be rotated about its
%                   "x" axis to make the principal axes coincide with the element axes.
%
%~~~~~~~~~~~~~~~~~~~~~~~~~~~~~~~~~~~~~~~~~~~~~~~~~~~~~~~~~~~~~~~~~~~~~~
% ID_arrays
%
% ID_G              : Global ID_array
% ID_F              : ID_array of free dofs (fixed dofs are set to be zero)
%                              (same as the "Freedom Vector" of Balfour Book)
% id_free           : id_array of free dofs (mapping of nonzero entities of ID_F
%                                     into ID_G)
% ID_FD             : ID_array after the rigid floor diaphragm removal
% ID_FD2            : ID_FD setting id's of slave dof to be zero
% ID_G              : ID_array after static condensation (Guyan reduction)
%~~~~~~~~~~~~~~~~~~~~~~~~~~~~~~~~~~~~~~~~~~~~~~~~~~~~~~~~~~~~~~~~~~~~~~
ID_G = [1:6*num_node];

id_free=find(node_rest==0);
Ndof_free=length(id_free);              % number of free dofs

ID_F=zeros(1,length(ID_G));
ID_F(id_free)=[1:Ndof_free];

% ~~~~~~~~~~~~~~~~~~~~~~~~~~~~~~~~~~~~~~~~~~~~~~~~~
% Assemble the Stiffness and Mass matrices, K & M
% ~~~~~~~~~~~~~~~~~~~~~~~~~~~~~~~~~~~~~~~~~~~~~~~~~
K=zeros(length(ID_G),length(ID_G));
M=zeros(length(ID_G),length(ID_G));
for kk=1:num_elem

  % ... 1) Calc. the element length
```

```
node_i=elem_prop(kk,2);
node_j=elem_prop(kk,3);

x1 = node_coord(node_i,2); x2 = node_coord(node_j,2);
y1 = node_coord(node_i,3); y2 = node_coord(node_j,3);
z1 = node_coord(node_i,4); z2 = node_coord(node_j,4);

L=sqrt((x1-x2)^2+(y1-y2)^2+(z1-z2)^2);

% ... 2) Calc. the directional cosine for the member x-axis
L11=(x2-x1)/L;
L12=(y2-y1)/L;
L13=(z2-z1)/L;

% ... 3) Calc. rest of the directional cosines
%            Based on "Computer Analysis of Structural Frameworks", pp.372-389
beta=pi*elem_prop(kk,5)/180;
if(abs(L13)>0.999)           % i.e. the element lies parallel to the coordinate z-axis
  L21=-L13*sin(beta);
  L22=cos(beta);
  L23=0;
  L31=-L13*cos(beta);
  L32=-sin(beta);
  L33=0;
else
  L21=(-L12*cos(beta)-L11*L13*sin(beta))/sqrt(1-L13^2);
  L22=(L11*cos(beta)-L12*L13*sin(beta))/sqrt(1-L13^2);
  L23=sin(beta)*sqrt(1-L13^2);
  L31=(L12*sin(beta)-L11*L13*cos(beta))/sqrt(1-L13^2);
  L32=(-L11*sin(beta)-L12*L13*cos(beta))/sqrt(1-L13^2);
  L33=cos(beta)*sqrt(1-L13^2);
end

L_hat=[L11 L12 L13;L21 L22 L23;L31 L32 L33];

T=[L_hat zeros(3,3) zeros(3,3) zeros(3,3); ...
  zeros(3,3) L_hat zeros(3,3) zeros(3,3); ...
  zeros(3,3) zeros(3,3) L_hat zeros(3,3); ...
  zeros(3,3) zeros(3,3) zeros(3,3) L_hat;];

% ... 4) Calc. the element stiffness matrix
prop_no=elem_prop(kk,4);

E=mat_table(prop_no,2);
```

```
A=mat_table(prop_no,3);
Iy=mat_table(prop_no,4);
Iz=mat_table(prop_no,5);
G=mat_table(prop_no,6);
J=mat_table(prop_no,7);

k11=zeros(6,6);
k11=diag([A*E/L 12*E*Iz/L^3 12*E*Iy/L^3 G*J/L 4*E*Iy/L 4*E*Iz/L]);
k11(2,6)=6*E*Iz/L^2;
k11(3,5)=-6*E*Iy/L^2;
k11(5,3)=k11(3,5);
k11(6,2)=k11(2,6);

k12=k11.*[-1 0 0 0 0 0;0 -1 0 0 0 1;0 0 -1 0 1 0;...
    0 0 0 -1 0 0;0 0 -1 0 1/2 0;0 -1 0 0 0 1/2];
k21=k12';
k22=k11.*[1 0 0 0 0 0;0 1 0 0 0 -1;0 0 1 0 -1 0;...
    0 0 0 1 0 0;0 0 -1 0 1 0;0 -1 0 0 0 1];
k_hat=[k11 k12;k21 k22];

k_elem=T'*k_hat*T;

% ... 5) Calc. the element mass matrix
%                  Lump mass matrix from Paz Book
%                  Consistent mass matrix from Ross Book
%                  13/35 is used instead of 13/15 for m11(2,2) & m11(3,3)
%                  in Paz Book and S.Z. Rad Ph.d. thesis (phd97ziaeirad.pdf)
ML = element_mass(kk)*L;        % element_mass(kk): mass per unit length

if(mass_type==1)            % lumped mass matrix
  small=1*10^-10;           % small numbers are added to rotational dofs
  m_hat=ML/2.*diag([1 1 1 J/A small small 1 1 1 J/A small small]);

elseif(mass_type==2)        % consistent mass matrix
  Ip=mat_table(prop_no,8);

  m11=zeros(6,6);
  m11=diag([1/3 13/35+6*Iz/(5*A*L^2) 13/35+6*Iy/(5*A*L^2)...
      Ip/(3*A) L^2/105+2*Iy/(15*A) L^2/105+2*Iz/(15*A)]);
  m11(2,6)=11*L/210+Iz/(10*A*L);
  m11(3,5)=-11*L/210-Iy/(10*A*L);
  m11(5,3)=m11(3,5);
  m11(6,2)=m11(2,6);
  m11=ML*m11;
```

```
    m12=zeros(6,6);
    m12=diag([1/6 9/70-6*Iz/(5*A*L^2) 9/70-6*Iy/(5*A*L^2)...
        Ip/(6*A) -L^2/140-Iy/(30*A) -L^2/140-Iz/(30*A)]);
    m12(2,6)=-13*L/420+Iz/(10*A*L);
    m12(3,5)=13*L/420-Iy/(10*A*L);
    m12(5,3)=m11(3,5);
    m12(6,2)=m11(2,6);
    m12=ML*m11;

    m21=m12';
    m22=m11.*[1 0 0 0 0 0;0 1 0 0 0 -1;0 0 1 0 -1 0;...
        0 0 0 1 0 0;0 0 -1 0 1 0;0 -1 0 0 0 1];

    m_hat=[m11 m12;m21 m22];
  else %(mass_type==3)                    % nodal mass
    m_hat=diag([0 0 0 0 0 0 0 0 0 0 0 0]);
  end
  m_elem=T'*m_hat*T;

  % ...6) set the elemnt ID_array (element code number according to the book)
  e_ID(1:6)=6*(node_i-1)+[1 2 3 4 5 6]; %ID_F(node_i*3-2:node_i*3);
  e_ID(7:12)=6*(node_j-1)+[1 2 3 4 5 6]; %ID_F(node_j*3-2:node_j*3);

  % ...7) assemble Global K & M
  for ii=1:12
    for jj=1:12
      row=e_ID(ii);
      col=e_ID(jj);
      %[kk jj row col];
      K(row,col)=K(row,col)+k_elem(ii,jj);
      M(row,col)=M(row,col)+m_elem(ii,jj);
    end
  end
end

% ...8) assemble Global M if mass_type==3, i.e. nadal mass
if(mass_type==3) % nodal mass
  M=diag(reshape(nodal_mass',6*num_node,1));
end

% ~~~~~~~~~~~~~~~~~~~~~~~~~~~~~~~~~~~~~~~~~~~~~~~~~~~~~~~~~~~~~~~~
% Elimination of Boundary Condition DOFs
% ... Condense out fixed dofs from M and K matrices
```

```
% ~~~~~~~~~~~~~~~~~~~~~~~~~~~~~~~~~~~~~~~~~~~~~~~~~~~~~~~~~~~~~~~~~~~~
K        = K(id_free,id_free);
M        = M(id_free,id_free);
MM=M;
KK=K;
%[eig_vec,eig_val] = eig(K,M);
%[omeg,w_order]    = sort(sqrt(diag(eig_val)));
%wn=omeg(1:3);
%fn=omeg/2/pi;

%~~~~~~~~~~~~~~~~~~~~~~~~~~~~~~~~~~~~~~~~~~~~~~~~~~~~~~~~~~~~~~~~~~~~~
% Rigid Floor Diaphragm Removal
%       Rigid Diaphragm Constraint (refer to SAP2000 Basic Analysis Manual p.64)
%                       ux_j=ux_i - deltaY * rz_i
%                       ux_j=uy_i + deltaX * rz_i
%                       rz_j=rz_i
%
%       Here,   ux_i, uy_i, and rz_i are called diagonal term
%               and deltaY & deltaX are called off-diagonal term
%
%  ritz_slv and ritz_mst vectors are mapping of slave dofs to master dofs
%               only in diagonal term sense (ritz_slv -> ritz_mst)
%~~~~~~~~~~~~~~~~~~~~~~~~~~~~~~~~~~~~~~~~~~~~~~~~~~~~~~~~~~~~~~~~~~~~~
ritz_slv = [ ]; % slave dofs vector
ritz_mst = [ ]; % master dofs vector

% ... 1) consider all dofs including support nodes
num_mst = length(slv_tbl(:,1));         % Number of Master Nodes
T_rigid = eye(6*num_node);
for i=1:num_mst
  for jj=1:3
    if jj==1
      dof_index=1;     % ux
    elseif jj==2
      dof_index=2;     % uy
    else
      dof_index=6;     % rz
    end

    node_mst=slv_tbl(i,1);                     % master node
    dof_mst = 6*(node_mst-1) + dof_index;  % master dof

    for kk=1:slv_tbl(i,2)                      % slv_tbl(i,3)= number of slave nodes
      node_slv=slv_tbl(i,2+kk);                % slave node
```

```
        dof_slv = 6*(node_slv-1) + dof_index; % slave dof

        ritz_mst= [ritz_mst dof_mst];    % dof_mst is added as many times as dof_slv added
        ritz_slv = [ritz_slv dof_slv];

        % ... diagonal terms
        T_rigid(dof_slv,dof_slv) = 0;
        T_rigid(dof_slv,dof_mst) = 1;

        % ... off-diagonal terms
        if(dof_index==1)
          deltaY = node_coord(node_slv,3)-node_coord(node_mst,3);
          T_rigid(dof_slv,6*(node_mst-1)+6)= -deltaY;
        elseif(dof_index==2)
          deltaX = node_coord(node_slv,2)-node_coord(node_mst,2);
          T_rigid(dof_slv,6*(node_mst-1)+6)= deltaX;
        end
      end
    end
end

% ... 2) consider free dofs only
ritz_slv            = ID_F(ritz_slv);
ritz_mst            = ID_F(ritz_mst);

Tr_free             = T_rigid(id_free,id_free);
mst_vec             = find(diag(Tr_free));
Tr        = Tr_free(:,mst_vec);
Nr        = length(mst_vec);

ID_FD               = zeros(1,Ndof_free);
ID_FD(mst_vec) = 1:length(mst_vec);
ID_FD2              = ID_FD;
ID_FD(ritz_slv)= ID_FD(ritz_mst);

M = Tr' * M * Tr;
K = Tr' * K * Tr;

% ... Tr and er
er = [mst_vec; ritz_slv'];
Tr_2nd = Tr(er,:);

%~~~~~~~~~~~~~~~~~~~~~~~~~~~~~~~~~~~~~~~~~~~~~~~~~~~~~~~~~~~~~~~~~~~~
% Static Condensation (Guyan Reduction)
```

```
% ... Reduce out two rotational dofs (rx and ry)
% ... and selected vertical dofs (uz)
%~~~~~~~~~~~~~~~~~~~~~~~~~~~~~~~~~~~~~~~~~~~~~~~~~~~~~~~~~~~~~~~~~~
% ... list of nodes whose vertical dofs are kept active, as of now none
guy_node        = [ ];

ind             = zeros(6,num_node);
indf            = reshape(ID_F,6,num_node);

% ... all of two horizontal and one vertical dofs are kept active
ind(1,:)                = indf(1,:);            % ux
ind(2,:)                = indf(2,:);            % uy
ind(6,:)                = indf(6,:);            % rz

% ... selected uz are kept active
ind(3,guy_node)= indf(3,guy_node);              % uz

% ... get a vector of active dofs
active_dofs     = ID_FD2(ind(find(ind(:))));
active_dofs     = active_dofs(find(active_dofs));
Ng              = length(active_dofs);                  % number of active dofs

condensed_dofs                  = 1:Nr;
condensed_dofs(active_dofs)= 0;
condensed_dofs                  = condensed_dofs(find(condensed_dofs));

ID_arrayGD                      = zeros(1,Nr);          % ID-F after the guyan reduction
ID_arrayGD(active_dofs)         = 1:Ng;

et      = [active_dofs condensed_dofs];

% partition mass and stiffness matrices for guyan reduction of rotational dof
K3      = K(et,et);
M3      = M(et,et);

Maa     = M3(1:Ng,1:Ng);
Mdd     = M3(Ng+1:Nr,Ng+1:Nr);
Mda     = M3(Ng+1:Nr,1:Ng);
Mad     = M3(1:Ng,Ng+1:Nr);

Kaa     = K3(1:Ng,1:Ng);
Kdd     = K3(Ng+1:Nr,Ng+1:Nr);
Kda     = K3(Ng+1:Nr,1:Ng);
Kad     = K3(1:Ng,Ng+1:Nr);
```

```
% find the transformation matrix
Tdag    = -Kdd\Kda;
Tg      = [eye(Ng);Tdag];

% determine the new reduced mass, stiffness and loading matrices
K       = Kaa+Kad*Tdag;
M       = Maa+Mad*Tdag+(Mad*Tdag)'+Tdag'*Mdd*Tdag;
```

APPENDIX C

SAP2000 DATA (S2K) FILES FOR 3D BUILDING EXAMPLES

C.1 EXAMPE 5.4.1

```
SYSTEM
 DOF=UX,UY,UZ,RX,RY,RZ  LENGTH=m  FORCE=N  PAGE=SECTIONS

JOINT
 1  X=-5.5  Y=-5.5  Z=0
 2  X=0  Y=-5.5  Z=0
 3  X=5.5  Y=-5.5  Z=0
 4  X=-5.5  Y=0  Z=0
 5  X=0  Y=0  Z=0
 6  X=5.5  Y=0  Z=0
 7  X=-5.5  Y=5.5  Z=0
 8  X=0  Y=5.5  Z=0
 9  X=5.5  Y=5.5  Z=0
 10  X=-5.5  Y=-5.5  Z=4.5
 11  X=0  Y=-5.5  Z=4.5
 12  X=5.5  Y=-5.5  Z=4.5
 13  X=-5.5  Y=0  Z=4.5
 14  X=0  Y=0  Z=4.5
 15  X=5.5  Y=0  Z=4.5
 16  X=-5.5  Y=5.5  Z=4.5
 17  X=0  Y=5.5  Z=4.5
 18  X=5.5  Y=5.5  Z=4.5
 19  X=-5.5  Y=-5.5  Z=9
 20  X=0  Y=-5.5  Z=9
 21  X=5.5  Y=-5.5  Z=9
 22  X=-5.5  Y=0  Z=9
 23  X=0  Y=0  Z=9
 24  X=5.5  Y=0  Z=9
 25  X=-5.5  Y=5.5  Z=9
```

26 X=0 Y=5.5 Z=9
27 X=5.5 Y=5.5 Z=9
28 X=-5.5 Y=-5.5 Z=13.5
29 X=0 Y=-5.5 Z=13.5
30 X=5.5 Y=-5.5 Z=13.5
31 X=-5.5 Y=0 Z=13.5
32 X=0 Y=0 Z=13.5
33 X=5.5 Y=0 Z=13.5
34 X=-5.5 Y=5.5 Z=13.5
35 X=0 Y=5.5 Z=13.5
36 X=5.5 Y=5.5 Z=13.5
37 X=-5.5 Y=-5.5 Z=18
38 X=0 Y=-5.5 Z=18
39 X=5.5 Y=-5.5 Z=18
40 X=-5.5 Y=0 Z=18
41 X=0 Y=0 Z=18
42 X=5.5 Y=0 Z=18
43 X=-5.5 Y=5.5 Z=18
44 X=0 Y=5.5 Z=18
45 X=5.5 Y=5.5 Z=18
46 X=0 Y=-5.5 Z=22.5
47 X=-5.5 Y=0 Z=22.5
48 X=5.5 Y=0 Z=22.5
49 X=0 Y=5.5 Z=22.5
50 X=0 Y=-5.5 Z=27
51 X=-5.5 Y=0 Z=27
52 X=5.5 Y=0 Z=27
53 X=0 Y=5.5 Z=27
54 X=0 Y=-5.5 Z=31.5
55 X=-5.5 Y=0 Z=31.5
56 X=5.5 Y=0 Z=31.5
57 X=0 Y=5.5 Z=31.5
58 X=0 Y=-5.5 Z=36
59 X=-5.5 Y=0 Z=36
60 X=5.5 Y=0 Z=36
61 X=0 Y=5.5 Z=36
62 X=0 Y=-5.5 Z=40.5
63 X=-5.5 Y=0 Z=40.5
64 X=5.5 Y=0 Z=40.5
65 X=0 Y=5.5 Z=40.5
66 X=0 Y=-5.5 Z=45
67 X=-5.5 Y=0 Z=45
68 X=5.5 Y=0 Z=45
69 X=0 Y=5.5 Z=45

```
 70  X=0  Y=-5.5  Z=49.5
 71  X=-5.5  Y=0  Z=49.5
 72  X=5.5  Y=0  Z=49.5
 73  X=0  Y=5.5  Z=49.5
 74  X=0  Y=-5.5  Z=54
 75  X=-5.5  Y=0  Z=54
 76  X=5.5  Y=0  Z=54
 77  X=0  Y=5.5  Z=54

RESTRAINT
 ADD=1  DOF=U1,U2,U3,R1,R2,R3
 ADD=2  DOF=U1,U2,U3,R1,R2,R3
 ADD=3  DOF=U1,U2,U3,R1,R2,R3
 ADD=4  DOF=U1,U2,U3,R1,R2,R3
 ADD=5  DOF=U1,U2,U3,R1,R2,R3
 ADD=6  DOF=U1,U2,U3,R1,R2,R3
 ADD=7  DOF=U1,U2,U3,R1,R2,R3
 ADD=8  DOF=U1,U2,U3,R1,R2,R3
 ADD=9  DOF=U1,U2,U3,R1,R2,R3

CONSTRAINT
 NAME=DIAPH2  TYPE=DIAPH  AXIS=Z  CSYS=0
  ADD=13
  ADD=16
  ADD=17
  ADD=18
  ADD=15
  ADD=14
  ADD=10
  ADD=11
  ADD=12
 NAME=DIAPH3  TYPE=DIAPH  AXIS=Z  CSYS=0
  ADD=19
  ADD=20
  ADD=21
  ADD=22
  ADD=23
  ADD=24
  ADD=25
  ADD=26
  ADD=27
 NAME=DIAPH4  TYPE=DIAPH  AXIS=Z  CSYS=0
  ADD=28
  ADD=29
```

```
  ADD=30
  ADD=31
  ADD=32
  ADD=33
  ADD=34
  ADD=35
  ADD=36
NAME=DIAPH5  TYPE=DIAPH  AXIS=Z  CSYS=0
  ADD=37
  ADD=38
  ADD=39
  ADD=40
  ADD=41
  ADD=42
  ADD=43
  ADD=44
  ADD=45
NAME=DIAPH6  TYPE=DIAPH  AXIS=Z  CSYS=0
  ADD=46
  ADD=47
  ADD=48
  ADD=49
NAME=DIAPH7  TYPE=DIAPH  AXIS=Z  CSYS=0
  ADD=50
  ADD=51
  ADD=52
  ADD=53
NAME=DIAPH8  TYPE=DIAPH  AXIS=Z  CSYS=0
  ADD=54
  ADD=55
  ADD=56
  ADD=57
NAME=DIAPH9  TYPE=DIAPH  AXIS=Z  CSYS=0
  ADD=58
  ADD=59
  ADD=60
  ADD=61
NAME=DIAPH10  TYPE=DIAPH  AXIS=Z  CSYS=0
  ADD=62
  ADD=63
  ADD=64
  ADD=65
NAME=DIAPH11  TYPE=DIAPH  AXIS=Z  CSYS=0
  ADD=66
```

```
   ADD=67
   ADD=68
   ADD=69
  NAME=DIAPH12  TYPE=DIAPH  AXIS=Z  CSYS=0
   ADD=70
   ADD=71
   ADD=72
   ADD=73
  NAME=DIAPH13  TYPE=DIAPH  AXIS=Z  CSYS=0
   ADD=74
   ADD=75
   ADD=76
   ADD=77

PATTERN
  NAME=DEFAULT

MASS
  ADD=46  U1=3693.877  U2=3693.877  U3=3693.877
  ADD=47  U1=3693.877  U2=3693.877  U3=3693.877
  ADD=48  U1=3693.877  U2=3693.877  U3=3693.877
  ADD=49  U1=3693.877  U2=3693.877  U3=3693.877
  ADD=50  U1=3693.877  U2=3693.877  U3=3693.877
  ADD=51  U1=3693.877  U2=3693.877  U3=3693.877
  ADD=52  U1=3693.877  U2=3693.877  U3=3693.877
  ADD=53  U1=3693.877  U2=3693.877  U3=3693.877
  ADD=54  U1=3693.877  U2=3693.877  U3=3693.877
  ADD=55  U1=3693.877  U2=3693.877  U3=3693.877
  ADD=56  U1=3693.877  U2=3693.877  U3=3693.877
  ADD=57  U1=3693.877  U2=3693.877  U3=3693.877
  ADD=58  U1=3693.877  U2=3693.877  U3=3693.877
  ADD=59  U1=3693.877  U2=3693.877  U3=3693.877
  ADD=60  U1=3693.877  U2=3693.877  U3=3693.877
  ADD=61  U1=3693.877  U2=3693.877  U3=3693.877
  ADD=62  U1=3693.877  U2=3693.877  U3=3693.877
  ADD=63  U1=3693.877  U2=3693.877  U3=3693.877
  ADD=64  U1=3693.877  U2=3693.877  U3=3693.877
  ADD=65  U1=3693.877  U2=3693.877  U3=3693.877
  ADD=66  U1=3693.877  U2=3693.877  U3=3693.877
  ADD=67  U1=3693.877  U2=3693.877  U3=3693.877
  ADD=68  U1=3693.877  U2=3693.877  U3=3693.877
  ADD=69  U1=3693.877  U2=3693.877  U3=3693.877
  ADD=70  U1=3693.877  U2=3693.877  U3=3693.877
  ADD=71  U1=3693.877  U2=3693.877  U3=3693.877
```

ADD=72 U1=3693.877 U2=3693.877 U3=3693.877
ADD=73 U1=3693.877 U2=3693.877 U3=3693.877
ADD=74 U1=3693.877 U2=3693.877 U3=3693.877
ADD=75 U1=3693.877 U2=3693.877 U3=3693.877
ADD=76 U1=3693.877 U2=3693.877 U3=3693.877
ADD=77 U1=3693.877 U2=3693.877 U3=3693.877
ADD=10 U1=3693.877 U2=3693.877 U3=3693.877
ADD=12 U1=3693.877 U2=3693.877 U3=3693.877
ADD=16 U1=3693.877 U2=3693.877 U3=3693.877
ADD=18 U1=3693.877 U2=3693.877 U3=3693.877
ADD=19 U1=3693.877 U2=3693.877 U3=3693.877
ADD=21 U1=3693.877 U2=3693.877 U3=3693.877
ADD=25 U1=3693.877 U2=3693.877 U3=3693.877
ADD=27 U1=3693.877 U2=3693.877 U3=3693.877
ADD=28 U1=3693.877 U2=3693.877 U3=3693.877
ADD=30 U1=3693.877 U2=3693.877 U3=3693.877
ADD=34 U1=3693.877 U2=3693.877 U3=3693.877
ADD=36 U1=3693.877 U2=3693.877 U3=3693.877
ADD=37 U1=3693.877 U2=3693.877 U3=3693.877
ADD=39 U1=3693.877 U2=3693.877 U3=3693.877
ADD=43 U1=3693.877 U2=3693.877 U3=3693.877
ADD=45 U1=3693.877 U2=3693.877 U3=3693.877
ADD=11 U1=7387.754 U2=7387.754 U3=7387.754
ADD=13 U1=7387.754 U2=7387.754 U3=7387.754
ADD=15 U1=7387.754 U2=7387.754 U3=7387.754
ADD=17 U1=7387.754 U2=7387.754 U3=7387.754
ADD=20 U1=7387.754 U2=7387.754 U3=7387.754
ADD=22 U1=7387.754 U2=7387.754 U3=7387.754
ADD=24 U1=7387.754 U2=7387.754 U3=7387.754
ADD=26 U1=7387.754 U2=7387.754 U3=7387.754
ADD=29 U1=7387.754 U2=7387.754 U3=7387.754
ADD=31 U1=7387.754 U2=7387.754 U3=7387.754
ADD=33 U1=7387.754 U2=7387.754 U3=7387.754
ADD=35 U1=7387.754 U2=7387.754 U3=7387.754
ADD=38 U1=7387.754 U2=7387.754 U3=7387.754
ADD=40 U1=7387.754 U2=7387.754 U3=7387.754
ADD=42 U1=7387.754 U2=7387.754 U3=7387.754
ADD=44 U1=7387.754 U2=7387.754 U3=7387.754
ADD=14 U1=14775.51 U2=14775.51 U3=14775.51
ADD=23 U1=14775.51 U2=14775.51 U3=14775.51
ADD=32 U1=14775.51 U2=14775.51 U3=14775.51
ADD=41 U1=14775.51 U2=14775.51 U3=14775.51

MATERIAL

```
  NAME=MAT1  IDES=S
    T=0  E=1.999E+11  U=.3  A=.0000117  FY=2.482E+08
  NAME=STEEL  IDES=S  M=7827.1  W=76819.55
    T=0  E=1.99948E+11  U=.3  A=.0000117  FY=2.482E+08
  NAME=CONC  IDES=C  M=2400.68  W=23561.61
    T=0  E=2.482113E+10  U=.2  A=.0000099

FRAME SECTION
  NAME=W14X61 MAT=MAT1 A=1.154836E-02 J=9.157092E-07 I=2.663881E-
04,4.453676E-05 AS=3.360509E-03,6.932244E-03 S=1.510111E-03,3.508586E-04
Z=1.67148E-03,5.374957E-04 R=.1518788,6.210107E-02
T=.352806,.253873,.016383,.009525,.253873,.016383 SHN=W14X61 DSG=W
  NAME=W14X68 MAT=MAT1 A=.0129032 J=1.257019E-06 I=3.009353E-
04,5.0364E-05 AS=3.759089E-03,7.769017E-03 S=1.687728E-03,3.951838E-04
Z=1.884512E-03,6.046827E-04 R=.1527172,6.247574E-02
T=.356616,.254889,.018288,.010541,.254889,.018288 SHN=W14X68 DSG=W
  NAME=W14X90 MAT=MAT1 A=1.709674E-02 J=1.6899E-06 I=4.158152E-
04,1.506758E-04 AS=3.979863E-03,1.108514E-02 S=2.335332E-03,8.17096E-04
Z=2.572769E-03,1.238862E-03 R=.1559529,9.387827E-02
T=.356108,.368808,.018034,.011176,.368808,.018034 SHN=W14X90 DSG=W
  NAME=W21X50 MAT=MAT1 A=9.483851E-03 J=4.745038E-07 I=4.095717E-
04,1.036416E-05 AS=.0051067,3.756508E-03 S=1.548235E-03,1.249733E-04
Z=1.802577E-03,1.999222E-04 R=.207813,3.305786E-02
T=.529082,.165862,.013589,.009652,.165862,.013589 SHN=W21X50 DSG=W
  NAME=W21X57 MAT=MAT1 A=1.077417E-02 J=7.367296E-07 I=4.869908E-
04,1.273668E-05 AS=5.502763E-03,4.58141E-03 S=1.820785E-03,1.529959E-04
Z=2.113931E-03,2.425285E-04 R=.2126025,.0343824
T=.534924,.166497,.01651,.010287,.166497,.01651 SHN=W21X57 DSG=W

FRAME
  1  J=1,10  SEC=W14X68  NSEG=2  ANG=90
  2  J=2,11  SEC=W14X90  NSEG=2  ANG=0
  3  J=3,12  SEC=W14X68  NSEG=2  ANG=0
  4  J=4,13  SEC=W14X90  NSEG=2  ANG=90
  5  J=5,14  SEC=W14X90  NSEG=2  ANG=0
  6  J=6,15  SEC=W14X90  NSEG=2  ANG=90
  7  J=7,16  SEC=W14X68  NSEG=2  ANG=0
  8  J=8,17  SEC=W14X90  NSEG=2  ANG=0
  9  J=9,18  SEC=W14X68  NSEG=2  ANG=90
  10  J=10,11  SEC=W21X50  NSEG=4  ANG=0
  11  J=11,12  SEC=W21X50  NSEG=4  ANG=0
  12  J=10,13  SEC=W21X50  NSEG=4  ANG=0
  13  J=11,14  SEC=W21X50  NSEG=4  ANG=0
  14  J=12,15  SEC=W21X50  NSEG=4  ANG=0
```

```
15  J=13,14  SEC=W21X50  NSEG=4  ANG=0
16  J=14,15  SEC=W21X50  NSEG=4  ANG=0
17  J=13,16  SEC=W21X50  NSEG=4  ANG=0
18  J=14,17  SEC=W21X50  NSEG=4  ANG=0
19  J=15,18  SEC=W21X50  NSEG=4  ANG=0
20  J=16,17  SEC=W21X50  NSEG=4  ANG=0
21  J=17,18  SEC=W21X50  NSEG=4  ANG=0
22  J=10,19  SEC=W14X68  NSEG=2  ANG=90
23  J=11,20  SEC=W14X90  NSEG=2  ANG=0
24  J=12,21  SEC=W14X68  NSEG=2  ANG=0
25  J=13,22  SEC=W14X90  NSEG=2  ANG=90
26  J=14,23  SEC=W14X90  NSEG=2  ANG=0
27  J=15,24  SEC=W14X90  NSEG=2  ANG=90
28  J=16,25  SEC=W14X68  NSEG=2  ANG=0
29  J=17,26  SEC=W14X90  NSEG=2  ANG=0
30  J=18,27  SEC=W14X68  NSEG=2  ANG=90
31  J=19,20  SEC=W21X50  NSEG=4  ANG=0
32  J=20,21  SEC=W21X50  NSEG=4  ANG=0
33  J=19,22  SEC=W21X50  NSEG=4  ANG=0
34  J=20,23  SEC=W21X50  NSEG=4  ANG=0
35  J=21,24  SEC=W21X50  NSEG=4  ANG=0
36  J=22,23  SEC=W21X50  NSEG=4  ANG=0
37  J=23,24  SEC=W21X50  NSEG=4  ANG=0
38  J=22,25  SEC=W21X50  NSEG=4  ANG=0
39  J=23,26  SEC=W21X50  NSEG=4  ANG=0
40  J=24,27  SEC=W21X50  NSEG=4  ANG=0
41  J=25,26  SEC=W21X50  NSEG=4  ANG=0
42  J=26,27  SEC=W21X50  NSEG=4  ANG=0
43  J=19,28  SEC=W14X68  NSEG=2  ANG=90
44  J=20,29  SEC=W14X90  NSEG=2  ANG=0
45  J=21,30  SEC=W14X68  NSEG=2  ANG=0
46  J=22,31  SEC=W14X90  NSEG=2  ANG=90
47  J=23,32  SEC=W14X68  NSEG=2  ANG=0
48  J=24,33  SEC=W14X90  NSEG=2  ANG=90
49  J=25,34  SEC=W14X68  NSEG=2  ANG=0
50  J=26,35  SEC=W14X90  NSEG=2  ANG=0
51  J=27,36  SEC=W14X68  NSEG=2  ANG=90
52  J=28,29  SEC=W21X50  NSEG=4  ANG=0
53  J=29,30  SEC=W21X50  NSEG=4  ANG=0
54  J=28,31  SEC=W21X50  NSEG=4  ANG=0
55  J=29,32  SEC=W21X50  NSEG=4  ANG=0
56  J=30,33  SEC=W21X50  NSEG=4  ANG=0
57  J=31,32  SEC=W21X50  NSEG=4  ANG=0
58  J=32,33  SEC=W21X50  NSEG=4  ANG=0
```

59 J=31,34 SEC=W21X50 NSEG=4 ANG=0
60 J=32,35 SEC=W21X50 NSEG=4 ANG=0
61 J=33,36 SEC=W21X50 NSEG=4 ANG=0
62 J=34,35 SEC=W21X50 NSEG=4 ANG=0
63 J=35,36 SEC=W21X50 NSEG=4 ANG=0
64 J=28,37 SEC=W14X68 NSEG=2 ANG=90
65 J=29,38 SEC=W14X90 NSEG=2 ANG=0
66 J=30,39 SEC=W14X68 NSEG=2 ANG=0
67 J=31,40 SEC=W14X90 NSEG=2 ANG=90
68 J=32,41 SEC=W14X68 NSEG=2 ANG=0
69 J=33,42 SEC=W14X90 NSEG=2 ANG=90
70 J=34,43 SEC=W14X68 NSEG=2 ANG=0
71 J=35,44 SEC=W14X90 NSEG=2 ANG=0
72 J=36,45 SEC=W14X68 NSEG=2 ANG=90
73 J=37,38 SEC=W21X50 NSEG=4 ANG=0
74 J=38,39 SEC=W21X50 NSEG=4 ANG=0
75 J=37,40 SEC=W21X50 NSEG=4 ANG=0
76 J=38,41 SEC=W21X50 NSEG=4 ANG=0
77 J=39,42 SEC=W21X50 NSEG=4 ANG=0
78 J=40,41 SEC=W21X50 NSEG=4 ANG=0
79 J=41,42 SEC=W21X50 NSEG=4 ANG=0
80 J=40,43 SEC=W21X50 NSEG=4 ANG=0
81 J=41,44 SEC=W21X50 NSEG=4 ANG=0
82 J=42,45 SEC=W21X50 NSEG=4 ANG=0
83 J=43,44 SEC=W21X50 NSEG=4 ANG=0
84 J=44,45 SEC=W21X50 NSEG=4 ANG=0
85 J=38,46 SEC=W14X90 NSEG=2 ANG=0
86 J=40,47 SEC=W14X90 NSEG=2 ANG=90
87 J=42,48 SEC=W14X90 NSEG=2 ANG=90
88 J=44,49 SEC=W14X90 NSEG=2 ANG=0
89 J=46,47 SEC=W21X57 NSEG=4 ANG=0
90 J=48,46 SEC=W21X50 NSEG=4 ANG=0
91 J=47,49 SEC=W21X50 NSEG=4 ANG=0
92 J=49,48 SEC=W21X57 NSEG=4 ANG=0
93 J=46,50 SEC=W14X90 NSEG=2 ANG=0
94 J=47,51 SEC=W14X90 NSEG=2 ANG=90
95 J=48,52 SEC=W14X90 NSEG=2 ANG=90
96 J=49,53 SEC=W14X90 NSEG=2 ANG=0
97 J=50,51 SEC=W21X57 NSEG=4 ANG=0
98 J=52,50 SEC=W21X50 NSEG=4 ANG=0
99 J=51,53 SEC=W21X50 NSEG=4 ANG=0
100 J=53,52 SEC=W21X57 NSEG=4 ANG=0
101 J=50,54 SEC=W14X90 NSEG=2 ANG=0
102 J=51,55 SEC=W14X90 NSEG=2 ANG=90

```
103  J=52,56  SEC=W14X90  NSEG=2  ANG=90
104  J=53,57  SEC=W14X90  NSEG=2  ANG=0
105  J=54,55  SEC=W21X57  NSEG=4  ANG=0
106  J=56,54  SEC=W21X50  NSEG=4  ANG=0
107  J=55,57  SEC=W21X50  NSEG=4  ANG=0
108  J=57,56  SEC=W21X57  NSEG=4  ANG=0
109  J=54,58  SEC=W14X90  NSEG=2  ANG=0
110  J=55,59  SEC=W14X90  NSEG=2  ANG=90
111  J=56,60  SEC=W14X90  NSEG=2  ANG=90
112  J=57,61  SEC=W14X90  NSEG=2  ANG=0
113  J=58,59  SEC=W21X57  NSEG=4  ANG=0
114  J=60,58  SEC=W21X50  NSEG=4  ANG=0
115  J=59,61  SEC=W21X50  NSEG=4  ANG=0
116  J=61,60  SEC=W21X57  NSEG=4  ANG=0
117  J=58,62  SEC=W14X90  NSEG=2  ANG=0
118  J=59,63  SEC=W14X90  NSEG=2  ANG=90
119  J=60,64  SEC=W14X90  NSEG=2  ANG=90
120  J=61,65  SEC=W14X90  NSEG=2  ANG=0
121  J=62,63  SEC=W21X57  NSEG=4  ANG=0
122  J=64,62  SEC=W21X50  NSEG=4  ANG=0
123  J=63,65  SEC=W21X50  NSEG=4  ANG=0
124  J=65,64  SEC=W21X57  NSEG=4  ANG=0
125  J=62,66  SEC=W14X90  NSEG=2  ANG=0
126  J=63,67  SEC=W14X90  NSEG=2  ANG=90
127  J=64,68  SEC=W14X90  NSEG=2  ANG=90
128  J=65,69  SEC=W14X90  NSEG=2  ANG=0
129  J=66,67  SEC=W21X57  NSEG=4  ANG=0
130  J=68,66  SEC=W21X50  NSEG=4  ANG=0
131  J=67,69  SEC=W21X50  NSEG=4  ANG=0
132  J=69,68  SEC=W21X57  NSEG=4  ANG=0
133  J=66,70  SEC=W14X61  NSEG=2  ANG=0
134  J=67,71  SEC=W14X61  NSEG=2  ANG=90
135  J=68,72  SEC=W14X61  NSEG=2  ANG=90
136  J=69,73  SEC=W14X61  NSEG=2  ANG=0
137  J=70,71  SEC=W21X57  NSEG=4  ANG=0
138  J=72,70  SEC=W21X50  NSEG=4  ANG=0
139  J=71,73  SEC=W21X50  NSEG=4  ANG=0
140  J=73,72  SEC=W21X57  NSEG=4  ANG=0
141  J=70,74  SEC=W14X61  NSEG=2  ANG=0
142  J=71,75  SEC=W14X61  NSEG=2  ANG=90
143  J=72,76  SEC=W14X61  NSEG=2  ANG=90
144  J=73,77  SEC=W14X61  NSEG=2  ANG=0
145  J=74,75  SEC=W21X57  NSEG=4  ANG=0
146  J=76,74  SEC=W21X50  NSEG=4  ANG=0
```

```
 147  J=75,77  SEC=W21X50  NSEG=4  ANG=0
 148  J=77,76  SEC=W21X57  NSEG=4  ANG=0

LOAD
 NAME=DL  CSYS=0
  TYPE=CONCENTRATED SPAN
   ADD=90  RD=.5  UZ=-36224.38
   ADD=91  RD=.5  UZ=-36224.38
   ADD=98  RD=.5  UZ=-36224.38
   ADD=99  RD=.5  UZ=-36224.38
   ADD=106  RD=.5  UZ=-36224.38
   ADD=107  RD=.5  UZ=-36224.38
   ADD=114  RD=.5  UZ=-36224.38
   ADD=115  RD=.5  UZ=-36224.38
   ADD=122  RD=.5  UZ=-36224.38
   ADD=123  RD=.5  UZ=-36224.38
   ADD=130  RD=.5  UZ=-36224.38
   ADD=131  RD=.5  UZ=-36224.38
   ADD=138  RD=.5  UZ=-36224.38
   ADD=139  RD=.5  UZ=-36224.38
   ADD=146  RD=.5  UZ=-36224.38
   ADD=147  RD=.5  UZ=-36224.38
   ADD=12  RD=.5  UZ=-36224.38
   ADD=14  RD=.5  UZ=-36224.38
   ADD=17  RD=.5  UZ=-36224.38
   ADD=19  RD=.5  UZ=-36224.38
   ADD=33  RD=.5  UZ=-36224.38
   ADD=35  RD=.5  UZ=-36224.38
   ADD=38  RD=.5  UZ=-36224.38
   ADD=40  RD=.5  UZ=-36224.38
   ADD=54  RD=.5  UZ=-36224.38
   ADD=56  RD=.5  UZ=-36224.38
   ADD=59  RD=.5  UZ=-36224.38
   ADD=61  RD=.5  UZ=-36224.38
   ADD=75  RD=.5  UZ=-36224.38
   ADD=77  RD=.5  UZ=-36224.38
   ADD=80  RD=.5  UZ=-36224.38
   ADD=82  RD=.5  UZ=-36224.38
   ADD=13  RD=.5  UZ=-72448.75
   ADD=18  RD=.5  UZ=-72448.75
   ADD=34  RD=.5  UZ=-72448.75
   ADD=39  RD=.5  UZ=-72448.75
   ADD=55  RD=.5  UZ=-72448.75
   ADD=60  RD=.5  UZ=-72448.75
```

```
  ADD=76  RD=.5  UZ=-72448.75
  ADD=81  RD=.5  UZ=-72448.75
 TYPE=DISTRIBUTED SPAN
  ADD=89  RD=0,1  UZ=-6586.25,-6586.25
  ADD=92  RD=0,1  UZ=-6586.25,-6586.25
  ADD=97  RD=0,1  UZ=-6586.25,-6586.25
  ADD=100  RD=0,1  UZ=-6586.25,-6586.25
  ADD=105  RD=0,1  UZ=-6586.25,-6586.25
  ADD=108  RD=0,1  UZ=-6586.25,-6586.25
  ADD=113  RD=0,1  UZ=-6586.25,-6586.25
  ADD=116  RD=0,1  UZ=-6586.25,-6586.25
  ADD=121  RD=0,1  UZ=-6586.25,-6586.25
  ADD=124  RD=0,1  UZ=-6586.25,-6586.25
  ADD=129  RD=0,1  UZ=-6586.25,-6586.25
  ADD=132  RD=0,1  UZ=-6586.25,-6586.25
  ADD=137  RD=0,1  UZ=-6586.25,-6586.25
  ADD=140  RD=0,1  UZ=-6586.25,-6586.25
  ADD=145  RD=0,1  UZ=-6586.25,-6586.25
  ADD=148  RD=0,1  UZ=-6586.25,-6586.25
  ADD=10  RD=0,1  UZ=-6586.25,-6586.25
  ADD=11  RD=0,1  UZ=-6586.25,-6586.25
  ADD=20  RD=0,1  UZ=-6586.25,-6586.25
  ADD=21  RD=0,1  UZ=-6586.25,-6586.25
  ADD=31  RD=0,1  UZ=-6586.25,-6586.25
  ADD=32  RD=0,1  UZ=-6586.25,-6586.25
  ADD=41  RD=0,1  UZ=-6586.25,-6586.25
  ADD=42  RD=0,1  UZ=-6586.25,-6586.25
  ADD=52  RD=0,1  UZ=-6586.25,-6586.25
  ADD=53  RD=0,1  UZ=-6586.25,-6586.25
  ADD=62  RD=0,1  UZ=-6586.25,-6586.25
  ADD=63  RD=0,1  UZ=-6586.25,-6586.25
  ADD=73  RD=0,1  UZ=-6586.25,-6586.25
  ADD=74  RD=0,1  UZ=-6586.25,-6586.25
  ADD=83  RD=0,1  UZ=-6586.25,-6586.25
  ADD=84  RD=0,1  UZ=-6586.25,-6586.25
  ADD=15  RD=0,1  UZ=-13172.5,-13172.5
  ADD=16  RD=0,1  UZ=-13172.5,-13172.5
  ADD=36  RD=0,1  UZ=-13172.5,-13172.5
  ADD=37  RD=0,1  UZ=-13172.5,-13172.5
  ADD=57  RD=0,1  UZ=-13172.5,-13172.5
  ADD=58  RD=0,1  UZ=-13172.5,-13172.5
  ADD=78  RD=0,1  UZ=-13172.5,-13172.5
  ADD=79  RD=0,1  UZ=-13172.5,-13172.5
NAME=LL  CSYS=0
```

```
TYPE=CONCENTRATED SPAN
  ADD=90  RD=.5  UZ=-25334.38
  ADD=91  RD=.5  UZ=-25334.38
  ADD=98  RD=.5  UZ=-25334.38
  ADD=99  RD=.5  UZ=-25334.38
  ADD=106  RD=.5  UZ=-25334.38
  ADD=107  RD=.5  UZ=-25334.38
  ADD=114  RD=.5  UZ=-25334.38
  ADD=115  RD=.5  UZ=-25334.38
  ADD=122  RD=.5  UZ=-25334.38
  ADD=123  RD=.5  UZ=-25334.38
  ADD=130  RD=.5  UZ=-25334.38
  ADD=131  RD=.5  UZ=-25334.38
  ADD=138  RD=.5  UZ=-25334.38
  ADD=139  RD=.5  UZ=-25334.38
  ADD=146  RD=.5  UZ=-25334.38
  ADD=147  RD=.5  UZ=-25334.38
  ADD=12  RD=.5  UZ=-25334.38
  ADD=14  RD=.5  UZ=-25334.38
  ADD=17  RD=.5  UZ=-25334.38
  ADD=19  RD=.5  UZ=-25334.38
  ADD=33  RD=.5  UZ=-25334.38
  ADD=35  RD=.5  UZ=-25334.38
  ADD=38  RD=.5  UZ=-25334.38
  ADD=40  RD=.5  UZ=-25334.38
  ADD=54  RD=.5  UZ=-25334.38
  ADD=56  RD=.5  UZ=-25334.38
  ADD=59  RD=.5  UZ=-25334.38
  ADD=61  RD=.5  UZ=-25334.38
  ADD=75  RD=.5  UZ=-25334.38
  ADD=77  RD=.5  UZ=-25334.38
  ADD=80  RD=.5  UZ=-25334.38
  ADD=82  RD=.5  UZ=-25334.38
  ADD=13  RD=.5  UZ=-50668.75
  ADD=18  RD=.5  UZ=-50668.75
  ADD=34  RD=.5  UZ=-50668.75
  ADD=39  RD=.5  UZ=-50668.75
  ADD=55  RD=.5  UZ=-50668.75
  ADD=60  RD=.5  UZ=-50668.75
  ADD=76  RD=.5  UZ=-50668.75
  ADD=81  RD=.5  UZ=-50668.75
TYPE=DISTRIBUTED SPAN
  ADD=89  RD=0,1  UZ=-4606.25,-4606.25
  ADD=92  RD=0,1  UZ=-4606.25,-4606.25
```

```
    ADD=97  RD=0,1  UZ=-4606.25,-4606.25
    ADD=100  RD=0,1  UZ=-4606.25,-4606.25
    ADD=105  RD=0,1  UZ=-4606.25,-4606.25
    ADD=108  RD=0,1  UZ=-4606.25,-4606.25
    ADD=113  RD=0,1  UZ=-4606.25,-4606.25
    ADD=116  RD=0,1  UZ=-4606.25,-4606.25
    ADD=121  RD=0,1  UZ=-4606.25,-4606.25
    ADD=124  RD=0,1  UZ=-4606.25,-4606.25
    ADD=129  RD=0,1  UZ=-4606.25,-4606.25
    ADD=132  RD=0,1  UZ=-4606.25,-4606.25
    ADD=137  RD=0,1  UZ=-4606.25,-4606.25
    ADD=140  RD=0,1  UZ=-4606.25,-4606.25
    ADD=145  RD=0,1  UZ=-4606.25,-4606.25
    ADD=148  RD=0,1  UZ=-4606.25,-4606.25
    ADD=10  RD=0,1  UZ=-4606.25,-4606.25
    ADD=11  RD=0,1  UZ=-4606.25,-4606.25
    ADD=20  RD=0,1  UZ=-4606.25,-4606.25
    ADD=21  RD=0,1  UZ=-4606.25,-4606.25
    ADD=31  RD=0,1  UZ=-4606.25,-4606.25
    ADD=32  RD=0,1  UZ=-4606.25,-4606.25
    ADD=41  RD=0,1  UZ=-4606.25,-4606.25
    ADD=42  RD=0,1  UZ=-4606.25,-4606.25
    ADD=52  RD=0,1  UZ=-4606.25,-4606.25
    ADD=53  RD=0,1  UZ=-4606.25,-4606.25
    ADD=62  RD=0,1  UZ=-4606.25,-4606.25
    ADD=63  RD=0,1  UZ=-4606.25,-4606.25
    ADD=73  RD=0,1  UZ=-4606.25,-4606.25
    ADD=74  RD=0,1  UZ=-4606.25,-4606.25
    ADD=83  RD=0,1  UZ=-4606.25,-4606.25
    ADD=84  RD=0,1  UZ=-4606.25,-4606.25
    ADD=15  RD=0,1  UZ=-9212.5,-9212.5
    ADD=16  RD=0,1  UZ=-9212.5,-9212.5
    ADD=36  RD=0,1  UZ=-9212.5,-9212.5
    ADD=37  RD=0,1  UZ=-9212.5,-9212.5
    ADD=57  RD=0,1  UZ=-9212.5,-9212.5
    ADD=58  RD=0,1  UZ=-9212.5,-9212.5
    ADD=78  RD=0,1  UZ=-9212.5,-9212.5
    ADD=79  RD=0,1  UZ=-9212.5,-9212.5
NAME=EQX  CSYS=0
  TYPE=FORCE
    ADD=74  UX=9825.165
    ADD=75  UX=9825.165
    ADD=76  UX=9825.165
    ADD=77  UX=9825.165
```

ADD=70 UX=8548.268
ADD=71 UX=8548.268
ADD=72 UX=8548.268
ADD=73 UX=8548.268
ADD=66 UX=7339.217
ADD=67 UX=7339.217
ADD=68 UX=7339.217
ADD=69 UX=7339.217
ADD=62 UX=6200.656
ADD=63 UX=6200.656
ADD=64 UX=6200.656
ADD=65 UX=6200.656
ADD=58 UX=5135.627
ADD=59 UX=5135.627
ADD=60 UX=5135.627
ADD=61 UX=5135.627
ADD=54 UX=4147.695
ADD=55 UX=4147.695
ADD=56 UX=4147.695
ADD=57 UX=4147.695
ADD=50 UX=3241.096
ADD=51 UX=3241.096
ADD=52 UX=3241.096
ADD=53 UX=3241.096
ADD=46 UX=2421.038
ADD=47 UX=2421.038
ADD=48 UX=2421.038
ADD=49 UX=2421.038
ADD=37 UX=1694.13
ADD=39 UX=1694.13
ADD=43 UX=1694.13
ADD=45 UX=1694.13
ADD=38 UX=3388.25
ADD=40 UX=3388.25
ADD=42 UX=3388.25
ADD=44 UX=3388.25
ADD=41 UX=6776.5
ADD=28 UX=1069.16
ADD=30 UX=1069.16
ADD=34 UX=1069.16
ADD=36 UX=1069.16
ADD=29 UX=2138.32
ADD=31 UX=2138.32
ADD=33 UX=2138.32

```
    ADD=35  UX=2138.32
    ADD=32  UX=4276.64
    ADD=19  UX=558.85
    ADD=21  UX=558.85
    ADD=25  UX=558.85
    ADD=27  UX=558.85
    ADD=20  UX=1117.71
    ADD=22  UX=1117.71
    ADD=24  UX=1117.71
    ADD=26  UX=1117.71
    ADD=23  UX=2235.42
    ADD=10  UX=184.35
    ADD=12  UX=184.35
    ADD=16  UX=184.35
    ADD=18  UX=184.35
    ADD=11  UX=368.71
    ADD=13  UX=368.71
    ADD=15  UX=368.71
    ADD=17  UX=368.71
    ADD=14  UX=737.41
  NAME=EQY  CSYS=0
   TYPE=FORCE
    ADD=74  UY=9825.165
    ADD=75  UY=9825.165
    ADD=76  UY=9825.165
    ADD=77  UY=9825.165
    ADD=70  UY=8548.268
    ADD=71  UY=8548.268
    ADD=72  UY=8548.268
    ADD=73  UY=8548.268
    ADD=66  UY=7339.217
    ADD=67  UY=7339.217
    ADD=68  UY=7339.217
    ADD=69  UY=7339.217
    ADD=62  UY=6200.656
    ADD=63  UY=6200.656
    ADD=64  UY=6200.656
    ADD=65  UY=6200.656
    ADD=58  UY=5135.627
    ADD=59  UY=5135.627
    ADD=60  UY=5135.627
    ADD=61  UY=5135.627
    ADD=54  UY=4147.695
    ADD=55  UY=4147.695
```

ADD=56 UY=4147.695
ADD=57 UY=4147.695
ADD=50 UY=3241.096
ADD=51 UY=3241.096
ADD=52 UY=3241.096
ADD=53 UY=3241.096
ADD=46 UY=2421.038
ADD=47 UY=2421.038
ADD=48 UY=2421.038
ADD=49 UY=2421.038
ADD=37 UY=1694.13
ADD=39 UY=1694.13
ADD=43 UY=1694.13
ADD=45 UY=1694.13
ADD=38 UY=3388.25
ADD=40 UY=3388.25
ADD=42 UY=3388.25
ADD=44 UY=3388.25
ADD=41 UY=6776.5
ADD=28 UY=1069.16
ADD=30 UY=1069.16
ADD=34 UY=1069.16
ADD=36 UY=1069.16
ADD=29 UY=2138.32
ADD=31 UY=2138.32
ADD=33 UY=2138.32
ADD=35 UY=2138.32
ADD=32 UY=4276.64
ADD=19 UY=558.85
ADD=21 UY=558.85
ADD=25 UY=558.85
ADD=27 UY=558.85
ADD=20 UY=1117.71
ADD=22 UY=1117.71
ADD=24 UY=1117.71
ADD=26 UY=1117.71
ADD=23 UY=2235.42
ADD=10 UY=184.35
ADD=12 UY=184.35
ADD=16 UY=184.35
ADD=18 UY=184.35
ADD=11 UY=368.71
ADD=13 UY=368.71
ADD=15 UY=368.71

```
    ADD=17  UY=368.71
    ADD=14  UY=737.41

PDELTA
 ITMAX=10  TOLD=.001  TOLP=.001
   LOAD=DL  SF=1
   LOAD=LL  SF=1

MODE
 TYPE=EIGEN  N=10  TOL=.00001

HISTORY
 NAME=HIST1 TYPE=LIN NSTEP=1500 DT=.02 DAMP=.02
   ACC=U1  ANG=0 FUNC=ELCENT2 SF=9.8146 AT=0

COMBO
 NAME=DSTL1
   LOAD=DL  SF=1.4
 NAME=DSTL2
   LOAD=DL  SF=1.2
   LOAD=LL  SF=1.6
 NAME=DSTL3
   LOAD=DL  SF=1.2
   LOAD=LL  SF=.5
   LOAD=EQX  SF=1
 NAME=DSTL4
   LOAD=DL  SF=1.2
   LOAD=LL  SF=.5
   LOAD=EQX  SF=-1
 NAME=DSTL5
   LOAD=DL  SF=1.2
   LOAD=LL  SF=.5
   LOAD=EQY  SF=1
 NAME=DSTL6
   LOAD=DL  SF=1.2
   LOAD=LL  SF=.5
   LOAD=EQY  SF=-1
 NAME=DSTL7
   LOAD=DL  SF=.9
   LOAD=EQX  SF=1
 NAME=DSTL8
   LOAD=DL  SF=.9
   LOAD=EQX  SF=-1
 NAME=DSTL9
```

```
    LOAD=DL  SF=.9
    LOAD=EQY  SF=1
  NAME=DSTL10
    LOAD=DL  SF=.9
    LOAD=EQY  SF=-1

OUTPUT
; No Output Requested

END

; The following data is used for graphics, design and pushover analysis.
; If changes are made to the analysis data above, then the following data
; should be checked for consistency.
SAP2000 V7.40 SUPPLEMENTAL DATA
  GRID GLOBAL  X "1"  -5.5
  GRID GLOBAL  X "2"  0
  GRID GLOBAL  X "3"  5.5
  GRID GLOBAL  Y "4"  -5.5
  GRID GLOBAL  Y "5"  0
  GRID GLOBAL  Y "6"  5.5
  GRID GLOBAL  Z "7"  0
  GRID GLOBAL  Z "8"  4.5
  GRID GLOBAL  Z "9"  9
  GRID GLOBAL  Z "10"  13.5
  GRID GLOBAL  Z "11"  18
  GRID GLOBAL  Z "12"  22.5
  GRID GLOBAL  Z "13"  27
  GRID GLOBAL  Z "14"  31.5
  GRID GLOBAL  Z "15"  36
  GRID GLOBAL  Z "16"  40.5
  GRID GLOBAL  Z "17"  45
  GRID GLOBAL  Z "18"  49.5
  GRID GLOBAL  Z "19"  54
  MATERIAL MAT1 FY 2.482E+08
  MATERIAL STEEL FY 2.482E+08
  MATERIAL CONC FYREBAR 4.136855E+08 FYSHEAR 2.757903E+08 FC
2.757903E+07 FCSHEAR 2.757903E+07
  STATICLOAD DL TYPE DEAD
  STATICLOAD LL TYPE LIVE
  STATICLOAD EQX TYPE QUAKE
  STATICLOAD EQY TYPE QUAKE
  COMBO DSTL1 DESIGN STEEL
  COMBO DSTL2 DESIGN STEEL
```

```
COMBO DSTL3 DESIGN STEEL
COMBO DSTL4 DESIGN STEEL
COMBO DSTL5 DESIGN STEEL
COMBO DSTL6 DESIGN STEEL
COMBO DSTL7 DESIGN STEEL
COMBO DSTL8 DESIGN STEEL
COMBO DSTL9 DESIGN STEEL
COMBO DSTL10 DESIGN STEEL
STEELDESIGN "AISC-LRFD93"
STEELFRAME 12 LMINOR .5
STEELFRAME 13 LMINOR .5
STEELFRAME 14 LMINOR .5
STEELFRAME 17 LMINOR .5
STEELFRAME 18 LMINOR .5
STEELFRAME 19 LMINOR .5
STEELFRAME 33 LMINOR .5
STEELFRAME 34 LMINOR .5
STEELFRAME 35 LMINOR .5
STEELFRAME 38 LMINOR .5
STEELFRAME 39 LMINOR .5
STEELFRAME 40 LMINOR .5
STEELFRAME 54 LMINOR .5
STEELFRAME 55 LMINOR .5
STEELFRAME 56 LMINOR .5
STEELFRAME 59 LMINOR .5
STEELFRAME 60 LMINOR .5
STEELFRAME 61 LMINOR .5
STEELFRAME 75 LMINOR .5
STEELFRAME 76 LMINOR .5
STEELFRAME 77 LMINOR .5
STEELFRAME 80 LMINOR .5
STEELFRAME 81 LMINOR .5
STEELFRAME 82 LMINOR .5
STEELFRAME 90 LMINOR .5
STEELFRAME 91 LMINOR .5
STEELFRAME 98 LMINOR .5
STEELFRAME 99 LMINOR .5
STEELFRAME 106 LMINOR .5
STEELFRAME 107 LMINOR .5
STEELFRAME 114 LMINOR .5
STEELFRAME 115 LMINOR .5
STEELFRAME 122 LMINOR .5
STEELFRAME 123 LMINOR .5
STEELFRAME 130 LMINOR .5
```

```
  STEELFRAME 131 LMINOR .5
  STEELFRAME 138 LMINOR .5
  STEELFRAME 139 LMINOR .5
  STEELFRAME 146 LMINOR .5
  STEELFRAME 147 LMINOR .5
END SUPPLEMENTAL DATA
```

C.2 EXAMPE 5.4.2

```
SYSTEM
 DOF=UX,UY,UZ,RX,RY,RZ  LENGTH=m  FORCE=N  PAGE=SECTIONS

JOINT
 1  X=-9  Y=-9  Z=0
 2  X=-3  Y=-9  Z=0
 3  X=3  Y=-9  Z=0
 4  X=9  Y=-9  Z=0
 5  X=-9  Y=-3  Z=0
 6  X=-3  Y=-3  Z=0
 7  X=3  Y=-3  Z=0
 8  X=9  Y=-3  Z=0
 9  X=-3  Y=3  Z=0
 10  X=3  Y=3  Z=0
 11  X=9  Y=3  Z=0
 12  X=-9  Y=-9  Z=4.5
 13  X=-3  Y=-9  Z=4.5
 14  X=3  Y=-9  Z=4.5
 15  X=9  Y=-9  Z=4.5
 16  X=-9  Y=-3  Z=4.5
 17  X=-3  Y=-3  Z=4.5
 18  X=3  Y=-3  Z=4.5
 19  X=9  Y=-3  Z=4.5
 20  X=-3  Y=3  Z=4.5
 21  X=3  Y=3  Z=4.5
 22  X=9  Y=3  Z=4.5
 23  X=-9  Y=-9  Z=9
 24  X=-3  Y=-9  Z=9
 25  X=3  Y=-9  Z=9
 26  X=9  Y=-9  Z=9
 27  X=-9  Y=-3  Z=9
 28  X=-3  Y=-3  Z=9
 29  X=3  Y=-3  Z=9
 30  X=9  Y=-3  Z=9
 31  X=-3  Y=3  Z=9
 32  X=3  Y=3  Z=9
 33  X=9  Y=3  Z=9
 34  X=-9  Y=-9  Z=13.5
 35  X=-3  Y=-9  Z=13.5
 36  X=3  Y=-9  Z=13.5
 37  X=9  Y=-9  Z=13.5
 38  X=-9  Y=-3  Z=13.5
```

39 X=-3 Y=-3 Z=13.5
40 X=3 Y=-3 Z=13.5
41 X=9 Y=-3 Z=13.5
42 X=-3 Y=3 Z=13.5
43 X=3 Y=3 Z=13.5
44 X=9 Y=3 Z=13.5
45 X=-9 Y=-9 Z=18
46 X=-3 Y=-9 Z=18
47 X=3 Y=-9 Z=18
48 X=9 Y=-9 Z=18
49 X=-9 Y=-3 Z=18
50 X=-3 Y=-3 Z=18
51 X=3 Y=-3 Z=18
52 X=9 Y=-3 Z=18
53 X=-3 Y=3 Z=18
54 X=3 Y=3 Z=18
55 X=9 Y=3 Z=18
56 X=-9 Y=-9 Z=22.5
57 X=-3 Y=-9 Z=22.5
58 X=3 Y=-9 Z=22.5
59 X=9 Y=-9 Z=22.5
60 X=-9 Y=-3 Z=22.5
61 X=-3 Y=-3 Z=22.5
62 X=3 Y=-3 Z=22.5
63 X=9 Y=-3 Z=22.5
64 X=-3 Y=3 Z=22.5
65 X=3 Y=3 Z=22.5
66 X=9 Y=3 Z=22.5
67 X=-9 Y=-9 Z=27
68 X=-3 Y=-9 Z=27
69 X=3 Y=-9 Z=27
70 X=9 Y=-9 Z=27
71 X=-9 Y=-3 Z=27
72 X=-3 Y=-3 Z=27
73 X=3 Y=-3 Z=27
74 X=9 Y=-3 Z=27
75 X=-3 Y=3 Z=27
76 X=3 Y=3 Z=27
77 X=9 Y=3 Z=27
78 X=-9 Y=-9 Z=31.5
79 X=-3 Y=-9 Z=31.5
80 X=3 Y=-9 Z=31.5
81 X=9 Y=-9 Z=31.5
82 X=-9 Y=-3 Z=31.5

```
 83  X=-3  Y=-3  Z=31.5
 84  X=3  Y=-3  Z=31.5
 85  X=9  Y=-3  Z=31.5
 86  X=-3  Y=3  Z=31.5
 87  X=3  Y=3  Z=31.5
 88  X=9  Y=3  Z=31.5
 89  X=-9  Y=-9  Z=36
 90  X=-3  Y=-9  Z=36
 91  X=3  Y=-9  Z=36
 92  X=9  Y=-9  Z=36
 93  X=-9  Y=-3  Z=36
 94  X=-3  Y=-3  Z=36
 95  X=3  Y=-3  Z=36
 96  X=9  Y=-3  Z=36
 97  X=-3  Y=3  Z=36
 98  X=3  Y=3  Z=36
 99  X=9  Y=3  Z=36

RESTRAINT
 ADD=1  DOF=U1,U2,U3,R1,R2,R3
 ADD=2  DOF=U1,U2,U3,R1,R2,R3
 ADD=3  DOF=U1,U2,U3,R1,R2,R3
 ADD=4  DOF=U1,U2,U3,R1,R2,R3
 ADD=5  DOF=U1,U2,U3,R1,R2,R3
 ADD=6  DOF=U1,U2,U3,R1,R2,R3
 ADD=7  DOF=U1,U2,U3,R1,R2,R3
 ADD=8  DOF=U1,U2,U3,R1,R2,R3
 ADD=9  DOF=U1,U2,U3,R1,R2,R3
 ADD=10  DOF=U1,U2,U3,R1,R2,R3
 ADD=11  DOF=U1,U2,U3,R1,R2,R3

CONSTRAINT
 NAME=DIAPH1  TYPE=DIAPH  AXIS=Z  CSYS=0
  ADD=12
  ADD=16
  ADD=13
  ADD=17
  ADD=20
  ADD=14
  ADD=18
  ADD=21
  ADD=15
  ADD=19
  ADD=22
```

```
NAME=DIAPH2  TYPE=DIAPH  AXIS=Z  CSYS=0
  ADD=23
  ADD=27
  ADD=24
  ADD=28
  ADD=31
  ADD=25
  ADD=29
  ADD=32
  ADD=26
  ADD=30
  ADD=33
NAME=DIAPH3  TYPE=DIAPH  AXIS=Z  CSYS=0
  ADD=34
  ADD=38
  ADD=35
  ADD=39
  ADD=42
  ADD=36
  ADD=40
  ADD=43
  ADD=37
  ADD=41
  ADD=44
NAME=DIAPH4  TYPE=DIAPH  AXIS=Z  CSYS=0
  ADD=45
  ADD=49
  ADD=46
  ADD=50
  ADD=53
  ADD=47
  ADD=51
  ADD=54
  ADD=48
  ADD=52
  ADD=55
NAME=DIAPH5  TYPE=DIAPH  AXIS=Z  CSYS=0
  ADD=56
  ADD=60
  ADD=57
  ADD=61
  ADD=64
  ADD=58
  ADD=62
```

```
   ADD=65
   ADD=59
   ADD=63
   ADD=66
  NAME=DIAPH6  TYPE=DIAPH  AXIS=Z  CSYS=0
   ADD=67
   ADD=71
   ADD=68
   ADD=72
   ADD=75
   ADD=69
   ADD=73
   ADD=76
   ADD=70
   ADD=74
   ADD=77
  NAME=DIAPH7  TYPE=DIAPH  AXIS=Z  CSYS=0
   ADD=78
   ADD=82
   ADD=79
   ADD=83
   ADD=86
   ADD=80
   ADD=84
   ADD=87
   ADD=81
   ADD=85
   ADD=88
  NAME=DIAPH8  TYPE=DIAPH  AXIS=Z  CSYS=0
   ADD=89
   ADD=93
   ADD=90
   ADD=94
   ADD=97
   ADD=91
   ADD=95
   ADD=98
   ADD=92
   ADD=96
   ADD=99

 PATTERN
  NAME=DEFAULT
```

```
MASS
 ADD=12  U1=4396  U2=4396  U3=4396
 ADD=13  U1=8972  U2=8972  U3=8972
 ADD=14  U1=8972  U2=8972  U3=8972
 ADD=15  U1=4396  U2=4396  U3=4396
 ADD=16  U1=4396  U2=4396  U3=4396
 ADD=17  U1=13188  U2=13188  U3=13188
 ADD=18  U1=17584  U2=17584  U3=17584
 ADD=19  U1=8972  U2=8972  U3=8972
 ADD=20  U1=4396  U2=4396  U3=4396
 ADD=21  U1=8972  U2=8972  U3=8972
 ADD=22  U1=4396  U2=4396  U3=4396
 ADD=23  U1=4396  U2=4396  U3=4396
 ADD=24  U1=8972  U2=8972  U3=8972
 ADD=25  U1=8972  U2=8972  U3=8972
 ADD=26  U1=4396  U2=4396  U3=4396
 ADD=27  U1=4396  U2=4396  U3=4396
 ADD=28  U1=13188  U2=13188  U3=13188
 ADD=29  U1=17584  U2=17584  U3=17584
 ADD=30  U1=8972  U2=8972  U3=8972
 ADD=31  U1=4396  U2=4396  U3=4396
 ADD=32  U1=8972  U2=8972  U3=8972
 ADD=33  U1=4396  U2=4396  U3=4396
 ADD=34  U1=4396  U2=4396  U3=4396
 ADD=35  U1=8972  U2=8972  U3=8972
 ADD=36  U1=8972  U2=8972  U3=8972
 ADD=37  U1=4396  U2=4396  U3=4396
 ADD=38  U1=4396  U2=4396  U3=4396
 ADD=39  U1=13188  U2=13188  U3=13188
 ADD=40  U1=17584  U2=17584  U3=17584
 ADD=41  U1=8972  U2=8972  U3=8972
 ADD=42  U1=4396  U2=4396  U3=4396
 ADD=43  U1=8972  U2=8972  U3=8972
 ADD=44  U1=4396  U2=4396  U3=4396
 ADD=45  U1=4396  U2=4396  U3=4396
 ADD=46  U1=8972  U2=8972  U3=8972
 ADD=47  U1=8972  U2=8972  U3=8972
 ADD=48  U1=4396  U2=4396  U3=4396
 ADD=49  U1=4396  U2=4396  U3=4396
 ADD=50  U1=13188  U2=13188  U3=13188
 ADD=51  U1=17584  U2=17584  U3=17584
 ADD=52  U1=8972  U2=8972  U3=8972
 ADD=53  U1=4396  U2=4396  U3=4396
 ADD=54  U1=8972  U2=8972  U3=8972
```

ADD=55 U1=4396 U2=4396 U3=4396
ADD=56 U1=4396 U2=4396 U3=4396
ADD=57 U1=8972 U2=8972 U3=8972
ADD=58 U1=8972 U2=8972 U3=8972
ADD=59 U1=4396 U2=4396 U3=4396
ADD=60 U1=4396 U2=4396 U3=4396
ADD=61 U1=13188 U2=13188 U3=13188
ADD=62 U1=17584 U2=17584 U3=17584
ADD=63 U1=8972 U2=8972 U3=8972
ADD=64 U1=4396 U2=4396 U3=4396
ADD=65 U1=8972 U2=8972 U3=8972
ADD=66 U1=4396 U2=4396 U3=4396
ADD=67 U1=4396 U2=4396 U3=4396
ADD=68 U1=8972 U2=8972 U3=8972
ADD=69 U1=8972 U2=8972 U3=8972
ADD=70 U1=4396 U2=4396 U3=4396
ADD=71 U1=4396 U2=4396 U3=4396
ADD=72 U1=13188 U2=13188 U3=13188
ADD=73 U1=17584 U2=17584 U3=17584
ADD=74 U1=8972 U2=8972 U3=8972
ADD=75 U1=4396 U2=4396 U3=4396
ADD=76 U1=8972 U2=8972 U3=8972
ADD=77 U1=4396 U2=4396 U3=4396
ADD=78 U1=4396 U2=4396 U3=4396
ADD=79 U1=8972 U2=8972 U3=8972
ADD=80 U1=8972 U2=8972 U3=8972
ADD=81 U1=4396 U2=4396 U3=4396
ADD=82 U1=4396 U2=4396 U3=4396
ADD=83 U1=13188 U2=13188 U3=13188
ADD=84 U1=17584 U2=17584 U3=17584
ADD=85 U1=8972 U2=8972 U3=8972
ADD=86 U1=4396 U2=4396 U3=4396
ADD=87 U1=8972 U2=8972 U3=8972
ADD=88 U1=4396 U2=4396 U3=4396
ADD=89 U1=4396 U2=4396 U3=4396
ADD=90 U1=8972 U2=8972 U3=8972
ADD=91 U1=8972 U2=8972 U3=8972
ADD=92 U1=4396 U2=4396 U3=4396
ADD=93 U1=4396 U2=4396 U3=4396
ADD=94 U1=13188 U2=13188 U3=13188
ADD=95 U1=17584 U2=17584 U3=17584
ADD=96 U1=8972 U2=8972 U3=8972
ADD=97 U1=4396 U2=4396 U3=4396
ADD=98 U1=8972 U2=8972 U3=8972

```
  ADD=99  U1=4396  U2=4396  U3=4396

MATERIAL
  NAME=STEEL  IDES=S
    T=0  E=1.999E+11  U=.3  A=.0000117  FY=2.482E+08
  NAME=CONC  IDES=C  M=2400.68  W=23561.61
    T=0  E=2.482113E+10  U=.2  A=.0000099
  NAME=OTHER  IDES=N  M=2400.68  W=23561.61
    T=0  E=2.482113E+10  U=.2  A=.0000099

FRAME SECTION
  NAME=FSEC1 MAT=STEEL SH=R T=.5,.3 A=.15 J=2.817371E-03
I=.003125,.001125 AS=.125,.125
  NAME=W14X109 MAT=STEEL A=2.064512E-02 J=2.963568E-06 I=5.16127E-
04,1.860554E-04 AS=4.850313E-03,1.350578E-02 S=2.837983E-03,1.003084E-03
Z=3.146316E-03,1.519081E-03 R=.1581137,9.493197E-02
T=.363728,.370967,.021844,.013335,.370967,.021844 SHN=W14X109 DSG=W
  NAME=W14X120 MAT=STEEL A=2.277415E-02 J=3.900088E-06 I=5.743994E-
04,2.060346E-04 AS=5.51173E-03,1.482771E-02 S=3.123501E-03,1.105875E-03
Z=3.474058E-03,1.67148E-03 R=.158813,9.511499E-02
T=.367792,.372618,.023876,.014986,.372618,.023876 SHN=W14X120 DSG=W
  NAME=W14X132 MAT=STEEL A=2.503221E-02 J=5.119647E-06 I=6.368341E-
04,2.280948E-04 AS=6.100439E-03,1.630835E-02 S=3.420492E-03,1.219709E-03
Z=3.834573E-03,1.851738E-03 R=.1595011,9.545708E-02
T=.372364,.374015,.026162,.016383,.374015,.026162 SHN=W14X132 DSG=W
  NAME=W14X159 MAT=STEEL A=3.012897E-02 J=8.241382E-06 I=7.908397E-
04,3.113411E-04 AS=7.199985E-03,1.991673E-02 S=4.156932E-03,1.575011E-03
Z=4.703087E-03,2.392511E-03 R=.1620138,.1016544
T=.380492,.395351,.030226,.018923,.395351,.030226 SHN=W14X159 DSG=W
  NAME=W14X68 MAT=STEEL A=.0129032 J=1.257019E-06 I=3.009353E-
04,5.0364E-05 AS=3.759089E-03,7.769017E-03 S=1.687728E-03,3.951838E-04
Z=1.884512E-03,6.046827E-04 R=.1527172,6.247574E-02
T=.356616,.254889,.018288,.010541,.254889,.018288 SHN=W14X68 DSG=W
  NAME=W14X74 MAT=STEEL A=1.406449E-02 J=1.614978E-06 I=3.313202E-
04,5.577501E-05 AS=4.113863E-03,8.499983E-03 S=1.841087E-03,4.361205E-04
Z=2.06477E-03,6.653148E-04 R=.1534836,6.297351E-02
T=.359918,.255778,.019939,.01143,.255778,.019939 SHN=W14X74 DSG=W
  NAME=W14X90 MAT=STEEL A=1.709674E-02 J=1.6899E-06 I=4.158152E-
04,1.506758E-04 AS=3.979863E-03,1.108514E-02 S=2.335332E-03,8.17096E-04
Z=2.572769E-03,1.238862E-03 R=.1559529,9.387827E-02
T=.356108,.368808,.018034,.011176,.368808,.018034 SHN=W14X90 DSG=W
  NAME=W14X99 MAT=STEEL A=1.877416E-02 J=2.235163E-06 I=4.620169E-
04,1.67325E-04 AS=4.430701E-03,1.221546E-02 S=2.569158E-03,9.045795E-04
```

```
Z=2.834962E-03,1.369959E-03 R=.1568732,9.440614E-02
T=.359664,.369951,.019812,.012319,.369951,.019812 SHN=W14X99 DSG=W
  NAME=W24X55 MAT=STEEL A=1.045159E-02 J=4.911531E-07 I=5.619124E-
04,1.211233E-05 AS=6.006569E-03,3.803799E-03 S=1.877178E-03,1.361495E-04
Z=2.195867E-03,2.179479E-04 R=.2318692,.0340426
T=.598678,.177927,.012827,.010033,.177927,.012827 SHN=W24X55 DSG=W
  NAME=W24X62 MAT=STEEL A=1.174191E-02 J=7.117558E-07 I=6.451587E-
04,1.435998E-05 AS=6.585794E-03,4.466249E-03 S=2.139844E-03,1.606118E-04
Z=2.507221E-03,2.572769E-04 R=.2344034,3.497096E-02
T=.602996,.178816,.014986,.010922,.178816,.014986 SHN=W24X62 DSG=W

FRAME
  1  J=1,12  SEC=W14X120  NSEG=2  ANG=0
  2  J=2,13  SEC=W14X132  NSEG=2  ANG=0
  3  J=3,14  SEC=W14X132  NSEG=2  ANG=0
  4  J=4,15  SEC=W14X120  NSEG=2  ANG=90
  5  J=5,16  SEC=W14X120  NSEG=2  ANG=0
  6  J=6,17  SEC=W14X159  NSEG=2  ANG=0
  7  J=7,18  SEC=W14X159  NSEG=2  ANG=0
  8  J=8,19  SEC=W14X120  NSEG=2  ANG=90
  9  J=9,20  SEC=W14X120  NSEG=2  ANG=0
  10  J=10,21  SEC=W14X132  NSEG=2  ANG=0
  11  J=11,22  SEC=W14X120  NSEG=2  ANG=90
  12  J=12,13  SEC=W24X62  NSEG=4  ANG=0
  13  J=13,14  SEC=W24X62  NSEG=4  ANG=0
  14  J=14,15  SEC=W24X62  NSEG=4  ANG=0
  15  J=12,16  SEC=W24X62  NSEG=4  ANG=0
  16  J=13,17  SEC=W24X62  NSEG=4  ANG=0
  17  J=14,18  SEC=W24X62  NSEG=4  ANG=0
  18  J=15,19  SEC=W24X62  NSEG=4  ANG=0
  19  J=16,17  SEC=W24X62  NSEG=4  ANG=0
  20  J=17,18  SEC=W24X62  NSEG=4  ANG=0
  21  J=18,19  SEC=W24X62  NSEG=4  ANG=0
  22  J=17,20  SEC=W24X62  NSEG=4  ANG=0
  23  J=18,21  SEC=W24X62  NSEG=4  ANG=0
  24  J=19,22  SEC=W24X62  NSEG=4  ANG=0
  25  J=20,21  SEC=W24X62  NSEG=4  ANG=0
  26  J=21,22  SEC=W24X62  NSEG=4  ANG=0
  27  J=12,23  SEC=W14X120  NSEG=2  ANG=0
  28  J=13,24  SEC=W14X132  NSEG=2  ANG=0
  29  J=14,25  SEC=W14X132  NSEG=2  ANG=0
  30  J=15,26  SEC=W14X120  NSEG=2  ANG=90
  31  J=16,27  SEC=W14X120  NSEG=2  ANG=0
  32  J=17,28  SEC=W14X159  NSEG=2  ANG=0
```

```
33  J=18,29  SEC=W14X159  NSEG=2  ANG=0
34  J=19,30  SEC=W14X120  NSEG=2  ANG=90
35  J=20,31  SEC=W14X120  NSEG=2  ANG=0
36  J=21,32  SEC=W14X132  NSEG=2  ANG=0
37  J=22,33  SEC=W14X120  NSEG=2  ANG=90
38  J=23,24  SEC=W24X62  NSEG=4  ANG=0
39  J=24,25  SEC=W24X62  NSEG=4  ANG=0
40  J=25,26  SEC=W24X62  NSEG=4  ANG=0
41  J=23,27  SEC=W24X62  NSEG=4  ANG=0
42  J=24,28  SEC=W24X62  NSEG=4  ANG=0
43  J=25,29  SEC=W24X62  NSEG=4  ANG=0
44  J=26,30  SEC=W24X62  NSEG=4  ANG=0
45  J=27,28  SEC=W24X62  NSEG=4  ANG=0
46  J=28,29  SEC=W24X62  NSEG=4  ANG=0
47  J=29,30  SEC=W24X62  NSEG=4  ANG=0
48  J=28,31  SEC=W24X62  NSEG=4  ANG=0
49  J=29,32  SEC=W24X62  NSEG=4  ANG=0
50  J=30,33  SEC=W24X62  NSEG=4  ANG=0
51  J=31,32  SEC=W24X62  NSEG=4  ANG=0
52  J=32,33  SEC=W24X62  NSEG=4  ANG=0
53  J=23,34  SEC=W14X99  NSEG=2  ANG=0
54  J=24,35  SEC=W14X109  NSEG=2  ANG=0
55  J=25,36  SEC=W14X109  NSEG=2  ANG=0
56  J=26,37  SEC=W14X99  NSEG=2  ANG=90
57  J=27,38  SEC=W14X109  NSEG=2  ANG=0
58  J=28,39  SEC=W14X132  NSEG=2  ANG=0
59  J=29,40  SEC=W14X132  NSEG=2  ANG=0
60  J=30,41  SEC=W14X109  NSEG=2  ANG=90
61  J=31,42  SEC=W14X99  NSEG=2  ANG=0
62  J=32,43  SEC=W14X109  NSEG=2  ANG=0
63  J=33,44  SEC=W14X99  NSEG=2  ANG=90
64  J=34,35  SEC=W24X62  NSEG=4  ANG=0
65  J=35,36  SEC=W24X62  NSEG=4  ANG=0
66  J=36,37  SEC=W24X62  NSEG=4  ANG=0
67  J=34,38  SEC=W24X62  NSEG=4  ANG=0
68  J=35,39  SEC=W24X62  NSEG=4  ANG=0
69  J=36,40  SEC=W24X62  NSEG=4  ANG=0
70  J=37,41  SEC=W24X62  NSEG=4  ANG=0
71  J=38,39  SEC=W24X62  NSEG=4  ANG=0
72  J=39,40  SEC=W24X62  NSEG=4  ANG=0
73  J=40,41  SEC=W24X62  NSEG=4  ANG=0
74  J=39,42  SEC=W24X62  NSEG=4  ANG=0
75  J=40,43  SEC=W24X62  NSEG=4  ANG=0
76  J=41,44  SEC=W24X62  NSEG=4  ANG=0
```

```
77  J=42,43  SEC=W24X62  NSEG=4  ANG=0
78  J=43,44  SEC=W24X62  NSEG=4  ANG=0
79  J=34,45  SEC=W14X99  NSEG=2  ANG=0
80  J=35,46  SEC=W14X109  NSEG=2  ANG=0
81  J=36,47  SEC=W14X109  NSEG=2  ANG=0
82  J=37,48  SEC=W14X99  NSEG=2  ANG=90
83  J=38,49  SEC=W14X109  NSEG=2  ANG=0
84  J=39,50  SEC=W14X132  NSEG=2  ANG=0
85  J=40,51  SEC=W14X132  NSEG=2  ANG=0
86  J=41,52  SEC=W14X109  NSEG=2  ANG=90
87  J=42,53  SEC=W14X99  NSEG=2  ANG=0
88  J=43,54  SEC=W14X109  NSEG=2  ANG=0
89  J=44,55  SEC=W14X99  NSEG=2  ANG=90
90  J=45,46  SEC=W24X62  NSEG=4  ANG=0
91  J=46,47  SEC=W24X62  NSEG=4  ANG=0
92  J=47,48  SEC=W24X62  NSEG=4  ANG=0
93  J=45,49  SEC=W24X62  NSEG=4  ANG=0
94  J=46,50  SEC=W24X62  NSEG=4  ANG=0
95  J=47,51  SEC=W24X62  NSEG=4  ANG=0
96  J=48,52  SEC=W24X62  NSEG=4  ANG=0
97  J=49,50  SEC=W24X62  NSEG=4  ANG=0
98  J=50,51  SEC=W24X62  NSEG=4  ANG=0
99  J=51,52  SEC=W24X62  NSEG=4  ANG=0
100  J=50,53  SEC=W24X62  NSEG=4  ANG=0
101  J=51,54  SEC=W24X62  NSEG=4  ANG=0
102  J=52,55  SEC=W24X62  NSEG=4  ANG=0
103  J=53,54  SEC=W24X62  NSEG=4  ANG=0
104  J=54,55  SEC=W24X62  NSEG=4  ANG=0
105  J=45,56  SEC=W14X90  NSEG=2  ANG=0
106  J=46,57  SEC=W14X99  NSEG=2  ANG=0
107  J=47,58  SEC=W14X99  NSEG=2  ANG=0
108  J=48,59  SEC=W14X90  NSEG=2  ANG=90
109  J=49,60  SEC=W14X99  NSEG=2  ANG=0
110  J=50,61  SEC=W14X109  NSEG=2  ANG=0
111  J=51,62  SEC=W14X109  NSEG=2  ANG=0
112  J=52,63  SEC=W14X99  NSEG=2  ANG=90
113  J=53,64  SEC=W14X90  NSEG=2  ANG=0
114  J=54,65  SEC=W14X99  NSEG=2  ANG=0
115  J=55,66  SEC=W14X90  NSEG=2  ANG=90
116  J=56,57  SEC=W24X55  NSEG=4  ANG=0
117  J=57,58  SEC=W24X55  NSEG=4  ANG=0
118  J=58,59  SEC=W24X55  NSEG=4  ANG=0
119  J=56,60  SEC=W24X55  NSEG=4  ANG=0
120  J=57,61  SEC=W24X55  NSEG=4  ANG=0
```

```
121  J=58,62  SEC=W24X55  NSEG=4  ANG=0
122  J=59,63  SEC=W24X55  NSEG=4  ANG=0
123  J=60,61  SEC=W24X55  NSEG=4  ANG=0
124  J=61,62  SEC=W24X55  NSEG=4  ANG=0
125  J=62,63  SEC=W24X55  NSEG=4  ANG=0
126  J=61,64  SEC=W24X55  NSEG=4  ANG=0
127  J=62,65  SEC=W24X55  NSEG=4  ANG=0
128  J=63,66  SEC=W24X55  NSEG=4  ANG=0
129  J=64,65  SEC=W24X55  NSEG=4  ANG=0
130  J=65,66  SEC=W24X55  NSEG=4  ANG=0
131  J=56,67  SEC=W14X90  NSEG=2  ANG=0
132  J=57,68  SEC=W14X99  NSEG=2  ANG=0
133  J=58,69  SEC=W14X99  NSEG=2  ANG=0
134  J=59,70  SEC=W14X90  NSEG=2  ANG=90
135  J=60,71  SEC=W14X99  NSEG=2  ANG=0
136  J=61,72  SEC=W14X109  NSEG=2  ANG=0
137  J=62,73  SEC=W14X109  NSEG=2  ANG=0
138  J=63,74  SEC=W14X99  NSEG=2  ANG=90
139  J=64,75  SEC=W14X90  NSEG=2  ANG=0
140  J=65,76  SEC=W14X99  NSEG=2  ANG=0
141  J=66,77  SEC=W14X90  NSEG=2  ANG=90
142  J=67,68  SEC=W24X55  NSEG=4  ANG=0
143  J=68,69  SEC=W24X55  NSEG=4  ANG=0
144  J=69,70  SEC=W24X55  NSEG=4  ANG=0
145  J=67,71  SEC=W24X55  NSEG=4  ANG=0
146  J=68,72  SEC=W24X55  NSEG=4  ANG=0
147  J=69,73  SEC=W24X55  NSEG=4  ANG=0
148  J=70,74  SEC=W24X55  NSEG=4  ANG=0
149  J=71,72  SEC=W24X55  NSEG=4  ANG=0
150  J=72,73  SEC=W24X55  NSEG=4  ANG=0
151  J=73,74  SEC=W24X55  NSEG=4  ANG=0
152  J=72,75  SEC=W24X55  NSEG=4  ANG=0
153  J=73,76  SEC=W24X55  NSEG=4  ANG=0
154  J=74,77  SEC=W24X55  NSEG=4  ANG=0
155  J=75,76  SEC=W24X55  NSEG=4  ANG=0
156  J=76,77  SEC=W24X55  NSEG=4  ANG=0
157  J=67,78  SEC=W14X68  NSEG=2  ANG=0
158  J=68,79  SEC=W14X74  NSEG=2  ANG=0
159  J=69,80  SEC=W14X74  NSEG=2  ANG=0
160  J=70,81  SEC=W14X68  NSEG=2  ANG=90
161  J=71,82  SEC=W14X68  NSEG=2  ANG=0
162  J=72,83  SEC=W14X90  NSEG=2  ANG=0
163  J=73,84  SEC=W14X90  NSEG=2  ANG=0
164  J=74,85  SEC=W14X68  NSEG=2  ANG=90
```

```
165  J=75,86  SEC=W14X68  NSEG=2  ANG=0
166  J=76,87  SEC=W14X74  NSEG=2  ANG=0
167  J=77,88  SEC=W14X68  NSEG=2  ANG=90
168  J=78,79  SEC=W24X55  NSEG=4  ANG=0
169  J=79,80  SEC=W24X55  NSEG=4  ANG=0
170  J=80,81  SEC=W24X55  NSEG=4  ANG=0
171  J=78,82  SEC=W24X55  NSEG=4  ANG=0
172  J=79,83  SEC=W24X55  NSEG=4  ANG=0
173  J=80,84  SEC=W24X55  NSEG=4  ANG=0
174  J=81,85  SEC=W24X55  NSEG=4  ANG=0
175  J=82,83  SEC=W24X55  NSEG=4  ANG=0
176  J=83,84  SEC=W24X55  NSEG=4  ANG=0
177  J=84,85  SEC=W24X55  NSEG=4  ANG=0
178  J=83,86  SEC=W24X55  NSEG=4  ANG=0
179  J=84,87  SEC=W24X55  NSEG=4  ANG=0
180  J=85,88  SEC=W24X55  NSEG=4  ANG=0
181  J=86,87  SEC=W24X55  NSEG=4  ANG=0
182  J=87,88  SEC=W24X55  NSEG=4  ANG=0
183  J=78,89  SEC=W14X68  NSEG=2  ANG=0
184  J=79,90  SEC=W14X74  NSEG=2  ANG=0
185  J=80,91  SEC=W14X74  NSEG=2  ANG=0
186  J=81,92  SEC=W14X68  NSEG=2  ANG=90
187  J=82,93  SEC=W14X68  NSEG=2  ANG=0
188  J=83,94  SEC=W14X90  NSEG=2  ANG=0
189  J=84,95  SEC=W14X90  NSEG=2  ANG=0
190  J=85,96  SEC=W14X68  NSEG=2  ANG=90
191  J=86,97  SEC=W14X68  NSEG=2  ANG=0
192  J=87,98  SEC=W14X74  NSEG=2  ANG=0
193  J=88,99  SEC=W14X68  NSEG=2  ANG=90
194  J=89,90  SEC=W24X55  NSEG=4  ANG=0
195  J=90,91  SEC=W24X55  NSEG=4  ANG=0
196  J=91,92  SEC=W24X55  NSEG=4  ANG=0
197  J=89,93  SEC=W24X55  NSEG=4  ANG=0
198  J=90,94  SEC=W24X55  NSEG=4  ANG=0
199  J=91,95  SEC=W24X55  NSEG=4  ANG=0
200  J=92,96  SEC=W24X55  NSEG=4  ANG=0
201  J=93,94  SEC=W24X55  NSEG=4  ANG=0
202  J=94,95  SEC=W24X55  NSEG=4  ANG=0
203  J=95,96  SEC=W24X55  NSEG=4  ANG=0
204  J=94,97  SEC=W24X55  NSEG=4  ANG=0
205  J=95,98  SEC=W24X55  NSEG=4  ANG=0
206  J=96,99  SEC=W24X55  NSEG=4  ANG=0
207  J=97,98  SEC=W24X55  NSEG=4  ANG=0
208  J=98,99  SEC=W24X55  NSEG=4  ANG=0
```

```
LOAD
  NAME=DL  CSYS=0
    TYPE=CONCENTRATED SPAN
      ADD=15  RD=.5  UZ=-43110
      ADD=41  RD=.5  UZ=-43110
      ADD=67  RD=.5  UZ=-43110
      ADD=93  RD=.5  UZ=-43110
      ADD=119  RD=.5  UZ=-43110
      ADD=145  RD=.5  UZ=-43110
      ADD=171  RD=.5  UZ=-43110
      ADD=197  RD=.5  UZ=-43110
      ADD=22  RD=.5  UZ=-43110
      ADD=48  RD=.5  UZ=-43110
      ADD=74  RD=.5  UZ=-43110
      ADD=100  RD=.5  UZ=-43110
      ADD=126  RD=.5  UZ=-43110
      ADD=152  RD=.5  UZ=-43110
      ADD=178  RD=.5  UZ=-43110
      ADD=204  RD=.5  UZ=-43110
      ADD=18  RD=.5  UZ=-43110
      ADD=44  RD=.5  UZ=-43110
      ADD=70  RD=.5  UZ=-43110
      ADD=96  RD=.5  UZ=-43110
      ADD=122  RD=.5  UZ=-43110
      ADD=148  RD=.5  UZ=-43110
      ADD=174  RD=.5  UZ=-43110
      ADD=200  RD=.5  UZ=-43110
      ADD=24  RD=.5  UZ=-43110
      ADD=50  RD=.5  UZ=-43110
      ADD=76  RD=.5  UZ=-43110
      ADD=102  RD=.5  UZ=-43110
      ADD=128  RD=.5  UZ=-43110
      ADD=154  RD=.5  UZ=-43110
      ADD=180  RD=.5  UZ=-43110
      ADD=206  RD=.5  UZ=-43110
      ADD=16  RD=.5  UZ=-86220
      ADD=42  RD=.5  UZ=-86220
      ADD=68  RD=.5  UZ=-86220
      ADD=94  RD=.5  UZ=-86220
      ADD=120  RD=.5  UZ=-86220
      ADD=146  RD=.5  UZ=-86220
      ADD=172  RD=.5  UZ=-86220
      ADD=198  RD=.5  UZ=-86220
```

```
  ADD=17  RD=.5  UZ=-86220
  ADD=43  RD=.5  UZ=-86220
  ADD=69  RD=.5  UZ=-86220
  ADD=95  RD=.5  UZ=-86220
  ADD=121  RD=.5  UZ=-86220
  ADD=147  RD=.5  UZ=-86220
  ADD=173  RD=.5  UZ=-86220
  ADD=199  RD=.5  UZ=-86220
  ADD=23  RD=.5  UZ=-86220
  ADD=49  RD=.5  UZ=-86220
  ADD=75  RD=.5  UZ=-86220
  ADD=101  RD=.5  UZ=-86220
  ADD=127  RD=.5  UZ=-86220
  ADD=153  RD=.5  UZ=-86220
  ADD=179  RD=.5  UZ=-86220
  ADD=205  RD=.5  UZ=-86220
 TYPE=DISTRIBUTED SPAN
  ADD=12  RD=0,1  UZ=-7185,-7185
  ADD=38  RD=0,1  UZ=-7185,-7185
  ADD=64  RD=0,1  UZ=-7185,-7185
  ADD=90  RD=0,1  UZ=-7185,-7185
  ADD=116  RD=0,1  UZ=-7185,-7185
  ADD=142  RD=0,1  UZ=-7185,-7185
  ADD=168  RD=0,1  UZ=-7185,-7185
  ADD=194  RD=0,1  UZ=-7185,-7185
  ADD=13  RD=0,1  UZ=-7185,-7185
  ADD=39  RD=0,1  UZ=-7185,-7185
  ADD=65  RD=0,1  UZ=-7185,-7185
  ADD=91  RD=0,1  UZ=-7185,-7185
  ADD=117  RD=0,1  UZ=-7185,-7185
  ADD=143  RD=0,1  UZ=-7185,-7185
  ADD=169  RD=0,1  UZ=-7185,-7185
  ADD=195  RD=0,1  UZ=-7185,-7185
  ADD=14  RD=0,1  UZ=-7185,-7185
  ADD=40  RD=0,1  UZ=-7185,-7185
  ADD=66  RD=0,1  UZ=-7185,-7185
  ADD=92  RD=0,1  UZ=-7185,-7185
  ADD=118  RD=0,1  UZ=-7185,-7185
  ADD=144  RD=0,1  UZ=-7185,-7185
  ADD=170  RD=0,1  UZ=-7185,-7185
  ADD=196  RD=0,1  UZ=-7185,-7185
  ADD=25  RD=0,1  UZ=-7185,-7185
  ADD=51  RD=0,1  UZ=-7185,-7185
  ADD=77  RD=0,1  UZ=-7185,-7185
```

```
    ADD=103  RD=0,1  UZ=-7185,-7185
    ADD=129  RD=0,1  UZ=-7185,-7185
    ADD=155  RD=0,1  UZ=-7185,-7185
    ADD=181  RD=0,1  UZ=-7185,-7185
    ADD=207  RD=0,1  UZ=-7185,-7185
    ADD=26  RD=0,1  UZ=-7185,-7185
    ADD=52  RD=0,1  UZ=-7185,-7185
    ADD=78  RD=0,1  UZ=-7185,-7185
    ADD=104  RD=0,1  UZ=-7185,-7185
    ADD=130  RD=0,1  UZ=-7185,-7185
    ADD=156  RD=0,1  UZ=-7185,-7185
    ADD=182  RD=0,1  UZ=-7185,-7185
    ADD=208  RD=0,1  UZ=-7185,-7185
    ADD=19  RD=0,1  UZ=-7185,-7185
    ADD=45  RD=0,1  UZ=-7185,-7185
    ADD=71  RD=0,1  UZ=-7185,-7185
    ADD=97  RD=0,1  UZ=-7185,-7185
    ADD=123  RD=0,1  UZ=-7185,-7185
    ADD=149  RD=0,1  UZ=-7185,-7185
    ADD=175  RD=0,1  UZ=-7185,-7185
    ADD=201  RD=0,1  UZ=-7185,-7185
    ADD=20  RD=0,1  UZ=-14370,-14370
    ADD=46  RD=0,1  UZ=-14370,-14370
    ADD=72  RD=0,1  UZ=-14370,-14370
    ADD=98  RD=0,1  UZ=-14370,-14370
    ADD=124  RD=0,1  UZ=-14370,-14370
    ADD=150  RD=0,1  UZ=-14370,-14370
    ADD=176  RD=0,1  UZ=-14370,-14370
    ADD=202  RD=0,1  UZ=-14370,-14370
    ADD=21  RD=0,1  UZ=-14370,-14370
    ADD=47  RD=0,1  UZ=-14370,-14370
    ADD=73  RD=0,1  UZ=-14370,-14370
    ADD=99  RD=0,1  UZ=-14370,-14370
    ADD=125  RD=0,1  UZ=-14370,-14370
    ADD=151  RD=0,1  UZ=-14370,-14370
    ADD=177  RD=0,1  UZ=-14370,-14370
    ADD=203  RD=0,1  UZ=-14370,-14370
NAME=LL  CSYS=0
  TYPE=CONCENTRATED SPAN
    ADD=15  RD=.5  UZ=-30150
    ADD=41  RD=.5  UZ=-30150
    ADD=67  RD=.5  UZ=-30150
    ADD=93  RD=.5  UZ=-30150
    ADD=119  RD=.5  UZ=-30150
```

ADD=145 RD=.5 UZ=-30150
ADD=171 RD=.5 UZ=-30150
ADD=197 RD=.5 UZ=-30150
ADD=22 RD=.5 UZ=-30150
ADD=48 RD=.5 UZ=-30150
ADD=74 RD=.5 UZ=-30150
ADD=100 RD=.5 UZ=-30150
ADD=126 RD=.5 UZ=-30150
ADD=152 RD=.5 UZ=-30150
ADD=178 RD=.5 UZ=-30150
ADD=204 RD=.5 UZ=-30150
ADD=18 RD=.5 UZ=-30150
ADD=44 RD=.5 UZ=-30150
ADD=70 RD=.5 UZ=-30150
ADD=96 RD=.5 UZ=-30150
ADD=122 RD=.5 UZ=-30150
ADD=148 RD=.5 UZ=-30150
ADD=174 RD=.5 UZ=-30150
ADD=200 RD=.5 UZ=-30150
ADD=24 RD=.5 UZ=-30150
ADD=50 RD=.5 UZ=-30150
ADD=76 RD=.5 UZ=-30150
ADD=102 RD=.5 UZ=-30150
ADD=128 RD=.5 UZ=-30150
ADD=154 RD=.5 UZ=-30150
ADD=180 RD=.5 UZ=-30150
ADD=206 RD=.5 UZ=-30150
ADD=16 RD=.5 UZ=-60300
ADD=42 RD=.5 UZ=-60300
ADD=68 RD=.5 UZ=-60300
ADD=94 RD=.5 UZ=-60300
ADD=120 RD=.5 UZ=-60300
ADD=146 RD=.5 UZ=-60300
ADD=172 RD=.5 UZ=-60300
ADD=198 RD=.5 UZ=-60300
ADD=17 RD=.5 UZ=-60300
ADD=43 RD=.5 UZ=-60300
ADD=69 RD=.5 UZ=-60300
ADD=95 RD=.5 UZ=-60300
ADD=121 RD=.5 UZ=-60300
ADD=147 RD=.5 UZ=-60300
ADD=173 RD=.5 UZ=-60300
ADD=199 RD=.5 UZ=-60300
ADD=23 RD=.5 UZ=-60300

```
  ADD=49  RD=.5  UZ=-60300
  ADD=75  RD=.5  UZ=-60300
  ADD=101  RD=.5  UZ=-60300
  ADD=127  RD=.5  UZ=-60300
  ADD=153  RD=.5  UZ=-60300
  ADD=179  RD=.5  UZ=-60300
  ADD=205  RD=.5  UZ=-60300
TYPE=DISTRIBUTED SPAN
  ADD=12  RD=0,1  UZ=-5025,-5025
  ADD=38  RD=0,1  UZ=-5025,-5025
  ADD=64  RD=0,1  UZ=-5025,-5025
  ADD=90  RD=0,1  UZ=-5025,-5025
  ADD=116  RD=0,1  UZ=-5025,-5025
  ADD=142  RD=0,1  UZ=-5025,-5025
  ADD=168  RD=0,1  UZ=-5025,-5025
  ADD=194  RD=0,1  UZ=-5025,-5025
  ADD=13  RD=0,1  UZ=-5025,-5025
  ADD=39  RD=0,1  UZ=-5025,-5025
  ADD=65  RD=0,1  UZ=-5025,-5025
  ADD=91  RD=0,1  UZ=-5025,-5025
  ADD=117  RD=0,1  UZ=-5025,-5025
  ADD=143  RD=0,1  UZ=-5025,-5025
  ADD=169  RD=0,1  UZ=-5025,-5025
  ADD=195  RD=0,1  UZ=-5025,-5025
  ADD=14  RD=0,1  UZ=-5025,-5025
  ADD=40  RD=0,1  UZ=-5025,-5025
  ADD=66  RD=0,1  UZ=-5025,-5025
  ADD=92  RD=0,1  UZ=-5025,-5025
  ADD=118  RD=0,1  UZ=-5025,-5025
  ADD=144  RD=0,1  UZ=-5025,-5025
  ADD=170  RD=0,1  UZ=-5025,-5025
  ADD=196  RD=0,1  UZ=-5025,-5025
  ADD=25  RD=0,1  UZ=-5025,-5025
  ADD=51  RD=0,1  UZ=-5025,-5025
  ADD=77  RD=0,1  UZ=-5025,-5025
  ADD=103  RD=0,1  UZ=-5025,-5025
  ADD=129  RD=0,1  UZ=-5025,-5025
  ADD=155  RD=0,1  UZ=-5025,-5025
  ADD=181  RD=0,1  UZ=-5025,-5025
  ADD=207  RD=0,1  UZ=-5025,-5025
  ADD=26  RD=0,1  UZ=-5025,-5025
  ADD=52  RD=0,1  UZ=-5025,-5025
  ADD=78  RD=0,1  UZ=-5025,-5025
  ADD=104  RD=0,1  UZ=-5025,-5025
```

```
    ADD=130  RD=0,1  UZ=-5025,-5025
    ADD=156  RD=0,1  UZ=-5025,-5025
    ADD=182  RD=0,1  UZ=-5025,-5025
    ADD=208  RD=0,1  UZ=-5025,-5025
    ADD=19  RD=0,1  UZ=-5025,-5025
    ADD=45  RD=0,1  UZ=-5025,-5025
    ADD=71  RD=0,1  UZ=-5025,-5025
    ADD=97  RD=0,1  UZ=-5025,-5025
    ADD=123  RD=0,1  UZ=-5025,-5025
    ADD=149  RD=0,1  UZ=-5025,-5025
    ADD=175  RD=0,1  UZ=-5025,-5025
    ADD=201  RD=0,1  UZ=-5025,-5025
    ADD=20  RD=0,1  UZ=-10050,-10050
    ADD=46  RD=0,1  UZ=-10050,-10050
    ADD=72  RD=0,1  UZ=-10050,-10050
    ADD=98  RD=0,1  UZ=-10050,-10050
    ADD=124  RD=0,1  UZ=-10050,-10050
    ADD=150  RD=0,1  UZ=-10050,-10050
    ADD=176  RD=0,1  UZ=-10050,-10050
    ADD=202  RD=0,1  UZ=-10050,-10050
    ADD=21  RD=0,1  UZ=-10050,-10050
    ADD=47  RD=0,1  UZ=-10050,-10050
    ADD=73  RD=0,1  UZ=-10050,-10050
    ADD=99  RD=0,1  UZ=-10050,-10050
    ADD=125  RD=0,1  UZ=-10050,-10050
    ADD=151  RD=0,1  UZ=-10050,-10050
    ADD=177  RD=0,1  UZ=-10050,-10050
    ADD=203  RD=0,1  UZ=-10050,-10050
NAME=EQX  CSYS=0
  TYPE=FORCE
    ADD=12  UX=708.31
    ADD=13  UX=1416.62
    ADD=14  UX=1416.62
    ADD=15  UX=708.31
    ADD=16  UX=708.31
    ADD=17  UX=2124.925
    ADD=18  UX=2833.23
    ADD=19  UX=1416.62
    ADD=20  UX=708.31
    ADD=21  UX=1416.62
    ADD=22  UX=708.31
    ADD=23  UX=1839.67
    ADD=24  UX=3679.35
    ADD=25  UX=3679.35
```

ADD=26 UX=1839.67
ADD=27 UX=1839.67
ADD=28 UX=5519.02
ADD=29 UX=7358.69
ADD=30 UX=3679.35
ADD=31 UX=1839.67
ADD=32 UX=3679.35
ADD=33 UX=1839.67
ADD=34 UX=3215.27
ADD=35 UX=6430.53
ADD=36 UX=6430.53
ADD=37 UX=3215.27
ADD=38 UX=3215.27
ADD=39 UX=9645.8
ADD=40 UX=12861.07
ADD=41 UX=6430.53
ADD=42 UX=3215.27
ADD=43 UX=6430.53
ADD=44 UX=3215.27
ADD=45 UX=4778.13
ADD=46 UX=9556.26
ADD=47 UX=9556.26
ADD=48 UX=4778.13
ADD=49 UX=4778.13
ADD=50 UX=14334.39
ADD=51 UX=19112.52
ADD=52 UX=9556.26
ADD=53 UX=4778.13
ADD=54 UX=9556.26
ADD=55 UX=4778.13
ADD=56 UX=6496.86
ADD=57 UX=12993.71
ADD=58 UX=12993.71
ADD=59 UX=6496.86
ADD=60 UX=6496.86
ADD=61 UX=19490.57
ADD=62 UX=25987.43
ADD=63 UX=12993.71
ADD=64 UX=6496.86
ADD=65 UX=12993.71
ADD=66 UX=6496.86
ADD=67 UX=8350.95
ADD=68 UX=16701.91
ADD=69 UX=16701.91

```
    ADD=70  UX=8350.95
    ADD=71  UX=8350.95
    ADD=72  UX=25052.86
    ADD=73  UX=33403.81
    ADD=74  UX=16701.91
    ADD=75  UX=8350.95
    ADD=76  UX=16701.91
    ADD=77  UX=8350.95
    ADD=78  UX=10325.76
    ADD=79  UX=20651.51
    ADD=80  UX=20651.51
    ADD=81  UX=10325.76
    ADD=82  UX=10325.76
    ADD=83  UX=30977.27
    ADD=84  UX=41303.02
    ADD=85  UX=20651.51
    ADD=86  UX=10325.76
    ADD=87  UX=20651.51
    ADD=88  UX=10325.76
    ADD=89  UX=12410.13
    ADD=90  UX=24820.26
    ADD=91  UX=24820.26
    ADD=92  UX=12410.13
    ADD=93  UX=12410.13
    ADD=94  UX=37230.39
    ADD=95  UX=49640.52
    ADD=96  UX=24820.26
    ADD=97  UX=12410.13
    ADD=98  UX=24820.26
    ADD=99  UX=12410.13
  NAME=EQY  CSYS=0
   TYPE=FORCE
    ADD=12  UY=708.31
    ADD=13  UY=1416.62
    ADD=14  UY=1416.62
    ADD=15  UY=708.31
    ADD=16  UY=708.31
    ADD=17  UY=2124.925
    ADD=18  UY=2833.23
    ADD=19  UY=1416.62
    ADD=20  UY=708.31
    ADD=21  UY=1416.62
    ADD=22  UY=708.31
    ADD=23  UY=1839.67
```

ADD=24 UY=3679.35
ADD=25 UY=3679.35
ADD=26 UY=1839.67
ADD=27 UY=1839.67
ADD=28 UY=5519.02
ADD=29 UY=7358.69
ADD=30 UY=3679.35
ADD=31 UY=1839.67
ADD=32 UY=3679.35
ADD=33 UY=1839.67
ADD=34 UY=3215.27
ADD=35 UY=6430.53
ADD=36 UY=6430.53
ADD=37 UY=3215.27
ADD=38 UY=3215.27
ADD=39 UY=9645.8
ADD=40 UY=12861.07
ADD=41 UY=6430.53
ADD=42 UY=3215.27
ADD=43 UY=6430.53
ADD=44 UY=3215.27
ADD=45 UY=4778.13
ADD=46 UY=9556.26
ADD=47 UY=9556.26
ADD=48 UY=4778.13
ADD=49 UY=4778.13
ADD=50 UY=14334.39
ADD=51 UY=19112.52
ADD=52 UY=9556.26
ADD=53 UY=4778.13
ADD=54 UY=9556.26
ADD=55 UY=4778.13
ADD=56 UY=6496.86
ADD=57 UY=12993.71
ADD=58 UY=12993.71
ADD=59 UY=6496.86
ADD=60 UY=6496.86
ADD=61 UY=19490.57
ADD=62 UY=25987.43
ADD=63 UY=12993.71
ADD=64 UY=6496.86
ADD=65 UY=12993.71
ADD=66 UY=6496.86
ADD=67 UY=8350.95

```
     ADD=68  UY=16701.91
     ADD=69  UY=16701.91
     ADD=70  UY=8350.95
     ADD=71  UY=8350.95
     ADD=72  UY=25052.86
     ADD=73  UY=33403.81
     ADD=74  UY=16701.91
     ADD=75  UY=8350.95
     ADD=76  UY=16701.91
     ADD=77  UY=8350.95
     ADD=78  UY=10325.76
     ADD=79  UY=20651.51
     ADD=80  UY=20651.51
     ADD=81  UY=10325.76
     ADD=82  UY=10325.76
     ADD=83  UY=30977.27
     ADD=84  UY=41303.02
     ADD=85  UY=20651.51
     ADD=86  UY=10325.76
     ADD=87  UY=20651.51
     ADD=88  UY=10325.76
     ADD=89  UY=12410.13
     ADD=90  UY=24820.26
     ADD=91  UY=24820.26
     ADD=92  UY=12410.13
     ADD=93  UY=12410.13
     ADD=94  UY=37230.39
     ADD=95  UY=49640.52
     ADD=96  UY=24820.26
     ADD=97  UY=12410.13
     ADD=98  UY=24820.26
     ADD=99  UY=12410.13

PDELTA
  ITMAX=10  TOLD=.001  TOLP=.001
    LOAD=DL  SF=1
    LOAD=LL  SF=1

MODE
  TYPE=EIGEN  N=100  TOL=.00001

HISTORY
  NAME=HIST1 TYPE=LIN NSTEP=1500 DT=.02 DAMP=.02
    ACC=U1  ANG=0 FUNC=ELCENTRO SF=9.8066 AT=0
```

```
COMBO
 NAME=DSTL1
  LOAD=DL  SF=1.4
 NAME=DSTL2
  LOAD=DL  SF=1.2
  LOAD=LL  SF=1.6
 NAME=DSTL3
  LOAD=DL  SF=1.2
  LOAD=LL  SF=.5
  LOAD=EQX  SF=1
 NAME=DSTL4
  LOAD=DL  SF=1.2
  LOAD=LL  SF=.5
  LOAD=EQX  SF=-1
 NAME=DSTL5
  LOAD=DL  SF=1.2
  LOAD=LL  SF=.5
  LOAD=EQY  SF=1
 NAME=DSTL6
  LOAD=DL  SF=1.2
  LOAD=LL  SF=.5
  LOAD=EQY  SF=-1
 NAME=DSTL7
  LOAD=DL  SF=.9
  LOAD=EQX  SF=1
 NAME=DSTL8
  LOAD=DL  SF=.9
  LOAD=EQX  SF=-1
 NAME=DSTL9
  LOAD=DL  SF=.9
  LOAD=EQY  SF=1
 NAME=DSTL10
  LOAD=DL  SF=.9
  LOAD=EQY  SF=-1

OUTPUT
; No Output Requested

END

; The following data is used for graphics, design and pushover analysis.
; If changes are made to the analysis data above, then the following data
; should be checked for consistency.
```

```
SAP2000 V7.40 SUPPLEMENTAL DATA
  GRID GLOBAL  X "1"  -9
  GRID GLOBAL  X "2"  -3
  GRID GLOBAL  X "3"  3
  GRID GLOBAL  X "4"  9
  GRID GLOBAL  Y "5"  -9
  GRID GLOBAL  Y "6"  -3
  GRID GLOBAL  Y "7"  3
  GRID GLOBAL  Z "8"  0
  GRID GLOBAL  Z "9"  4.5
  GRID GLOBAL  Z "10"  9
  GRID GLOBAL  Z "11"  13.5
  GRID GLOBAL  Z "12"  18
  GRID GLOBAL  Z "13"  22.5
  GRID GLOBAL  Z "14"  27
  GRID GLOBAL  Z "15"  31.5
  GRID GLOBAL  Z "16"  36
  MATERIAL STEEL FY 2.482E+08
  MATERIAL CONC FYREBAR 4.136855E+08 FYSHEAR 2.757903E+08 FC
2.757903E+07 FCSHEAR 2.757903E+07
  STATICLOAD DL TYPE DEAD
  STATICLOAD LL TYPE LIVE
  STATICLOAD EQX TYPE QUAKE
  STATICLOAD EQY TYPE QUAKE
  COMBO DSTL1 DESIGN STEEL
  COMBO DSTL2 DESIGN STEEL
  COMBO DSTL3 DESIGN STEEL
  COMBO DSTL4 DESIGN STEEL
  COMBO DSTL5 DESIGN STEEL
  COMBO DSTL6 DESIGN STEEL
  COMBO DSTL7 DESIGN STEEL
  COMBO DSTL8 DESIGN STEEL
  COMBO DSTL9 DESIGN STEEL
  COMBO DSTL10 DESIGN STEEL
  STEELDESIGN "AISC-LRFD93"
  STEELFRAME 15 LMINOR .5
  STEELFRAME 16 LMINOR .5
  STEELFRAME 17 LMINOR .5
  STEELFRAME 18 LMINOR .5
  STEELFRAME 22 LMINOR .5
  STEELFRAME 23 LMINOR .5
  STEELFRAME 24 LMINOR .5
  STEELFRAME 41 LMINOR .5
  STEELFRAME 42 LMINOR .5
```

STEELFRAME 43 LMINOR .5
STEELFRAME 44 LMINOR .5
STEELFRAME 48 LMINOR .5
STEELFRAME 49 LMINOR .5
STEELFRAME 50 LMINOR .5
STEELFRAME 67 LMINOR .5
STEELFRAME 68 LMINOR .5
STEELFRAME 69 LMINOR .5
STEELFRAME 70 LMINOR .5
STEELFRAME 74 LMINOR .5
STEELFRAME 75 LMINOR .5
STEELFRAME 76 LMINOR .5
STEELFRAME 93 LMINOR .5
STEELFRAME 94 LMINOR .5
STEELFRAME 95 LMINOR .5
STEELFRAME 96 LMINOR .5
STEELFRAME 100 LMINOR .5
STEELFRAME 101 LMINOR .5
STEELFRAME 102 LMINOR .5
STEELFRAME 119 LMINOR .5
STEELFRAME 120 LMINOR .5
STEELFRAME 121 LMINOR .5
STEELFRAME 122 LMINOR .5
STEELFRAME 126 LMINOR .5
STEELFRAME 127 LMINOR .5
STEELFRAME 128 LMINOR .5
STEELFRAME 145 LMINOR .5
STEELFRAME 146 LMINOR .5
STEELFRAME 147 LMINOR .5
STEELFRAME 148 LMINOR .5
STEELFRAME 152 LMINOR .5
STEELFRAME 153 LMINOR .5
STEELFRAME 154 LMINOR .5
STEELFRAME 171 LMINOR .5
STEELFRAME 172 LMINOR .5
STEELFRAME 173 LMINOR .5
STEELFRAME 174 LMINOR .5
STEELFRAME 178 LMINOR .5
STEELFRAME 179 LMINOR .5
STEELFRAME 180 LMINOR .5
STEELFRAME 197 LMINOR .5
STEELFRAME 198 LMINOR .5
STEELFRAME 199 LMINOR .5
STEELFRAME 200 LMINOR .5

```
  STEELFRAME 204 LMINOR .5
  STEELFRAME 205 LMINOR .5
  STEELFRAME 206 LMINOR .5
END SUPPLEMENTAL DATA
```